MATHEMATICAL MODELING OF EPIDEMICS SPREADING DEALING WITH TEMPORARY TREATMENT EFFICIENCY

GRÉGOIRE RANSON

A DISSERTATION SUBMITTED TO
THE FACULTY OF GRADUATE STUDIES
IN PARTIAL FULFILLMENT OF THE REQUIREMENTS
FOR THE DEGREE OF
DOCTOR OF PHILOSOPHY

GRADUATE PROGRAM IN MATHEMATICS AND STATISTICS
YORK UNIVERSITY
TORONTO, ONTARIO

April 2026

© Grégoire Ranson, 2026

YORK U

Université Claude Bernard Lyon 1

THÈSE de DOCTORAT DE L'UNIVERSITÉ CLAUDE BERNARD LYON 1
EN COTUTELLE AVEC YORK UNIVERSITY

École Doctorale N° 512
ED InfoMaths

Discipline : Mathématiques

Soutenue publiquement le 17 Avril 2026, par :

Grégoire Ranson

Mathematical modeling of epidemics spreading dealing with temporary treatment efficiency

Devant le jury composé de :

ADIMY, Mostafa	DR, Centre Inria de Lyon	Directeur
AÏNSEBA, Bedr'Eddine	PR, Université de Bordeaux	Rapporteur
ASGARY, Ali	Professeur, York University	Rapporteur
CIUPERCA, Gabriela	PR, Université Claude Bernard Lyon 1	Examinatrice
GREER, Meredith	Professeure, Bates College	Rapporteuse
MACKEY, Michael C.	Professeur, McGill University	Examinateur
RUAN, Shigui	Professeur, University of Miami	Examinateur
WU, Jianhnong	Professeur, York University	Co-directeur

MATHEMATICAL MODELING OF EPIDEMICS SPREADING DEALING WITH TEMPORARY TREATMENT EFFICIENCY

by **Grégoire Ranson**

a dissertation submitted to the Faculty of Graduate Studies of York University in partial fulfilment of the requirements for the degree of

DOCTOR OF PHILOSOPHY

© 2026

Permission has been granted to: a) YORK UNIVERSITY LIBRARIES to lend or sell copies of this dissertation in paper, microform or electronic formats, and b) LIBRARY AND ARCHIVES CANADA to reproduce, lend, distribute, or sell copies of this dissertation anywhere in the world in microform, paper or electronic formats *and* to authorise or procure the reproduction, loan, distribution or sale of copies of this dissertation anywhere in the world in microform, paper or electronic formats.

The author reserves other publication rights, and neither the dissertation nor extensive extracts for it may be printed or otherwise reproduced without the author's written permission.

MATHEMATICAL MODELING OF EPIDEMICS SPREADING DEALING WITH TEMPORARY TREATMENT EFFICIENCY

by **Grégoire Ranson**

By virtue of submitting this document electronically, the author certifies that this is a true electronic equivalent of the copy of the dissertation approved by York University for the award of the degree. No alteration of the content has occurred and if there are any minor variations in formatting, they are as a result of the coversion to Adobe Acrobat format (or similar software application).

Colloquium Committee Members:

1. Jianhong Wu
2. Neal Madras
3. Woldegebriel Assefa Woldegerima

Abstract

This dissertation focuses on the mathematical modeling and epidemiological impact analysis of two major biomedical interventions for sexually transmitted diseases (STDs): Pre-Exposure Prophylaxis (PrEP) for the Human Immunodeficiency Virus (HIV) and vaccination against Chlamydia trachomatis (CT). In the first part, we develop HIV compartmental models that incorporate a specific PrEP compartment. The originality of the model lies in accounting for the limited duration of protection through an age-structured hyperbolic equation (where age represents the time elapsed since the last dose). This formalism allows the model to be reduced to a hybrid system of differential-difference equations with a discrete delay, representing the interval between medical appointments according to WHO guidelines. We perform a rigorous mathematical analysis (including local and global stability) and explore the influence of non-linear recruitment rates. Our results highlight the existence of hysteresis phenomena and the emergence of Hopf bifurcations, identifying critical delays beyond which epidemic dynamics become oscillatory. Numerical simulations, calibrated using French data (Truvada), quantify the impact of treatment adherence and protection duration on epidemic control. In the second part, the thesis shifts scale to evaluate the population-level impact of a potential vaccine for Chlamydia in the United States. We developed an Agent-Based Model (ABM), calibrated using National Health and Nutrition Examination Survey (NHANES) data, to simulate transmission networks. This model tests various vaccination strategies, demonstrating that age-targeted approaches or gender-inclusive strategies are essential for significantly reducing infection prevalence. This interdisciplinary work combines the qualitative analysis of dynami-

cal systems with stochastic simulations to provide decision-support tools for public health, emphasizing the importance of behavioral and economic factors in the success of prevention policies.

Acknowledgements

First and foremost, I would like to thank my thesis supervisors, Mostafa Adimy, Laurent Pujo-Menjouet, and Jianhong Wu, for their guidance and for enabling me to bring this work to completion. Your kindness, your rigor, and your scientific curiosity have been a true source of inspiration for me and have given me a passion for research. Thanks to you, I was able to benefit from the exceptional framework of a cotutelle program. This journey has not always been easy, but it has proven to be extremely formative, and for that, I thank you.

I would also like to thank all the members of the laboratories and institutes that welcomed me, whether at LIAM, the Department of Mathematics at York University, the Institut Camille Jordan (ICJ), or at Inria. Having had the opportunity to work in so many different environments and to cross paths with so many people has been an immensely enriching experience for which I am deeply grateful.

I wish to extend a very special thank you to the research group at Sanofi. Taking part in such an intensive project, with such fascinating and crucial challenges, has been a true honor. I have grown immensely, both personally and scientifically, throughout this collaboration.

Finally, I want to thank my family, without whom none of this would have been possible. Thank you to my parents, my brother, and my sister for always being there for me during the difficult times and for continually pushing me to give my very best.

Table of Contents

Copyright ii

Authenticity iii

Abstract iv

Acknowledgements vi

Table of Contents vii

List of Tables xi

List of Figures xiii

Résumé substantiel en français xv

Preface xx

Abbreviations xxii

1 Introduction 1

1.1 Human immunodeficiency virus: a chronic irreversible infection 2

1.2 Epidemiological persistence and concentration of HIV transmission . 4

1.3 HIV prevention strategies and the specific role of PrEP 6

1.4 PrEP as a temporally structured prevention strategy . . . 8
1.5 Political and economic impact . . . 10
1.6 Limitations of standard approaches for PrEP . . . 12
1.7 Temporally structured prevention and the role of delay . . . 13
1.8 Contributions . . . 14

2 Forecasting the effect of Pre-Exposure Prophylaxis (PrEP) on HIV propagation with a system of differential-difference equations with delay 19
2.1 Introduction . . . 19
2.2 Introducing our model . . . 22
2.3 Mathematical analysis . . . 27
2.3.1 Wellposedness of the model . . . 27
2.3.2 Steady-states . . . 28
2.4 Global stability analysis . . . 39
2.4.1 Disease-free steady-state . . . 40
2.4.2 Endemic equilibrium . . . 44
2.5 French clinical data . . . 46
2.5.1 Parameters . . . 47
2.5.2 MSM . . . 53
2.5.3 High-risks . . . 56
2.5.4 Sensitivity analysis . . . 59
2.6 Comparaison of PrEP costs in France from 2016 to 2026 . . . 62
2.7 Conclusion and discussion . . . 70

3 Stability analysis of a new differential-difference model applied to the Pre-Exposure Prophylaxis (PrEP) effect on the spread of HIV 72
3.1 Introduction . . . 72
3.2 Age-structured model with fixed maximum age . . . 76
3.3 Existence of steady-states . . . 80

3.4 Stability of the two steady-states and persistence analysis 84
3.4.1 Disease-free equilibrium: $\mathcal{E}_0 := (\Lambda/\mu, 0, 0)$ 86
3.4.2 Global asymptotic stability of $\mathcal{E}_0 := (\Lambda/\mu, 0, 0)$ 87
3.4.3 Persistence analysis 88
3.4.4 The dynamical behavior of the endemic steady state 93
3.5 Discussion 105

4 Qualtitative impact of political and economic decisions on PrEP users under HIV epidemic control 107
4.1 Introduction 107
4.2 The SI model with protection 110
4.3 Existence of equilibria 115
4.3.1 System without any infection 115
4.3.2 Existence of disease-free equilibria 119
4.3.3 Existence of the endemic equilibrium 120
4.4 Local asymptotic stability 124
4.4.1 Disease-free equilibria 125
4.4.2 Endemic steady state 129
4.5 Discussion 144
4.6 Comparaison between deterministic and stochastic approaches 148

5 An agent-based platform for simulating the impact of chlamydia vaccine in the US population 152
5.1 Introduction 152
5.2 Methods 154
5.3 Results 174
5.4 Discussion 185

6 Conclusion 190
6.1 Discussion 190
6.2 Future works 193

Bibliography **195**

List of Tables

2.1 Parameters used in model (1.1) with values applied to the French population estimated from [92] 48
2.2 Summary of initial conditions for susceptibles and infected among general MSM and MSM high risks populations 49
2.3 Total number of PrEP users in France since 2016, given by semester (See [92], Table 3). 50
2.4 Values of parameters ψ and θ per month accordingly to each semester, computed according to Table 2.2 and 2.3. 51
2.5 Values of parameters K and r depending on the population 52
2.6 Values of parameters S_{sat}, γ and n depending on the general French MSM and the high risk French MSM. 53

4.1 Parameters of the model and their description. 114
4.2 Existence of equilibria with respect to d, the death rate of the susceptible population. 119

5.1 Calibration prevalence targets for Chlamydia and PID 160
5.2 Parameters for the model simulation (No vaccination case) 169
5.3 Vaccination scenarios 173
5.4 Relative reduction in chlamydia and PID prevalence across VE and VC combinations 181
5.5 Relative reduction in chlamydia across VE waning rates 183
5.6 Relative reduction in chlamydia across vaccination scale-up years . . 183

5.7 Relative reduction in chlamydia and PID prevalence across vaccine mechanisms 184
5.8 Relative reduction in chlamydia and PID prevalence across different vaccine programs 184

List of Figures

1.1 Progression of HIV infection without treatment. 3
1.2 Global HIV Epidemic Incidence and Mortality in 2024 5
1.3 WHO and HIV: 40-Year Timeline. Source: World Health Organization (WHO), 2023 6

2.1 Schematic representation of the compartmental model (2.1). Continuous arrows represent movements between the compartments. Dashed ones represents the transmission of the infection. 23
2.2 Plot of the evolution of the French MSM population over 15 years . . 54
2.3 Plot of the evolution of the different compartments of the model over 15 years 55
2.4 Plot of the evolution of the incidence with and without PrEP for MSM population over 15 years 55
2.5 Plot of the $\mathcal{R}_0$ as a function of ψ. 56
2.6 Plot of the evolution of the incidence with PrEP over 15 years 57
2.7 Plot of the evolution of the incidence with and without PrEP (2.4) over 15 years among French high risk MSM. 57
2.8 Plot of the $\mathcal{R}_0$ as a function of ψ. 58
2.9 Plot of the susceptibles and infected if PrEP was stopped in 15 years 58
2.10 Local sensitivity analysis on $\mathcal{R}_0$ for MSM population 60
2.11 Local sensitivity analysis on $\mathcal{R}_0$ for high-risk MSM population 61

3.1 Flow diagram of SIP model with non-linear recruitment with respect to I . . . 79
3.2 Numericla simulation holding condition on $\vartheta(\tau) \geq \vartheta^*(\tau)$ . . . 100
3.3 Stability of th endemic equilibrium . . . 101
3.4 Condiiton for $0 \leq \vartheta(\tau) \leq \vartheta_-(\tau)$ . . . 104
3.5 Functions $T_k^{\pm}$ are drawn for $\tau \in [0, 6$ . . . 105

4.1 Representation of PrEP uptake through unimodal function . . . 111
4.2 Flow diagram of SIP model with non-linear recruitment rate with unimodal function . . . 113
4.3 Reprensentation of possible equilibrium of the model . . . 117
4.4 Schematic representation of conditions existence of equilibria . . . 119
4.5 Representation of conditon the $\vartheta(\tau) \leq 0$ for $\tau \in [0, 17.219$ . . . 143
4.6 Numerical simulation of existence of equilibriium E_f^3 . . . 143
4.7 Numerical simulation of Hopf bifurcation . . . 144
4.8 Co-existence of the equilibria . . . 144
4.9 Diagram of bifurcation and the amplitude of the oscillations . . . 145

5.1 Model calibration of CT prevalence . . . 164
5.2 PID prevalence calibration results. . . . 165
5.3 Model validation results . . . 168
5.4 Chlamydia a and PID b prevalence rates across combinations of vaccine efficacy and coverage . . . 175
5.5 Vaccine efficacy changes with time over 20 years and Chlamydia prevalence under different vaccine efficacy dynamics . . . 176
5.6 Immunity level and Chlamydia prevalence under vaccination scale-up scenarios . . . 177
5.7 Projected weekly CT prevalence over 20 years under four vaccination scenarios . . . 179
5.8 Impact of vaccination programs foucsing on age . . . 182

Résumé substantiel en français

Ce travail de thèse s'inscrit dans le domaine des biomathématiques et de l'épidémiologie théorique. Il vise à modéliser et à quantifier l'impact épidémiologique des interventions biomédicales préventives dont la caractéristique principale est de posséder une efficacité intrinsèquement limitée dans le temps. La recherche se concentre sur deux problèmes majeurs de santé publique sexuelle : le Virus de l'Immunodéficience Humaine (VIH) et l'infection bactérienne à Chlamydia trachomatis (CT). Historiquement, les modèles épidémiologiques compartimentaux classiques considèrent
l'immunité (acquise ou vaccinale) comme permanente ou décroissante de manière exponentielle simple. Or, les prophylaxies modernes, telles que la Prophylaxie Pré-Exposition (PrEP) contre le VIH, exigent une observance stricte et des renouvellements réguliers (généralement tous les trois mois selon les directives de l'Organisation Mondiale de la Santé). De même, les candidats vaccins contre la Chlamydia présentent une décroissance immunitaire complexe. La problématique centrale de cette thèse est donc d'intégrer rigoureusement cette « temporalité » clinique et comportementale dans des modèles mathématiques déterministes et stochastiques afin d'évaluer l'efficacité de différentes stratégies de santé publique. La première grande partie du manuscrit est consacrée à la modélisation de la PrEP. Contrairement aux traitements antirétroviraux (TAR) administrés aux personnes séropositives, la PrEP est destinée aux individus séronégatifs à haut risque, modifiant ainsi le vivier des personnes susceptibles (S).

Dans le chapitre 2, nous avons développé un système compartimental innovant de type SIP (Susceptibles, Infectés, Protégés). La population protégée est modélisée par une équation aux dérivées partielles (EDP) hyperbolique, structurée par « l'âge », qui représente ici le temps écoulé depuis la dernière prescription médicale. Le processus de renouvellement du traitement est mathématiquement intégré sous forme de condition aux limites. Grâce à la méthode des caractéristiques, ce modèle EDP a pu être réduit à un système d'équations différentielles à retard discret (DDE), le retard correspondant au délai d'efficacité maximale défini par la prescription (par exemple, 90 jours). L'analyse de la stabilité de ce système repose sur le calcul du taux de reproduction de base ($\mathcal{R}_0$). Nos résultats analytiques démontrent que le $\mathcal{R}_0$ est une fonction strictement décroissante de ce délai de protection. Nous avons ensuite appliqué ce modèle aux données épidémiologiques françaises concernant les hommes ayant des relations sexuelles avec des hommes (HSH), en utilisant les paramètres cliniques du médicament proposé par Truvada. Les simulations numériques soulignent qu'une stratégie ciblant spécifiquement la sous-population à haut risque est fondamentalement plus efficace pour contrôler l'épidémie qu'une distribution élargie, validant ainsi l'approche ciblée des politiques publiques actuelles. Le recrutement dans un programme PrEP n'est pas un processus constant. Le chapitre 3 enrichit le modèle précédent en introduisant des taux de recrutement non linéaires qui dépendent de la dynamique de l'épidémie elle-même, afin de traduire la « perception du risque » par la population. Spécifiquement, le taux d'adoption de la PrEP est formulé comme une fonction de la prévalence (le nombre d'individus infectés). L'analyse mathématique se concentre sur l'étude de la stabilité asymptotique locale et globale des équilibres du système (sans maladie et endémique). Nous démontrons la persistance de l'infection lorsque $\mathcal{R}_0 > 1$. De plus, bien que l'introduction de retards discrets dans les équations différentielles soit connue pour pouvoir générer des instabilités dynamiques, telles que des bifurcations de Hopf (entraînant des oscillations périodiques de l'épidémie), nos analyses théoriques et numériques prouvent que, pour des paramètres biologiquement et sociologiquement réalistes, de telles bifurcations n'émergent pas dans cette configuration spécifique. L'implémentation de la PrEP à grande échelle se heurte à des limites budgétaires, logistiques et infrastructurelles (capacité des centres de

dépistage, coût des médicaments). Dans le chapitre 4, nous modélisons ces limitations en introduisant un taux de recrutement non monotone, inspiré d'une fonction de réponse fonctionnelle unimodale. Cette modification structurelle engendre une dynamique mathématique particulièrement riche. Le modèle permet l'existence de multiples états d'équilibre, notamment la coexistence de plusieurs équilibres sans maladie, mettant en évidence un phénomène d'hystérésis : si le système perd le contrôle de l'épidémie en raison d'une baisse temporaire du financement de la PrEP, un retour aux conditions financières initiales ne suffira pas nécessairement à rétablir le contrôle épidémique. Plus remarquablement, contrairement aux résultats du chapitre 3, les limitations de ressources couplées aux retards de protection peuvent franchir des valeurs critiques, entraînant l'apparition de bifurcations de Hopf. En termes de santé publique, cela signifie que des capacités de renouvellement des prescriptions mal calibrées peuvent provoquer des vagues épidémiques récurrentes (oscillations). La deuxième thématique de la thèse se tourne vers Chlamydia trachomatis, l'infection bactérienne sexuellement transmissible la plus fréquente, souvent asymptomatique mais responsable de graves séquelles à long terme (maladies inflammatoires pelviennes, infertilité). Bien qu'il n'existe actuellement aucun vaccin commercialisé, la modélisation de candidats vaccins est essentielle pour orienter les futurs essais cliniques. Pour capturer la complexité des comportements sexuels hétérogènes et l'histoire clinique individuelle (y compris l'accumulation de séquelles au fil des infections), nous avons abandonné l'approche par équations différentielles au profit d'un Modèle Basé sur les Agents (Agent-Based Model, ABM) appliqué à la population des États-Unis. Ce modèle simule un réseau dynamique intégrant les comportements des hétérosexuels, des HSH et des travailleuses du sexe, rigoureusement calibré en trois étapes sur les données des enquêtes nationales américaines (NHANES, NSFG). Les résultats des simulations mettent en évidence plusieurs points critiques pour la formulation d'une stratégie vaccinale optimale. La vaccination prioritaire de la cohorte des 15-24 ans est significativement plus impactante sur la prévalence globale qu'un ciblage des adultes plus âgés, même à couverture vaccinale égale. Un vaccin dit "bloquant" (réduisant à la fois la susceptibilité à l'infection et l'infectiosité en cas d'échec vaccinal) offre les meilleures perspectives d'élimination de la maladie à un horizon de 20 ans. La durée

de protection est le paramètre le plus sensible. Une protection s'estompant avec une demi-vie de 10 ans permettrait une réduction de près de 60 % de la prévalence. Toutefois, une décroissance immunitaire plus rapide annihilerait presque totalement les bénéfices du programme de vaccination à l'échelle populationnelle. Nous démontrons qu'il existe un continuum d'équivalence où une moindre efficacité biologique du vaccin peut être parfaitement compensée par un déploiement logistique accéléré et une couverture vaccinale élargie.

Cette thèse démontre la nécessité d'intégrer les contraintes temporelles (délais cliniques de protection, décroissance de l'immunité) et structurelles (budgets, comportements d'adhésion) dans l'évaluation mathématique des interventions biomédicales. Les modèles développés soulignent que la réussite de stratégies telles que la PrEP ne repose pas uniquement sur l'efficacité pharmacologique de la molécule, mais fortement sur l'infrastructure de santé publique capable de soutenir le rythme des renouvellements. Sur le plan vaccinal, nos travaux sur la Chlamydia fournissent une matrice décisionnelle claire pour les autorités de santé américaines en vue des futurs lancements. En guise de perspectives, ces travaux de recherche appellent à plusieurs développements futurs. D'abord le couplage des dynamiques de la PrEP avec celles du TasP (Treatment as Prevention, pour les individus séropositifs avec charge virale indétectable). Ensuite, l'application de la théorie du contrôle optimal à ces systèmes à retard pour déterminer des stratégies d'allocation budgétaire dynamiques minimisant le coût tout en maximisant l'évitement des infections.Enfin, le développement de modèles hybrides, combinant la finesse comportementale des modèles basés sur les agents (ABM) pour les populations à haut risque, et l'efficacité calculatoire des équations différentielles (EDP/DDE) pour la population générale. Cette thèse démontre la nécessité d'intégrer les contraintes temporelles (délais cliniques de protection, décroissance de l'immunité) et structurelles (budgets, comportements d'adhésion) dans l'évaluation mathématique des interventions biomédicales. Les modèles développés soulignent que la réussite de stratégies telles que la PrEP ne repose pas uniquement sur l'efficacité pharmacologique de la molécule, mais fortement sur l'infrastructure de santé publique capable de soutenir le rythme des renouvellements. Sur le plan

vaccinal, nos travaux sur la Chlamydia fournissent une feuile de route claire pour les autorités de santé américaines en vue des futurs lancements.

Preface

I, Grégoire Ranson, declare that this thesis titled "Mathematical modeling of epidemics spreading dealing with temporary treatment efficiency" has been witten by me under the supervision of Mostafa Adimy, Laurent Pujo-Menjouet et Jianhong Wu. Chapter 2 of this thesis has been published in *Mathematics* as

> Adimy, M., Molina, J., Pujo-Menjouet, L., **Ranson, G.**, Wu, J. (2022). Forecasting the Effect of Pre-Exposure Prophylaxis (PrEP) on HIV Propagation with a System of Differential-Difference Equations with Delay. *Mathematics*, 10(21), 4093.
> doi.org/10.3390/math10214093

My primary contributions were as follows: data collection and processing, numerical simulations, mathematical validation. I was actively involved in the drafting of the manuscript. I took a leading role in writing the Introduction, detailing the numerical results, and writing the Conclusion. I also participated in the comprehensive review and editing of the final manuscript. My co-first author, Julien Molina, led the initial drafting of the manuscript. Mostafa Adimy, Laurent Pujo-Menjouet, and Jianhong Wu supervised the research project. All authors read and agreed to the published version of the manuscript.

The content of Chapter 3 is based on the following published peer-reviewed article:

> Adimy, M., Chekroun, A., **Ranson, G.**, Pujo-Menjouet, L. (2024). Stability Analysis of a New Differential-Difference Model Applied to the

Pre-exposure Prophylaxis (PrEP) Effect on the Spread of HIV. *Qualitative Theory of Dynamical Systems*, 23(238).
doi.org/10.1007/s12346-024-01093-x

As stated in the published manuscript, all authors contributed equally to this work.

Chapter 4 of this thesis, "Qualtitative impact of political and economic decisions on PrEP users under HIV epidemic control", is being prepared for submission for publication. The draft of the paper was prepared by Grégoire Ranson and Abdennasser Chekroun and then revised by Mostafa Adimy, Abdennasser Chekroun, Laurent Pujo-Menjouet et Grégoire Ranson. Mostafa Adimy and Laurent Pujo-Menjouet supervised the project. The content of Chapter 5 is based on the following manuscript:

Deng, Q., **Ranson, G.**, Bragazzi, N. L., Bosch Castells, V., Chaves, S. S., Thommes, E., Wu, J. An agent-based platform for simulating the impact of chlamydia vaccine in the US population. Nat Commun (2026). doi.org/10.1038/s41467-026-74025-9

My specific contributions to this chapter were as follows: I contributed to the conceptualization of the study, data curation, formal analysis and writing of the original manuscipt. The first author, Qi Deng, took the lead in methodology, software development, visualization, and validation. The project was supervised by Jianhong Wu, Edward Thommes, Valerie Bosch Castells, and Sandra Sandra Chaves. All authors participated in data curation, formal analysis, and drafting the original manuscript. Qi Deng, Nicola Luigi Bragazzi, Valérie Bosch Castells, Sandra S. Chavez, Edward Thommes and Jianhong Wu reviewed and edited the manuscript.

Abbreviations

ABM	Agent-Based Model
AIDS	Acquired Immune Deficiency Syndrome
CT	*Chlamydia trachomatis*
DFE	Disease-Free Equilibrium
FSW	Female Sex Workers
HIV	Human Immunodeficiency Virus
MSM	Men who have Sex with Men
NHANES	National Health and Nutrition Examination Survey
NSFG	National Survey of Family Growth
PID	Pelvic Inflammatory Disease
PrEP	Pre-Exposure Prophylaxis
SEIRS	Susceptible - Exposed - Infected - Recovered - Susceptible
SICA	Susceptible - Infected - Infected under ART - Infected with AIDS symptom

SIP	Susceptible - Infected - Protected
SIR	Susceptible - Infected - Recovered
STI	Sexually Transmitted Infections
UNAIDS	Joint United Nations Programme on AIDS
VC	Vaccine Coverage
VE	Vaccine Efficacy
WHO	World Health Organization

Chapter 1

Introduction

The objective of this thesis is to develop mathematical models for studying the impact of biomedical prevention strategies on sexually transmitted infections (STIs). To capture the diverse epidemiological challenges posed by different pathogens, this work is structured around two main axes. In a first part, we study the transmission of the Human Immunodeficiency Virus (HIV), with a particular focus on the epidemiological impact of pre-exposure prophylaxis (PrEP). Motivated by the clinical organization of PrEP delivery, we use temporally structured compartmental models to investigate how finite protection and renewal mechanisms shape epidemic dynamics. In a second part, we shift our focus to Chlamydia Trachomatis (CT), the most frequently reported bacterial STI worldwide. Because addressing long-term sequelae like pelvic inflammatory disease (PID) requires explicit tracking of individual infection histories and dynamic sexual partnerships , we develop an agent-based modeling (ABM) framework to evaluate the potential impact of a candidate vaccination program

1.1 Human immunodeficiency virus: a chronic irreversible infection

Human immunodeficiency virus (HIV) is a chronic viral infection. It is characterized by irreversible integration of its genetic material into host cells and by prolonged asymptomatic phases during which infected individuals remain infectious. Following initial exposure, viral replication rapidly establishes a persistent infection through integration into the host genome. Unlike many acute infections, HIV does not admit a natural recovery process at the individual level. Effective treatment can not remove HIV infection from infected individuals [136, 156]. This biological persistence fundamentally shapes the structure of HIV epidemics, as transmission may occur over extended periods in the absence of symptoms 1.1. At the population level, this irreversibility has important epidemiological consequences. Since infection cannot be cleared, epidemic control cannot rely on recovery dynamics to reduce prevalence. Instead, the pool of infected individuals accumulates over time, and reductions in transmission can only be achieved by preventing new infections or by suppressing infectiousness through treatment [139].

While antiretroviral therapy effectively reduces viral load and transmission risk, it does not eliminate infection, and therefore does not restore susceptibility [124, 152]. As a result, the long-term dynamics of HIV epidemics are primarily driven by the rate at which new individuals become infected. This irreversibility distinguishes HIV from many acute infectious diseases commonly modeled using susceptible–infected–recovered (SIR) frameworks, in which recovery plays a central role in shaping epidemic trajectories. In the case of HIV, infected compartments must instead be treated as absorbing states, and epidemic dynamics are governed by transitions occurring upstream of infection. Consequently, interventions cannot be modeled as mechanisms shortening infectious periods, but must be represented as acting on exposure or susceptibility prior to infection. This modeling constraint directly affects the mathematical structure of HIV transmission model, in which prevention modifies transmission processes rather than disease progression. From a modeling perspec-

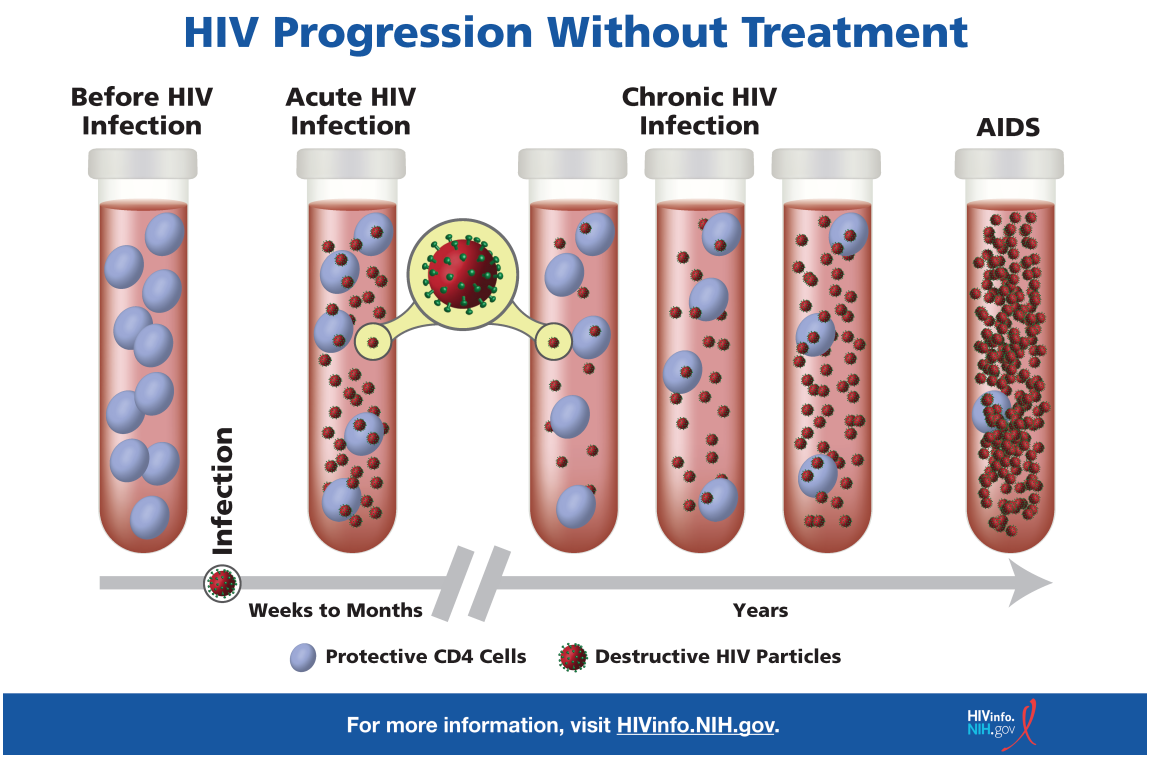


Figure 1.1: Progression of HIV infection without treatment.
Source: HIVinfo.NIH.gov, National Institutes of Health (NIH). Royalty-free image (public domain)

tive, these features place prevention mechanisms at the center of HIV epidemiology. Understanding the impact of preventive strategies therefore requires frameworks capable of capturing how protection alters transmission over extended time scales. This focus naturally leads to the study of interventions acting before infection occurs, and motivates the explicit representation of preventive dynamics in mathematical models of HIV transmission.

1.2 Epidemiological persistence and concentration of HIV transmission

Despite major advances in antiretroviral therapy and widespread treatment coverage in many regions, HIV remains a persistent global public health issue, with 40.8 millions of individuals living with the virus worldwide in 2024 1.1,[157, 165]. Antiretroviral treatment has profoundly transformed the natural history of HIV infection by suppressing viral replication, improving life expectancy, and substantially reducing onward transmission 1.2, [142, 168]. However, treatment does not eliminate infection and does not restore susceptibility, such that individuals remain infected for life even under sustained viral suppression. As a result, while treatment is essential for individual and public health, it does not, by itself, interrupt epidemic dynamics or lead to disease elimination [142]. In many high-income countries, the epidemiological profile of HIV has evolved from generalized transmission toward concentrated epidemics. Ongoing transmission is no longer uniformly distributed across the population but is instead concentrated within specific groups, notably men who have sex with men, people who inject drugs, and sex workers. These populations experience higher exposure risks due to biological, behavioral, and social factors, and they often form partially connected transmission networks in which infection can persist despite high overall treatment availability [173].

Consequently, even in settings with extensive access to care, transmission continues within subpopulations that are insufficiently protected by treatment alone. This concentration of transmission highlights the central role of heterogeneity in HIV epidemiology. Differences in exposure risk, contact patterns, and access to prevention and care generate uneven transmission dynamics that cannot be captured by homogeneous population assumptions. In particular, transmission within key populations may be sustained by network structures and behavioral patterns that amplify local risk, while remaining largely decoupled from the broader population. These features imply that epidemic control cannot rely solely on population-wide averages, but must explicitly address differential risk and selective intervention uptake [173].

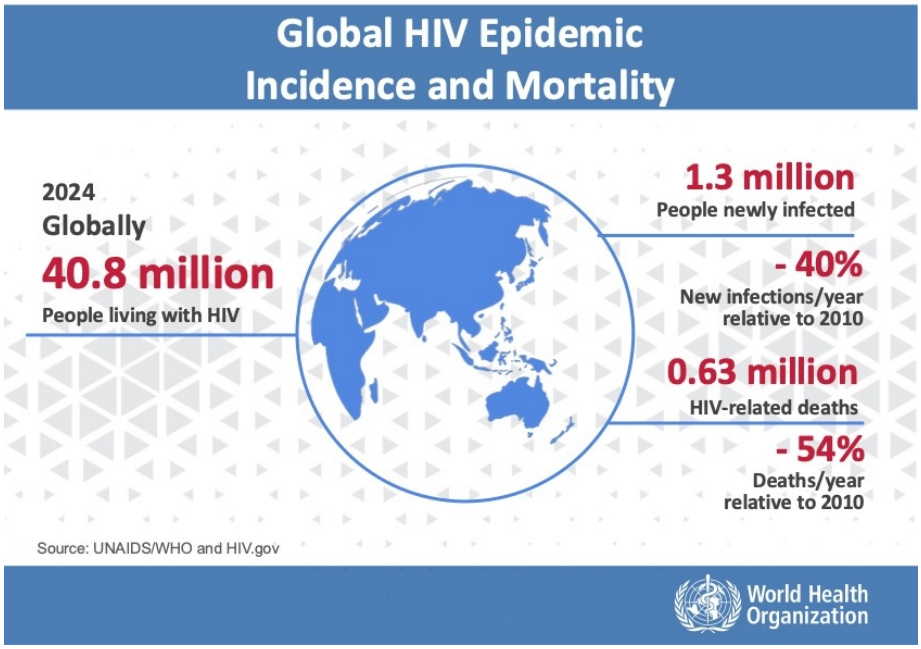


Figure 1.2: Global HIV Epidemic Incidence and Mortality in 2024. Source: World Health Organization (WHO), 2024

From a modeling perspective, the presence of concentrated epidemics fundamentally shapes the structure of effective prevention strategies. Interventions aimed at reducing susceptibility or exposure must be targeted toward populations at sustained risk, and their impact depends on patterns of initiation, coverage, and adherence within these groups. Consequently, prevention dynamics cannot be treated as uniform across the population, but must account for selective uptake and differentiated risk profiles. This observation motivates the study of prevention tools specifically designed for individuals at high risk of infection, and naturally leads to the consideration of biomedical interventions such as pre-exposure prophylaxis.

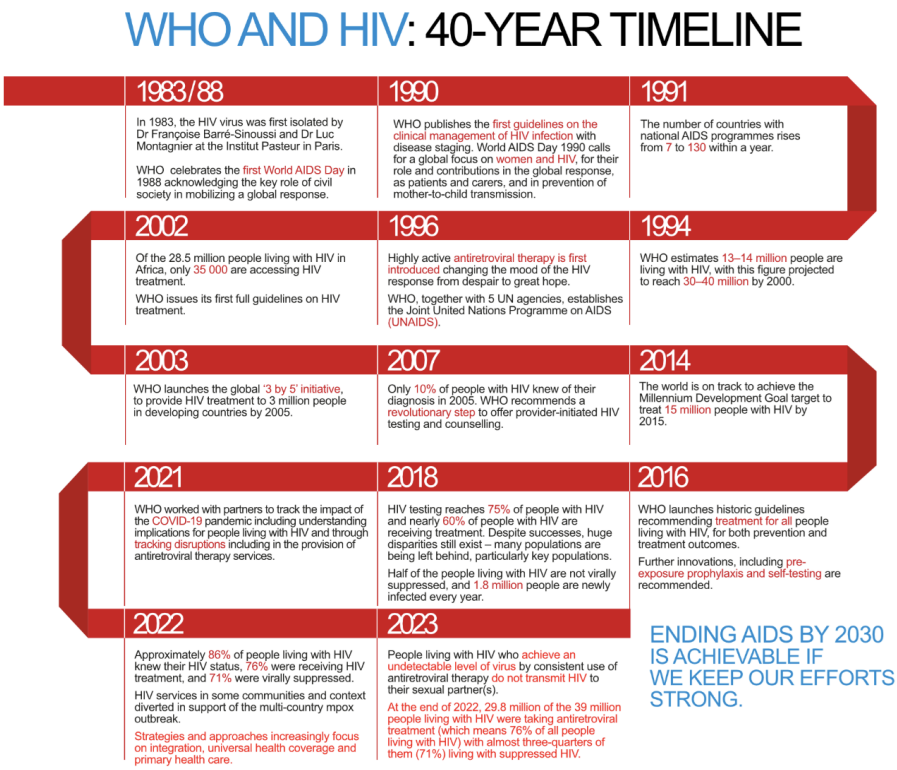


Figure 1.3: WHO and HIV: 40-Year Timeline. Source: World Health Organization (WHO), 2023

1.3 HIV prevention strategies and the specific role of PrEP

In the absence of an effective vaccine, HIV prevention relies on a combination of behavioral, biomedical, and treatment-based strategies aimed at reducing exposure or susceptibility to infection [116, 157].

Behavioral interventions, including condom use, harm reduction programs, and risk-reduction counseling, have played a central role in prevention efforts. These programs are designed to minimize the impact of drug use and drug policies on users. They are aimed at increase risk awareness about sexual practices as well. Treatment as

prevention leverages viral suppression to decrease onward transmission from infected individuals [44].

Together, these approaches have contributed substantially to reducing HIV incidence in many settings and remain essential components of comprehensive prevention strategies [127].

However, the effectiveness of both behavioral interventions and treatment as prevention critically depends on sustained adherence, early diagnosis, and continuous engagement in care. Behavioral prevention requires long-term compliance with protective practices, while treatment as prevention is contingent on timely diagnosis and durable viral suppression. As a result, these strategies may fail to fully protect individuals experiencing intermittent care, delayed diagnosis, or fluctuating risk behaviors. Consequently, prevention gaps persist, particularly within populations exposed to sustained or episodic high risk, highlighting the need for complementary approaches that act directly on susceptibility prior to infection.

Among biomedical prevention tools, pre-exposure prophylaxis (PrEP) has emerged as one of the most effective interventions for individuals at high risk of HIV infection, substantially reducing the probability of transmission when taken as prescribed [49, 64, 107]. Unlike post-infection treatments, PrEP acts before exposure occurs and modifies individual susceptibility rather than disease progression. Its protective effect is therefore independent of infection status within the population and directly targets the biological risk of acquisition. This pre-exposure mechanism distinguishes PrEP from other prevention strategies and makes it particularly well suited for targeted deployment within high-risk populations.

Importantly, the population-level impact of PrEP depends not only on its biological efficacy but also on patterns of initiation, adherence, and discontinuation within exposed groups [158]. Individuals may initiate PrEP during periods of elevated risk and discontinue it when perceived risk decreases, leading to time-varying protection at the individual level [158]. These features introduce dynamic processes that directly shape epidemic outcomes and cannot be reduced to static reductions in transmission probability. As such, PrEP constitutes a prevention strategy whose effectiveness is intrinsically linked to its temporal implementation, motivating a detailed examination

of how PrEP use is organized and sustained in practice.

1.4 PrEP as a temporally structured prevention strategy

Initiation and finite protection

PrEP, provided by Truvada, has been approved in July 2012 by the US Food and Drug administration [51]. The initial annual cost of PrEP was $22,000 and decreases to $360 with generic versions [125]. However, European Medecines Agency provided EU-wide authorization in 2016. [123]. A great variability of cost and access exist in Europe with three types of situations. In France, PrEP is fully reimbursed for the persons at risk. In Italy, PrEP is paid out-of-pocket. Finally, Belgium set a co-payments system [123].
Pre-exposure prophylaxis (PrEP) is not a permanent preventive state but a temporally structured intervention whose effectiveness is limited in time. Individuals typically initiate PrEP during periods of perceived elevated risk of HIV exposure, such as changes in sexual behavior, partnership patterns, or substance use [57, 97]. Once initiated, PrEP provides a high level of protection against infection, conditional on adherence to the prescribed regimen. However, this protection is inherently finite, as it depends on continued drug intake and clinical follow-up. According to WHO guidelines, persons following PrEP are recommended to attend follow-up visits every three months. These visits include HIV testing, screening for STI and adherence counselling [121, 115, 159]. PrEP is highly dependent on adherence as missed doses quickly reduce effectiveness oppositely to vaccination. Unlike vaccination or permanent immunity, PrEP does not confer lasting protection beyond the period of use, and its preventive effect ceases shortly after discontinuation.

From an epidemiological standpoint, this finite duration implies that protection

cannot be treated as a permanent attribute of individuals. Instead, PrEP use defines time-limited protection episodes embedded within longer individual life histories [180]. As a result, the impact of PrEP at the population level depends not only on the proportion of individuals who ever initiate treatment, but also on the duration of protection and the timing of initiation relative to exposure risk [118]. These features already suggest that PrEP dynamics cannot be adequately represented by static preventive compartments.

Clinical follow-up and renewal

In most clinical settings, PrEP use is organized around discrete follow-up intervals, typically of three months, during which individuals undergo biological screening and clinical evaluation [121]. At each visit, HIV seronegativity is confirmed, potential side effects are assessed, and prescriptions are renewed for the subsequent interval. Continuation of PrEP is therefore conditional on successful completion of this follow-up process, introducing explicit decision points at which individuals may renew or discontinue treatment.

This clinical organization induces a renewal mechanism that is fundamentally discontinuous in time. Protection does not decay continuously but is reassessed and reauthorized at specific intervals, creating a structured sequence of protection windows. Consequently, the probability of remaining protected depends not only on current PrEP status but also on the time elapsed since initiation and the proximity to the next renewal event. Such renewal-driven dynamics differ qualitatively from standard continuous-time transition processes commonly assumed in compartmental models .

Cycling between susceptibility and protection

Due to changes in perceived risk, access to care, side effects, or social and structural constraints, individuals may repeatedly initiate and discontinue PrEP over time [180]. This leads to cycling behavior in which individuals alternate between periods of

susceptibility and periods of protection. Importantly, these cycles are not random fluctuations but are structured by clinical follow-up schedules and behavioral decision-making processes [121].
At the population level, this repeated entry and exit from the protected state generates time-dependent coverage patterns that directly influence transmission dynamics. The effectiveness of PrEP therefore depends not only on average coverage levels but also on the distribution of protection durations and the synchronization between protection windows and exposure risk. These considerations highlight the importance of explicitly representing transitions between susceptibility and protection over time, rather than aggregating them into average effects.

Modeling implications: time since initiation

Taken together, these features imply that PrEP induces a time-dependent protection mechanism governed by the elapsed time since initiation. The level and persistence of protection cannot be described solely by the current compartmental state of an individual, but depend on how long that individual has been under prophylaxis and whether renewal has occurred. Capturing such dynamics therefore requires models that explicitly track time since entry into the protected state.
Delay and age-structured formulations provide a natural and mechanistically consistent framework to represent these processes [12, 47, 60]. By embedding protection duration and renewal directly into the model structure, these approaches allow finite protection, renewal decisions, and protection loss to be represented explicitly. This modeling perspective forms the foundation of the mathematical frameworks developed in the remainder of this thesis and underpins the analysis of how temporally structured prevention reshapes HIV epidemic dynamics.

1.5 Political and economic impact

Beyond its clinical and epidemiological characteristics, the implementation of PrEP is strongly shaped by political and economic factors that influence access, uptake,

and continuity of use. Unlike vaccines or one-time interventions, PrEP requires sustained public investment, repeated clinical follow-up, and long-term engagement with healthcare systems. As a result, national and regional policies play a central role in determining who can access PrEP, under which conditions, and for how long protection is maintained [115, 157, 159, 167].

The cost of antiretroviral drugs, healthcare infrastructure constraints, and reimbursement policies directly affect PrEP availability and coverage [127]. In many settings, PrEP is fully subsidized and integrated into public health programs, whereas in others it remains partially reimbursed or restricted to specific populations. These differences lead to heterogeneous patterns of initiation and discontinuation across countries and risk groups, reflecting not only individual behavior but also structural and economic constraints [171]. Consequently, PrEP uptake is often uneven in time and across populations, reinforcing the need to account for nonuniform and temporally varying recruitment processes.

Political prioritization of HIV prevention further shapes PrEP deployment through eligibility criteria, awareness campaigns, and monitoring requirements [159]. Policy decisions regarding screening frequency, prescription renewal, and eligibility thresholds implicitly define the temporal structure of PrEP use, including the duration of protection windows and the conditions under which treatment is continued or discontinued [127]. These institutional design choices translate directly into model parameters governing recruitment, renewal, and protection duration.

From a modeling perspective, these political and economic dimensions do not act as external noise but as structural determinants of PrEP dynamics. They influence the rate at which individuals enter prevention programs, the persistence of protection over time, and the stability of coverage within high-risk populations. Incorporating temporally structured prevention into epidemiological models therefore provides a framework for exploring how policy-driven constraints interact with biological protection mechanisms to shape epidemic outcomes, without explicitly modeling political processes themselves.

1.6 Limitations of standard approaches for PrEP

Most compartmental models of HIV transmission represent prevention as an instantaneous transition from susceptibility to a protected class or as a permanent preventive state [138]. In such formulations, individuals are assumed to enter a protected compartment at a given rate and to remain there indefinitely or to leave it according to constant transition rates [10, 20, 28]. This representation is mathematically convenient and has been successfully used to model acute interventions or forms of permanent immunity, where protection does not depend on the duration spent in the protected state. In these settings, prevention can be treated as a static modification of transmission parameters.

These approaches rely on a memoryless, or Markovian, assumption, whereby the probability of leaving a compartment depends only on the current state of an individual and not on the time already spent in that state. While this assumption simplifies analysis and is appropriate for many epidemiological processes, it imposes a specific structure on prevention dynamics. In particular, it implies that protection does not age, expire, or require renewal, and that transitions occur continuously in time without reference to prior history. As a consequence, all individuals within a given compartment are treated as epidemiologically identical, regardless of how long they have been protected.

Biomedical prevention strategies such as pre-exposure prophylaxis fundamentally violate these assumptions. PrEP confers protection that is intrinsically time-limited and conditional on periodic clinical renewal [121]. The probability of remaining protected is therefore strongly dependent on the elapsed time since initiation and on whether a renewal event occurs at the end of a protection interval. Standard compartmental formulations cannot represent these features, as they lack the ability to encode protection duration or to distinguish individuals according to time since entry into the protected state. As a result, renewal and discontinuation processes are either ignored or approximated by constant transition rates, obscuring their temporal

structure.

This limitation has important consequences for the analysis of epidemic dynamics. By neglecting protection duration, standard models fail to capture how the timing of initiation and renewal influences epidemic thresholds, stability properties, and long-term behavior [8]. In contrast, modeling frameworks that explicitly track time since initiation allow finite protection, renewal decisions, and protection loss to be represented in a mechanistically consistent manner. Delay and age-structured formulations therefore provide a natural extension of classical compartmental models, enabling the study of temporally structured prevention strategies such as PrEP within a rigorous mathematical framework [15].

1.7 Temporally structured prevention and the role of delay

The finite duration of protection conferred by pre-exposure prophylaxis introduces an intrinsic time scale into the dynamics of HIV transmission. Unlike interventions that act instantaneously or confer permanent immunity, PrEP protection unfolds over a defined time window, during which individuals are protected only as long as treatment is maintained and renewed. This temporal dimension is not imposed externally but arises from the biological and clinical organization of PrEP use itself, making time since initiation a fundamental variable governing protection at the individual level.

In such a context, protection cannot be adequately represented by memoryless transitions. The level of protection experienced by an individual depends explicitly on the time elapsed since treatment initiation and on whether renewal occurs at the end of a protection interval. Two individuals classified as "protected" may therefore face markedly different risks depending on how long they have been under prophylaxis and how close they are to a renewal event. Standard compartmental models, which treat transitions as independent of prior history, are unable to capture these distinctions and consequently obscure the role of protection duration in shaping transmission

dynamics.

Capturing this dependence requires modeling frameworks that explicitly track time since entry into the protected state, rather than treating protection as an instantaneous or permanent attribute. Delay and age-structured formulations provide a natural and mechanistically consistent way to represent such [41, 78, 144]. By introducing an explicit temporal structure, these approaches allow renewal, discontinuation, and protection loss to be incorporated directly into the model dynamics, without resorting to ad hoc approximations or averaged transition rates. Importantly, delay-based models retain the compartmental structure while extending it to account for duration-dependent effects [145].

Embedding protection duration directly into the model structure enables a rigorous analysis of how temporally structured prevention reshapes epidemic behavior. In particular, these frameworks make it possible to investigate how finite-time protection influences epidemic thresholds, equilibrium stability, and long-term dynamics, and to identify conditions under which prevention may succeed or fail. This perspective forms the conceptual foundation of the mathematical models developed in this thesis, which aim to characterize the epidemiological impact of PrEP within a temporally explicit and analytically tractable framework.

1.8 Contributions

The main contribution of this work is the dynamic description of PrEP protected as a compartment structured by age. The protected population is structured by an age variable $a \in [0, \tau]$, representing the time elapsed since the last PrEP renewal or initiation. The density $p(t, a)$ denotes the number of individuals at time t who have been under PrEP for a duration a. Its dynamics are governed by the transport equation

$$\partial_t p(t, a) + \partial_a p(t, a) = -\mu p(t, a), \qquad 0 < a < \tau, \tag{1.1}$$

where μ is the natural mortality rate, assumed identical across compartments, reflecting the fact that neither HIV infection nor PrEP is assumed to directly affect mortality at the population scale considered. The chapters following on PrEP take interest into the description of the uptake mechanisms. We explore different scenarios. They are all based on the availabilities of ressources and effort that health insitutions may provide to bring treatment to population.

In chapter 2, we introduced a system of differential equations SI-type coupled with an age-structured partial differential equation representing persons protected by PrEP since initiation until the next STI screening and renewal decision. We consider the recruitment term for the PrEP compartment as Hill function type depending on the susceptible representing political and economic decisions taken depending on HIV exposed. We include the personal choice of continuation of the treatment at the end of protection period. We show that our model can be written as a nonlinear differential-difference system with discrete delay, the latter representing the full duration of the protection. This formulation allows a better tractability of the impact of the protection period induced by PrEP treatment. We derive positivity and uniqueness of solutions depending on initial conditions. When deriving the basic reproduction number, we note that it is a decreasing function of the delay. This indicates that the longer the protection the better the impact on the epidemic. This is not a surprising result at first sight but it is important to mention that large delay has tendency to destabilize system, which is not the case here.

We derive the classic stability threshold based on the reproduction number but nuanced by the dependance on the delay. In a second part of this chapter, we consider that recruitment is linear. By introducing an auxiliary differential-difference system and deriving a Lyapunov function, we show that the unique steady-state of the auxiliary system is globally asymptotically stable. Then, by comparaison principle we can establish that the disease-free equilibria of the initial system is globally asymptotically stable as well depending on the classic reproduction number threshold.

For the endemic equilibrium, we follow the same procedure and we obtain the global asymptotical stability. In a last part of this chapter, we fit our model using French data from PrEP initiation extracted from Truvada speadsheets. For more realistic

purpose, we assume that the recruitment is a coupled term depending on susceptibles through a Hill function and time through a logistic function. We realize numerical sismulations for two sets of population: general MSM population and MSM high risks population. We show that targeted intervention on specific population is much more effective than diluting the intervention in a larger population.

In chapter 3, we explore the risk perception that induces PrEP uptake. In that matter, we introduce a new recruitment rate not only depending on susceptibles but also on infected. Again this term is presented through a coupled term of linear or saturation functions. Through this formulation, we can investigate different scenarios with high prevalence but low access to PrEP. We carry the same transformation of the system into a differential-difference system with discrete delay. However, in order to generalize the study of the model, we analyze the original age-structured model. We derive the existence of the disease-free equilibrium and endemic equilibrium. The definition of the basic reproduction number slightly changes due to the coupling term depending on infected on the recruitment term for PrEP users. This term neutralizes the PrEP contribution and we can keep the definition of basic reproduction number. We then prove the global asymptotic stability of the disease-free equilibrium. We derive a persistence analysis of our model and show that we have strong persistence. Then, we divide the stability analysis of the endemic equilibrium in sub-regions where we are able to derive local stability depending on destabilisation by the delay. We prove for all but one subregion the local asymptotic stability. Following the method proposed by Fan et al. in [32], we provide numerical simulations exhibiting the non-feasibility of Hopf bifurcation occuring in the subregion latter aforementionned given specific sets of parameter Uncertainty remains about occurence of Hopf bifurcation induced by the delay. This seems unlikely based on monotone dynamical system theory.

In chapter 4, we investigate the impact of political and economic decision by supposing that the uptake rate of PrEP compartment is define by a non-monotonic function depending on the susceptible exclusively. This function represents three possible

situations: first, a increasing coverage targeted the most at risk popualtion like multi-partners, injectable drug users. Secondly, the coverage is maximal for the initial targeted population, mostly MSM Finally, the treatment is used by a bigger fraction of the population and a saturation effect decreases the uptake. PrEP is an expensive treatment and cannot be availlable for everyone. This change adds complexity in the analysis of the model. Up to three disease-free equilibrium can coexist. Each of them correspond to the forementionned scenarios. We derive existence conditions depending on the demography of the model. We define the basic reproduction number associated to each equilibrium. More importantly, we prove that the model admits a bistability situation: the low and high uptake equilibrium are locally asymptotically stable depending on the classic basic reproduction criteria but the maximal coverage one is always unstable.
Then, we derive existence condition for the unique endemic equilibrium of the model. We identify a maximal protection duration preventing the existence of the endemic equilibrium. Finally we derive a stability analysis of the endemic equilibrium and show that in the increasing uptake interval the endemic equilibrium is locally asymptotically stable .However, the rich dynamic of the maximal target equilibrium makes it difficult to derive clear criterion for the stability. We prove the existence of Hopf bifurcation occuring at a critical delay destabilizing the system. Persistent oscillations appear. Using implicit method we cannot clarify the stabilty situation.
Moerover, we identify hysteresis situation where we have coexistence of the three disease-free equilibria and the endemic equilibrium but the epidemic converge to one of the locally asymptotically stable equilibria.

In Chapter 5, we develop an agent-based model to study the impact of a potential vaccine on Chlamydia trachomatis (CT) epidemics and Pelvic Inflammatory Disease (PID) in the United States, for which CT is a primary cause. This approach extends previous works [33, 24, 154] by incorporating a dynamic relationship and sexual network.
Agents are stratified into distinct subpopulations to account for varying transmission risks, specifically focusing on heterosexual individuals, men who have sex with

men (MSM), and female sex workers (FSW). A rigorous three-step calibration and validation process is applied: (i) sexual network calibration using National Survey of Family Growth (NSFG) data, (ii) chlamydia prevalence calibration across age and sex using NHANES data, and (iii) all-cause PID calibration across age using NHANES data.

Simulations demonstrate that vaccines against CT infection may significantly reduce both CT cases and all-cause PID in the U.S. population. Various scenarios are evaluated involving different levels of vaccine coverage and efficacy. The results indicate that targeting younger individuals aged 15–24 years is more effective than achieving higher coverage in older adult populations. Furthermore, this modeling framework can be readily adapted to other sexually transmitted infections (STIs), as the underlying sexual network is disease-agnostic

Chapter 2

Forecasting the effect of Pre-Exposure Prophylaxis (PrEP) on HIV propagation with a system of differential-difference equations with delay

2.1 Introduction

Since its onset in the early eighties and its clear identification in 1983, Human Immunodeficiency Virus (HIV) and then Acquired Immune Deficiency Syndrome (AIDS) has still been one of the most deadly active worldwide epidemics. In the 2019 UNAIDS study, about 38 million persons lived with HIV, 1.7 million got infected and $690,000$ died of AIDS-related diseases becoming one of the most serious public health challenges [106].

It is well known now that this infection evolves in 3 stages: first a short acute phase where flu-like symptoms appear followed by a symptom free chronic phase that lasts

between 10 and 15 years. It eventually ends up with AIDS when the virus has killed enough TCD4 leading to a failure of the immune system [177]. Note here that the latency stage appears as one of the crucial problems. Indeed, the dormant period of the virus drastically delays HIV/AIDS-diagnosis if not detected and plays a major role in the epidemics spread (Figure 1, [45]). Despite extensive investigations, there is still no existing therapy that helps the organism to fully get rid of the virus.
However, since 1996, the AntiRetroviral Therapy, consisting in a combination of 3 (or more) antiretroviral agents taken daily appeared to reduce significantly the presence of the virus under a detectable threshold. Nowadays, not only efficient to avoid a fatal issue to the disease, AntiRetroviral Therapy allows also HIV infected individuals to stop spreading the disease. In 2019, 25.4 million of them successfully accessed antiretroviral therapy [106, 184]. In the late 2010's, the Pre-Exposure Prophylaxis (PrEP) was introduced as a new way of preventing HIV transmission. This successful treatment addresses HIV-free individuals showing a high risk of getting infected. PrEP consists in taking a combination of 2 antiretrovirals in two different protocols: either on a daily basis (continuous treatment) or on demand (discrete treatment) that is just at least 2 hours before and 2 days after sexual intercourse. Every 3 months, continuous PrEP users need to get a global STI (Sexually Transmitted Infections) screening in order to get a prescription for another 3 months [**hivgov_symptoms**, 106]. Theoretically, they can stop anytime, but they are practically more likely to choose at the end of each quarter. We remind here that PrEP is preventive and does not cure HIV. However, it effectively reduces HIV transmission [106].
Our objective here is to design a new model to mathematically forecast the influence of PrEP users among high risk profiles on the epidemic. The application of our study focuses only on the French population, where PrEP has been used since 2016, and is currently followed by an average of $20,000$ individuals [92]. In the past decades, many epidemiological models have been describing HIV dynamics. Some of them used the standard $SICA$ (Susceptible (S) - Infected (I) - Infected under AntiRetroviral Therapy (C) with low viral charge - Infected with AIDS symptom (A)) ([76] for instance) and for a good review we suggest [36] and [58].
This is only in the past years that new models including a PrEP user compartment

appeared and started to keep our attention. A good example is the preliminary work [53] where the authors suggested vaccination approach which could be seen as the precursor of PrEP. Their numerical simulations showed that the epidemic spread could be controlled thanks to vaccination, even if the basic reproduction number remains above 1. In [81, 83], an explicit PrEP compartment was included into the $SICA$ model. Parameters in [83] were adjusted with clinical data and PrEP effectiveness mathematically proven. In [77], the authors divided the PrEP compartment according to the adherence of users to the treatment. They showed that with at least 70% of PrEP users in the male homosexual population, the HIV epidemic could be effectively controlled. Finally, in [82], PrEP was combined with screening and the result was compared to Portuguese data showing that these two processes appeared necessary to fight control the HIV epidemic.

In our paper, we introduce a new approach with a SIP (Susceptible - Infected - Protected) model. Inspired by [83] and [95], it includes an age structure on the PrEP (protected) compartment, corresponding to the time spent after the onset of the new 3 month treatment period. Once the term reached, the user chooses either to keep on taking the PrEP or to stop it, becoming susceptible again. On the other side, individuals of the S compartment may decide to start or resume this preventing process and hence reach the P population.

Our goal is to propose a more accurate model than [83], still possible to handle analytically, by considering a more complex susceptible interaction $F(t, S)$ depending both on time t (through a function ψ) and the total S population (through a function f that can be seen as political or economic decision taken depending on the size of HIV exposed (see Section 2.2 for details). After standard modifications, we prove in Section 2.2 that our new model can be written as a nonlinear differential-difference system with discrete delay. As presented below in Section 2.3 and Section 2.4, the stability analysis is then possible when the ψ term is constant. However, since it may take a while to convince a population set to start PrEP, it appears natural to us that ψ may follow a logistic equation. The model becomes then too challenging to be investigated in an analytical way, and thus numerical simulations numerically take over this work in Section 2.5. Thanks to this new assumption, we show eventually

that it is possible to fit the data with realistic values. Before this, we proceed to its well-posedness and stability study and investigate the constant and non constant joining PrEP rate subcases in Section 2.3 and Section 2.4. Then, we compare our theoretical work to official clinical French data in order to understand the role taken by PrEP dynamics on the HIV/AIDS epidemic in Section 2.5. With some numerical simulations, we observe that, by choosing a logistic equation for the non linear joining PrEP rate and a Hill function for the dynamics of $f(S)$, we perfectly fit our data.

2.2 Introducing our model

In order to keep the model as simple as possible, we consider only three compartments: Susceptible (S), individuals that may be infected by the HIV; Infected (I) and Protected (P), individuals under PrEP treatment (see Figure 2.1). The total population is

$$N(t) = S(t) + I(t) + P(t).$$

To take into account the limited protection duration offered by PrEP, we structure the compartment of protected individuals in age. Here, age a corresponds to the time since the last test and the renewal of PrEP treatment. The maximum duration of the protection period is generally three months, $\tau = 3$ months. Therefore, $a \in [0, \tau]$. If an individual decides to renew the treatment, the age a is reset to zero.
We denote by $p(t, a)$ the population under PrEP at time t who started their new treatment period a days ago. Thus, the total population of PrEP users at time t is

$$P(t) = \int_0^\tau p(t, a)da.$$

The model is designed taking into account the input and output rates of each compartment with appropriate parameters (see Figure 2.1). At each time t, there is a constant number of individuals (source term σ) who become susceptible by reaching

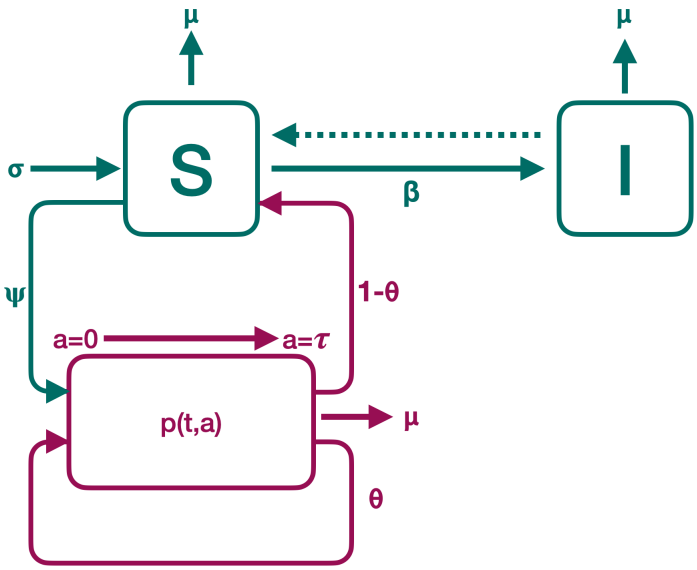


Figure 2.1: Schematic representation of the compartmental model (2.1). Continuous arrows represent movements between the compartments. Dashed ones represents the transmission of the infection.

the age of sexual consent, becoming single again, or deciding to start new intercourse experiences. At the same time, some susceptible individuals become infected with HIV at a rate β. A part,

$$F(t, S(t)) = \psi(t) f(S(t)),$$

of susceptible individuals decide to start PrEP. The choice of functions f and ψ allows us to consider many scenarios. The function f is an increasing function of the total population of susceptible individuals with $f(0) = 0$. Examples could be

$$f(S) = S^n \quad \text{or} \quad f(S) = \frac{S^n}{1 + S^n}, \quad n \geq 1.$$

The first choice is well adapted to rich countries or countries with a low number of susceptible individuals (the proposed treatment, for example the case $f(S) = S$, $n = 1$, is proportional to the total population of susceptible individuals).

The second choice is better adapted to poor countries or countries with a large number of susceptible individuals, which for budgetary reasons cannot increase the treatment indefinitely. The fact that the function ψ is time-dependent is dictated by the data we wish to use on PrEP, which began in 2016 in France and continues to increase. For cost reasons, this PrEP prescription rate will eventually reach a maximum threshold. A well-fitting example of function ψ is

$$\psi(t) = \psi_0 + \frac{\kappa_1 t^m}{t^m + \kappa_2}, \quad m \geq 1,\ \kappa_1,\ \kappa_2 > 0.$$

For the analytical study of the model, we assume that this threshold has already been reached and therefore consider

$$\psi \equiv K := \psi_0 + \kappa_1$$

to be a constant. We can also choose $t \mapsto \psi(t)$ as a solution of logistic equation with K as the carrying capacity. Finally, we suppose that the disease and treatment do not affect mortality (death rate μ is consequently the same for all). The system satisfied by S and I is then given, for all $t > 0$, by

$$\begin{cases} S'(t) &= \sigma - \beta I(t)S(t) - \mu S(t) - Kf(S(t)) + (1-\theta)p(t,\tau), \\ I'(t) &= \beta I(t)S(t) - \mu I(t). \end{cases} \tag{2.1}$$

The density p satisfies, for $t > 0$, the following age-structured partial differential equation

$$\begin{cases} \dfrac{\partial p}{\partial t}(t,a) + \dfrac{\partial p}{\partial a}(t,a) = -\mu p(t,a), \quad 0 < a < \tau, \\ p(t,0) = Kf(S(t)) + \theta p(t,\tau). \end{cases} \tag{2.2}$$

We remind here that $a \in [0,\tau]$ is the time elapsed from the new period of time under treatment. If an individual decides to renew the treatment, the age a is reset to zero.

We denote by $p(t,a)$ the population under PrEP at time t who started their new treatment period a days ago. The initial condition is given by

$$S(0) = S_0, \quad I(0) = I_0 \quad \text{and} \quad p(0,a) = p_0(a), \quad 0 < a < \tau.$$

The boundary condition

$$p(t,0) = Kf(S(t)) + \theta p(t,\tau),$$

represents individuals who renewed their PrEP, $\theta p(t,\tau)$, or those who started it, $Kf(S(t))$.
Using the characteristics method and the boundary condition from (2.2), see [4], we obtain, for $t > 0$ and $a \in [0,\tau]$,

$$p(t,a) = \begin{cases} e^{-\mu a} p(t-a,0), & t > a, \\ e^{-\mu t} p(0,a-t) = e^{-\mu t} p_0(a-t), & 0 \le t \le a. \end{cases} \tag{2.3}$$

To write the equation (2.3) in a convenient form, we suppose that the initial condition p_0 is continuous on $[0,\tau]$ and satisfies the compatibility condition

$$p_0(0) = Kf(S_0) + \theta p_0(\tau).$$

We put

$$\varphi(t) := e^{-\mu t} p_0(-t), \quad -\tau \le t \le 0,$$

and we define the function

$$u(t) := p(t,0), \quad t \ge 0.$$

We then get from (2.3), the expression

$$p(t,\tau) = e^{-\mu\tau}\begin{cases} u(t-\tau), & t > \tau, \\ \varphi(t-\tau), & 0 \leq t \leq \tau. \end{cases}$$

This means that we can extend the function u to the interval $[-\tau, 0]$, by putting $u(t) = \varphi(t)$ for $t \in [-\tau, 0]$. Then, we have directly $p(t,\tau) = e^{-\mu\tau}u(t-\tau)$, for all $t \geq 0$. Consequently, using the boundary condition of the system (2.2), u satisfies the difference equation

$$u(t) = \begin{cases} Kf(S(t)) + \theta e^{-\mu\tau}u(t-\tau), & t > 0, \\ \varphi(t), & -\tau \leq t \leq 0. \end{cases}$$

Furthermore, the total population $P(t)$ can be explicitly expressed, for $t \geq 0$, in terms of the function u

$$P(t) = \int_0^\tau e^{-\mu a}u(t-a)da = e^{-\mu t}\int_{t-\tau}^t e^{\mu a}u(a)da.$$

Thus, we get the complete model, for $t > 0$,

$$\begin{cases} S'(t) &= \sigma - \beta I(t)S(t) - \mu S(t) - Kf(S(t)) + (1-\theta)e^{-\mu\tau}u(t-\tau), \\ I'(t) &= \beta I(t)S(t) - \mu I(t), \\ u(t) &= Kf(S(t)) + \theta e^{-\mu\tau}u(t-\tau), \end{cases} \tag{2.4}$$

with the initial condition

$$S(0) = S_0, \quad I(0) = I_0 \quad \text{and} \quad u(t) = \varphi(t), \quad t \in [-\tau, 0]. \tag{2.5}$$

Knowing that $P(t) = e^{-\mu t}\int_{t-\tau}^{t} e^{\mu a}u(a)da$, we get

$$P'(t) = -\mu P(t) + Kf(S(t)) - (1-\theta)e^{-\mu\tau}u(t-\tau).$$

We then have

$$N'(t) = S'(t) + I'(t) + P'(t) = \sigma - \mu N(t).$$

We easily get

$$N(t) = \left(N_0 - \frac{\sigma}{\mu}\right)e^{-\mu t} + \frac{\sigma}{\mu} \to \frac{\sigma}{\mu}, \text{ as } t \to +\infty. \tag{2.6}$$

2.3 Mathematical analysis

In this section, we discuss the wellposedness of the model, steady-states, basic reproduction number and local asymptotic stability.

2.3.1 Wellposedness of the model

The problem (2.4)-(2.5) is a coupled system of nonlinear differential and difference equations with discrete delay. We directly derive the following proposition about the wellposedness of the model.

Proposition 2.1. *For any nonnegative initial condition (S_0, I_0, φ), where φ is a nonnegative continuous function on $[-\tau, 0]$, there exists a unique nonnegative solution to Problem (2.4)-(2.5) defined on $[0, +\infty)$. Moreover, this solution is uniformly bounded on $[0, +\infty)$.*

Proof. We first solve the system (2.4)-(2.5) on the interval $[0, \tau]$. In this case, since u is completely defined, the Cauchy-Lipschitz theorem gives the existence and uniqueness of the solution on $[0, \tau]$ and this solution is nonnegative. Then, we repeat this method on each interval of type $[k\tau, (k+1)\tau]$ with $k \in \mathbb{N}$. Thus, we get a unique

nonnegative solution on the interval $[0, +\infty)$. Furthermore, using (2.6) and the fact that $S(t) + I(t) + u(t) \leq S(t) + I(t) + P(t) = N(t)$, we deduce that (S, I, u) is uniformly bounded on $[0, +\infty)$. □

2.3.2 Steady-states and basic reproduction number

In this subsection, we compute the steady-states of the system and study their local asymptotic stability. Let us consider a steady-state (S^*, I^*, u^*) of (2.4). We then have

$$\begin{cases} 0 &= \sigma - \beta I^* S^* - \mu S^* - K f(S^*) + (1-\theta) e^{-\mu\tau} u^*, \\ 0 &= (\beta S^* - \mu) I^*, \\ u^* &= K f(S^*) + \theta e^{-\mu\tau} u^*. \end{cases} \tag{2.7}$$

The third equation of the system (2.7) leads to

$$u^* = \frac{K f(S^*)}{1 - \theta e^{-\mu\tau}}.$$

Remark that as $\theta \in (0, 1)$, we always have $1 - \theta e^{-\mu\tau} > 0$.

Assume that $I^* = 0$. Then, the first equation of (2.7) implies that S^* satisfies the equation

$$\Phi(S^*) := S^* + \frac{K(1 - e^{-\mu\tau})}{\mu(1 - \theta e^{-\mu\tau})} f(S^*) = \frac{\sigma}{\mu}. \tag{2.8}$$

Since Φ is increasing, tends to infinity and satisfies $\Phi(0) = 0$, we get the existence of a unique S^* such that $\Phi(S^*) = \sigma/\mu$. We can therefore write $S^* = \Phi^{-1}(\sigma/\mu)$. Thus, we obtain the disease free steady-state

$$(S^*, I^*, u^*) = \left(\Phi^{-1}(\sigma/\mu) \ , \ 0 \ , \ \frac{K f(\Phi^{-1}(\sigma/\mu))}{1 - \theta e^{-\tau\mu}} \right). \tag{2.9}$$

Now suppose that $S^* = \mu/\beta$. We immediately obtain that

$$u^* = \frac{Kf(\mu/\beta)}{1 - \theta e^{-\mu\tau}}.$$

We inject these two last expressions into the first equation of (2.7) to obtain

$$I^* = \frac{\sigma}{\mu} - \Phi\left(\frac{\mu}{\beta}\right),$$

where the function Φ is given by the expression (2.8). Then, $I^* > 0$ exists if and only if

$$\Phi^{-1}\left(\frac{\sigma}{\mu}\right) > \frac{\mu}{\beta}.$$

Let us define the basic reproduction number $\mathcal{R}_0$ as a threshold for the existence of the endemic steady-state

$$\mathcal{R}_0 := \frac{\beta}{\mu}\Phi^{-1}\left(\frac{\sigma}{\mu}\right).$$

Hence, we get the existence of a unique endemic steady-sate

$$(S^*, I^*, u^*) = \left(\frac{\mu}{\beta}\,,\ \frac{\sigma}{\mu} - \Phi\left(\frac{\mu}{\beta}\right)\,,\ \frac{Kf(\mu/\beta)}{1 - \theta e^{-\mu\tau}}\right) \tag{2.10}$$

if and only if

$$\mathcal{R}_0 > 1.$$

We will need to know the variation of $\mathcal{R}_0$ as a function of $\tau \in [0, +\infty)$. We have the following lemma.

Lemma 2.1. *The basic reproduction number $\mathcal{R}_0 : \tau \in [0, +\infty) \mapsto \mathcal{R}_0(\tau)$ is a decreasing function such that*

$$\mathcal{R}_0(0) = \frac{\beta\sigma}{\mu^2} \quad \textit{and} \quad \mathcal{R}_0(\infty) = \frac{\beta}{\mu}\Phi_\infty^{-1}\left(\frac{\sigma}{\mu}\right),$$

with

$$\Phi_\infty(S) := S + \frac{K}{\mu} f(S).$$

Proof. Consider the dependence of the function Φ on τ by putting

$$\Phi(S,\tau) := S + \frac{K(1-e^{-\mu\tau})}{\mu(1-\theta e^{-\mu\tau})} f(S).$$

We want to study the variation of $\tau \mapsto \mathcal{R}_0(\tau) = \dfrac{\beta}{\mu}\Phi^{-1}\left(\dfrac{\sigma}{\mu},\tau\right)$. Then, we set $S(\tau) := \Phi^{-1}(\sigma/\mu,\tau)$. In fact, we have $\Phi(S(\tau),\tau) = \sigma/\mu$. By differentiating, we deduce that

$$\frac{\partial\Phi}{\partial S}(S(\tau),\tau)\frac{d}{d\tau}S(\tau) + \frac{\partial\Phi}{\partial\tau}(S(\tau),\tau) = 0.$$

Thus, we get

$$\frac{d}{d\tau}\mathcal{R}_0(\tau) = \frac{\beta}{\mu}\frac{d}{d\tau}S(\tau) = -\frac{\beta}{\mu}\frac{\frac{\partial\Phi}{\partial\tau}(S(\tau),\tau)}{\frac{\partial\Phi}{\partial S}(S(\tau),\tau)} < 0.$$

Then, the function $\tau \mapsto \mathcal{R}_0(\tau)$ is decreasing on $[0,+\infty)$. Furthermore, by taking $\tau = 0$ and $\tau \to +\infty$ in the equality

$$\Phi(S,\tau) := S(\tau) + \frac{K(1-e^{-\mu\tau})}{\mu(1-\theta e^{-\mu\tau})} f(S(\tau)) = \frac{\sigma}{\mu},$$

we get that

$$\mathcal{R}_0(0) = \frac{\beta\sigma}{\mu^2} \quad \text{and} \quad \mathcal{R}_0(\infty) = \frac{\beta}{\mu}\Phi_\infty^{-1}\left(\frac{\sigma}{\mu}\right),$$

with

$$\Phi_\infty(S) := S + \frac{K}{\mu} f(S).$$

□

We conclude from Lemma 2.1 that $\mathcal{R}_0(\infty) < \mathcal{R}_0(\tau) < \mathcal{R}_0(0)$, for all $\tau \in (0, +\infty)$, and we immediately obtain the following result.

Proposition 2.2. *Suppose that $\tau \geq 0$. Then, we have three cases:*

- *If $\mathcal{R}_0(0) < 1$, then we have $\mathcal{R}_0(\tau) < 1$, for all $\tau \geq 0$.*
- *If $\mathcal{R}_0(\infty) > 1$, then we have $\mathcal{R}_0(\tau) > 1$, for all $\tau \geq 0$.*
- *If $\mathcal{R}_0(0) > 1$ and $\mathcal{R}_0(\infty) < 1$, then there exists a unique $\bar{\tau} > 0$ such that $\mathcal{R}_0(\tau) > 1$ for $0 \leq \tau < \bar{\tau}$ and $\mathcal{R}_0(\tau) < 1$ for $\tau > \bar{\tau}$, with $\mathcal{R}_0(\bar{\tau}) = 1$.*

We linearize System (2.4) around any equilibrium (S^*, I^*, u^*) and we get

$$\begin{cases} S'(t) &= -\beta I^* S(t) - \beta S^* I(t) - \mu S(t) - K f'(S^*) S(t) + (1-\theta) e^{-\mu\tau} u(t-\tau), \\ I'(t) &= \beta I^* S(t) + \beta S^* I(t) - \mu I(t), \\ u(t) &= K f'(S^*) S(t) + \theta e^{-\mu\tau} u(t-\tau). \end{cases}$$

We look for solutions of the form $S(t) = e^{-\lambda t} S_0$, $I(t) = e^{-\lambda t} I_0$ and $u(t) = e^{-\lambda t} u_0$, $t > 0$ and $\lambda \in \mathbb{C}$. Then, we obtain the following characteristic equation

$$\Delta(\lambda, \tau) := \begin{vmatrix} \lambda + \beta I^* + \mu + K f'(S^*) & \beta S^* & -(1-\theta) e^{-\mu\tau} e^{-\lambda\tau} \\ -\beta I^* & \lambda - \beta S^* + \mu & 0 \\ -K f'(S^*) & 0 & 1 - \theta e^{-\mu\tau} e^{-\lambda\tau} \end{vmatrix} = 0.$$

We develop the determinant and obtain

$$\begin{aligned} \Delta(\tau, \lambda) &= (\lambda - \beta S^* + \mu) \left[(\lambda + \mu)(1 - \theta e^{-\mu\tau} e^{-\lambda\tau}) + K f'(S^*)(1 - e^{-\mu\tau} e^{-\lambda\tau}) \right] \\ &\quad + (\lambda + \mu) \beta I^* (1 - \theta e^{-\mu\tau} e^{-\lambda\tau}), \\ &= 0. \end{aligned}$$

First, consider the disease-free equilibrium (2.9). Then, the characteristic equation becomes

$$[\lambda - \mu(\mathcal{R}_0 - 1)] \left[(\lambda + \mu)(1 - \theta e^{-\mu\tau} e^{-\lambda\tau}) + K f'\left(\Phi^{-1}\left(\sigma/\mu\right)\right)\left(1 - e^{-\mu\tau} e^{-\lambda\tau}\right)\right] = 0.$$

We have an immediate real eigenvalue

$$\lambda_0 = \mu(\mathcal{R}_0 - 1).$$

The other eigenvalues are solutions of the transcendental equation

$$\bar{\Delta}(\lambda) := P(\lambda) - Q(\lambda) e^{-\lambda\tau} = 0, \tag{2.11}$$

with

$$P(\lambda) := \lambda + \mu + K f'(\Phi^{-1}(\sigma/\mu)) \quad \text{and} \quad Q(\lambda) := e^{-\mu\tau}[\theta\lambda + \theta\mu + K f'(\Phi^{-1}(\sigma/\mu))].$$

We have the following properties.

Proposition 2.3. *(i) The equation* (2.11) *has no purely imaginary root.*

(ii) There exists $A > 0$ such that every roots λ of 2.3.2 with $|\lambda| > A$ has a negative real part.

Proof. (i) First, we seek for pure imaginary roots $\lambda = \pm i\omega$, $\omega > 0$, of (2.11). Splitting in (2.11) the real and the imaginary part, we obtain

$$\begin{cases} \gamma \cos(\omega\tau) e^{-\mu\tau} + \theta\omega \sin(\omega\tau) e^{-\mu\tau} &= \mu + K f'(\Phi^{-1}(\sigma/\mu)), \\ -\theta\omega \cos(\omega\tau) e^{-\mu\tau} + \gamma \sin(\omega\tau) e^{-\mu\tau} &= -\omega, \end{cases}$$

where $\gamma := \theta\mu + Kf'(\Phi^{-1}(\sigma/\mu))$. Solving this system, we find that

$$\begin{cases} \cos(\omega\tau) &= \dfrac{1}{(\theta^2\omega^2+\gamma^2)e^{-\mu\tau}}\left[\theta\omega^2+\gamma(\mu+Kf'(\Phi^{-1}(\sigma/\mu))\right], \\ \sin(\omega\tau) &= \dfrac{1}{(\theta^2\omega^2+\gamma^2)e^{-\mu\tau}}\left[-\omega\gamma+\theta\omega(\mu+Kf'(\Phi^{-1}(\sigma/\mu))\right]. \end{cases}$$

Using the trigonometric identity $\cos^2(\omega\tau)+\sin^2(\omega\tau)=1$, we get that ω satisfies

$$(\theta^2\omega^2+\gamma^2)(e^{-\mu\tau})^2 = \omega^2 + (\mu + Kf'(\Phi^{-1}(\sigma/\mu)))^2.$$

Then, we obtain

$$\omega^2 = \frac{\left[\gamma e^{-\mu\tau} - \left(\mu + Kf'\left(\Phi^{-1}\left(\frac{\sigma}{\mu}\right)\right)\right)\right]\left[\left(\mu + Kf'\left(\Phi^{-1}\left(\frac{\sigma}{\mu}\right)\right)\right) + \gamma e^{-\mu\tau}\right]}{1-\theta^2 e^{-2\mu\tau}}. \tag{2.12}$$

Notice that $1-\theta^2e^{-2\mu\tau} > 0$ and

$$\gamma e^{-\mu\tau} - (\mu + Kf'(\Phi^{-1}(\sigma/\mu))) = [\theta\mu + Kf'(\Phi^{-1}(\sigma/\mu))]e^{-\mu\tau} - [\mu + Kf'(\Phi^{-1}(\sigma/\mu))] < 0.$$

Thus the right-hand side of (2.12) is negative which is absurd. We conclude that the equation (2.11) has no purely imaginary root.
(ii) As the function $\bar{\Delta}$ is entire, the set of its roots has no accumulation points in $\mathbb{C}$.

Let us analyze the asymptotic behavior of the roots for large moduli. For any non-zero root λ, the characteristic equation $\bar{\Delta}(\lambda)=0$ can be rewritten as:

$$e^{\lambda\tau}\left(\frac{P(\lambda)}{\lambda}\right) - \frac{Q(\lambda)}{\lambda} = 0.$$

Since P and Q are polynomials, we have the limits:

$$\lim_{|\lambda|\to+\infty}\frac{P(\lambda)}{\lambda} = 1 \quad \text{and} \quad \lim_{|\lambda|\to+\infty}\frac{Q(\lambda)}{\lambda} = \theta e^{-\mu\tau}.$$

Therefore, for roots λ with arbitrarily large modulus ($|\lambda| \to +\infty$), the characteristic equation is asymptotic to the reference equation:

$$e^{\lambda\tau} - \theta e^{-\mu\tau} = 0.$$

The roots of this asymptotic equation are given by the complex numbers:

$$\bar{\lambda}_p = \frac{1}{\tau}\ln(\theta) - \mu + \frac{2p\pi}{\tau}i, \quad p \in \mathbb{Z}.$$

Since $\theta \in (0,1)$, we have $\ln(\theta) < 0$. It follows that the real part of these asymptotic roots is strictly negative, bounded away from zero by:

$$\mathcal{R}e(\bar{\lambda}_p) = \frac{1}{\tau}\ln(\theta) - \mu < 0.$$

By the continuous dependence of roots on the parameters for large moduli, the roots λ of the original equation approach the roots $\bar{\lambda}_p$ as $|\lambda| \to +\infty$. Thus, $\lim_{|\lambda|\to+\infty} \mathcal{R}e(\lambda) = \frac{1}{\tau}\ln(\theta) - \mu < 0$.

Consequently, there exists a constant $A > 0$ such that every root λ satisfying $|\lambda| > A$ has a strictly negative real part.

□

We state the stability of the disease-free equilibrium (2.9).

Corollary 1. *(i) Suppose that there exists $\tau_0 \geq 0$ such that $\mathcal{R}_0(\tau_0) > 1$. Then, the disease-free equilibrium (2.9) is unstable for $\tau = \tau_0$.*

(ii) Suppose that there exists $\tau_1 \geq 0$ such that $\mathcal{R}_0(\tau_1) < 1$ and the disease-free equilibrium (2.9) is locally asymptotically stable for $\tau = \tau_1$. Then, it is locally asymptotically stable for all $\tau \geq \tau_1$.

(iii) Suppose that $\mathcal{R}_0(0) < 1$. Then, the disease-free equilibrium (2.9) is locally asymptotically stable for all $\tau \geq 0$.

Proof. (i) The real eigenvalue

$$\lambda_0 = \mu(\mathcal{R}_0(\tau_0) - 1)$$

is positive because $\mathcal{R}_0(\tau_0) > 1$. Then, the disease-free equilibrium (2.9) is unstable for $\tau = \tau_0$.
(ii) Suppose that there exits $\tau_1 \geq 0$ such that $\mathcal{R}_0(\tau_1) < 1$ and the disease-free equilibrium (2.9) is locally asymptotically stable for $\tau = \tau_1$. As $\tau \mapsto \mathcal{R}_0(\tau)$ is decreasing, we have $\mathcal{R}_0(\tau) < 1$ for all $\tau \geq \tau_1$. Then, the real eigenvalue λ_0 is negative for all $\tau \geq \tau_1$. The other eigenvalues given by

$$\bar{\Delta}(\tau, \lambda) := P(\tau, \lambda) - Q(\tau, \lambda)e^{-\lambda\tau} = 0,$$

with

$$P(\tau, \lambda) := \lambda + \mu + Kf'(\Phi^{-1}(\sigma/\mu)) \quad \text{and} \quad Q(\tau, \lambda) := e^{-\mu\tau}[\theta\lambda + \theta\mu + Kf'(\Phi^{-1}(\sigma/\mu))],$$

cannot cross the imaginary axis when we increase τ starting from τ_1. The disease-free equilibrium (2.9) thus keeps the same stability as for $\tau = \tau_1$, i.e. it remains locally asymptotically stable for all $\tau \leq \tau_1$.

(iii) Let us consider the case $\tau = 0$. Then, the equation (2.11) becomes

$$(\lambda + \mu)(1 - \theta) = 0.$$

This means that $\lambda = -\mu < 0$. Then, the disease-free equilibrium (2.9) is locally asymptotically stable for $\tau = 0$. We use the previous property, *(ii)*, to conclude that the disease-free equilibrium (2.9) is locally asymptotically stable for all $\tau \geq 0$.
One can prove this corollary directly by proving that Equation (2.11) has no root with a non-negative real part and therefore the stability of the endemic equilibrium is determined by the sign of $\mathcal{R}_0 - 1$. Indeed, let us suppose by contradiction the

existence of such a root $\lambda = \alpha + i\omega$, with $\alpha \geq 0$. Then, we obtain

$$\frac{|P(\alpha + i\omega)|}{|Q(\alpha + i\omega)|} = e^{-\alpha\tau} \leq 1.$$

This gives the following inequality

$$[P(\alpha) - Q(\alpha)]\,[P(\alpha) + Q(\alpha)] + \left(1 - e^{-2\mu\tau}\theta^2\right)\omega^2 \leq 0,$$

with

$$P(\alpha) - Q(\alpha) = (1 - e^{-\mu\tau}\theta)(\alpha + \mu) + (1 - e^{-\mu\tau})Kf'(\Phi^{-1}(\sigma/\mu)) > 0.$$

This leads to a contradiction. □

Now we focus on the endemic equilibrium (2.10)

$$(S^*, I^*, u^*) = \left(\frac{\mu}{\beta}\ ,\ \frac{\sigma}{\mu} - \Phi\left(\frac{\mu}{\beta}\right)\ ,\ \frac{Kf(\mu/\beta)}{1 - \theta e^{-\mu\tau}}\right).$$

Proposition 2.4. *Suppose that $\mathcal{R}_0(0) > 1$. Then, for all $\tau \geq 0$ such that $\mathcal{R}_0(\tau) > 1$, the endemic steady-state is locally asymptotically stable.*

Proof. We suppose that $\mathcal{R}_0(\tau) > 1$ and we consider the endemic equilibrium. The characteristic equation becomes

$$\Delta(\tau, \lambda) := \lambda^2 + A\lambda + \mu\beta I^* - e^{-\mu\tau}e^{-\lambda\tau}\left[\theta\lambda^2 + (\theta A + Kf'(S^*))\lambda + \theta\mu\beta I^*\right] = 0, \tag{2.13}$$

with $A := \mu + \beta I^* > 0$. We follow the same steps as in the proof of the stability of the disease-free equilibrium. First, we consider the case $\tau = 0$. Then, the endemic

steady-state becomes

$$(S^*, I^*, u^*) = \left(\frac{\mu}{\beta} \, , \, \frac{\sigma}{\mu} - \frac{\mu}{\beta} \, , \, \frac{Kf(\mu/\beta)}{1-\theta} \right),$$

with $\mathcal{R}_0(0) = \beta\sigma/\mu^2$ and the characteristic equation is reduced to

$$\Delta(\lambda, \tau) := (1-\theta) \begin{vmatrix} \lambda + \beta I^* + \mu & \beta S^* \\ -\beta I^* & \lambda - \beta S^* + \mu \end{vmatrix} = 0.$$

We obtain two eigenvalues $\lambda_1 = -\mu < 0$ and $\lambda_2 = -\mu - \beta(I^* - S^*) = -\mu(\mathcal{R}_0(0) - 1) < 0$.

Hence, the endemic steady-state is locally asymptotically stable for $\tau = 0$. We then look for pure imaginary roots $\lambda = \pm i\omega$, $\omega > 0$. Then, splitting the real and imaginary parts in (2.13), we have the following system

$$\begin{cases} \omega\Gamma\cos(\omega\tau)e^{-\mu\tau} + \rho_\omega \sin(\omega\tau)e^{-\mu\tau} &= \omega(A + \psi f'(\mu/\beta)), \\ \rho_\omega \cos(\omega\tau)e^{-\mu\tau} - \omega\Gamma\sin(\omega\tau)e^{-\mu\tau} &= \omega^2 - \mu\beta I^*, \end{cases}$$

with $\rho_\omega := (\omega^2 - \mu\beta I^*)\theta e^{-\mu\tau}$ and $\Gamma = (\theta A + \psi f'(\mu/\beta))e^{-\mu\tau}$. Using the identity $\cos^2(\omega\tau) + \sin^2(\omega\tau) = 1$, we obtain the polynomial equation in ω

$$\begin{aligned} [1 - (\theta e^{-\mu\tau})^2]\omega^4 + [2\mu\beta I^*(\theta e^{-\mu\tau})^2 - 2\mu\beta I^* + (A + \psi f'(\mu/\beta))^2 - \Gamma^2]\omega^2 & \\ + (\mu\beta I^*)^2(1 - (\theta e^{-\mu\tau})^2) &= 0. \end{aligned}$$

Let us set

$$N := \frac{1}{1 - (\theta e^{-\mu\tau})^2}[2\mu\beta I^*(\theta e^{-\mu\tau})^2 - 2\mu\beta I^* + (A + \psi f'(\mu/\beta))^2 - \Gamma^2] \quad \text{and} \quad X := \omega^2.$$

Then, we get the following polynomial

$$X^2 + NX + (\mu\beta I^*)^2 = 0. \tag{2.14}$$

First, if $N > 0$, then the Routh-Hurwitz criterion implies that all roots of (2.14) have negative real part. This leads to a contradiction.
Suppose now that $N \leq 0$. We compute the discriminant of the equation (2.14) to obtain

$$\Delta = N^2 - 4(\mu\beta I^*)^2 = (N + 2\mu\beta I^*)(N - 2\mu\beta I^*).$$

As we suppose that $N \leq 0$, we have that $N - \mu\beta I^* < 0$. On the other hand, we have that

$$(1 - (\theta e^{-\mu\tau})^2)(N + 2\mu\beta I^*) = (A + Kf'(\mu/\beta))^2 - \Gamma^2.$$

But, as $\theta < 1$ and $e^{-\mu\tau} < 1$, we obtain

$$\Gamma^2 = [(\theta A + Kf'(\mu/\beta))e^{-\mu\tau}]^2 < (A + Kf'(\mu/\beta))^2.$$

We conclude that $\Delta < 0$. So there is no positive real root of (2.14) and $\omega > 0$ cannot exist.
Furthermore, as for the disease-free equilibrium, if Δ has infinitely many different zeros, $\lambda_n \in \mathbb{C}$, $n \in \mathbb{N}$, then

$$\lim_{n\to+\infty} |\lambda_n| = +\infty.$$

The sequence λ_n, $n \in \mathbb{N}$, satisfies

$$e^{\lambda_n\tau}\left(\frac{P(\lambda_n)}{\lambda_n^2}\right) - \frac{Q(\lambda_n)}{\lambda_n^2} = 0,$$

with

$$P(\lambda) := \lambda^2 + A\lambda + \mu\beta I^* \quad \text{and} \quad Q(\lambda) := e^{-\mu\tau}\left[\theta\lambda^2 + (\theta A + Kf'(S^*))\lambda + \theta\mu\beta I^*\right].$$

We have

$$\lim_{n\to\infty}\left|\frac{P(\lambda_n)}{\lambda_n^2}-1\right|=0 \quad \text{and} \quad \lim_{n\to\infty}\left|\frac{Q(\lambda_n)}{\lambda_n^2}-\theta e^{-\mu\tau}\right|=0.$$

Then, as for the case of the disease-free steady-state, the closed forms of the roots λ_n are

$$\bar{\lambda}_p=\frac{1}{\tau}\ln(\theta)-\mu+\frac{2p\pi}{\tau}i, \quad p\in\mathbb{Z}.$$

Thus, all roots such that $|\lambda_n|\to+\infty$ have negative real part for n large enough. We conclude that all roots of (2.13) have negative real part and then the endemic equilibrium is locally asymptotically stable. □

Remark 1. As for the proof of Corollary 1, we can also prove directly by contradiction that there is no root $\lambda=\alpha+i\omega$ of (2.13) with $\alpha\geq 0$.

2.4 Global stability analysis

We consider in this section the case

$$f(S)=S.$$

The model becomes

$$\begin{cases} S'(t) &= \sigma-\beta I(t)S(t)-\mu S(t)-KS(t)+(1-\theta)e^{-\mu\tau}u(t-\tau), \\ I'(t) &= \beta I(t)S(t)-\mu I(t), \\ u(t) &= KS(t)+\theta e^{-\mu\tau}u(t-\tau), \end{cases} \tag{2.15}$$

with the initial condition

$$S(0)=S_0, \quad I(0)=I_0 \quad \text{and} \quad u(t)=\varphi(t), \ \ t\in[-\tau,0].$$

The function Φ given by (2.8) becomes

$$\Phi(S^*) = \left[1 + \frac{K(1 - e^{-\mu\tau})}{\mu(1 - \theta e^{-\mu\tau})}\right] S^*.$$

The corresponding disease-free equilibrium is

$$(S^0, I^0, u^0) := \left(\frac{\sigma(1 - \theta e^{-\mu\tau})}{\mu + K - (\mu\theta + K)e^{-\mu\tau}} \ , \ 0 \ , \ \frac{K\sigma}{\mu + K - (\mu\theta + K)e^{-\mu\tau}}\right), \tag{2.16}$$

and the endemic steady-state is

$$(S^*, I^*, u^*) = \left(\frac{\mu}{\beta} \ , \ \frac{\sigma}{\mu} - \Phi\left(\frac{\mu}{\beta}\right) \ , \ \frac{K\mu}{\beta(1 - \theta e^{-\mu\tau})}\right). \tag{2.17}$$

The basic reproduction number becomes

$$\mathcal{R}_0 := \frac{\beta}{\mu}\Phi^{-1}\left(\frac{\sigma}{\mu}\right) = \frac{\beta}{\mu}S^0 = \frac{\beta\sigma(1 - \theta e^{-\mu\tau})}{\mu^2(1 - \theta e^{-\mu\tau}) + \mu K(1 - e^{-\mu\tau})}. \tag{2.18}$$

A model similar to (2.15) has been studied in [95] as a generalization of a Kermack-McKendrick SIR model with age-structured protection phase. Authors have established the global asymptotic stability of the two steady-states. They showed that if $\mathcal{R}_0 < 1$, then the disease-free steady-state is globally asymptotically stable, and if $\mathcal{R}_0 > 1$, then the endemic steady-state is globally asymptotically stable. They constructed quadratic and logarithmic Lyapunov functions to establish this global stability. In the following subsections, we also present results on the global asymptotic stability of the two steady-states. We use similar techniques to those used for the proofs of the global stability results in [95].

2.4.1 Global asymptotic stability of the disease-free steady-state

In this subsection, we assume that $\mathcal{R}_0 < 1$ and we show that the disease-free equilibrium (S^0, I^0, u^0) is globally asymptotically stable. The proof is based on the use of

the following auxiliary differential-difference system, for $t > 0$,

$$\begin{cases} \dfrac{dS^+}{dt}(t) &= \sigma - (\mu + K)S^+(t) + (1-\theta)e^{-\mu\tau}u^+(t-\tau), \\ u^+(t) &= KS^+(t) + \theta e^{-\mu\tau}u^+(t-\tau), \end{cases} \tag{2.19}$$

with the same initial condition as the main system

$$S^+(0) = S_0 \quad \text{and} \quad u^+(t) = \varphi(t), \;\; t \in [-\tau, 0].$$

By using a comparison principle, we get that $S(t) \leq S^+(t)$ and $u(t) \leq u^+(t)$ for all $t > 0$. Furthermore, the system (2.19) has a unique equilibrium that corresponds to the disease-free equilibrium of the system (2.15). The basic reproduction number associated to (2.19) is also given by (2.18). The global asymptotic stability of the auxiliary system (2.19) has been established in [95]. Indeed, by setting

$$\hat{S}(t) := S^+(t) - S^0, \quad \hat{u}(t) := u^+(t) - u^0$$

and considering the Lyapunov function $V : \mathbb{R} \times \mathcal{C}([-\tau, 0], \mathbb{R}) \longrightarrow \mathbb{R}^+$,

$$V(S_0, \varphi) = \frac{S_0^2}{2} + \xi \int_{-\tau}^{0} \varphi^2(s)ds, \quad \text{with } \xi = \frac{1}{2K^2}\left[\mu(1 - \theta^2 e^{-2\mu\tau}) + K\right] > 0,$$

Authors proved in [95] the following lemma.

Lemma 2.2. *Suppose that $\mathcal{R}_0 < 1$. Then, the unique steady-state (S^0, u^0) of the system* (2.19) *is globally asymptotically stable.*

Thanks to a comparison principle and the global attractivity of the set

$$\begin{aligned} \Omega_\varepsilon \;:=\; & \{(S, I, u) \in \mathbb{R}^+ \times \mathbb{R}^+ \times \mathcal{C}([-\tau, 0], \mathbb{R}^+) : \\ & 0 \leq S \leq S^0 + \varepsilon, \; 0 \leq u(s) \leq u^0 + \varepsilon, \; s \in [-\tau, 0]\}, \end{aligned}$$

for $\varepsilon > 0$ arbitrarily small, we are able to obtain the global asymptotic stability of the disease-free equilibrium of (2.15). More precisely, the proof of the global asymptotic stability of the disease-free steady-state (2.16) is based on the following lemma.

Lemma 2.3. *Suppose that $\mathcal{R}_0 < 1$. Then, for any sufficiently small $\varepsilon > 0$, the subset Ω_ε of $\mathbb{R}^+ \times \mathbb{R}^+ \times \mathcal{C}([-\tau, 0], \mathbb{R}^+)$ is global attractor for the system* (2.15)*.*

Proof. The solutions of (2.15) satisfy, for all $t > 0$, the system

$$\begin{cases} S'(t) & \leq & \sigma - (\mu + K)S(t) + (1-\theta)e^{-\mu\tau}u(t-\tau), \\ u(t) & = & KS(t) + \theta e^{-\mu\tau}u(t-\tau). \end{cases}$$

By the comparison principle and the positivity of the solutions, we have $0 \leq S(t) \leq S^+(t)$ and $0 \leq u(t) \leq u^+(t)$, for all $t > 0$, where (S^+, u^+) is the solution of the system (2.19). Lemma 2.2 implies that $(S^+(t), u^+(t)) \to (S^0, u^0)$ as $t \to +\infty$. This convergence means that the subset Ω_ε, with $\varepsilon > 0$ is arbitrarily small, is a global attractor for the system (2.15). □

Lemma 2.3 allows us to restrict the analysis of the global stability of the disease-free steady-state (2.16) of (2.15) to the subset Ω_ε with $\varepsilon > 0$ small enough.

Theorem 2.1. *Suppose that $\mathcal{R}_0 < 1$. Then, the disease-free steady-state $(S^0, 0, u^0)$ given by* (2.16) *of the model* (2.15) *is globally asymptotically stable.*

Proof. We consider the solutions of System (2.15) in the subset Ω_ε, with $\varepsilon > 0$ small enough. It is clear that the second equation of (2.15) implies that

$$I'(t) \leq \beta(S^0 + \varepsilon)I(t) - \mu I(t) = -\mu\left(1 - \frac{\beta(S^0 + \varepsilon)}{\mu}\right)I(t).$$

Since $\mathcal{R}_0 = \dfrac{\beta}{\mu} S^0 < 1$, we can choose $\varepsilon > 0$ such that $\dfrac{\beta(S^0+\varepsilon)}{\mu} < 1$. This implies that $\lim_{t\to+\infty} I(t) = 0$. Then, there exists $T_\varepsilon > 0$ such that $0 \leq I(t) \leq \varepsilon$, for all $t > T_\varepsilon$. We then have, for $t > T_\varepsilon$

$$\begin{cases} S'(t) &\geq \sigma - (\mu + K)S(t) - \varepsilon\beta S(t) + (1-\theta)e^{-\mu\tau}u(t-\tau), \\ u(t) &= KS(t) + \theta e^{-\mu\tau}u(t-\tau). \end{cases}$$

We again use the comparison principle to obtain $S(t) \geq S_\varepsilon(t)$ and $u(t) \geq u_\varepsilon(t)$, for all $t > T_\varepsilon$, where $(S_\varepsilon, u_\varepsilon)$ is the solution of the problem, for $t > 0$,

$$\begin{cases} S'_\varepsilon(t) &= \sigma - (\mu + K)S_\varepsilon(t) - \varepsilon\beta S_\varepsilon(t) + (1-\theta)e^{-\mu\tau}u_\varepsilon(t-\tau), \\ u_\varepsilon(t) &= KS_\varepsilon(t) + \theta e^{-\mu\tau}u_\varepsilon(t-\tau), \\ S_\varepsilon(0) &= S_0, \quad u_\varepsilon(s) = \varphi(s), \quad \text{for } -\tau \leq s \leq 0. \end{cases} \tag{2.20}$$

We use the same techniques as for the proof of the lemmas 2.2 and 2.3, to show that $(S_\varepsilon(t), u_\varepsilon(t)) \to (S^0_\varepsilon, u^0_\varepsilon)$ as $t \to +\infty$, with $(S^0_\varepsilon, u^0_\varepsilon)$ the steady-state of System (2.20). In fact, $(S^0_\varepsilon, u^0_\varepsilon)$ is given by the expression

$$(S^0_\varepsilon, u^0_\varepsilon) := \left(\frac{\sigma(1-\theta e^{-\mu\tau})}{\mu_\varepsilon + K - (\mu_\varepsilon\theta + K)e^{-\mu\tau}} \ , \ \frac{K\sigma}{\mu_\varepsilon + K - (\mu_\varepsilon\theta + K)e^{-\mu\tau}} \right),$$

with $\mu_\varepsilon := \mu + \varepsilon\beta$. Then, there exists $\tilde{T}_\varepsilon > T_\varepsilon > 0$ such that, for $t > \tilde{T}_\varepsilon$,

$$S^0_\varepsilon - \varepsilon \leq S(t) \leq S^0 + \varepsilon \quad \text{and} \quad u^0_\varepsilon - \varepsilon \leq u(t) \leq u^0 + \varepsilon.$$

As $\varepsilon \to 0$, we have $S^0_\varepsilon \to S^0$ and $u^0_\varepsilon \to u^0$. Then, we obtain

$$\lim_{t\to+\infty} S(t) = S^0 \quad \text{and} \quad \lim_{t\to+\infty} u(t) = u^0.$$

Recalling that $(S^0, 0, u^0)$ is locally asymptotically stable. Then, it is globally asymptotically stable. □

2.4.2 Global asymptotic stability of the endemic equilibrium

In this subsection, we assume that

$$\mathcal{R}_0 > 1,$$

where $\mathcal{R}_0$ is given by (2.18), and we study the global asymptotic stability of the endemic steady-state (2.17). Let us define

$$\tilde{S}(t) := S(t) - S^* \quad \text{and} \quad \tilde{u}(t) := u(t) - u^*.$$

Then, the system (2.15) becomes, with $\beta S^* = \mu$,

$$\begin{cases} \tilde{S}'(t) &= -(\mu + K)\tilde{S}(t) - \beta\tilde{S}(t)I(t) - \beta S^* I(t) + \beta S^* I^* + (1-\theta)e^{-\mu\tau}\tilde{u}(t-\tau), \\ I'(t) &= \beta\tilde{S}(t)I(t), \\ \tilde{u}(t) &= K\tilde{S}(t) + \theta e^{-\mu\tau}\tilde{u}(t-\tau). \end{cases} \tag{2.21}$$

The endemic steady-state (2.17) of the system (2.15) becomes $(0, I^*, 0)$ (as a steady-state of the system (2.21)). We then get the following result.

Theorem 2.2. *Let us suppose that $\mathcal{R}_0 > 1$. Then, the endemic steady-state (S^*, I^*, u^*) given by (2.17) of the model (2.15) is globally asymptotically stable.*

Proof. The proof of this theorem is based on the use of the following Lyapunov function $V : \mathbb{R} \times \mathbb{R}^+ \times \mathcal{C}([-\tau, 0], \mathbb{R}) \to \mathbb{R}^+$ defined by

$$V(S_0, I_0, \varphi) = \frac{S_0^2}{2} + \xi \int_{-\tau}^{0} \varphi^2(s)ds + S^* \left[I_0 - I^* - I^* \ln\left(\frac{I_0}{I^*}\right) \right],$$

with $\xi = \dfrac{1}{2K^2}\left[K + \mu(1 - (\theta^2 e^{-2\mu\tau})\right]$.

First, we note that the function $G : (0 + \infty) \to [0 + \infty)$ defined by

$$G(I_0) = I_0 - I^* - I^* \ln\left(\frac{I_0}{I^*}\right), \quad I_0 > 0,$$

satisfies $G(I_0) \geq 0$ for all $I_0 > 0$ and $G(I_0) = 0$ if and only if $I_0 = I^*$. Then, we have $V(S_0, I_0, u_0) = 0$ if and only if $(S_0, I_0, u_0) = (0, I^*, 0)$. We set

$$\tilde{V}(t) := V(\tilde{S}(t), I(t), \tilde{u}_t), \;\; t \geq 0,$$

where $(\tilde{S}(t), I(t), \tilde{u}_t)$ is the solution of (2.21). Then, we obtain

$$\begin{aligned} \tilde{V}'(t) &= -a\tilde{S}^2(t) + b\tilde{S}(t)\tilde{u}(t-\tau) - c\tilde{u}^2(t-\tau) - \beta I(t)\tilde{S}^2(t), \\ &\leq \frac{b^2 - 4ac}{4c}\tilde{S}^2(t), \\ &= -\kappa\tilde{S}^2(t), \end{aligned} \tag{2.22}$$

with

$$\begin{cases} a &= \mu + K - \xi K^2, \\ b &= (1-\theta)e^{-\mu\tau} + 2\xi K\theta e^{-\mu\tau} \;>\; 0, \\ c &= \xi(1 - \theta e^{-\mu\tau})(1 + \theta e^{-\mu\tau}) \;>\; 0, \\ \kappa &= (4ac - b^2)/4c \;>\; 0. \end{cases}$$

We conclude that the function $t \mapsto V(\tilde{S}(t), I(t), \tilde{u}_t)$ is nonincreasing. Then, we get

$$\lim_{t\to+\infty} V(\tilde{S}(t), I(t), \tilde{u}_t) = \inf_{s\geq 0} V(\tilde{S}(s), I(s), \tilde{u}_s) =: V^* \geq 0.$$

By integrating (2.22) from 0 to $t > 0$, we obtain

$$\kappa \int_0^t \tilde{S}^2(s)ds \leq V(\tilde{S}(0), I(0), \tilde{u}_0) - V(\tilde{S}(t), I(t), \tilde{u}_t).$$

It is clear that the limits on both sides exist when $t \to +\infty$ and we have

$$\lim_{t\to+\infty} \int_0^t \tilde{S}^2(s)ds \leq \frac{1}{\kappa}\left[V(\tilde{S}(0), I(0), \tilde{u}_0) - V^*\right]. \tag{2.23}$$

Furthermore, the first equation of System (2.21) implies that $t \mapsto \tilde{S}'(t)$ is uniformly bounded. Then, the function $t \mapsto \tilde{S}(t)$ is uniformly continuous. We conclude from (2.23), that $\lim_{t\to+\infty} \tilde{S}(t) = 0$ and the fluctuations lemma implies that there exists a sequence $(t_k)_{k\in\mathbb{N}}$, $t_k \to +\infty$ such that $\lim_{k\to+\infty} \tilde{S}'(t_k) = 0$. On the other hand, using the difference equation satisfied by $\tilde{u}$, we also have $\lim_{t\to+\infty} \tilde{u}(t) = 0$. Then, the first equation of System (2.21) implies that $\lim_{k\to+\infty} I(t_k) = I^*$. We also have from the expression of V that

$$\lim_{t\to+\infty} G(I(t)) = \frac{V^*}{S^*}.$$

Furthermore, the continuity of the function G implies that $\lim_{k\to+\infty} G(I(t_k)) = G(I^*) = 0$. Then, $V^* = 0$. This means that $\lim_{t\to+\infty} G(I(t)) = 0$. The properties of the function G imply that $\lim_{t\to+\infty} I(t) = I^*$. We conclude that the endemic steady-sate (S^*, I^*, u^*) is globally asymptotically stable. □

We assumed, in a first time, that the rate of start PrEP treatment was constant and that $f(S) = S$. Thus, the model admits two equilibrium points, the disease-free equilibrium and the endemic equilibrium. By considering $\mathcal{R}_0$ as a function of the delay, we have shown that if $\mathcal{R}_0 < 1$ the disease-free equilibrium is globally asymptotically stable and that if $\mathcal{R}_0 > 1$ then it is the endemic equilibrium that becomes globally asymptotically stable.

2.5 Applications to French clinical data

In order to apply our model to real data, we choose the French MSM population and later, we will focus more specifically to the high risk individuals within this group. We define here the high risk MSM population as the multi-partners gay men as well as sexual intercourse under drug usually called chemsex, or new generations

not inclined to use any protection anymore (mainly condom). Of course, this reduces our study to a small part of the population, but, because of their highest rate of infectivity they belong to the target of PrEP treatments in the infectious disease center in France.
Furthermore, for a more realistic approach, ψ is considered time-dependent and ψ is defined by the logistic equation for a more accurate data fit (details and parameters in the first subsection below). The PrEP users had been collected between January 2016 (starting year of PrEP in France) to June 2019 (before the SARS-COV 2 outbreak) (see [92]).
Section 2.5 is structured in three subsection: first, we introduce the data and the methods to approximate the parameters. Then, we propose a set of simulations adapted to the general French MSM population. The last subsection is a focus on the so-called high risk individuals as described previously.
It is important at this stage to the reader that HIV is not curable and then PrEP does not have a direct influence on the decreasing number of infected compartment over the time which is mainly due to natural death (with a life expectancy for treated persons as high as non infected ones) or, more rarely now, thus neglected here for the French group, untreated-AIDS individuals. However, PrEP policy in the population may have an important impact on the infectivity rate. And since PrEP efficiency can be measured in a long term range and using incidence we simulated over 15 years (that is 180 months) for a forecast of this prevention strategy over time.

2.5.1 Choice of the parameters

In Table 2.1, we remind the parameters used in model (2.1) as well as their meaning and values for the general and high risk MSM in France estimated from [92], assuming that 60% of the the population considered in the dataset of the study are MSM.

PrEP treatment in France has started in 2016, and since the SARS-COV2 epidemics modified drastically the sexual habits (through the successive lock down), we considered the population data until 2019 only. Then after, we simulate our model based on the estimated parameter values for the following 15 years. Note here that we do

Symbol	Signification	Value for general MSM	Value for high risks	Unit
θ	Probability to keep the PrEP treatment	0.83	0.83	–
σ	Recruitment	$3,000$	562	$(\text{indiv}).(\text{months})^{-1}$
μ	Removal rate from the compartments	0.000758	0.0076	$(\text{months})^{-1}$
β	HIV transmission rate per infected individual	1.82×10^{-10}	2.85×10^{-7}	$(\text{indiv.months})^{-1}$
τ	Duration of the period of PrEP taking	3	3	months

Table 2.1: Parameters used in model (1.1) with values applied to the French population estimated from [92]

take neither the SARS-COV2 nor the monkey pox epidemic into account for three reasons: first, because these periods are a bias to our model and need to be carefully adjusted with updated parameter values, second, to the best of our knowledge, the official French data related to these past two years have not been released yet, and finally, we prefer keeping our model as simple as possible for this present work. A more complex approach will be the object of a future work.

In [92], information between 2016 and 2019 had been collected every 6 months. We remind here that at the end of a 3 month period, the patient decides whether to give up the treatment or to continue. This is the reason why our simulations below are computed on a monthly basis. Initial conditions for functions $t \mapsto S(t)$, $t \mapsto I(t)$ and $t \mapsto u(t)$ are chosen to be January, the 1^{st} of 2016 according to [92]. Because of the delay equation on u, the function $u_{\text{init}} : [-3, 0] \to \mathbb{R}^+$, $t \mapsto u_{\text{init}}(t)$ is adjusted with the cubic spline interpolation of 60% of each total number of the last column in Table 2.2. Note that u_{init} is the same for both population (general MSM and its high risk subset) simulations because we assume that here that most of the French PrEP users belong to the high MSM risk group. Regarding the susceptible: based on an

AVAC studies [176], page 5. $4-10\%$ of the French males declare to belong to the MSM group. Assuming that France counts about $65,000,000$ inhabitants, it seems then reasonable to assume that $S(0) = 2,600,000$.
Furthermore, on the official website of UNAIDS , we get that $170,000$ individuals were infected by HIV in France in 2016 [182]. We assume that a majority belongs to the MSM group but not the entire number (indeed a large portion of new cases was reported to be foreign heterosexual, among other subcases). This is why we take $I(0) = 90,000$. It is important to remind here that this value may not be the exact one, since the number of HIV detected is always below the real number of HIV infected (the HIV testing is not compulsory and thus several individuals may carry the virus for years without knowing it). Finally, when simulating the MSM high risk population, the estimate susceptible number would be between $30,000$ and $50,000$ depending on the literature. Thus, we take $S(0) = 40,000$ according to [92]. According to French data , French infections have been stable since 2010. On average, there are 6500 contaminations per year and infections within the MSM population represent 43%. Then, we choose $I(0) = 9,000$ [94].

Initial conditions	**Value for MSM**	**Value for high risks MSM**
$S(0)$	2,600,0000	40,000
$I(0)$	90,000	9,000

Table 2.2: Summary of initial conditions for susceptibles and infected among general MSM and MSM high risks populations

According to the official French data $\mu = 0.000758333$ individuals. months^{-1} at the country scale[178]. We choose this value for the French MSM removal rate (death as well as removed from sexual life). For the high risk MSM, μ is considered much larger because high risk sexual life style does not last longer than the average MSM ones.

Thus, $\mu = 0.0076$ individuals. months^{-1} in this subgroup. The 2016-2019 semester official French data sets are given in Tables 2.3.

Semester	**Initiation of PrEP**	**Renewal of the treatment**	**Total of PrEP users**
S1 - 2016	1,166	###	1,166
S2 - 2016	1,826	911	2,737
S1 - 2017	2,193	2,273	4,466
S2 - 2017	2,564	3,807	6,371
S1 - 2018	3,138	5,413	8,551
S2 - 2018	4,488	7,647	12,135
S1 - 2019	5,103	10,398	15,501

Table 2.3: Total number of PrEP users in France since 2016, given by semester (See [92], Table 3).

Thanks to Table 2.2 and 2.3, we are able to assess values of functions θ and ψ for the years 2016-2019. Indeed, for each semester, we get a different θ by using the following formula coming from its definition

$$\theta(\text{semester}) = \frac{\text{Number of renewal treatment of the current semester}}{\text{Total of PrEP users of the previous semester}}.$$

We assume that this value is the same for every months of the semester. And then we choose ψ, per months, as follows

$$\psi(\text{months}) = \frac{\text{Number of individuals who begins the treatment}}{S(0) * 6},$$

where $S(0)$ is the initial condition for the susceptible compartment S (2.4).

Semester	**Values of ψ for general MSM**	**Values of ψ for high risks MSMS**	**Values of θ**
S1 - 2016	0.0000747	0.0048583	###
S2 - 2016	0.000117	0.007608	0.7813
S1 - 2017	0.00014	0.00913	0.8305
S2 - 2017	0.000164	0.0106	0.8159
S1 - 2018	0.000201	0.0130	0.8496
S2 - 2018	0.00029	0.0187	0.8943
S1 - 2019	0.00033	0.0216	0.8569

Table 2.4: Values of parameters ψ and θ per month accordingly to each semester, computed according to Table 2.2 and 2.3.

We select $\theta = 0.83$ as the average value of all the previous θ from Table 2.4. As

mentioned in Section 2.2, we assume that ψ is solution of a logistic equation given by:

$$\frac{d\psi}{dt} = r\psi\left(1 - \frac{\psi}{K}\right),$$

where K is the carrying capacity and r the exponential growth. We remind that the explicit form of ψ is then written by the following expression :

$$\psi(t) = \frac{K}{1 + \left(\frac{K}{\psi_0} - 1\right)\exp(-rt)},$$

where ψ_0 is the initial condition depending on the population type. Using data for ψ given in Table 2.4 we summarize our results in Table 2.5.

Parameters	**Values for general MSM**	**Values for high risks MSM**
K	0.0007	0.072
r	0.0000222	0.000026

Table 2.5: Values of parameters K and r depending on the population

We assume a Hill function for the dynamics of the function f

$$f(S) = S_{sat}\frac{S^n}{\gamma^n + S^n},$$

with S_{sat} the saturation of the Hill function, γ is the abscissa of the inflection point and n the intensity of the slope. We summarize the value of these parameters in Table 2.6.

Parameters	Values for MSM	Values for high risks MSM
S_{sat}	5×10^6	$230,000$
γ	120	50
n	2	1.56

Table 2.6: Values of parameters S_{sat}, γ and n depending on the general French MSM and the high risk French MSM.

One of our goals is to estimate the HIV epidemics $\mathcal{R}_0$ for French MSM. We use the package in R® language untitled R0, and precisely the function *est.R0.SB* that estimates the $\mathcal{R}_0$ using a Bayesian approach following the idea developed in [29]. Thanks to our data of new HIV contamination ([62] and [85]), we get $\mathcal{R}_0 = 0.93$ for the normal MSM French population.
The two remaining parameters, β and σ are estimated to keep $\mathcal{R}_0$ equal to 0.93. We decide to choose $\sigma = 3,000$, in other words, each month, $3,000$ individuals might join the susceptible compartment (by reaching the sexual consent age, or deciding to join the MSM group). Thus, $\beta = 1.821 \times 10^{-10}(\text{individuals.months})^{-1}$ is estimated for the French general MSM.
On the other hand, according to the official French data, the basic reproduction number related to the high risk MSM ranges between 1.27 to 1.44 [34]. We take $\mathcal{R}_0 = 1.31$ and estimate $\beta = 2.85 \times 10^{-7}(\text{individuals.months})^{-1}$, with $\mu = 0.0076$ months^{-1} and $\sigma = 562$ given by Table 2.1.

2.5.2 Numerical simulations for the general French MSM

In Figure 2.2, protected (P) in green (graph on the right) keeps the track of the exact data (crosses) for the first semesters then reaches a threshold due to the French policy

of regulating the PrEP users. Indeed, the treatment is fully taken care by the health insurance in France. Thus, a threshold needs to be set up (estimated at $60,000$ MSM individuals here). With this threshold, it seems that within 15 years the number of infected drops and keeps on decreasing. The number of susceptibles (blue curve in left on the graph) keeps on growing with a lower slope between 50 and 100 months due to the increase of protected and then the threshold. But even with the increase of the susceptibles, the infected remains low. The protected compartment plays the role of reservoir to prevent the HIV epidemic to grow back.
Just as a comparison point, we simulated our model with a function f defined as identity (and not a Hill function anymore) (see Figure 2.3). We easily observe that the graph of the protected population does not fit the data in the first months with the same realistic parameter sets. Then, it seems that f needs to be more complex than identity for the case of the French MSM, and the Hill function seems to be validated here.

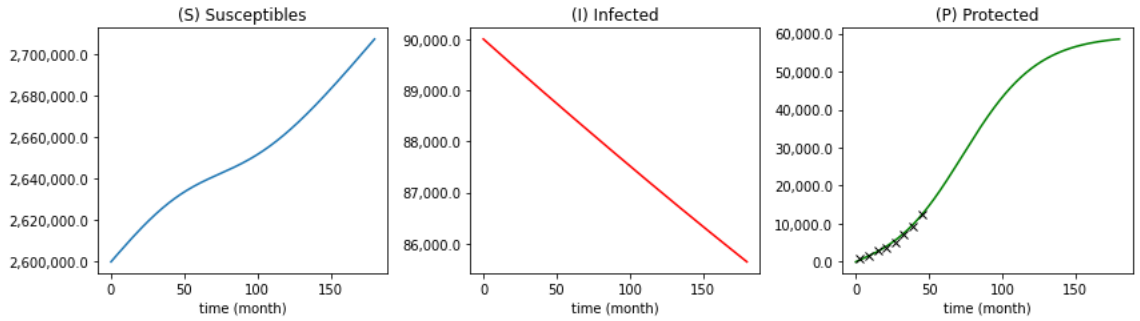


Figure 2.2: Plot of the evolution of the French MSM population (2.4) along the time (over 15 years). The crosses in the last plot represent the real values of PrEP users taken from Table 2.3. Function ψ verifies the logistic equation and f is a hill function.

In Figure 2.4 we plot the incidence with or without PrEP treatment. It seems obvious that without the PrEP reservoir (in blue), the incidence keeps on growing with no chance for the HIV epidemics to be controlled.
On the other hand, with the PrEP compartment (in red) it is possible to keep the incidence at a low level (and even to decrease it significantly for the first years). The

slight increase at the end (after month 125) is due to the threshold of the number of PrEP users imposed in our model and likely used by the French health insurance policy.

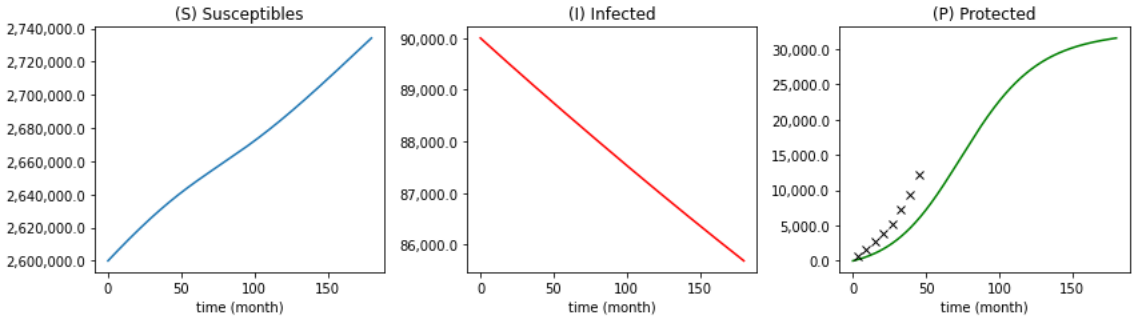


Figure 2.3: Plot of the evolution of the different compartments of the model (2.4) along the time (over 15 years). The crosses in the last plot represent the real values of PrEP users taken from Table 2.3. ψ verifies the logistic equation and f is identity.

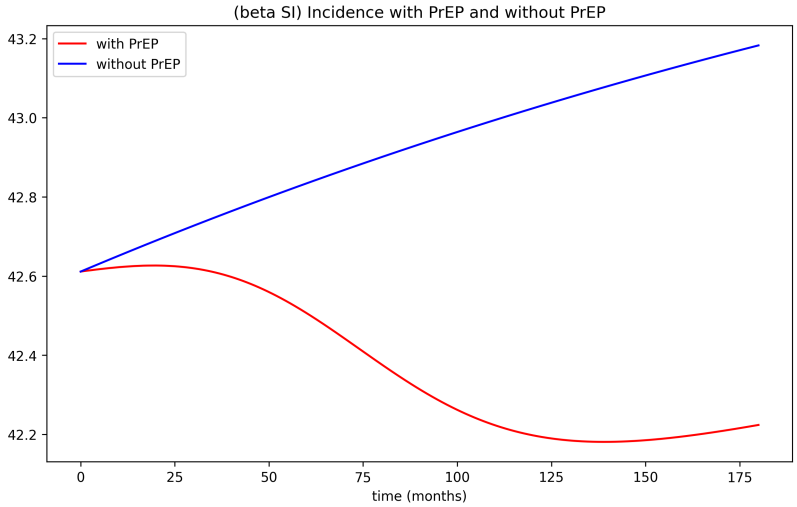


Figure 2.4: Plot of the evolution of the incidence with PrEP (in red) and without (in blue) from the system (2.4) over 15 years among the general French MSM.

In Figure 2.5, we depict the effect of the variation of $\mathcal{R}_0$ in function of ψ. It appears clearly here that as ψ increases (that is the number of PrEP users rises), the $\mathcal{R}_0$

declines drastically. This is however not linear and a plateau may be reached after a certain threshold (above 0.2), which indicates that the flow of new PrEP users does not need to expand in drastically. Indeed, even at ψ larger than 0.125 we get $\mathcal{R}_0$ already below 0.3 which is quite satisfactory. Augmenting ψ would decrease $\mathcal{R}_0$ but not as fast as the first values of ψ.

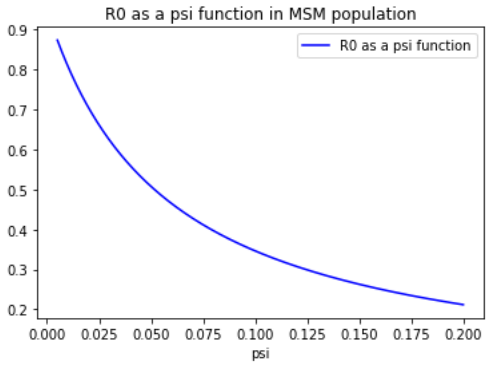


Figure 2.5: Plot of the $\mathcal{R}_0$ as a function of ψ.

2.5.3 Numerical simulations for high risks population

In this subsection, we focus our attention to the French MSM high risk population. We remind that this MSM subgroup consists in individuals with multi partner inter courses, sex relationship under drugs (chemsex), *etc.*). The HIV risk of infection is thus much higher than the rest of the MSM population. This is one of the reasons why this subgroup is the PrEP treatment target for the French health insurance. Protected compartment in this particular case plays a major role of reservoir. It is clearly confirmed in our model simulations as shown in Figure 2.6, where the number of susceptibles clearly drops as the number of protected individuals increases. Note that the infected population rises but for the first time reaches a threshold. This means that barely any new infected cases appear. We remind here that the model is a SI and not a SIR, that is no recovered individuals can appear since HIV is a disease with a lifetime treatment.

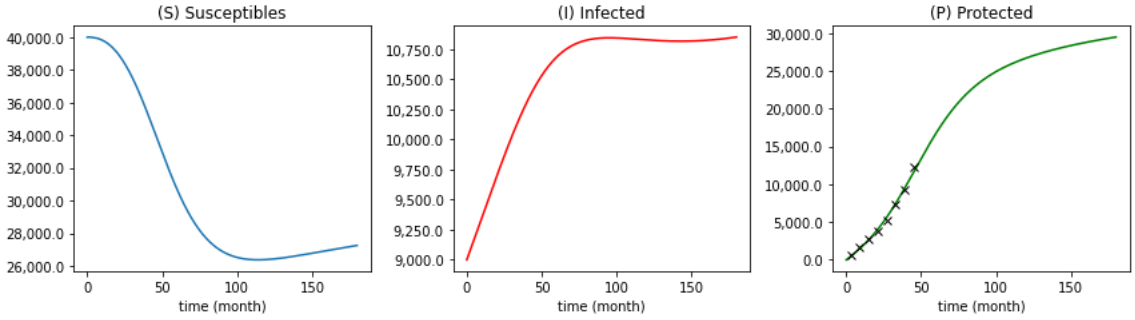


Figure 2.6: Plot of the evolution of the incidence with PrEP along the time (over 15 years). The crosses in the last plot represent the real values of the number of PrEP users got in Table 2.4. ψ verifies the logistic equation and f is a hill function.

In Figure 2.7 incidence evolution is plotted with or without PrEP treatment. The reservoir effect is even more explicit there in the sense that with PrEP the incidence declines to reach a low plateau, while without it keeps on growing indefinitely.

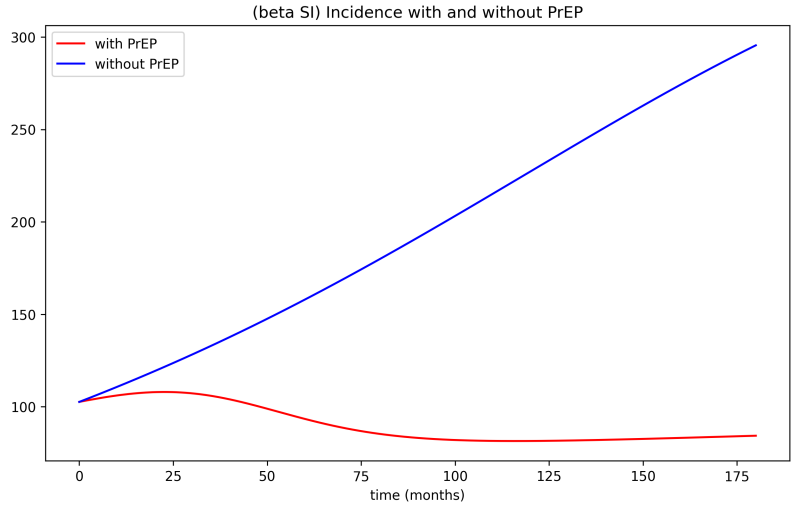


Figure 2.7: Plot of the evolution of the incidence with and without PrEP (2.4) over 15 years among French high risk MSM.

Finally, as mentioned before, for MSM high risk populations, the $\mathcal{R}_0$ in France is higher than 1. And Figure 2.8 reveals that as the number ψ of new PrEP users

increase, the $\mathcal{R}_0$ not only decreases below one, but also keeps on falling off. Here, the critical value of ψ which keeps $\mathcal{R}_0$ below one is $\psi_{critical} = 0.113$ person.months^{-1}. According to our data, $\psi = 0.071$person.months^{-1} as we assume the maximum threshold has been reached. The decay appears however with a smaller slope which means, as in the previous subsection, that after a certain threshold (0.2 here) very large values of ψ do not influence much the $\mathcal{R}_0$ reduction.

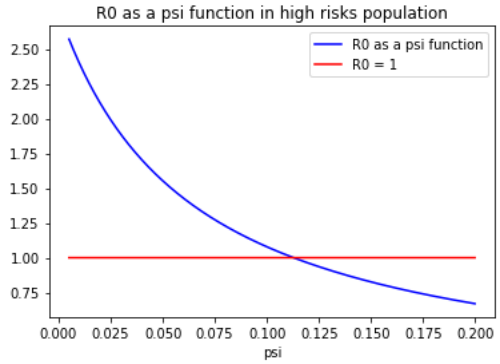


Figure 2.8: Plot of the $\mathcal{R}_0$ as a function of ψ.

This reservoir effect is so important that if for any reason the decision to stop PrEP treatment for this MSM group, the rise of new infected individuals would be inevitable as shown in Figure 2.9.

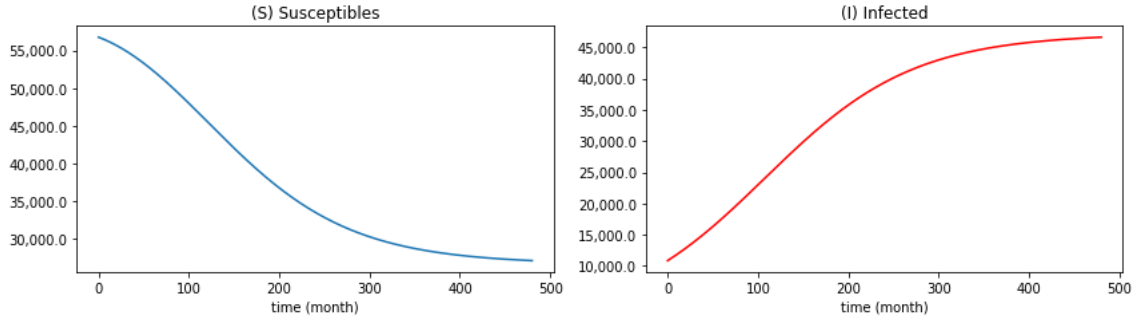


Figure 2.9: Plot of the susceptibles and infected if PrEP was stopped in 15 years. Time 0 corresponds to the end of the 15 years. We consider that all the protected individuals become susceptibles again.

2.5.4 Sensitivity analysis

In order to evaluate the influence of specific parameters on the value of $\mathcal{R}_0$, we conduct a sensitivity analysis of $\mathcal{R}_0$ using elasticity indices. Our approach was guided by the definition proposed in [63]. We use a numerical approximation due to the implicit definition of the DFE from equation 2.8. In doing so, we avoid heavy calculations involving the use of implicit function theorem to obtain analytical expression of $\mathcal{R}_0$.

$$\Upsilon_p^{\mathcal{R}_0} = \frac{\partial \mathcal{R}_0}{\partial p} \frac{p}{\mathcal{R}_0} \approx \frac{\%\Delta \mathcal{R}_0}{\%\Delta p}. \tag{2.24}$$

$\Upsilon_p^{\mathcal{R}_0}$ can be either negative or positive. The negative and positive sign denote respectively an increase and a decrease in $\mathcal{R}_0$ when the parameter p increases. Approximately, 1% change in the numerical value of p leads to $\Upsilon_p^{\mathcal{R}_0}\%$ in $\mathcal{R}_0$.

The local sensitivity analysis quantifies the necessity of targeted interventions in HIV prevention. In the general MSM population 2.10, the near-zero elasticity of PrEP-related parameters (e.g., $\Upsilon_\theta^{\mathcal{R}_0} = -0.079$) demonstrates a mathematical dilution effect. The high demographic influx (σ) marginalizes the impact of the prophylactic reservoir.

Conversely, in the high-risk MSM cohort, the protected compartment acts as a massive epidemiological sink. The results of sensitivity analysis aligns with core group theory in infectious disease epidemiology, confirming that widespread and untargeted PrEP prescription is inefficient, whereas focusing on multi-partner and high-risk networks is essential to drive $\mathcal{R}_0$ below the epidemic threshold. The extreme elasticity ($\Upsilon_\theta^{\mathcal{R}_0} = -3.824$) of the adherence and retention parameter θ in the high-risk cohort is the most critical finding of this analysis 2.11. It demonstrates that the long-term success of PrEP does not rely solely on initial prescription rates (K), but disproportionately on preventing drop-outs at the end of each 3-month cycle. If retention drops even marginally, the susceptible reservoir rapidly replenishes, and $\mathcal{R}_0$ immediately crosses the critical threshold of 1. This mathematical result echoes recent clinical literature emphasizing the "PrEP cascade," where loss to follow-up—often exacerbated by stigma, clinic accessibility, or external shocks like the COVID-19 pandemic—remains

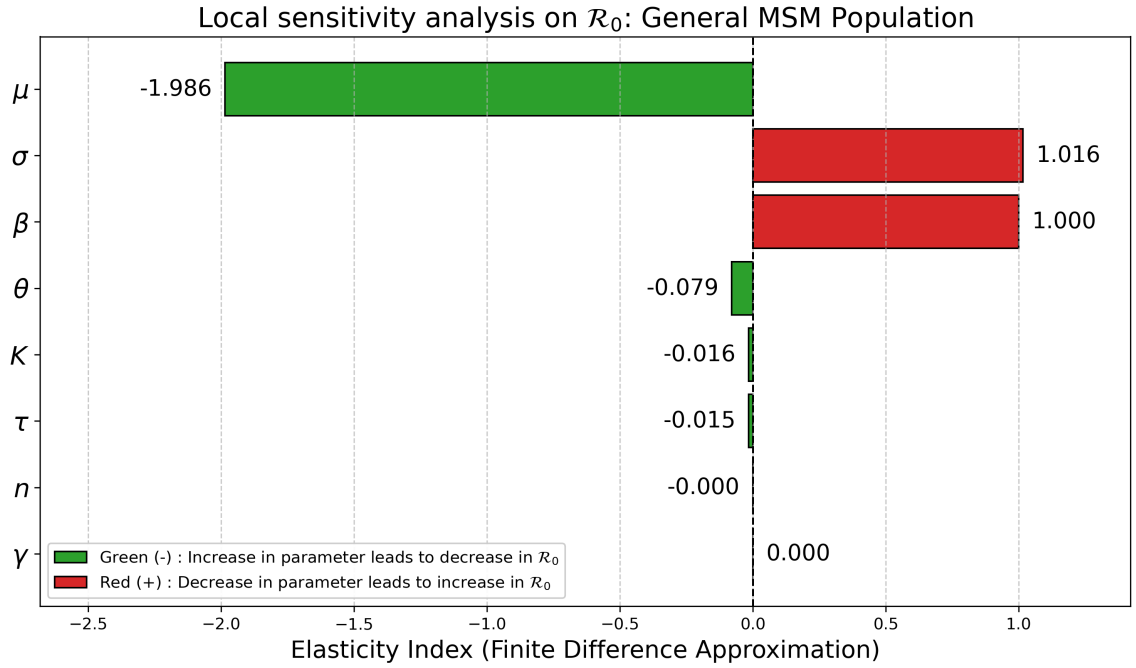


Figure 2.10: Local sensitivity analysis (elasticity index) of $\mathcal{R}_0$ for the general MSM population. Indices were computed numerically using finite difference approximations ($\Delta = 1\%$). The color coding and signs indicate the direction of the epidemiological impact: green bars and negative signs (-) correspond to parameters whose increase leads to a reduction in $\mathcal{R}_0$; red bars and positive signs (+) highlight parameters that exacerbate the epidemic when increased. The bar length quantifies the relative magnitude of this impact.

the greatest threat to HIV eradication [174].Pharmaco-Economic validation of the French health policy from a health economics perspective, the model's extreme sensitivity to treatment accessibility provides a mathematical validation for the French public health strategy.

In France, the introduction of generic Truvada has drastically reduced costs, allowing the national health insurance system to offer fully reimbursed PrEP. By removing financial barriers, this policy maximizes both the initiation rate (K) and the retention probability (θ). Our sensitivity analysis shows that financing continuous access to PrEP for high-risk individuals is not just a clinical benefit, but a mathematical lever

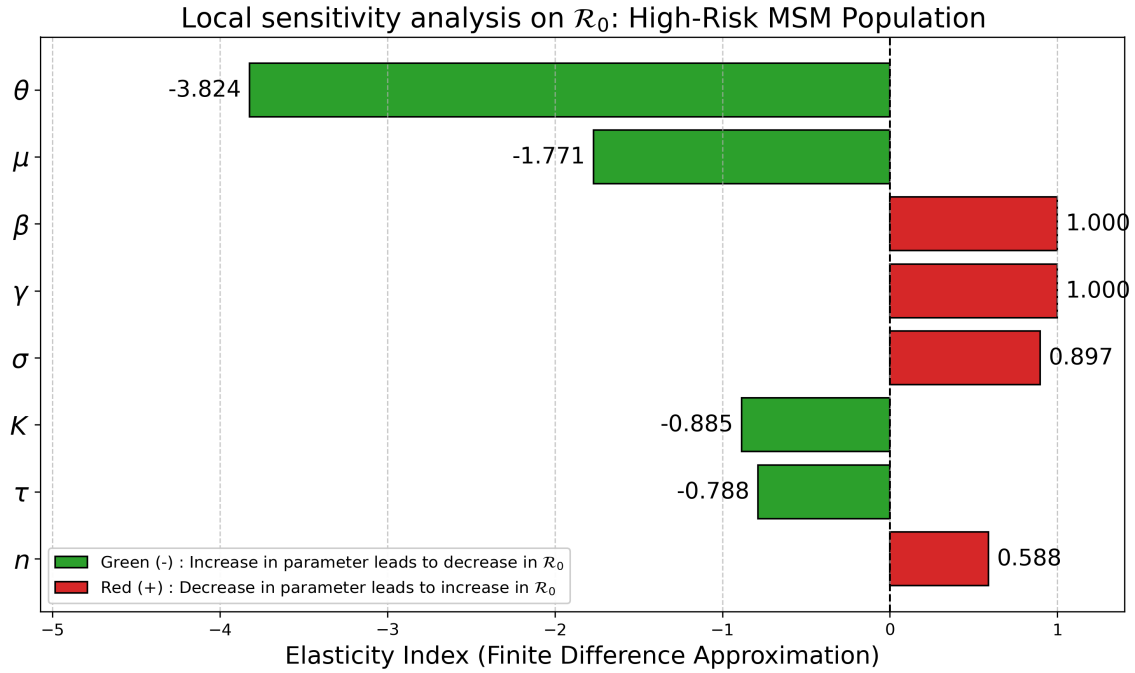


Figure 2.11: Local sensitivity analysis of $\mathcal{R}_0$ for the High-Risk MSM population. Indices were computed numerically using finite difference approximations ($\Delta = 1\%$). The color coding and signs indicate the direction of the epidemiological impact: green bars and negative signs (-) correspond to parameters whose increase leads to a reduction in $\mathcal{R}_0$; red bars and positive signs (+) highlight parameters that exacerbate the epidemic when increased. The bar length quantifies the relative magnitude of this impact.

to control the epidemic at a macroeconomic scale. The unit elasticity ($\Upsilon_{\gamma}^{\mathcal{R}_0} = 1.000$) of the Hill function's inflection parameter highlights a critical non-linear dynamic in the recruitment of PrEP users. As the easiest-to-reach individuals are enrolled, identifying and recruiting the remaining high-risk susceptible population becomes increasingly difficult. This mathematically justifies the current shift in public health strategies towards decentralized PrEP delivery—such as community-based testing, sexual health centers (CeGIDD in France), and telemedicine which are specifically designed to shift the γ parameter and reach marginalized populations who do not engage with traditional healthcare systems.

2.6 Comparaison of PrEP costs in France from 2016 to 2026

To quantify the economic impact on the carrying capacity parameter K of our model, it is essential to trace the precise evolution of the monthly cost per patient. The coverage of PrEP in France is based on 100% reimbursement by the National Health Insurance. This free access for the user shifts the economic constraint from the individual to the state. Thus, the actual cost dictates the asymptotic budgetary limit K that can be allocated by national solidarity.

The Truvada® era (2016-2018)

During the official launch of PrEP in France in January 2016, the only treatment holding a marketing authorization (MA) for this indication was Truvada®, developed by Gilead Sciences. It is a fixed-dose combination of emtricitabine (200 mg) and tenofovir disoproxil (245 mg) [146]. At that time, Truvada® enjoyed an absolute monopoly. The retail price for a box of 30 tablets, corresponding to a one-month prophylactic coverage under a continuous regimen, was initially negotiated and set at around €340 to €350 [146]. However, the economic modeling of PrEP cannot be limited solely to the cost of antiretrovirals. The clinical protocol imposes a rigorous care pathway. Before any dispensation, and quarterly thereafter, the patient must undergo a specialized medical consultation and comprehensive biological testing. This testing includes HIV screening via serology, screening for other STIs (chlamydia, gonorrhea, syphilis), and monitoring of renal function via serum creatinine levels, as tenofovir presents potential nephrotoxicity [115]. Medico-economic studies conducted on French cohorts, extrapolating data from the foundational ANRS IPERGAY trial [64, 80], estimated these additional biology and consultation costs at approximately €1,142 per year per patient. Consequently, during the initial deployment years (2016-2018), the PrEP strategy generated an overall annual cost of approximately €5,217 (i.e., €4,075 for medications and €1,142 for monitoring). The total monthly cost borne by the Health Insurance therefore amounted to roughly €435 per month

per person [80]. This extremely heavy financial burden translated into a relatively restricted carrying capacity parameter K in our model. The deployment, while real, had to be meticulously controlled so as not to destabilize the National Health Insurance Expenditure Target (ONDAM). The cost-effectiveness evaluation of this strategy was heavily debated, with some reports highlighting that the Number Needed to Treat (NNT) to prevent a single HIV infection could exceed €84,000—more than four times the lifetime care cost of an HIV-positive patient—if the originator's prices were maintained.

Price collapse via generics (2018-2025)

The year 2017 marked a decisive turning point. The primary patent protecting tenofovir disoproxil expired in Europe. Although the MA holder attempted to extend its exclusivity via a supplementary protection certificate (SPC), citing the combination with emtricitabine, several European jurisdictions and patent offices, including those in France, ultimately rejected this evergreening maneuver (artificial patent extension) [125]. This legal decision opened the market floodgates to generic drug manufacturers. By late 2017 and massively throughout 2018, generic versions of the emtricitabine/tenofovir disoproxil combination were marketed in France by laboratories such as Biogaran, Mylan, Krka, and Zentiva [125]. The arrival of competition caused the cost of the molecule to drop by more than half. The retail price, including dispensing fees, for a box of 30 tablets fell into a range of €151.46 to €168.93 . Taking a representative average, the strictly pharmaceutical cost stabilized around €156 per month. Factoring in the clinical biology costs, which remain incompressible (€1,142 per year), the overall annual cost per user dropped to approximately €3,169. Thus, the total monthly cost covered fell from €435 to about €264 per person [80]. This therapeutic deflation has a direct and major consequence on our logistic function $\psi(t) = \dfrac{K}{1 + (\frac{K}{\psi_0} - 1)e^{-rt}}$. With a constant public health budget, a reduction in unit cost of nearly 40% allows the carrying capacity K to increase almost proportionally. This is precisely what the empirical data from the scientific interest group EPI-PHARE observed [146]. Following the price drop, PrEP initiations expe-

rienced exponential growth, reaching peaks of over 1,000 monthly initiations at the dawn of 2020. Lifting the economic lock allowed the system to more closely follow the curvature of the Hill function $f(S)$, massively responding to the demand of the MSM population.

Injectable PrEP (2026)

Until now, the oral PrEP model relied on daily administration or on-demand dosing (via the 2-1-1 protocol). However, this mode of administration exposes the system to the risk of non-adherence, which, in our SIP model, decreases protection efficacy. To mitigate this weakness, clinical research developed long-acting (LA) injectable formulations [168]. On February 26, 2026, an order published in the Official Journal of the French Republic formalized the full reimbursement of Apretude® (cabotegravir injectable suspension), developed by ViiV Healthcare. This treatment represents a major breakthrough: after two initial injections spaced four weeks apart, subsequent injections are administered every eight weeks (approximately 2 months) in a medical setting. However, this innovation comes with a substantial additional cost. Following 18 months of highly tense negotiations between the manufacturer and the Economic Committee for Health Products, the public price was set at €1,312.07 per bimonthly injection. Over a steady-state year (6 injections), the strictly pharmaceutical cost amounts to €7,872, or €656 per month [161]. Moreover, the monitoring protocol for cabotegravir is more demanding. To minimize the risk of developing a viral strain resistant to integrase inhibitors, the French National Authority for Health (HAS) requires an HIV viral load (HIV RNA) test before each injection,a costly exam that generates concern regarding potential out-of-pocket costs for users without complementary health insurance [168]. Including these new exams, the overall cost to the healthcare system jumps to over €800 per month per patient. The introduction of this ultra-expensive treatment creates a budgetary dichotomy. If we apply economic logic to the SIP model, the asymptotic capacity parameter K allocated to Apretude® will mathematically be much lower than that of oral generics, barring a massive increase in the prevention budget. This reality implies that injectable PrEP will not, initially, be able to entirely replace the oral form. It will need to be targeted

at individuals for whom the adherence parameter is problematic, thus justifying a premium cost aimed at optimizing the retention rate θ.

The Impact of exogenous shocks on modeling parameters

The trajectory of PrEP adoption, while influenced by prices, has been profoundly disrupted by external health shocks. The robustness of our mathematical model relies on its ability to integrate these shocks as alterations to parameters $\psi(t)$, $f(S)$, τ, and θ. Beginning in March 2020, France implemented strict lockdown measures to stem the spread of the SARS-CoV-2 virus. This event caused a sharp break in the dynamics of pre-exposure prophylaxis. EPI-PHARE reports measured a collapse in PrEP initiations of 40% to 80% during March, April, and May 2020, compared to the historical peak of 1,027 initiations observed in February of that same year [146]. Within the equations of our SIP model, this staggering drop is explained by the simultaneous contraction of the two components of the initiation function $F(t, S(t)) = \psi(t)f(S(t))$. Screening infrastructures, notably the Free Information, Screening, and Diagnostic Centers (CeGIDD), were partially closed or requisitioned for the fight against COVID-19 [146]. The reallocation of medical staff caused an instantaneous drop in capacity K. Physical distancing mandates drastically reduced exposure to sexual risk. In the equation $f(S) = S_{\text{sat}} \dfrac{S^n}{\gamma^n + S^n}$, the perceived decrease in risk translates into an abrupt increase in the parameter γ, making the fraction $\dfrac{S^n}{\gamma^n + S^n}$ marginal.

The opening of initial prescription (June 2021)

The COVID-19 pandemic acted as an eye-opener to the structural vulnerabilities of the healthcare system. Prior to 2021, French law mandated that the very first PrEP prescription (initial prescription) be exclusively carried out by a specialist doctor practicing in a hospital or CeGIDD. This restriction created a significant bottleneck. The capacity K of the logistic function $\psi(t)$ was physically capped by the limited number of available consultation slots in these specialized structures. To relaunch the prophylactic dynamic post-lockdown and decongest the CeGIDDs,

the HAS and the government made the historic decision to authorize any doctor, primarily private practice general practitioners (GPs), to initiate PrEP starting June 1, 2021. From a modeler's perspective, this regulatory reform translates into a structural release of the parameter K. By integrating thousands of private GPs into the equation, the healthcare system artificially pushed back the asymptotic limit of care supply. The impact was immediate. Initiations resumed vigorous growth as early as the second half of 2021. According to EPI-PHARE statistics updated in 2024, community medicine now absorbs roughly 52% of new initiations, 90% of which are performed by general practitioners. The growth rate r of the logistic equation is thereby sustained, allowing France to cross the 64,000 user mark in mid-2022, reaching 124,181 cumulative initiators by June 2025.

The Mpox Epidemic (2022)

While initial prescription in primary care increased the elasticity of $\psi(t)$, a new crisis emerged to test the elasticity of specialized reception capacities: the outbreak of the Mpox (monkeypox) epidemic in May 2022. The epidemiology of the Mpox virus in France presented a specific features. The epidemic spread almost exclusively within multi-partner sexual networks, precisely affecting the same sub-population targeted by PrEP. Sexual health and community centers, already tasked with quarterly PrEP monitoring, were requisitioned as an absolute emergency to administer post-exposure and pre-exposure Mpox vaccines (Imvanex® and Jynneos®), as well as to diagnose suspected cases [170]. In the renewal equation of our SIP model, $u(t) = Kf(S(t)) + \theta e^{-\mu\tau}u(t-\tau)$, the protection time τ is theoretically 3 months. However, the bottleneck in centers artificially dilated this waiting time for many patients seeking to renew their prescriptions. From a clinical standpoint, a τ that extends beyond the prescription's expiration means that antiretroviral coverage is interrupted. The individual, despite wishing to maintain protection ($\theta \approx 1$), suffers a treatment rupture and is forced to return to the Susceptible (S) compartment, making them vulnerable to HIV once again precisely when community sexual activity remains intense. This crisis highlights the limitations of a differential equation model if τ is considered a strict constant. In reality, infrastructural shocks make τ stochastic, underscoring the vital importance

of community medicine relays.

Global mathematical consequences on HIV dynamics and $\mathcal{R}_0$

The relevance of a public health intervention is judged by its capacity to control viral diffusion, that is, to keep the basic reproduction number $\mathcal{R}_0$ strictly below unity ($\mathcal{R}_0 < 1$). In the model defined by the delay system, the reproduction rate is analytically proven to be a decreasing function of the carrying capacity K and the renewal rate θ, as well as a decreasing function of the protection delay τ. The formula is expressed as follows:

$$\mathcal{R}_0(\tau) = \frac{\beta}{\mu}\Phi^{-1}\left(\frac{\sigma}{\mu}\right)$$

where the asymptotic equilibrium function is given by:

$$\Phi(S^*) = S^* + \frac{K(1-e^{-\mu\tau})}{\mu(1-\theta e^{-\mu\tau})}f(S^*)$$

The analysis of this equation reveals the direct impact of the price drop (generics) and the increase in prescribers (general practitioners). By increasing the asymptotic constant K, the second term of the function $\Phi(S^*)$ is considerably increased. To satisfy the asymptotic equilibrium equality $\Phi(S^*) = \sigma/\mu$, the increase on the right side forces the equilibrium value of the Susceptibles (S^*) to mathematically decrease. Since $\mathcal{R}_0$ is proportional to S^* ($\mathcal{R}_0 = \frac{\beta}{\mu}S^*$), the price reduction of PrEP is the essential economic engine to drive $\mathcal{R}_0$ below the critical threshold. Numerical simulations conducted on the high-risk MSM population in France suggest that optimal deployment could crush the local $\mathcal{R}_0$ from values above 1.30 down to manageable levels below 0.30, provided that K remains high. The integration of injectable PrEP into the therapeutic arsenal in 2026 not only alters costs; it requires a reprogramming of the delay parameter τ in our differential equations. The shift from daily oral treatment (renewed every quarter, hence $\tau = 3$) to an intramuscular injection changes the protection interval to 8 weeks ($\tau = 2$ months). At first glance, the decrease in τ within the formula $\Phi(S^*)$ seems to mathematically reduce the magnitude of protection. The

numerator $(1 - e^{-\mu\tau})$ decreases. Nevertheless, the power of cabotegravir lies in its drastic effect on the retention parameter θ. The attrition linked to forgetting daily pills, commonly referred to as "treatment fatigue," is erased by the episodic clinical act. The literature anticipates that the injection pushes the retention probability θ toward a value close to 1. Let us examine the denominator of the fraction in $\Phi(S^*)$: $\mu(1 - \theta e^{-\mu\tau})$. If θ tends toward unity, the term $(1 - \theta e^{-\mu\tau})$ approaches its absolute minimum value, causing the quotient to explode. The impact of the Hill function $f(S^*)$ is thus multiplied. Consequently, the mathematical efficacy of the injectable in compressing the Susceptible reservoir and collapsing the $\mathcal{R}_0$ is colossal, thereby compensating for the potential decrease in K induced by the exorbitant cost of the molecule (over €1,300 per injection). This is a classic trade-off in health economics: accepting a major unit premium cost to secure adherence (θ) whose failure would ultimately cost the system more in terms of new infections.

The limit of the function S_{sat}

Finally, the efficacy of the French prophylactic strategy runs up against a sociological reality translated by the parameter S_{sat} of the Hill function $f(S)$. Successive epidemiological reports from EPI-PHARE draw a striking conclusion of inequity: PrEP adoption is massively concentrated on a stereotyped population. Up until 2025, approximately 97% to 98% of initiators are men (primarily MSM), averaging 36 years of age, residing mostly in large metropolitan areas (over 70%), and displaying a privileged socio-economic profile (barely 7% to 8% are beneficiaries of Supplementary Universal Health Insurance or State Medical Assistance). In the mathematical model, the saturation S_{sat} was therefore calibrated on this specific subgroup of the population. Data from 2024 and 2025 show a stabilization of annual initiations around 20,000 new users. This asymptotic stagnation demonstrates that the logistic function $\psi(t)$ has reached its carrying capacity for the current S_{sat} reservoir. The challenge for French public health in the coming years is no longer so much about increasing capacity K largely made possible by generics and community medicine, but rather about modifying the parameters γ (the socio-cultural threshold of access) and S_{sat} the total targeted volume of the Hill function. To continue driving down the global

epidemic's $\mathcal{R}_0$, public authorities must implement proactive outreach strategies to include migrant populations, sex workers, and exposed heterosexual women, lest the mathematical potential of PrEP hit an epidemiological glass ceiling.

Conclusion

At the end of this analysis, the ten-year evolution (2016-2026) of PrEP deployment in France stands as a true laboratory of health economics and mathematical modeling. The transposition of empirical events into the discrete delay Susceptible-Infected-Protected (SIP) model validates the relevance of an approach that integrates both the finite protection time (τ) and non-autonomous variations in prescription dynamics. It is clear that the cost of therapy is the primary control variable of the system. The transition from an originator monopoly charging nearly €435 per month (including clinical fees) to a generic supply lowering the overall cost to around €264 per month unlocked the carrying capacity parameter K. This budgetary elasticity made it possible to meet a growing demand modeled by a Hill function, propelling the number of users beyond 120,000 cumulative initiations in a decade. However, the deterministic equations collided with the stochastic shocks of pandemics. The COVID-19 crisis induced a simultaneous contraction of supply through an abrupt drop in $\psi(t)$) and risk perception by increase in parameter γ. Even though the very high propensity for retention in care ($\theta \approx 0.85$) proved the efficacy of the Protected compartment's therapeutic inertia. The decentralization of prescription to general practitioners in the summer of 2021 corrected the infrastructural ceiling of specialized centers, durably relaunching the logistic dynamics of vaccine coverage. Similarly, the Mpox episode highlighted the risks associated with the competitive saturation of clinical capacities targeting the same population, temporarily threatening therapeutic continuity and virtually lengthening the discrete delay τ. Finally, the horizon opens onto the new pharmacological era of injectable cabotegravir (Apretude®). By redefining the granularity of the protection time and pushing the overall monthly cost beyond €800, this innovation presents a new challenge. Mathematically, it offers the promise of optimal retention θ, an indispensable driving force for crushing the basic reproduction number $\mathcal{R}_0$. Economically, it demands a rigorous allocation of

National Health Insurance resources. Mathematical modeling ultimately asserts itself not only as a descriptive tool but as an indispensable analytical compass to balance, for the benefit of public health, the cost of innovation against the imperative of viral eradication.

2.7 Conclusion and discussion

The aim of this work is to propose a brand new model for prescribing PrEP for 3 months, with the choice to continue treatment or to stop it at any time after this period. This choice changes many things in the new modeling approach by introducing difference equations with delay and thus the possibility of describing the effect of inertia and the reservoir of protected individuals not only analytically but also numerically. This approach could also be generalized to other epidemiological models describing the effect of vaccine or booster doses for improved efficacy of protection.

Furthermore, the double insights of MSM general and high-risk populations seemed very important to us, especially to depict the effect of PrEP treatment on disease incidence of the disease and the French health insurance policy to target the high-risk subgroup. With our model and simulations, it appeared that these strategies are much more effective than random targeting of any MSM individual.

Our future work, in production, will take into account that the exponential growth of susceptibilities is not realistic for a longer period of time, it would be better to model it as a logistic growth and then numerically simulated on a longer period of time. The data we worked on are from 2016 to 2019. It would be interesting to analyze the effect of the SARS-COV2 lockdown effect on the incidence and PrEP users. It would also be informative to analyze the booster effect of the unlocked period (mid-2021 and after). For this purpose, it is necessary to wait a few more years to collect a sufficient amount of data. A future model should also consider the θ time dependent. Indeed, depending on certain periods (a lockdown, for example, or a seasonal effect), the number of PrEP users willing to take the treatment at the end of their 3 months

prescription may vary over time. Some users may also take it for a short period of time (*e.g.*, 2 years on average) and discontinue treatment after choosing a long-term closed relationship.

The addition of a compartment of infected population under tritherapy should also be more realistic. Indeed, with tritherapy, HIV individuals can no longer be infectious and can be removed from the I compartment. The estimate of β would then be more accurate and reflect a more realistic situation.

Finally, it would be interesting to add the cost of treatment and the cost-efficiency strategy with the threshold of PrEP users in the compartment for optimal disease control and eventually its disappearance. For this purpose, our next goal is to compare data and policies across multiple countries (some with full financial support for treatment, some with partial support, and some with no support).

Chapter 3

Stability analysis of a new differential-difference model applied to the Pre-Exposure Prophylaxis (PrEP) effect on the spread of HIV

3.1 Introduction

HIV (Human Immunodeficiency Virus) is a retrovirus that infects humans and leads to AIDS (Acquired Immunodeficiency Syndrome). AIDS marks the advanced stage of the infection, wherein the virus has depleted a substantial count of CD4 T-cells, leading to immune system failure. It is crucial to note that this stage can be fatal if left untreated. Typically, this stage manifests between 5 and 10 years after initial infection, with an average survival time of 9.2 months [25]. At present, there is no cure or vaccine available for HIV, and treatment options become limited once AIDS has developed. In 2019, UNAIDS reported that around 38 million people worldwide were

living with HIV. Within that year, approximately 1.7 million individuals contracted the virus, while 690,000 deaths resulted from AIDS-related illnesses [140]. HIV can be transmitted through various means, including unprotected sex, mother-to-child transmission, and exposure to contaminated blood through activities like drug injections. While prevention methods may seem straightforward in theory, implementing them systematically in practice proves more challenging for several reasons. One key factor is that younger generations are less inclined to consistently use condoms during sexual activity [132] while older generations [65] tend to underestimate their risk of infection. A number of initiatives are already in place to help combat the current HIV epidemic. Among these, two treatments appear to be effective in preventing the spread of the epidemic. Namely, PrEP (Pre-Exposure Prophylaxis) and Treatment as Prevention.

PrEP is a treatment taken to reduce the risk of HIV infection. It is used by people who are not HIV-positive but who are at high risk of exposure to HIV through sexual intercourse or injecting drug use. PrEP combines several antiretroviral drugs and is available in both oral and injectable forms. The oral form can be taken according to continuous (daily) or discrete (on-demand) protocols. The on-demand regimen involves taking the drug approximately 2 hours before and up to 2 days after each sexual encounter. This worldwide approach has proven highly effective, offering excellent protection against HIV transmission [129]. PrEP users have a significantly reduced risk of HIV infection for three months. However, as PrEP does not protect against other Sexually Transmitted Infections (STIs) [114], they are required to undergo STI screening after this period, to renew their prescription of PrEP. They can then choose to continue treatment if they wish. When correctly implemented, PrEP has a proven impact on HIV transmission [68].

Treatment as prevention, on the other hand, targets people who are already infected (HIV-positive). Individuals taking this drug are then unable to transmit the disease, thus protecting their sexual partners [52, 101]. Treatment as prevention is able to significantly reduce the viral load to undetectable levels and maintain a nearly unchanged lifespan [88]. Treatment as prevention, when implemented at the population level, can effectively reduce the rate of transmission and bring the epidemic under

control.

PrEP and Treatment as prevention have in common the need for total adherence to treatment to fully exploit their potential to prevent the spread of HIV. However, many factors can lead to treatment failure, such as forgetting to take the medication, stigma-related problems, and side effects [66, 103, 91].

Many mathematical models have been investigated with the intent to bring light to difficult questions arising from HIV/AIDS conditions [5, 11]. For a good review, we suggest [102, 30, 6]. Delay differential equations have been one of the main tools in HIV immunology modeling over the years [19, 22]. In [119], researchers examined the influence of spatial factors on the MSM (Men who have Sex with Men) population, segmented into immunity-based compartments. They integrated this approach with an optimal control case to investigate the effects of varying PrEP costs. Similarly, [145] explored a combined approach involving both ART (Anti-Retroviral Therapy) and PrEP. They proposed an age-structured model incorporating infection ages and conducted qualitative analysis alongside numerical simulations utilizing data from China. In [74], the authors developed a model for HIV/AIDS to evaluate the impact of combining PrEP and ART drugs. They conducted mathematical and numerical analyses to explore the effects of these combined controls in the context of PrEP drug resistance. The findings indicated a significant reduction in new HIV infections when both PrEP and ART are applied at high levels. However, the study also showed that resistance to PrEP drugs could diminish or negate PrEP's effects, especially at lower efficacy levels. In [104], a mathematical model was proposed to understand HIV/AIDS transmission dynamics within a worker population, divided into isolated and non-isolated groups. Isolated workers were HIV-negative individuals who disclosed their status and committed to maintaining it, while non-isolated workers included those either HIV-positive or not wishing to reveal their status. The model extended the work of [74] by considering PrEP use and effectiveness. The study aimed to assess the impact of isolated groups on HIV/AIDS dynamics, revealing that high individual awareness and PrEP efficacy significantly reduce the epidemic. In [119], the authors designed and calibrated a compartmental model using Canadian data to observe changes in serosorting patterns due to PrEP. The model underscored the

critical importance of maintaining high PrEP effectiveness. Finally, in [151], the authors investigated the issue of reduced PrEP efficacy, primarily due to non-adherence, and its effect on HIV/AIDS infection dynamics. The study aimed to determine the critical threshold of PrEP efficacy needed to prevent backward bifurcation, which occurs when efficacy falls below 100%. Conversely, with 100% efficacy, indicating full adherence, the model exhibited a forward bifurcation. The numerical analysis highlighted the crucial role of adherence in enhancing PrEP efficacy.

Here, we base our model on the classic Kermack-McKendrick SI model [1], integrating an age-structured phase to depict the impact of PrEP only. We do not deal with other STIs or other treatments. These latter will be the object of further work. The age variable is exclusive to the PrEP user compartment, symbolizing the duration spent between prescription renewals. To the best of our knowledge, this is the first model that includes the time between two consecutive prescriptions. Individuals who remain protected during this period are described by an age-structured equation. The age structure allows for a more comprehensive system by adding the age variable alongside the time variable (in our case, the protection age). This system extends a previously published model outlined in [122]. As detailed in [122], it can be reformulated into a delay differential-difference system, where the delay corresponds to the duration of HIV protection provided by PrEP, approximately three months between two prescriptions. The primary alteration concerns the nonlinear force of infection [3] among PrEP users recruited from susceptible individuals. While previously considered as a constant parameter [95], we argue that it should depend not only on the infected population (increasing with the number of infected individuals) but also on factors associated with the political or economic context of a government. Additionally, we propose that only a fraction of the population can afford to utilize PrEP due to economic and political constraints, which we will now elucidate. On one hand, a country might opt to limit the number of PrEP users, either due to the treatment's cost or because the prevalence of infection is deemed too low to justify widespread use. On the other hand, some governments may choose to fully subsidize the treatment and actively promote its utilization among high-risk individuals. Conversely, other governments might allow individuals to decide whether to

pursue PrEP at their own expense or opt not to include any PrEP options in their healthcare plans [128]. Our study aims to examine the behavior of solutions with a rate of new PrEP users, recruited from the susceptible population, assumed to model a government's political or economic context. We are investigating whether, under specific conditions, the endemic equilibrium of this system may become unstable. Could a specific series of political and economic measures lead to a destabilization of this equilibrium, allowing periodic oscillations to occur? We meticulously analyze the stability of each steady state, achieving local asymptotic stability for both disease-free and endemic equilibria. Furthermore, we demonstrate global asymptotic stability for the disease-free steady state. Finally, we establish persistence when the endemic equilibrium exists. Although our study focuses on a simplified model, we believe the results hold validity for the PDE system. Given certain compatibility conditions on initial conditions, equivalence between the two systems can be achieved.
The organization of this paper is as follows. In the next section (Section 3.2), we formulate the age-structured model by introducing a protection phase by PrEP. We carefully detail the role of each term and parameter. Section 3.3 focuses on establishing the existence of two steady-states. A threshold basic reproduction number is also defined. In Section 3.4, we provide stability of the disease and disease-free equilibria: local, global, and persistence. We conclude with a discussion of our results in Section 3.5.

3.2 Age-structured model with fixed maximum age

Let us first remind the model introduced in [122]. We consider a population with three categories of individuals: susceptible $S(t)$, infected $I(t)$, and PrEP users $p(t, a)$, where $a \in [0, \tau)$ represents the time since an individual started a new prescription (usually $\tau = 3$ months is the recommended duration between two prescription renewals).

Then, the total protected population of all ages is given by

$$P(t) = \int_0^\tau p(t,a)da,$$

and the entire population studied by

$$N(t) := S(t) + I(t) + P(t).$$

In order to generalize a previous work, we define the recruitment rate of starting PrEP as a function depending on infected I and we note $\varphi(I)$. We assume that a large number of infected people in a population will push susceptible people to protect themselves. Then, $I \in \mathbb{R}^+ \mapsto \psi(I)$ is an increasing function. Consequently, we assume $\psi(0) = 0$. If there is no infection there is no individual seeking PrEP. For political and economic reasons, we consider that only a fraction of the population of susceptible is able to start taking PrEP and we note $f(S)$, where f is an increasing function.

Then, the part of the population starting PrEP is represented by $\psi(I)f(S)$. This term allows us to consider different scenarios. We are giving interpretations in 3.2, 3.3 and 3.4. At the end of the prescription period τ, only a proportion $0 < \theta < 1$ of PrEP users decide to renew their treatment and remain protected. Thus, $(1-\theta)p(t,\tau)$ represents the proportion of individuals who decide to stop renewing the prescription and lose their protection. They re-enter the susceptible phase. We denote μ as the constant death rate common to the three categories and Λ be the susceptible recruitment rate. We neglect here vertical (mother/child) transmission. We denote by β the rate at which the susceptibles become infected. Now and using the previous description (see Figure 3.1), we are ready to set up the whole system for $t > 0$ as

follows,

$$\begin{cases} \dfrac{dS(t)}{dt} = \Lambda - \mu S(t) - \beta I(t)S(t) - \psi(I(t))f(S(t)) + (1-\theta)p(t,\tau), \\ \dfrac{dI(t)}{dt} = \beta I(t)S(t) - \mu I(t), \\ \dfrac{\partial p}{\partial t}(t,a) + \dfrac{\partial p}{\partial a}(t,a) = -\mu p(t,a), \qquad 0 < a < \tau, \\ p(t,0) = \psi(I(t))f(S(t)) + \theta p(t,\tau), \end{cases} \tag{3.1}$$

with initial conditions

$$S(0) = S_0, \quad I(0) = I_0 \quad \text{and} \quad p(0,a) = p_0(a), \quad 0 < a < \tau.$$

We can reduce the model by using the method of characteristics (see [95, 60, 122] for the details) and introducing the function ϕ defined by

$$\phi(t) = e^{-\mu t} p_0(-t), \quad t \in [-\tau, 0],$$

and putting the new state

$$u(t) := p(t,0), \quad t > 0,$$

it is possible to obtain

$$p(t,\tau) = e^{-\mu\tau} \begin{cases} u(t-\tau), & t > \tau, \\ \phi(t-\tau), & t \in [0,\tau]. \end{cases}$$

Then, we have the following coupled differential-delayed difference equations, for

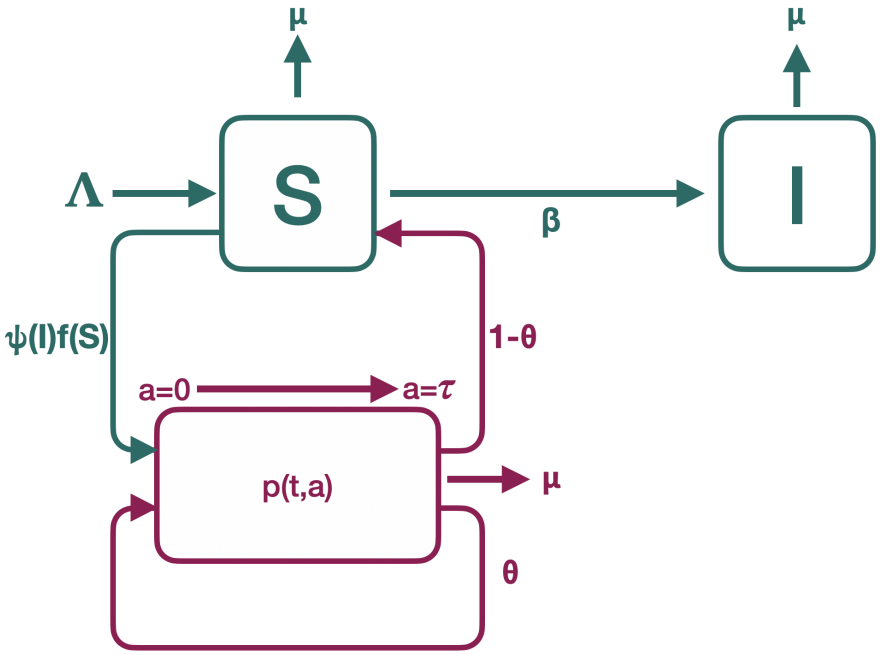


Figure 3.1: Schematic representation of the process. The population splits into susceptible $S(t)$, infected $I(t)$, and protected individuals under PrEP $p(t,a)$, where a stands for the elapsed time (finite time: less than τ, between to prescription renewals) in the PrEP compartment.

$t > 0$,

$$\begin{cases} \dfrac{dS(t)}{dt} &= \Lambda - \mu S(t) - \beta S(t)I(t) - \psi(I(t))f(S(t)) + (1-\theta)e^{-\mu\tau}u(t-\tau), \\ \dfrac{dI(t)}{dt} &= -\mu I(t) + \beta S(t)I(t), \\ u(t) &= \psi(I(t))f(S(t)) + \theta e^{-\mu\tau}u(t-\tau), \end{cases} \tag{3.2}$$

which is completed by the initial conditions

$$S(0) = S_0, \;\; I(0) = I_0 \;\text{ and }\; u(t) = \phi(t), \;\; \text{for} \;\; -\tau \leq t \leq 0.$$

The existence, uniqueness, and positivity of the solution of this system may be deduced in a classic way [95] or [60].
However, in the context of our objective to generalize the study of [122] where only the homogeneous steady-states were investigated, we decided to analyze the dynamics of the age-distributed equilibria from the original age-structured model (3.1). Moreover, both systems can be linked by the same states S, I and considering, for $a \in (0, \tau)$,

$$p(t,a) = e^{-\mu a} \begin{cases} \phi(t-a), & 0 < t \leq a, \\ \\ u(t-a), & t > a. \end{cases}$$

3.3 Existence of steady-states

Beforehand, observe first that the equation on $p(t,a)$ can be simplified by integrating over the age, for $t > 0$,

$$\frac{dP(t)}{dt} = -\mu P(t) - p(t,\tau) + p(t,0) = -\mu P(t) + \psi(I(t)) f(S(t)) - (1-\theta) p(t,\tau).$$

Then, by adding it to the two first equations of the system (3.1), we obtain, for $t > 0$,

$$\frac{dN(t)}{dt} = \frac{dS(t)}{dt} + \frac{dI(t)}{dt} + \frac{dP(t)}{dt} = \Lambda - \mu(S(t) + I(t) + P(t)) = \Lambda - \mu N(t).$$

This means that

$$\lim_{t \to +\infty} N(t) = \frac{\Lambda}{\mu}. \tag{3.3}$$

Then, we denote the steady-states by $(S^*, I^*, p^*(a))$, $0 < a < \tau$. They satisfy the following system

$$\begin{cases} \Lambda - \mu S^* - \beta I^* S^* - \psi(I^*) f(S^*) + (1-\theta) p^*(\tau) = 0, \\ \beta I^* S^* - \mu I^* = 0, \\ \dfrac{d}{da} p^*(a) = -\mu p^*(a), \\ p^*(0) = \psi(I^*) f(S^*) + \theta p^*(\tau). \end{cases} \tag{3.4}$$

The equation of p^* has an analytical expression given by

$$p^*(a) = e^{-\mu a} p^*(0).$$

Two possible steady-states may arise then: the disease-free equilibrium (DFE) characterized by the fact that $I^* = 0$, and the endemic one for which $I^* > 0$. Let us investigate the disease-free steady-state. Considering $I^* = 0$ yields to

$$\begin{cases} \Lambda - \mu S^* + (1-\theta) e^{-\mu\tau} p^*(0) = 0, \\ \left(1 - \theta e^{-\mu\tau}\right) p^*(0) = 0. \end{cases}$$

Since $\theta < 1 < e^{\mu\tau}$, then $1 - \theta e^{-\mu\tau} > 0$ and the second equation of the system implies that

$$p^*(0) = 0 \quad \text{and} \quad S^* = \frac{\Lambda}{\mu}.$$

It follows that there is a unique DFE and is given by

$$\mathcal{E}_0 = \left(\frac{\Lambda}{\mu}, 0, 0\right).$$

As previously mentioned, for an endemic steady-state, we consider $I^* > 0$. From the second equation of (3.4) we have

$$S^* = \frac{\mu}{\beta}.$$

Substituting the expression of S^* in (3.4) leads to

$$\begin{cases} \Lambda - \dfrac{\mu^2}{\beta} - \mu I^* - \psi(I^*) f\left(\dfrac{\mu}{\beta}\right) + (1-\theta)e^{-\mu\tau} p^*(0) = 0, \\ p^*(a) = e^{-\mu a} p^*(0), \\ p^*(0) = \dfrac{1}{1-\theta e^{-\mu\tau}} \psi(I^*) f\left(\dfrac{\mu}{\beta}\right). \end{cases}$$

Then, by replacing the expression of $p^*(0)$ into the first equation, we obtain

$$\Lambda - \frac{\mu^2}{\beta} - \mu I^* - \left[1 - \frac{(1-\theta)e^{-\mu\tau}}{1-\theta e^{-\mu\tau}}\right] \psi(I^*) f\left(\frac{\mu}{\beta}\right) = 0.$$

To prove the existence of a solution to this equation, we consider the function $\mathcal{H}$ defined on $\mathbb{R}^+$ by

$$\mathcal{H}(I^*) := \frac{\beta\Lambda}{\mu^2 + \beta\mu I^* + \left[\dfrac{\beta(1-e^{-\mu\tau})}{1-\theta e^{-\mu\tau}}\right] \psi(I^*) f\left(\dfrac{\mu}{\beta}\right)}.$$

The existence of an endemic steady-state is then equivalent to solving the equation

$$\mathcal{H}(I^*) = 1.$$

Since all the parameters of the system are positive, we easily check that $\mathcal{H}$ is a decreasing function on $\mathbb{R}^+$ with $\lim\limits_{I^* \to +\infty} \mathcal{H}(I^*) = 0$. We are then able to define the basic reproduction number $\mathcal{R}_0$ as

$$\mathcal{R}_0 := \mathcal{H}(0) = \frac{\beta\Lambda}{\mu^2}.$$

Therefore, we conclude that

- If $\mathcal{R}_0 > 1$, then there is a unique endemic steady-state.
- If $\mathcal{R}_0 < 1$, then the maximal value of the function $\mathcal{H}$ is $\mathcal{R}_0$ and there is no endemic steady-state.

We summarize the existence of equilibria in the following theorem.

Theorem 3.1. *If $\mathcal{R}_0 > 1$, then the system (3.1) has two distinct steady-states: a disease-free steady-state $\mathcal{E}_0$ and an endemic steady-state $\mathcal{E}^* := (S^*, I^*, p^*(a))$. If $\mathcal{R}_0 < 1$, then $\mathcal{E}_0$ is the only steady-state.*

Based on the equilibrium $\mathcal{E}^* := (S^*, I^*, p^*(a))$ of System (3.1) where

$$\begin{cases} S^* = \dfrac{\mu}{\beta}, \\ p^*(a) = e^{-\mu a} p^*(0), \\ p^*(0) = \dfrac{1}{1 - \theta e^{-\mu\tau}} \psi(I^*) f\left(\dfrac{\mu}{\beta}\right), \end{cases}$$

we notice that the positive equilibrium of System (4.2) is given by

$$(S^*, I^*, u^*) = (S^*, I^*, p^*(0)).$$

3.4 Stability of the two steady-states and persistence analysis

To study the stability of the two steady-states, we linearize the system (3.1) about each steady-state $(S^*, I^*, p^*(a))$. We put, for $t > 0$,

$$\begin{cases} S(t) &= S^* + s(t), \\ I(t) &= I^* + i(t), \\ p(t,a) &= p^*(a) + q(t,a). \end{cases}$$

Then, differentiating these expressions, the system (3.1) yields to

$$\begin{cases} \dfrac{dS(t)}{dt} = \Lambda - \mu S(t) - \beta I(t)S(t) - \psi(I(t))f(S(t)) + (1-\theta)p(t,\tau), \\ \dfrac{dI(t)}{dt} = \beta I(t)S(t) - \mu I(t), \\ \dfrac{\partial q}{\partial t}(t,a) + \dfrac{\partial q}{\partial a}(t,a) + \dfrac{d}{da}p^*(a) = -\mu p(t,a), \qquad 0 < a < \tau, \\ q(t,0) + p^*(0) = \psi(I(t))f(S(t)) + \theta p(t,\tau). \end{cases}$$

We replace the functions S, I and p by their expressions

$$\begin{cases} \dfrac{dS(t)}{dt} = -(\mu + \beta I^* + \psi(I^*)\dfrac{df(S^*)}{dS}s(t) - (\beta S^* + \dfrac{d\psi(I^*)}{dI}(f(S^*))i(t) \\ \qquad\qquad +(1-\theta)q(t,\tau), \\ \dfrac{dI(t)}{dt} = \beta I^* s(t) + (\beta S^* - \mu)i(t), \\ \dfrac{\partial q}{\partial t}(t,a) + \dfrac{\partial q}{\partial a}(t,a) = -\mu q(t,a), \qquad 0 < a < \tau, \\ q(t,0) = \psi(I^*)\dfrac{df(S^*)}{dS}s(t) + \dfrac{d\psi(I^*)}{dI}f(S^*)i(t) + \theta q(t,\tau). \end{cases}$$

We look for solutions with exponential growth of the form

$$s(t) = e^{\lambda t} s_0, \quad i(t) = e^{\lambda t} i_0, \quad \text{and} \quad q(t,a) = e^{\lambda t} q_0(a), \quad \lambda \in \mathbb{C}.$$

We substitute in the previous system and we simplify by $e^{\lambda t}$, to obtain

$$\begin{cases} \lambda s_0 = -\left(\mu + \beta I^* + \psi(I^*)\dfrac{df(S^*)}{dS}\right) s_0 - \left(\beta S^* + \dfrac{d\psi(I^*)}{dI} f(S^*)\right) i_0 \\ \qquad\qquad +(1-\theta) q_0(\tau), \\ \lambda i_0 = \beta I^* s_0 + (\beta S^* - \mu) i_0, \\ \lambda q_0(a) + q_0'(a) = -\mu q_0(a), \\ q_0(0) = \psi(I^*)\dfrac{df(S^*)}{dS} s_0 + \dfrac{d\psi(I^*)}{dI} f(S^*) i_0 + \theta q_0(\tau). \end{cases}$$

The equation on q_0 can be solved analytically and we have the exact solution

$$q_0(a) = e^{-(\lambda+\mu)a} q_0(0).$$

This leads to the following linear system

$$\begin{cases} \left(\lambda + \mu + \beta I^* + \psi(I^*)\dfrac{df(S^*)}{dS}\right) s_0 + \left(\beta S^* + \dfrac{d\psi(I^*)}{dI} f(S^*)\right) i_0 \\ \qquad\qquad -(1-\theta) e^{-(\lambda+\mu)\tau} q_0(0) = 0, \\ -\beta I^* s_0 + (\lambda - \beta S^* + \mu) i_0 = 0, \\ -\psi(I^*)\dfrac{df(S^*)}{dS} s_0 - \dfrac{d\psi(I^*)}{dI} f(S^*) i_0 + (1 - \theta e^{-(\lambda+\mu)\tau}) q_0(0) = 0. \end{cases}$$

This system can be written with a matrix of the form $A(s_0, i_0, q_0(0))^T = 0$, where

$$A = \begin{pmatrix} \lambda + \mu + \beta I^* + \psi(I^*)\dfrac{df(S^*)}{dS} & \beta S^* + \dfrac{d\psi(I^*)}{dI} f(S^*) & -(1-\theta)e^{-(\lambda+\mu)\tau} \\ -\beta I^* & \lambda - \beta S^* + \mu & 0 \\ -\psi(I^*)\dfrac{df(S^*)}{dS} & -\dfrac{d\psi(I^*)}{dI} f(S^*) & 1 - \theta e^{-(\lambda+\mu)\tau} \end{pmatrix}.$$

Then, the characteristic equation is

$$\det(A) = 0,$$

where $\det(A)$ is the determinant of the matrix A. We treat the two steady-states separately.

3.4.1 Disease-free equilibrium: $\mathcal{E}_0 := (\Lambda/\mu, 0, 0)$

For this case, we have to write and study the characteristic equation for $\mathcal{E}_0 := (\Lambda/\mu, 0, 0)$.

Theorem 3.2. *Assume that $\mathcal{R}_0 < 1$. Then, $\mathcal{E}_0 := (\Lambda/\mu, 0, 0)$ is the only steady-state and is locally asymptotically stable. If $\mathcal{R}_0 > 1$, then the disease-free steady-state $\mathcal{E}_0 := (\Lambda/\mu, 0, 0)$ is unstable.*

Proof. The characteristic equation is given, for $\mathcal{E}_0$, by

$$\begin{vmatrix} \lambda + \mu & \beta S^* + \dfrac{d\psi(0)}{dI} f\left(\frac{\Lambda}{\mu}\right) & -(1-\theta)e^{-(\lambda+\mu)\tau} \\ 0 & \lambda - \frac{\beta\Lambda - \mu^2}{\mu} & 0 \\ 0 & \dfrac{d\psi(0)}{dI} f\left(\frac{\Lambda}{\mu}\right) & -1 + \theta e^{-(\lambda+\mu)\tau} \end{vmatrix} = 0.$$

This is equivalent to

$$(\lambda+\mu)\left(\lambda-\frac{\beta\Lambda-\mu^2}{\mu}\right)\left(-1+\theta e^{-(\lambda+\mu)\tau}\right)=0.$$

Then, we have three eigenvalues

$$-\mu<0, \qquad \mu\left(\mathcal{R}_0-1\right), \qquad \frac{1}{\tau}\ln(\theta)-\mu<0.$$

We easily conclude on the local asymptotic stability of the disease-free equilibrium.

- If $\mathcal{R}_0<1$, then the disease-free equilibrium $\mathcal{E}_0$ is locally asymptotically stable.
- If $\mathcal{R}_0>1$, then the disease-free equilibrium $\mathcal{E}_0$ is unstable.

□

3.4.2 Global asymptotic stability of $\mathcal{E}_0 := (\Lambda/\mu, 0, 0)$

Global attractivity of $\mathcal{E}_0$ may be seen with the following arguments. Note

$$\left(\liminf_{t\to+\infty} S(t), \limsup_{t\to+\infty} S(t)\right)=(S_\infty, S^\infty), \quad S_\infty\le S^\infty<+\infty,$$

and

$$\limsup_{t\to+\infty} I(t)=I^\infty<+\infty, \quad \limsup_{t\to+\infty} p(t,0)=p^\infty<+\infty.$$

By (3.3), we get $S^\infty<\Lambda/\mu+\epsilon$, where $\epsilon>0$ is arbitrarily small. Then, for a large time, the function $I(t)$ obeys the following inequality

$$\frac{dI(t)}{dt}\le\mu I(t)\left(\mathcal{R}_0-1+\frac{\epsilon\beta}{\mu}\right).$$

Therefore, for $\mathcal{R}_0<1$, $I(t)$ is decreasing for t large enough and tends to zero as t goes to $+\infty$, keeping in mind that ϵ is very small. Moreover, from the age structured equation of p (third equation of System (3.1)), when time is large, we

have $p(t,\tau) = e^{-\mu\tau}p(t-\tau,0)$. Then, using the fact that $\psi(0) = 0$, we obtain

$$p^\infty = \frac{\psi(I^\infty)f(S^\infty)}{1-\theta e^{-\mu\tau}} = 0.$$

We directly use Lemma 3.5 of [2] to prove that $p(t,0)$ tends to zero as t goes to $+\infty$. Using the fluctuation lemma (see Lemma A.14 of [42]), there exist two sequences $(t_n)_{n\in\mathbb{N}}$ and $(s_n)_{n\in\mathbb{N}}$ tending to infinity as n goes to infinity such that $S(t_n) \to S^\infty$, $S(s_n) \to S_\infty$, $\frac{dS(t_n)}{dt} \to 0$ and $\frac{dS(s_n)}{dt} \to 0$. We conclude from the equation of S (first equation of System (3.1)) that $S^\infty = S_\infty = \Lambda/\mu$. Consequently, we have the following theorem.

Theorem 3.3. *Assume that $\mathcal{R}_0 < 1$. Then, the disease-free steady-state $\mathcal{E}_0 := (\Lambda/\mu, 0, 0)$ is globally asymptotically stable.*

3.4.3 Persistence analysis

In this section, we examine the persistence of the solution of the system (3.1) (*i.e.*, when the solution remains positive) in the presence of an unstable disease-free steady-state. For technical reasons, we consider the reduced system (4.2) instead of the original system (3.1).
We prove the following lemma on the weak persistence of the disease.

Lemma 3.1. *Assume that $\mathcal{R}_0 > 1$. Then, there exists $\epsilon > 0$ such that*

$$\limsup_{t\to+\infty} I(t) > \epsilon,$$

for any initial condition $(S_0, I_0, \phi) \in \mathbb{R}^+ \times \mathbb{R}^{+*} \times C([-\tau, 0], \mathbb{R}^+)$ of the system (4.2).

Proof. Let us prove by contradiction that $\limsup_{t\to+\infty} I(t) > \epsilon$.
We assume that $\limsup_{t\to+\infty} I(t) \leq \epsilon$. Then, there exists a sufficiently large $t_\epsilon > 0$

such that $I(t) \leq \epsilon$, for all $t \geq t_\epsilon$. Therefore, we have for all $t \geq t_\epsilon$

$$\frac{dS(t)}{dt} \geq \Lambda - \mu S(t) - \beta\epsilon S(t) - \psi(\epsilon) f(S(t)).$$

If we set $\liminf_{t\to+\infty} S(t) = S_\infty$, then there exists a sequence $(t_k)_{k\in\mathbb{N}}$ tending to infinity as k tends to infinity such that $S(t_k) \to S_\infty$ and $S'(t_k) \to 0$. Necessarily, we have

$$S_\infty \geq F_\epsilon^{-1}(\Lambda), \qquad \text{with} \quad F_\epsilon(x) = \mu x + \beta\epsilon x + \psi(\epsilon) f(x), \qquad x \geq 0.$$

Remember that for $\epsilon = 0$, we have $F_0^{-1}(\Lambda) = S^0 = \Lambda/\mu$ and $\mathcal{R}_0 = \beta S^0/\mu$. Hence, by using $\mathcal{R}_0 > 1$, we can choose $\epsilon > 0$ and $\nu > 0$ sufficiently smalls such that

$$\mathcal{R}_0^\epsilon := \frac{\beta S_\epsilon^0}{\nu + \mu} > 1, \qquad \text{where} \quad S_\epsilon^0 := F_\epsilon^{-1}(\Lambda).$$

Multiplying the equation of $I(t)$ by $e^{-\nu t}$ and integrating from t_ϵ to $+\infty$, we obtain

$$0 > -e^{-\nu t_\epsilon} I(t_\epsilon) > \left[-(\nu + \mu) + \beta S_\epsilon^0\right] \int_{t_\epsilon}^{+\infty} e^{-\nu t} I(t) dt > 0.$$

This is a contradiction with the positivity of the solution. Hence, the conclusion of the lemma holds true. □

We now give the following result on the strong persistence of the disease, see [42]. We use the same idea as in the paper [9, the proof of Theorem 1].

Theorem 3.4. *Suppose that $\mathcal{R}_0 > 1$. There exists a positive constant $\epsilon_1 > 0$ such that $\liminf_{t\to+\infty} I(t) > \epsilon_1$, for any initial condition $(S_0, I_0, \phi) \in \mathbb{R}^+ \times \mathbb{R}^{+*} \times C([-\tau, 0], \mathbb{R}^+)$ of the system (4.2).*

Proof. By using the weak persistence proved in Lemma 3.1, we have

$$\limsup_{t\to+\infty} I(t) > \epsilon$$

for a given $\epsilon > 0$. This yields to the existence of an increasing sequence $(\eta_k)_{k\in\mathbb{N}}$, which is positive, with $\eta_k \to +\infty$ such that $I(\eta_k) > \epsilon$. Suppose by contradiction that for all $\tilde{\epsilon} \in (0, \epsilon]$ there exists an initial condition $(S_0, I_0, \phi) \in \mathbb{R}^+ \times \mathbb{R}^{+*} \times C([-\tau, 0], \mathbb{R}^+)$, such that

$$\liminf_{t\to+\infty} I(t) \leq \tilde{\epsilon}.$$

There exists a positive increasing sequence $(t_k)_{k\in\mathbb{N}}$ and a positive decreasing sequence $(t'_k)_{k\in\mathbb{N}}$ with $t_k > \eta_k$, $\lim_{k\to+\infty} t'_k = 0$ and

$$I(t_k) < t'_k < \tilde{\epsilon} \leq \epsilon. \tag{3.5}$$

Therefore, there exists a sequence $(\nu_k)_{k\in\mathbb{N}}$ where $\nu_k \in (\eta_k, t_k)$ such that

$$I(\nu_k) = \epsilon \text{ and } I(t) < \epsilon, \text{ for all } t \in (\nu_k, t_k). \tag{3.6}$$

Let $(I_k)_{k\in\mathbb{N}}$ and $(S_k)_{k\in\mathbb{N}}$ be the sequences such that $I_k := I(\nu_k) = \epsilon$ and $S_k := S(\nu_k) \in \mathbb{R}^+$. We point out that the sequence $(I_k)_{k\in\mathbb{N}}$ is constant and the sequence $(S_k)_{k\in\mathbb{N}}$ is uniformly bounded. Accordingly to the boundedness, there exist convergent subsequences of $(I_k)_{k\in\mathbb{N}}$ and $(S_k)_{k\in\mathbb{N}}$ (we keep the same notation for these two subsequences). Then, we have $I_k = \epsilon$ and $\lim_{k\to+\infty} S_k = l$, with $l \in \mathbb{R}^+$. Consider the following problem

$$v(t) = \begin{cases} \psi(\epsilon)f(l) + \theta e^{-\mu\tau} v(t-\tau), & t > 0, \\ \phi(t), & t \in [-\tau, 0]. \end{cases}$$

It admits a unique continuous solution v on $(0, +\infty)$, for any initial condition $\phi \in C([-\tau, 0], \mathbb{R}^+)$. Let $(u_k)_{k\in\mathbb{N}}$ be the functional sequence in $C([-\tau, 0], \mathbb{R}^+)$ defined by $u_k(\theta) := v(\nu_k + \theta)$, $\theta \in [-\tau, 0]$ with $\nu_k > \tau$ for k large enough. Without loss of generality, we can consider $\nu_k > \tau$, for all $k \in \mathbb{N}$. Thus,

$$u_k(\theta) = \psi(\epsilon)f(l) + \theta e^{-\mu\tau} u_k(\theta - \tau), \quad \text{for all } \theta \in [-\tau, 0].$$

Clearly, we have the uniform boundedness of the sequence $(u_k)_{k\in\mathbb{N}}$. By taking $\alpha, \alpha' \in [-\tau, 0]$, we have

$$\begin{aligned}
|u_k(\alpha) - u_k(\alpha')| &= \theta e^{-\mu\tau} \left|u_k(\alpha-\tau) - u_k(\alpha'-\tau)\right|, \\
&\leq \left(\theta e^{-\mu\tau}\right)^{n_k+1} \left|\phi(\nu_k+\alpha-(n_k+1)\tau) - \phi(\nu_k+\alpha'-(n_k+1)\tau)\right|, \\
&\leq \left|\phi(\nu_k+\alpha-(n_k+1)\tau) - \phi(\nu_k+\alpha'-(n_k+1)\tau)\right|,
\end{aligned}$$

where $n_k := \lfloor \nu_k/\tau \rfloor$. By the fact that ϕ is uniformly continuous on $[-\tau, 0]$, then the last inequality implies that the sequence $(u_k)_{k\in\mathbb{N}}$ is equicontinuous. It follows from the Ascoli-Arzela theorem that there exists a convergent subsequence of $(u_k)_{k\in\mathbb{N}}$ (we denote it again $(u_k)_{k\in\mathbb{N}}$). Then, $\lim_{k\to+\infty} u_k = u^*$ and $u^* \in C([-\tau, 0], \mathbb{R}^+)$.

We consider now the solution, denoted $(S^\infty, I^\infty, u^\infty)$, of System (4.2), with the initial condition $S_0 = l$, $I_0 = \epsilon$ and $\phi = u^* \in C([-\tau, 0], \mathbb{R}^+)$. From Lemma 3.1, there exists $\varrho > 0$ and we can find $0 < m < \epsilon$, such that

$$I^\infty(\varrho) > \epsilon \quad \text{and} \quad I^\infty(t) > m, \quad \text{for all } t \in (0, \varrho). \tag{3.7}$$

Now, we are going to prove that a contradiction occurs. For each $k \in \mathbb{N}$, we put $\tilde{I}_k(t) := I(\nu_k + t)$, $t > 0$. From (3.7), the continuity and the fact that

$$\tilde{I}_k(0) = I_k = \epsilon, \qquad \lim_{k\to+\infty} S_k = l \quad \text{and} \quad \lim_{k\to+\infty} u_k = u^*,$$

we have, for k large enough and by $\lim_{k\to+\infty} t'_k = 0$,

$$\tilde{I}_k(\varrho) > \epsilon \quad \text{and} \quad \tilde{I}_k(t) > m > t'_k, \quad \text{for all } t \in (0, \varrho). \tag{3.8}$$

In a parallel way, by putting $\tilde{t}_k := t_k - \nu_k$, we have from (3.5) and (3.6) that

$$\tilde{I}_k(\tilde{t}_k) = I(t_k) < t'_k < \epsilon \quad \text{and} \quad \tilde{I}_k(t) = I(\nu_k + t) < \epsilon, \quad \text{for all } t \in (0, \tilde{t}_k). \tag{3.9}$$

We distinguish the following cases:

- If $\varrho < \tilde{t}_k$, then the second inequality of (3.9) which gives $\tilde{I}_k(\varrho) < \epsilon$ and the first inequality of (3.8) are in contradiction.
- If $\varrho = \tilde{t}_k$, then the first inequality of (3.8) and the first inequality of (3.9) are in contradiction.
- If $\tilde{t}_k < \varrho$, then the second inequality of (3.8) which gives $\tilde{I}_k(\tilde{t}_k) > t'_k$ and the first inequality of (3.9) are in contradiction.

Consequently, there exists $\tilde{\epsilon} \in (0, \epsilon]$ such that for any initial condition $(S_0, I_0, \phi) \in \mathbb{R}^+ \times \mathbb{R}^{+*} \times C([-\tau, 0], \mathbb{R}^+)$, we have

$$\liminf_{t \to +\infty} I(t) > \tilde{\epsilon}.$$

□

This result suggests that given a set of parameters where the basic reproduction number $\mathcal{R}_0 > 1$, the number of infected will not die out by itself, and the disease will become endemic. The number of infected will always be greater than a strictly positive constant ϵ. Thus, any outbreak related to the disease will last in time because there is always infection. PrEP is then effective by reducing the reproduction number and has an impact on the persistence of the disease.

3.4.4 The dynamical behavior of the endemic steady state

Let us focus now on the stability of the endemic steady-state. Suppose that $\tau > 0$. We have

$$\begin{aligned} S^* &= \frac{\mu}{\beta}, \\ \mathcal{H}(I^*) :&= \frac{\beta\Lambda}{\mu^2 + \beta\mu I^* + \left[\dfrac{\beta(1-e^{-\mu\tau})}{1-\theta e^{-\mu\tau}}\right]\psi(I^*)f\left(\dfrac{\mu}{\beta}\right)} = 1, \\ p^*(a) &= \frac{e^{-\mu a}}{1-\theta e^{-\mu\tau}}\psi(I^*)f\left(\frac{\mu}{\beta}\right). \end{aligned}$$

Then, the characteristic equation is given by $\det(A) = 0$, where the determinant of the matrix A is

$$\det(A) = \begin{vmatrix} \lambda+\mu+\beta I^* + \psi(I^*)\dfrac{df(S^*)}{dS} & \beta S^* + \dfrac{d\psi(I^*)}{dI}f(S^*) & -(1-\theta)e^{-(\lambda+\mu)\tau} \\ -\beta I^* & \lambda - \beta S^* + \mu & 0 \\ -\psi(I^*)\dfrac{df(S^*)}{dS} & -\dfrac{d\psi(I^*)}{dI}f(S^*) & 1-\theta e^{-(\lambda+\mu)\tau} \end{vmatrix}.$$

To simplify the expression of the determinant, we add the three lines to the first line and we obtain

$$\begin{vmatrix} \lambda+\mu & \lambda+\mu & 1-e^{-(\lambda+\mu)\tau} \\ -\beta I^* & \lambda-\beta S^*+\mu & 0 \\ -\psi(I^*)\dfrac{df(S^*)}{dS} & -\dfrac{d\psi(I^*)}{dI}f(S^*) & 1-\theta e^{-(\lambda+\mu)\tau} \end{vmatrix} = 0.$$

This implies the following factorization

$$(\lambda+\mu)\begin{vmatrix} 1 & 1 & \dfrac{1-e^{-(\lambda+\mu)\tau}}{\lambda+\mu} \\ -\beta I^* & \lambda-\beta S^*+\mu & 0 \\ -\psi(I^*)\dfrac{df(S^*)}{dS} & -\dfrac{d\psi(I^*)}{dI}f(S^*) & 1-\theta e^{-(\lambda+\mu)\tau} \end{vmatrix} = 0.$$

Remark that the following limit is finite

$$\lim_{\lambda\to-\mu}\frac{1-e^{-(\lambda+\mu)\tau}}{\lambda+\mu} = \tau \neq 0.$$

Therefore, $\lambda = -\mu < 0$ is a root of the characteristic equation. Other roots verify

$$\begin{vmatrix} 1 & 0 & \dfrac{1-e^{-(\lambda+\mu)\tau}}{\lambda+\mu} \\ -\beta I^* & \lambda-\beta(S^*-I^*)+\mu & 0 \\ -\psi(I^*)\dfrac{df(S^*)}{dS} & \psi(I^*)\dfrac{df(S^*)}{dS}-\dfrac{d\psi(I^*)}{dI}f(S^*) & 1-\theta e^{-(\lambda+\mu)\tau} \end{vmatrix} = 0.$$

By observing that $\beta S^* - \mu = 0$, we develop the determinant following the first line

$$(\lambda+\beta I^*)\left(1-\theta e^{-(\lambda+\mu)\tau}\right)$$

$$+\frac{1-e^{-(\lambda+\mu)\tau}}{\lambda+\mu}\begin{vmatrix} -\beta I^* & \lambda+\beta I^* \\ -\psi(I^*)\dfrac{df(S^*)}{dS} & \psi(I^*)\dfrac{df(S^*)}{dS}-\dfrac{d\psi(I^*)}{dI}f(S^*) \end{vmatrix} = 0.$$

This implies that

$$\begin{aligned}
&(\lambda+\beta I^*)\left(1-\theta e^{-(\lambda+\mu)\tau}\right)\\
&+\frac{1-e^{-(\lambda+\mu)\tau}}{\lambda+\mu}\left(-\beta I^*(\psi(I^*)\frac{df(S^*)}{dS}-\frac{d\psi(I^*)}{dI}f(S^*))\right)\\
&+\frac{1-e^{-(\lambda+\mu)\tau}}{\lambda+\mu}\left(\psi(I^*)\frac{df(S^*)}{dS}(\lambda+\beta I^*)\right)=0.
\end{aligned}$$

To simplify the notations, we note

$$\begin{aligned}
b &:= \beta I^*\frac{d\psi(I^*)}{dI}f(S^*)>0,\\
c &:= \psi(I^*)\frac{df(S^*)}{dS}>0.
\end{aligned}$$

With these notations, we define the function $\mathcal{F}$ by

$$\mathcal{F}(\lambda) := (\lambda+\mu)(\lambda+\beta I^*)\left(1-\theta e^{-(\lambda+\mu)\tau}\right)+(c\lambda+b)\left(1-e^{-(\lambda+\mu)\tau}\right)=0. \quad (3.10)$$

We easily prove that $\mathcal{F}$ is strictly increasing on $[0,+\infty)$ due to the positive parameters. Moreover, we have

$$\lim_{\lambda\to+\infty}\mathcal{F}(\lambda)=+\infty.$$

Furthermore,

$$\mathcal{F}(0)=\mu\beta I^*\left(1-\theta e^{-\mu\tau}\right)+(1-e^{-\mu\tau})b>0.$$

Then, the function $\mathcal{F}$ has no positive real root. We also remark

$$\mathcal{F}(\lambda) := \left(1-\theta e^{-(\lambda+\mu)\tau}\right)(c\lambda+b)\left[\frac{(\lambda+\mu)(\lambda+\beta I^*)}{c\lambda+b}+\frac{1-e^{-(\lambda+\mu)\tau}}{1-\theta e^{-(\lambda+\mu)\tau}}\right],$$

with

$$\lim_{\lambda\to-\infty}\frac{1-e^{-(\lambda+\mu)\tau}}{1-\theta e^{-(\lambda+\mu)\tau}}=\frac{1}{\theta}.$$

Then,

$$\lim_{\lambda \to -\infty} \mathcal{F}(\lambda) = -\infty.$$

This means there is a negative real root and all real roots are negative.

- Case $\tau = 0$: the characteristic equation is simplified to

$$\mathcal{F}(\lambda) := (\lambda + \mu)(\lambda + \beta I^*)(1 - \theta) = 0.$$

It has two roots $\lambda = -\mu < 0$ and $\lambda = -\beta I^* < 0$ which are negative. This implies that the endemic steady-state is locally asymptotically stable.

- Case $\tau > 0$: we need to go further in our analysis and investigate the behavior of complex roots. Before that, we check that there is no infinite sequence of complex roots $\{\lambda_n\}_n$ with strict positive real parts. We suppose by contradiction that there exists a sequence of roots $\{\lambda_n\}_n$ with

$$\lim_{n \to +\infty} |\lambda_n| = +\infty.$$

In this case, every λ_n satisfies

$$\left(1 + \frac{\beta I^*}{\lambda_n}\right)\left(1 - \theta e^{-(\lambda_n + \mu)\tau}\right) + \frac{1 - e^{-(\lambda_n + \mu)\tau}}{\lambda_n + \mu}\left(c + \frac{b}{\lambda_n}\right) = 0.$$

By taking the limit for $n \to \infty$, we obtain

$$\lim_{n \to \infty} \left(1 - \theta e^{-(\lambda_n + \mu)\tau}\right) = 0.$$

This implies that

$$\lim_{n \to \infty} e^{\Re(\lambda_n)\tau} = \theta e^{-\mu\tau}.$$

Therefore

$$\lim_{n\to\infty} \Re(\lambda_n) = \frac{1}{\tau}\ln\left(\theta e^{-\mu\tau}\right) = \frac{1}{\tau}\ln(\theta) - \mu < 0.$$

Then, the roots have negative real parts. At this step, we conclude with the following proposition.

Proposition 3.1. *There exists some $\tau_0^* > 0$ such that for $\tau \in [0, \tau_0^*)$ all characteristic roots have negative real parts.*

Next, we prove the existence or non-existence of complex roots with positive real parts.

- Case $\tau = 0$: we first notice again the non-existence of such roots.

- Case $\tau > 0$: we prove the non-existence or the existence of pure complex roots of the form iw, with $w > 0$. We rewrite the equation (3.10) as, for $\lambda \in \mathbb{C}$,

$$\begin{aligned} \mathcal{F}(\lambda) := \quad & \lambda^2 + (\beta I^* + \mu + c)\lambda + \mu\beta I^* + b \\ & -e^{-(\lambda+\mu)\tau}\left[\theta\lambda^2 + (\theta\beta I^* + \theta\mu + c)\lambda + \theta\mu\beta I^* + b\right] = 0. \end{aligned} \tag{3.11}$$

For $\lambda = iw$ and by separating the real and the imaginary part in (3.11), we get

$$\begin{cases} A\cos(w\tau) - Bw\sin(w\tau) = w^2 - \mu\beta I^* - b, \\ Bw\cos(w\tau) + A\sin(w\tau) = w(\beta I^* + \mu + c), \end{cases}$$

where

$$A = e^{-\mu\tau}[\theta w^2 - \theta\mu\beta I^* - b] \quad \text{and} \quad B = e^{-\mu\tau}[\theta\beta I^* + \theta\mu + c].$$

It follows that

$$\begin{cases} \cos(w\tau) = \dfrac{A(w^2 - \mu\beta I^* - b) + w^2 B(\beta I^* + \mu + c)}{A^2 + (Bw)^2}, \\ \sin(w\tau) = \dfrac{wA(\beta I^* + \mu + c) - Bw(w^2 - \mu\beta I^* - b)}{A^2 + (Bw)^2}. \end{cases} \tag{3.12}$$

Then, we get

$$A^2 + w^2 B^2 = (w^2 - \mu\beta I^* - b)^2 + w^2(\beta I^* + \mu + c)^2.$$

Hence, it implies that w must be a root of the following equation

$$\begin{aligned} (1 - (\theta e^{-\mu\tau})^2)w^4 + (-2(\mu\beta I^* + b) + 2\theta e^{-2\mu\tau}(\theta\mu\beta I^* + b) + \vartheta(\tau))w^2 & \\ +(\mu\beta I^* + b)^2 - e^{-2\mu\tau}(\theta\mu\beta I^* + b)^2 &= 0, \end{aligned}$$

where $\vartheta(\tau) := (\beta I^* + \mu + c)^2 - e^{-2\mu\tau}(\theta\beta I^* + \mu\theta + c)^2 \geq 0$. We note $X = w^2$ and analyze a second-degree polynomial function for $X \geq 0$. If $(-2(\mu\beta I^* + b) + 2\theta e^{-2\mu\tau}(\theta\mu\beta I^* + b) + \vartheta(\tau))$ is nonnegative for $\tau \in [0, \tau_1^*)$ with $\tau_1^* > 0$, then the Routh-Hurwitz criterion implies that no positive real roots exist. So, we have the following property.

Proposition 3.2. *Assume that $\mathcal{R}_0 > 1$ and $\vartheta(\tau) \geq \vartheta^*(\tau) := 2(\mu\beta I^* + b) - 2\theta e^{-2\mu\tau}(\theta\mu\beta I^* + b)$ for all $\tau \in [0, \tau_1^*)$ with $\tau_1^* > 0$. Then, the endemic steady-state $\mathcal{E}^* := (S^*, I^*, p^*(a))$ is locally asymptotically stable for $\tau \in [0, \tau_1^*)$.*

To illustrate the previous proposition, we give the following two examples associated with the bilinear case and a saturated case with a function as in [3] which is more realistic.

Example 3.1. Let ψ and f be given by

$$\psi(I) = l_1 I, \qquad f(S) = l_2 S, \quad \text{with} \quad l_1, l_2 > 0.$$

This set-up would describe a population of small size or living in a rich country where no competition effect would occur when individuals are seeking treatment. The choice of the function ψ means that recruitment is motivated by the number of infected with no restriction from political or economic decisions.
We note $l := l_1 l_2$. The condition $\vartheta(\tau) \geq 2(\mu\beta I^* + b) - 2\theta e^{-2\mu\tau}(\theta\mu\beta I^* + b)$ is always true for any $\tau \geq 0$. Then, the endemic equilibrium is always asymptotically stable (see Figure 3.2). In fact, in this case, we have

$$c := \psi(I^*)\frac{df(S^*)}{dS} = lI^* \quad \text{and} \quad b := \beta I^* \frac{d\psi(I^*)}{dI} f(S^*) = \mu l I^* = \mu c.$$

Therefore, we get

$$\begin{aligned}
\vartheta(\tau) - \vartheta^*(\tau) &= (\beta I^* + \mu + c)^2 - e^{-2\mu\tau}(\theta\beta I^* + \mu\theta + c)^2 \\
&\quad - 2(\mu\beta I^* + \mu c) - 2\theta e^{-2\mu\tau}(\theta\mu\beta I^* + \mu c), \\
&= [(\beta + l)^2 - e^{-2\mu\tau}(\theta\beta + l)^2](I^*)^2 + \mu^2(1 - \theta^2 e^{-2\mu\tau}), \\
&\geq 0.
\end{aligned}$$

Thus, the endemic steady-state $\mathcal{E}^* := (S^*, I^*, p^*(a))$ is locally asymptotically stable for $\tau \geq 0$.
Example 3.2. Let ψ and f given by

$$\psi(I) = \frac{a_I I}{b_I + I}, \qquad f(S) = a_S S, \quad \text{with} \quad a_I, a_S, b_I > 0.$$

The choice of function would describe a saturation effect in recruitment due to a high number of infected. It would describe an outbreak in a very specific population where the ones targeted by PrEP and the very persons supposed to begin treatment are unable as they are infected.

We check that the condition $\vartheta(\tau) \geq 2(\mu\beta I^* + b) - 2\theta e^{-2\mu\tau}(\theta\mu\beta I^* + b)$ is always true

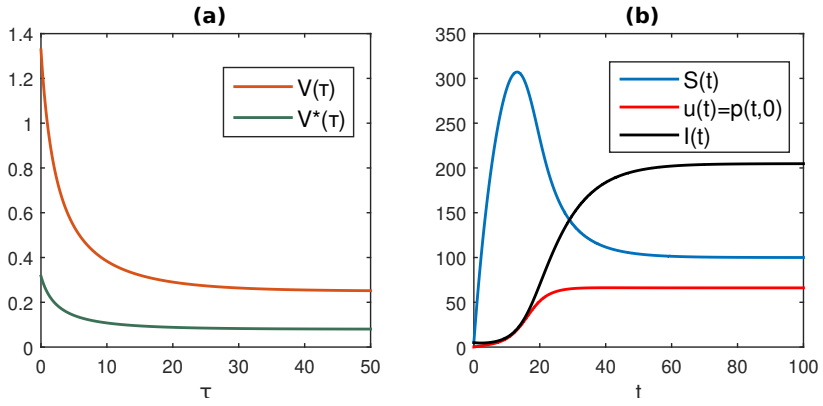


Figure 3.2: Left: we observe that the condition $\vartheta(\tau) \geq \vartheta^*(\tau)$ of Proposition 4.3 is satisfied for the selected parameters. Right: a simulation is carried out for the stability of the endemic equilibrium. Parameters are $\Lambda = 50$, $\mu = 0.1$, $\beta = 0.001$, $\theta = 0.1$, $l_1 = 0.01$, $l_2 = 0.3$ and $\tau = 3.5$. In this case $\mathcal{R}_0 = 5 > 1$.

for any $\tau \geq 0$ (see Figure 3.3). In this case, we have

$$c := \psi(I^*)\frac{df(S^*)}{dS} = \frac{a_S a_I}{b_I + I^*} I^* =: l(I^*)I^*$$

and

$$b := \mu L(I^*)c, \qquad \text{where} \quad L(I^*) := \frac{b_I}{b_I + I^*} < 1.$$

After an easy computation, we get

$$\begin{aligned}
\vartheta(\tau) - \vartheta^*(\tau) &= (\beta I^* + \mu + c)^2 - e^{-2\mu\tau}(\theta\beta I^* + \mu\theta + c)^2 \\
&\quad - 2(\mu\beta I^* + \mu L(I^*)c) - 2\theta e^{-2\mu\tau}(\theta\mu\beta I^* + \mu L(I^*)c), \\
&= [(\beta + l(I^*))^2 - e^{-2\mu\tau}(\theta\beta + l(I^*))^2](I^*)^2 + \mu^2(1 - \theta^2 e^{-2\mu\tau}) \\
&\quad + 2\mu l(I^*)I^*(1 - L(I^*))(1 - \theta e^{-2\mu\tau}), \\
&\geq 0.
\end{aligned}$$

Consequently, the endemic steady-state $\mathcal{E}^* := (S^*, I^*, p^*(a))$ is locally asymptotically stable for $\tau \geq 0$.

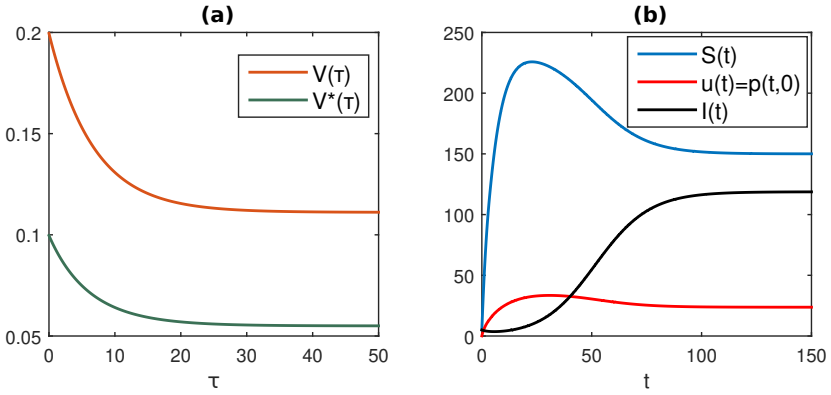


Figure 3.3: Left: we observe that the condition of Proposition 4.3 is satisfied for the selected parameters. Right: a simulation is carried out for the stability of the endemic equilibrium. Parameters are $\Lambda = 50$, $\mu = 0.15$, $\beta = 0.001$, $\theta = 0.1$, $a_S = 0.3$, $a_I = 0.5$, $b_I = 1$ and $\tau = 3.5$. In this case $\mathcal{R}_0 = 2.22 > 1$.

Next, we suppose that $\vartheta(\tau) < \vartheta^*(\tau) = 2(\mu\beta I^* + b) - 2\theta e^{-2\mu\tau}(\theta\mu\beta I^* + b)$ for some $\tau > 0$. After tedious calculations, the discriminant is given by

$$\Delta(\vartheta(\tau)) = \vartheta^2(\tau) - 4[(\mu\beta I^* + b) - \theta e^{-2\mu\tau}(\theta\mu\beta I^* + b)]\vartheta(\tau)$$
$$+[2e^{-\mu\tau}\theta(\mu\beta I^* + b) - 2e^{-\mu\tau}(\theta\mu\beta I^* + b)]^2.$$

Furthermore, the discriminant of the last polynomial of the second degree is

$$\begin{aligned}\bar{\Delta} &= 16[(1 + \theta e^{-\mu\tau})(\mu\beta I^* + b) - (\theta e^{-2\mu\tau} + e^{-\mu\tau})(\theta\mu\beta I^* + b)] \\ &\quad \times[(1 - \theta e^{-\mu\tau})(\mu\beta I^* + b) - (\theta e^{-2\mu\tau} - e^{-\mu\tau})(\theta\mu\beta I^* + b)], \\ &\geq 0.\end{aligned}$$

Define

$$\vartheta_-(\tau) := 2[(\mu\beta I^* + b) - \theta e^{-2\mu\tau}(\theta\mu\beta I^* + b)] - \frac{\sqrt{\bar{\Delta}}}{2} \geq 0.$$

Clearly, the discriminant $\Delta(\vartheta(\tau))$ is either negative for $\vartheta_-(\tau) < \vartheta(\tau) < \vartheta^*(\tau)$ or nonnegative for $0 \leq \vartheta(\tau) \leq \vartheta_-(\tau)$.

Proposition 3.3. *Assume that $\mathcal{R}_0 > 1$ and $\vartheta_-(\tau) < \vartheta(\tau) < \vartheta^*(\tau)$ for all $\tau \in [0, \tau_2^*)$ with $\tau_2^* > 0$. Then, the endemic steady-state $\mathcal{E}^* := (S^*, I^*, p^*(a))$ is locally asymptotically stable for $\tau \in [0, \tau_2^*)$.*

Now, we focus on the case where $0 \leq \vartheta(\tau) \leq \vartheta_-(\tau)$ for some $\tau > 0$ (see example given in Figure 3.4). Then, there are two possible roots $w_\pm(\tau)$ given by

$$w_-(\tau) = \left[\frac{-(-2(\mu\beta I^* + b) + 2\theta e^{-2\mu\tau}(\theta\mu\beta I^* + b) + \vartheta(\tau)) - \sqrt{\Delta(\vartheta(\tau))}}{2(1 - (\theta e^{-\mu\tau})^2)}\right]^{\frac{1}{2}},$$

and

$$w_+(\tau) = \left[\frac{-(-2(\mu\beta I^* + b) + 2\theta e^{-2\mu\tau}(\theta\mu\beta I^* + b) + \vartheta(\tau)) + \sqrt{\Delta(\vartheta(\tau))}}{2(1 - (\theta e^{-\mu\tau})^2)}\right]^{\frac{1}{2}}.$$

From (4.27), we define the angles $\Theta_\pm(\tau) \in [0, 2\pi]$ solution of

$$\begin{cases} \cos(\Theta_\pm(\tau)) = \dfrac{A(w_\pm^2(\tau) - \mu\beta I^* - b) + w_\pm^2(\tau)B(\beta I^* + \mu + c)}{A^2 + (Bw_\pm(\tau))^2}, \\ \sin(\Theta_\pm(\tau)) = \dfrac{w_\pm(\tau)A(\beta I^* + \mu + c) - Bw_\pm(\tau)(w_\pm^2(\tau) - \mu\beta I^* - b)}{A^2 + (Bw_\pm(\tau))^2}. \end{cases}$$

We get $w_\pm(\tau)\tau = \Theta_\pm(\tau) + 2k\pi$ with $k \in \mathbb{N}$. A deep analysis of the existence of such

angles can be referred to [32]. We also get

$$\Theta_{\pm}(\tau) = \arctan(H_1(\tau)/H_2(\tau)), \quad \text{if} \quad \sin(\Theta_{\pm}(\tau)) > 0, \quad \cos(\Theta_{\pm}(\tau)) > 0,$$

$$\Theta_{\pm}(\tau) = \pi/2, \quad \text{if} \quad \sin(\Theta_{\pm}(\tau)) = 1, \quad \cos(\Theta_{\pm}(\tau)) = 0,$$

$$\Theta_{\pm}(\tau) = \pi + \arctan(H_1(\tau)/H_2(\tau)), \quad \text{if} \quad \cos(\Theta_{\pm}(\tau)) < 0,$$

$$\Theta_{\pm}(\tau) = 3\pi/2, \quad \text{if} \quad \sin(\Theta_{\pm}(\tau)) = -1, \quad \cos(\Theta_{\pm}(\tau)) = 0,$$

$$\Theta_{\pm}(\tau) = 2\pi + \arctan(H_1(\tau)/H_2(\tau)), \quad \text{if} \quad \sin(\Theta_{\pm}(\tau)) < 0, \quad \cos(\Theta_{\pm}(\tau)) > 0,$$

with

$$H_1(\tau) := w_{\pm}(\tau)A(\beta I^* + \mu + c) - Bw_{\pm}(\tau)(w_{\pm}^2(\tau) - \mu\beta I^* - b),$$

$$H_2(\tau) := A(w_{\pm}^2(\tau) - \mu\beta I^* - b) + w_{\pm}^2(\tau)B(\beta I^* + \mu + c).$$

We keep in mind that the endemic equilibrium exists for $\mathcal{R}_0 > 1$ and τ ranges on $\mathbb{R}^+$. To obtain a critical value of τ for the stability change, we define the following functions, for $k \in \mathbb{N}$,

$$\begin{aligned} T_k^{\pm} : \ \mathbb{R}^+ &\to \mathbb{R}, \\ \tau &\mapsto T_k^{\pm}(\tau) = \tau - \frac{\Theta_{\pm}(\tau) + 2k\pi}{w_{\pm}(\tau)}. \end{aligned}$$

Note that a pair of simple conjugate pure imaginary roots $\lambda = \pm iw(\tau^*)$ exist at τ^* if and only if τ^* is a root of T_k^+ or T_k^-, $k \in \mathbb{N}$. Then, the stability may switch at any root of $T_k^{\pm}$. We are now ready to conclude with the following theorem.

Theorem 3.5. *Let $\mathcal{R}_0 > 1$. If $T_k^{\pm}$ has no root on $\mathbb{R}^+$, for any $k \in \mathbb{N}$, then the endemic equilibrium is locally asymptotically stable for all $\tau \in \mathbb{R}^+$. If T_k^+ or T_k^- has at least one root in $\mathbb{R}^+$ and if we denote by τ^* the smallest root among all, then the*

endemic equilibrium is locally asymptotically stable for $\tau \in [0, \tau^*)$.

Example 3.3. Let ψ and f given by

$$\psi(I) = a_I I, \qquad f(S) = \frac{a_S S}{b_S + S}, \quad \text{with} \quad a_I, a_S, b_S > 0.$$

For this last example, the situation described would take place in a poor country or in a very large population where we would observe competition between individuals. For a given parameter, we check that the condition $0 \leq \vartheta(\tau) \leq \vartheta_-(\tau)$ is true for $\tau \in [0, 6]$ in Figure 3.4.

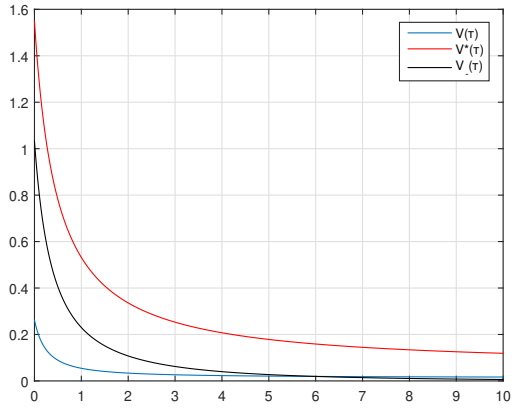


Figure 3.4: We observe that the condition $0 \leq \vartheta(\tau) \leq \vartheta_-(\tau)$ is satisfied for a selected parameters. Parameters are $\Lambda = 50$, $\mu = 0.1$, $\beta = 0.001$, $\theta = 0.1$, $a_S = 1$, $a_I = 2$, $b_S = 0.2$.

In this example, we remark that the functions $T_k^{\pm}$ plotted do not admit any roots and this is valid for all the values of the parameters. So, we conclude that the characteristic equation cannot have a purely imaginary root and therefore no destabilization of the endemic equilibrium is possible.

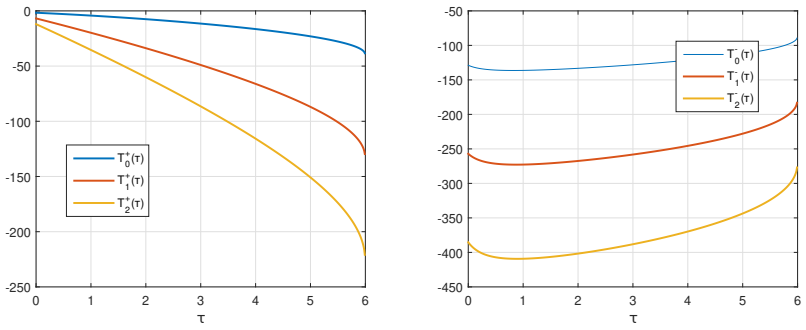


Figure 3.5:
]Functions $T_k^{\pm}$ are drawn for $\tau \in [0, 6]$. We observe that these functions exhibit no root in this interval where a possible purely imaginary root could exist. In this case, no possible Hopf bifurcation occurs. Parameters are $\Lambda = 50$, $\mu = 0.1$, $\beta = 0.001$, $\theta = 0.1$, $a_S = 1$, $a_I = 2$, $b_S = 0.2$.

3.5 Discussion

In this study, we concentrated on an epidemiological SI (Susceptible-Infected) model that characterizes HIV epidemics, with an additional external compartment denoted as P to represent Pre-Exposure Prophylaxis (PrEP) treatment. We assumed the P compartment to be age-structured, where age corresponds to the time elapsed since the last PrEP prescription. Our goal is to introduce a novel framework to assess the effects of PrEP on HIV transmission dynamics. Our approach builds upon prior models [95, 134, 135, 122], in which the initiation rate (ψ) of the protection phase remained constant. However, unlike these works, we now consider ψ to be dependent on the infected population I, emphasizing the influence of the HIV epidemic on the protection phase.

Employing the method of characteristics, we derived a coupled system of differential-difference equations with delay. We pinpointed two steady states – the disease-free equilibrium and the endemic equilibrium – and scrutinized their stability and existence using the classic criterion associated with the basic reproduction number $\mathcal{R}_0$. We confirmed the global asymptotic stability of the disease-free equilibrium and investigated the system's persistence when $\mathcal{R}_0 > 1$.

Remarkably, the basic reproduction number of the system reflects that of any standard SI model due to ψ being an I-dependent function, with the assumption $\psi(0) = 0$. This differs from a previous study [122], where ψ was assumed to be constant, resulting in a more complex expression for $\mathcal{R}_0$ involving delay dependence. Since ψ now varies with I, the disease-free equilibrium relies solely on the susceptible component, unlike in [122]. However, the equilibrium and its stability are affected by the delay. We demonstrated the weak persistence of the disease, leading to the proof of strong persistence. Subsequently, we analyzed the stability of the endemic state, uncovering various stability regions. While the case with zero delay is straightforward, the non-trivial case presents challenges, and we could not fully determine the occurrence of Hopf bifurcations.

We maintain that the occurrence of a Hopf bifurcation in this system is unlikely, supported by heuristic reasoning from the theory of monotone systems. However, further investigation is necessary to confirm this. It is important to note that the behavior of the recruitment function was based on pre-COVID-19 data, and the pandemic likely affected data collection and access to treatment services, including PrEP. Nevertheless, it appears that the recruitment rate has returned to pre-pandemic levels. Future research will focus on the impact of various policies, economic factors, and cultural influences from different countries on the evolution of the epidemic, as well as on the development of STIs. We have included numerical simulations to visually demonstrate the established stability conditions.

As far as we know, this study presents a more realistic depiction of PrEP's influence on new HIV cases and introduces fresh theoretical perspectives on stability. In essence, our approach offers a more efficient method of modeling the HIV epidemic, considering political and economic decisions regarding PrEP treatment for high-risk populations.

Chapter 4

Qualtitative impact of political and economic decisions on PrEP users under HIV epidemic control

4.1 Introduction

HIV (Human Immunodeficiency Virus) is a retrovirus that infects humans, leading to AIDS (Acquired Immunodeficiency Syndrome). AIDS represents the advanced stage of the infection, where the virus significantly reduces the number of CD4+ T-cells, causing immune system failure. This stage can be fatal if not treated. Typically, it develops between 5 and 10 years after initial infection, with an average survival time of 9.2 months [31]. Currently, there is no cure or vaccine for HIV, and treatment options become very limited once AIDS has developed. In 2022, UNAIDS reported between 33.1 million and 45.7 million people living with HIV worldwide. That same year, around 1.3 million people contracted the virus, and 630,000 deaths were due to AIDS-related illnesses [141]. This is still far from the target of maximum 200,000 new infections by 2030 [140].

HIV can be transmitted through various means, including unprotected sex, mother-

to-child transmission, and exposure to contaminated blood from activities like drug injections. Although prevention methods seem straightforward in theory, implementing them systematically in practice is challenging. One significant factor is that younger generations are less consistent in using condoms during sexual activity [**CACERES2008**], while older generations [65] often underestimate their risk of infection. Several initiatives are currently being implemented to address the ongoing HIV epidemic. One of them is the Pre-Exposure Prophylaxis also known as PrEP.
PrEP is a preventive treatment for individuals who are not HIV-positive but are at high-risk exposure through sexual activity involving several partners or injecting drug use. PrEP, which combines several antiretroviral drugs, is available in oral form. The treatment can be taken daily or on-demand, with the latter regimen involving intake approximately 2 hours before and up to 2 days after each sexual intercourse. This globally adopted approach has been proven highly effective, offering excellent protection against HIV transmission [57, 129]. PrEP users experience a significantly reduced risk of HIV infection for three months. However, as PrEP does not protect against other Sexually Transmitted Infections (STIs) [114], users are required to undergo STI screening after 3 months to renew their prescription. They can then choose to continue treatment or nor as they wish. When correctly implemented, PrEP significantly impacts HIV transmission rates [68, 70].
Political and economic decisions play a critical role in the uptake and availability of PrEP by shaping healthcare policies, funding mechanisms, and regulatory frameworks [61]. Government-led initiatives, such as national health insurance coverage and targeted public health programs, have been instrumental in reducing financial barriers and expanding access [126]. However, disparities persist due to decentralized healthcare systems, regional policy variations, and legal challenges to coverage mandates [100]. The cost of PrEP—historically influenced by pharmaceutical monopolies and patent protections—has been a significant determinant of accessibility, with the introduction of generics improving affordability in some settings. Despite evidence of PrEP's cost-effectiveness in HIV prevention, structural and logistical barriers, including provider restrictions and healthcare system fragmentation, continue to limit equitable distribution, particularly among marginalized populations [143].

A large variety of mathematical models have been developed to tackle complex questions surrounding HIV/AIDS conditions [5, 11]. Comprehensive reviews can be found in [102, 30, 6]. Over the years, delay differential equations have been extensively used in HIV immunology modeling [19, 22]. Additionally, other modeling techniques, such as stochastic models and agent-based models, have provided significant insights into the transmission dynamics and intervention strategies for HIV [26, 37]. These diverse approaches help to deepen the understanding of the disease and improve the effectiveness of public health interventions.

Our approach is based on the classic Kermack-Mckendrick SI model [1] with a protection compartment. We integrate an age-structured phase to describe the impact of PrEP. Other interventions are not considered in this work and should be considered in further works. The PrEP compartment is described by an age variable to assess the role of protection duration between prescription renewals every 3 months. To the best of our knowledge, this approach has been rarely described by mathematical models [122, 147, 135]. Individuals who remain protected during this period are modeled using an age-structured equation. The novelty of this model resides in the non-monotonic recruitment rate. Our approach is the following: we suppose that some government policies allow a free (or low fare) access to PrEP treatment to a targeted population at risk. However, as susceptible population increases and targeted population is exceeded, ressources may run out and healthcare system cannot provide for the whole population. For example, PrEP is fully accessible in France to people aged 15 and over who are at risk of sexual transmission. To take into account this phenomenon, we introduce h as a function of S the susceptible which is decreasing. The recruitement term for the PrEP compartment is then $h(S)S$ to highlight the effect of saturation reached when the population oversteps the maximum capacity of healthcare providers. The term $h(S)S$ is Holling type III modified [72]. It is representing ressources to keep PrEP uptake stable and sustain the adherence at an acceptable level.

Through this paper, we aim to explore the study of our SI model with protection phase and with a non-monotonic recruitment to this phase. The system is presented in Section 4.2. It is based on an age-structured partial differential equation with

a system of two ordinaries differential equations and reduced to a delayed coupled differential-difference system. In Section 4.3, we start by analyzing the system and the existence of equilibiria. The local asymptotic stability is treated for each equilibrium along the Section 4.4. Mainly, the stability of the unique endemic equilibrium is treated with a possible Hopf bifurcation. We finish this part by carrying out some numerical simulations to show the occurrence of oscillations. The last Section 4.5 is dedicated to discussion.

4.2 The SI model with protection

The mathematical model includes the two classic compartments: susceptible individuals $S(t)$ and infected individuals $I(t)$, to which we add a new compartment for protected individuals $P(t)$. We denote by $p(t, a)$ the age distribution of protected individuals, as introduced in [135]. Here, $t \geq 0$, $a \in [0, \tau)$, and $\tau > 0$. The variable a represents the time elapsed since the beginning of a new protection period following a prescription, and τ is the total duration of prescription validity. So, the total number of protected individuals at time t is

$$P(t) := \int_0^\tau p(t, a)da.$$

We aim to investigate the impact of potential economic and political decisions on PrEP uptake depending on the population level. PrEP is an expensive treatment that cannot be made available to everyone due to cost constraints. We assume that the recruitment rate depends only on the number of susceptible individuals and is denoted by $h(S)$.

The function h is assumed to be decreasing: at low population levels, a large number of individuals can initiate PrEP. A low population level may represent a high-risk profile for HIV, such as individuals with multiple sexual partners over a short period or people who use injectable drugs. However, initiating PrEP at the population level would occur at a lower rate due to limited stock and high treatment costs. Therefore,

we define

$$h(S)S = \frac{\gamma S}{K^2 + S^2}$$

as a unimodal function. The parameter γ represents the maximal effort according to ressources available. The parameter K represents the size of population targeted by PrEP.

A visual representation of the recruitment term given by $h(S)S$ is provided in Figure 4.1.

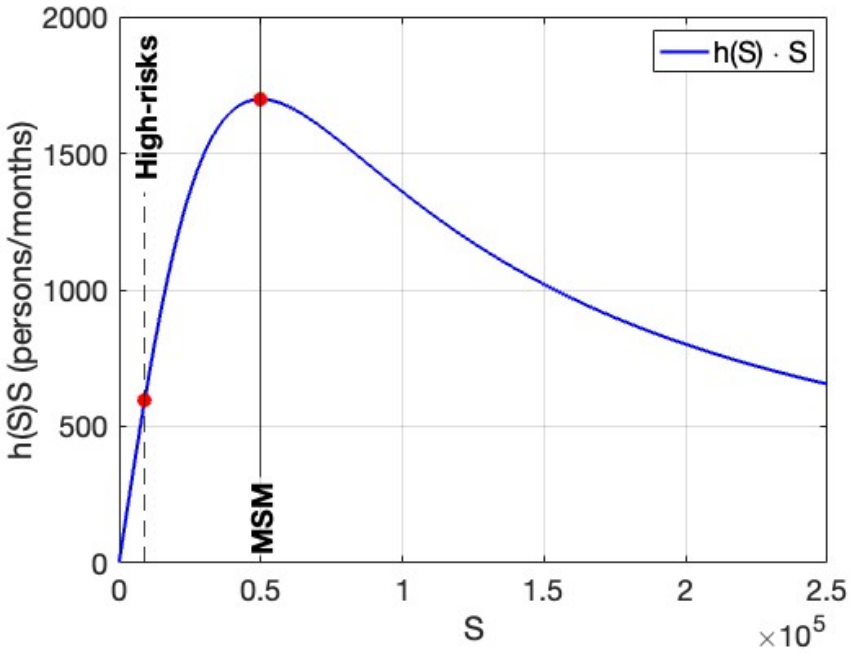


Figure 4.1: This figure provides an unofficial estimate of the reality, generated solely from [146]. It represents PrEP uptake in France in 2024 per unit of time with respect to population size. High-risk profiles are the primary targets of PrEP; dotted line; the recruitment is low because it is a subgroup of men who have sex with men (MSM). MSM; full line; recruitment is maximal, they represent 95 % of PrEP uptake in France [146]. As populations increases, monthly recruitment decreases to take into account logistic constraints.

The model is given by, for $t > 0$,

$$\begin{cases} S'(t) = \Lambda - (d + h(S(t)))S(t) - \beta S(t)I(t) + (1-\alpha)p(t,\tau), \\ I'(t) = \beta S(t)I(t) - (d+\mu)I(t), \\ \dfrac{\partial}{\partial t}p(t,a) + \dfrac{\partial}{\partial a}p(t,a) = -dp(t,a), \qquad 0 < a < \tau. \end{cases} \tag{4.1}$$

We consider a constant inflow of new susceptible represented by the parameter Λ. The definition of this parameter depends on the population studied. For the overall population, Λ represents the number of persons per months reaching their sexual majority. For MSM population, Λ represents individuals per months deciding to start at risk sexual intercourses like multi-partners or non-protected sexual intercourses. The parameter $\alpha \in [0, 1)$ represents probability to keep following the PrEP and renew treatment after the HIV and STD screening performed during the medical follow-up. The boundary condition is, for $t > 0$,

$$p(t, 0) = h(S(t))S(t) + \alpha p(t, \tau).$$

The first right-hand side term represents susceptible uptaking PrEP. The second right-hand side term denote protected individual who choose to renew their prescription. The system is combined with nonnegative initial conditions

$$S(0) = S_0, \;\; I(0) = I_0 \;\text{ and }\; p(0, a) = p_0(a), \quad 0 < a < \tau.$$

All the parameters of the model are nonnegative constants, and they are described in Table 4.1. Figure 4.2 provides a schematic representation of the epidemiological model.

In order to study the system, we use the method of characteristics, see for instance

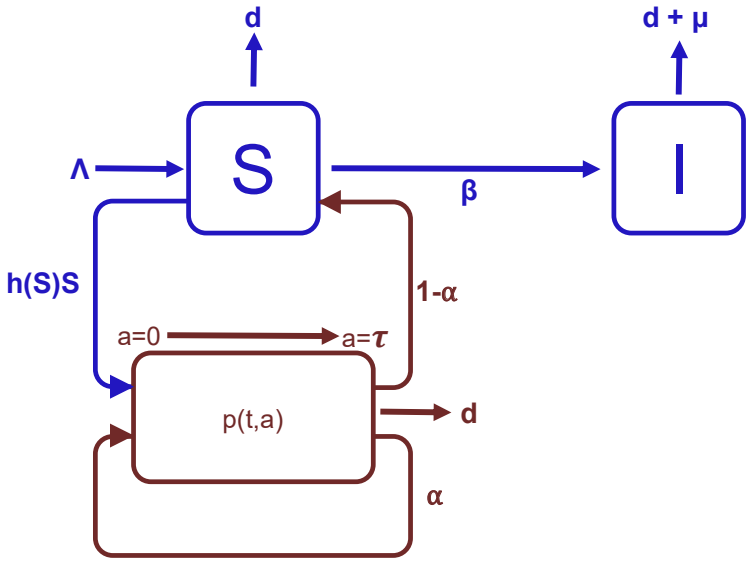


Figure 4.2: Flow diagram: the structure of the model is based on an SI-model (blue) in which we added an age-structured equation with nonmonotonic $h(s)$ recruitment rate.

[4], to reduce it to an appropriate one. We obtain, for $t > 0$ and $a \in [0, \tau]$,

$$p(t,a) = \begin{cases} e^{-dt} p(0, a-t) = e^{-dt} p_0(a-t), & 0 \le t \le a, \\ e^{-da} p(t-a, 0), & t > a. \end{cases}$$

We denote by $u(t) := p(t, 0)$, $t > \tau$, then, the expression of $p(t, a)$ becomes, for $t > \tau$ and $a \in [0, \tau]$,

$$p(t,a) = e^{-da} u(t-a).$$

Table 4.1: Parameters of the model and their description.

Parameter	**Description**	**Unit**
S, I, P	Number of individuals	Individuals
u	New individuals starting PrEP	Individuals $\cdot$ (time)$^{-1}$
t	Time	e.g., Days
Λ	Recruitment/immigration	Individuals $\cdot$ (time)$^{-1}$
$h(S)S$	PrEP uptake term	Individuals $\cdot$ (time)$^{-1}$
β	Infectious rate	(Indiv $\cdot$ time)$^{-1}$
d	Death rate and end of sexual life	(time)$^{-1}$
μ	Death rate induced by the disease	(time)$^{-1}$
α	Renewal rate ($0 \leq \alpha < 1$)	Dimensionless
τ	Temporary protection phase duration	Time

Consequently,

$$P(t) = \int_0^\tau e^{-da} u(t-a) da, \qquad t > \tau.$$

Finally, we obtain the following system, for $t > \tau$,

$$\begin{cases} S'(t) &= \Lambda - (d + h(S(t)))S(t) - \beta S(t) I(t) + (1-\alpha) e^{-d\tau} u(t-\tau), \\ I'(t) &= \beta S(t) I(t) - (d+\mu) I(t), \\ u(t) &= h(S(t)) S(t) + \alpha e^{-d\tau} u(t-\tau), \\ P(t) &= \int_0^\tau e^{-da} u(t-a) da. \end{cases}$$

By doing a translation in time ($t \mapsto t - \tau$), we can consider the initial conditions defined on $[-\tau, 0]$. Moreover, the equations of S, I and u are independent on P.

Then, we focus on the reduced system, for $t > 0$,

$$\begin{cases} S'(t) &= \Lambda - (d + h(S(t)))S(t) - \beta S(t)I(t) + (1-\alpha)e^{-d\tau}u(t-\tau), \\ I'(t) &= \beta S(t)I(t) - (d+\mu)I(t), \\ u(t) &= h(S(t))S(t) + \alpha e^{-d\tau}u(t-\tau), \end{cases} \tag{4.2}$$

which is completed by the initial conditions

$$S(0) = S_0, \;\; I(0) = I_0 \;\text{ and }\; u(t) = \phi(t), \;\; \text{for} \;\; -\tau \leq t \leq 0. \tag{4.3}$$

System (4.2)–(4.16) is known as a coupled system of differential and difference equations with discrete delay. The existence, uniqueness, positivity and regularity of the solution is easily proved by steps on the intervals $[m\tau, (m+1)\tau]$ with $m = 0, 1, 2, ...$, see [95] and the book [47]. The boundedness of solutions is also standard by considering the total population (see Theorem 2 of [135]).

4.3 Existence of equilibria

4.3.1 System without any infection

In the context of a nonlinear and nonmontonic recruitment term, the system presents quite rich dynamics. The difference equation on u does not depend on I. We choose to set $I = 0$ in (4.2) to focus on dynamics related to the recruitment rate in the system (4.3.1).
Let us first investigate the existence of the multiple equilibrium. In this paragraph,

we give the global study of the following system, for $t \geq 0$,

$$\begin{cases} S'(t) &= \Lambda - (d + h(S(t)))S(t) + (1-\alpha)e^{-d\tau}u(t-\tau), \\ u(t) &= h(S(t))S(t) + \alpha e^{-d\tau}u(t-\tau), \end{cases} \tag{4.4}$$

for which the initial conditions given by

$$S(0) = S_0 \text{ and } u(t) = \phi(t), \text{ for } -\tau \leq t \leq 0.$$

Depending on the parameter values, between one and three positive equilibrium can be exhibited. Indeed, if we consider any stationary state $(\overline{S}, \overline{I}, \overline{u})$, we have

$$\begin{cases} 0 &= \Lambda - (d + h(\overline{S}))\overline{S} + (1-\alpha)e^{-d\tau}\overline{u}, \\ \overline{u} &= h(\overline{S})\overline{S} + \alpha e^{-d\tau}\overline{u}. \end{cases}$$

As $0 \leq \alpha < 1$, we obtain:

$$\overline{u} = \frac{h(\overline{S})\overline{S}}{1 - \alpha e^{-d\tau}}.$$

Therefore, we get

$$0 = \Lambda - (d + h(\overline{S}))\overline{S} + (1-\alpha)e^{-d\tau}\frac{h(\overline{S})\overline{S}}{1 - \alpha e^{-d\tau}},$$

which can be written as follows:

$$Mh(\overline{S})\overline{S} = \Lambda - d\overline{S}, \qquad \text{where} \quad M := \frac{1 - e^{-d\tau}}{1 - \alpha e^{-d\tau}}.$$

Let us denote $f(S) := Mh(S)S$. Then, f is increasing then decreasing (see Figure 4.1) and allows us to deduce the existence of one to three equilibria, see Figure 4.3 . Let S_f^l and S_f^r, with $S_f^l < S_f^r$, be the solutions of the following system

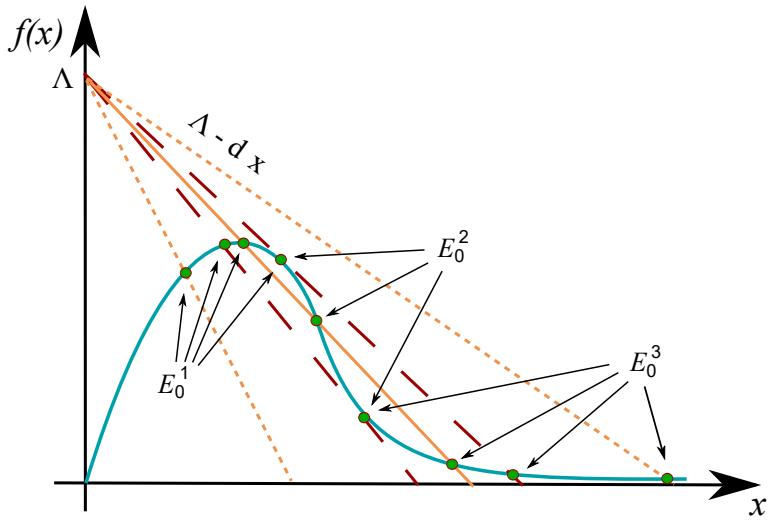


Figure 4.3: Representation for the possible intersections between the graph of f (in blue) and the straight line of equation $\Lambda - dx$ in orange. The intersections indicate the number of equilibria. As shown in Table 4.2, in each respective region: the solid line represents three intersections, the small dotted line represents one intersection, and the large dashed line represents two intersections.

$$\begin{cases} f(x) = \Lambda - dx, \\ \\ f'(x) = -d. \end{cases}$$

We denote by $d_{S_f^l} := -f'(S_f^l)$ and $d_{S_f^r} := -f'(S_f^r)$. Then

- If $d_{S_f^l} < d < d_{S_f^r}$, this ensures the existence of three equilibrium $E_0^i = (\overline{S}^i, \overline{u}^i) = (S_f^i, u_f^i)$, for $i = 1, 2, 3$, where

$$u_f^i = \frac{h(S_f^i)S_f^i}{1 - \alpha e^{-d\tau}}.$$

- If $d < d_{S_f^l}$, this ensures the existence of a unique equilibria denoted $E_0^3 =$

$(\overline{S}^3, \overline{u}^3) = (S_f^3, u_f^3)$ where

$$u_f^3 = \frac{h(S_f^3)S_f^3}{1 - \alpha e^{-d\tau}}.$$

- If $d > d_{S_f^r}$, this ensures the existence of a unique equilibria denoted $E_0^1 = (\overline{S}^1, \overline{u}^1) = (S_f^1, u_f^1)$ where

$$u_f^1 = \frac{h(S_f^1)S_f^1}{1 - \alpha e^{-d\tau}}.$$

- If $d = d_{S_f^l}$, this ensures the existence of two equilibrium denoted $E_0^{1,2} = (S_f^{1,2}, u_f^{1,2})$ and $E_0^3 = (S_f^3, u_f^3)$.
- If $d = d_{S_f^r}$, this ensures the existence of two equilibrium denoted $E_0^1 = (S_f^1, u_f^1)$ and $E_0^{2,3} = (S_f^{2,3}, u_f^{2,3})$.

For more clarity, E_0^1 is the equilibrium attaches to low population size like high-risks population with low recruitment rate due to difficulty to reach the targeted population.
E_0^2 represents medium population density with maximal recruitement rate. It is MSM population which has a highest uptaking rate for PrEP.
Finally, E_0^3 is connected to general population with the highest density but saturation effect is reached due to logistical constraints.
The following remark is useful for the next sections.
Remark 2. When $d \neq d_{S_f^r}$ and $d \neq d_{S_f^l}$, from the steady-states study, we deduce that

$$d + M\frac{d[h(x)x]}{dx}\Big|_{x=S_f^1} > 0, \qquad d + M\frac{d[h(x)x]}{dx}\Big|_{x=S_f^3} > 0,$$

and

$$d + M\frac{d[h(x)x]}{dx}\Big|_{x=S_f^2} < 0.$$

We summarize the existence of these equilibria in Table 4.2:

Table 4.2: Existence of equilibria with respect to d, the death rate of the susceptible population.

Condition on d	**Number**	**Equilibrium**
$d < d_{S_f^l}$	1	E_0^3
$d = d_{S_f^l}$	2	$E_0^{1,2} = E_0^1 = E_0^2$ and E_0^3
$d_{S_f^l} < d < d_{S_f^r}$	3	E_0^1, E_0^2, E_0^3
$d = d_{S_f^r}$	2	E_0^1 and $E_0^{2,3} = E_0^2 = E_0^3$
$d > d_{S_f^r}$	1	E_0^1

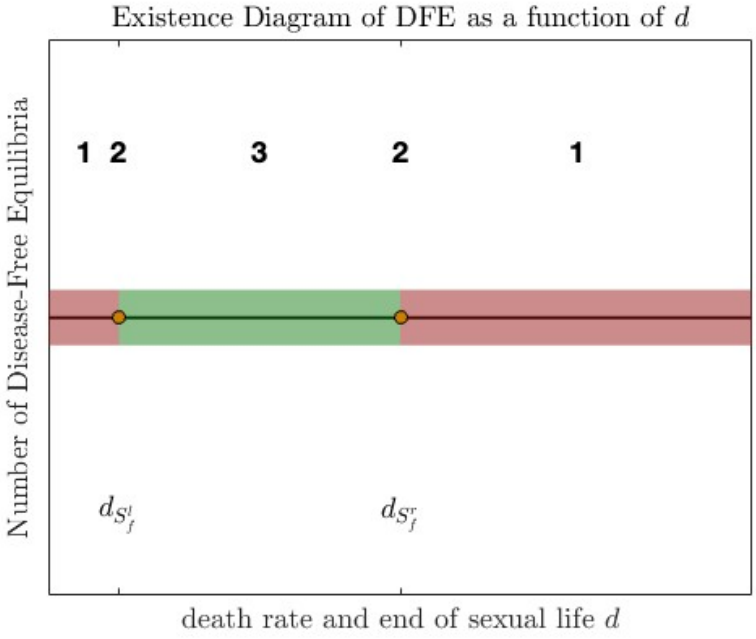


Figure 4.4: Schematic representation of conditions existence of equilibria

4.3.2 Existence of disease-free equilibria

We study now the full system (4.2). We investigate the existence of steady-states (S^*, I^*, u^*). We have

$$\begin{cases} 0 &= \Lambda - (d + h(S^*))S^* + (1-\alpha)e^{-d\tau}u^*, \\ 0 &= (\beta S^* - (d+\mu))I^*, \\ u^* &= h(S^*)S^* + \alpha e^{-d\tau}u^*. \end{cases} \tag{4.5}$$

By setting $I^* = 0$, we get

$$\begin{cases} 0 &= \Lambda - (d + h(S^*))S^* + (1-\alpha)e^{-d\tau}u^*, \\ u^* &= h(S^*)S^* + \alpha e^{-d\tau}u^*. \end{cases}$$

We notice it is the same system as 4.3.1. Then, the study of the latter stytem is the same. We unify notations and note the multiple disease-free equilibrium that may co-exist $E_0^i = (S_f^i, 0, u_f^i)$ with $i = 1, 2, 3$.

4.3.3 Existence of the endemic equilibrium

We consider the full system by setting $I^* \neq 0$.

Proposition 4.1. *A non-trivial (endemic) equilibrium E_I exists if and only if*

$$\Lambda > dS_I + \frac{1 - e^{-d\tau}}{1 - \alpha e^{-d\tau}} h(S_I)S_I, \qquad \textit{with} \quad S_I := \frac{d+\mu}{\beta}.$$

Furthermore, between one and three disease-free equilibria can coexist.

Proof. For any stationary state with $I^* \neq 0$ $(\overline{S}, \overline{I}, \overline{u})$, we have

$$\begin{cases} 0 &= \Lambda - (d + h(\overline{S}))\overline{S} - \beta\overline{SI} + (1-\alpha)e^{-d\tau}\overline{u}, \\ 0 &= \beta\overline{SI} - (d+\mu)\overline{I}, \\ \overline{u} &= h(\overline{S})\overline{S} + \alpha e^{-d\tau}\overline{u}. \end{cases} \tag{4.6}$$

Clearly, we obtain again

$$\overline{u} = \frac{h(\overline{S})\overline{S}}{1 - \alpha e^{-d\tau}}.$$

Considering $\overline{I} > 0$

$$\overline{S} = \frac{d+\mu}{\beta} =: S_I.$$

Substituting this expression in (4.6), we get

$$\Lambda - (d + h(S_I))S_I - \beta S_I \overline{I} + \frac{(1-\alpha)e^{-d\tau}}{1 - \alpha e^{-d\tau}} h(S_I)S_I = 0.$$

We set

$$I_I := \overline{I} = \frac{\Lambda - dS_I - \dfrac{1 - e^{-d\tau}}{1 - \alpha e^{-d\tau}} h(S_I)S_I}{\beta S_I}.$$

This expression is biologically relevant, if

$$\Lambda > dS_I + \frac{1 - e^{-d\tau}}{1 - \alpha e^{-d\tau}} h(S_I)S_I.$$

This expression means that an epidemic can occur only if the in-flow number of susceptible is higher than the ones leaving the compartment by dying at the natural death rate d or the ones starting PrEP. Consequently, under this condition we get the existence of non-trivial (endemic) equilibrium $E_I = (S_I, I_I, u_I)$ where $u_I = h(S_I)S_I/(1 - \alpha e^{-d\tau})$. □

Now, we define the basic reproduction number, denoted R_0, which is the expected number of secondary cases produced, in a completely susceptible population, by a typical infective individual, see [8, 21].
When the disease-free equilibrium is unique, denoted $E_0 = (S_f, 0, u_f)$ (It could be E_0^1 or E_0^3), we define

$$R_0 := \frac{\beta S_f}{d+\mu}, \tag{4.7}$$

where S_f is the unique positive solution of

$$\frac{\Lambda}{d + \dfrac{1-e^{-d\tau}}{1-\alpha e^{-d\tau}} h(x)} = x, \qquad x > 0.$$

This is the natural way to define this quantity. In this case, we show that the condition in Proposition 4.1 is insured if and only if $R_0 > 1$. In fact, if I_I exists, then we have

$$\frac{\Lambda}{d + Mh(S_I) + \beta I_I} = S_I \quad \text{and} \quad \frac{\Lambda}{d + Mh(S_f)} = S_f,$$

We remind that h is a nonincreasing function. By considering another function defined for all $x \in \mathbb{R}^+$, by

$$g_\alpha(x) = \frac{\Lambda}{d + Mh(x) + \beta\alpha}, \qquad \alpha \geq 0.$$

Then, the intersections of both function $g_0(x)$ and $g_I(x)$ with the first bisector lead to get $S_I < S_f$. This means that $R_0 > 1$.
Inversely, if $R_0 > 1$, then clearly $S_I < S_f$. Since the graph of $g_0(x)$ is above the graph of x when $x \in [0, S_f]$, then

$$\frac{\Lambda}{d + Mh(S_I)} > S_I.$$

Therefore, the condition in Proposition 4.1 holds. Combining the above results and statements, we get the following theorem.

Theorem 4.1. *A non-trivial (endemic) equilibrium E_I exists if and only if $R_0 > 1$ and the disease-free equilibrium E_0 is unique.*

Remark 3. Some condition could be considered if we want to guarantee the uniqueness of the disease-free equilibrium. In fact, if we consider

$$g_0(x) = x, \qquad x > 0.$$

Since, h is a nonincreasing function satisfying $\lim_{s\to+\infty} h(s) = 0$, then there exists at least one positive S_f where the above equality holds. Moreover, if we suppose that $g_0''(x) < 0$ for all $x \geq 0$, then the DFE is unique.

When the disease-free equilibrium is not unique, denoted before $E_0^i = (S_f^i, 0, u_f^i)$, for $i = 1, 2, 3$, we will use the following thresholds

$$R_0^i := \frac{\beta S_f^i}{d+\mu}, \qquad i = 1, 2, 3.$$

We have $R_0^1 \leq R_0^2 \leq R_0^3$. In this case, the conditions of existence of the endemic steady state are given in term of R_0^i by

$$R_0^3 \geq R_0^2 \geq R_0^1 > 1 \qquad \text{or} \qquad R_0^1 \leq R_0^2 \leq 1 < R_0^3,$$

which is equivalent to

$$R_0^1 > 1 \qquad \text{or} \qquad R_0^2 \leq 1 < R_0^3.$$

The stability of the equilibria is important for disease control and this is the purpose of the rest of the paper.

4.4 Local asymptotic stability

In this section, we study at the local stability of each equilibrium from the previous section. To do so, we linearize system (4.2) about any equilibrium (S^*, I^*, u^*):

$$\begin{cases} \dfrac{dS(t)}{dt} = -dS(t) - \overline{h}(S^*)S(t) - \beta S^* I(t) - \beta I^* S(t) + (1-\alpha)e^{-d\tau}u(t-\tau), \\ \dfrac{dI(t)}{dt} = \beta S^* I(t) + \beta I^* S(t) - (d+\mu)I(t), \\ u(t) = \overline{h}(S^*)S(t) + \alpha e^{-d\tau}u(t-\tau), \end{cases} \tag{4.8}$$

where

$$\overline{h}(S^*) := \frac{d[h(x)x]}{dx}\,|_{x=S^*} = h(S^*) + h'(S^*)S^*.$$

We look for solutions of the form $S(t) = e^{\lambda t}s_0$, $I(t) = e^{\lambda t}i_0$ and $u(t) = e^{\lambda t}u_0$, with $\lambda \in \mathbb{C}$. We plug these expressions into (4.4) and by simplifying by $e^{\lambda t}$:

$$\begin{cases} \lambda s_0 = -ds_0 - \overline{h}(S^*)s_0 - \beta s_0 I^* - \beta i_0 S^* + (1-\alpha)e^{-(d+\lambda)\tau}u_0, \\ \lambda i_0 = \beta i_0 S^* + \beta I^* s_0 - (d+\mu)i_0, \\ u_0 = \overline{h}(S^*)s_0 + \alpha e^{-(d+\lambda)\tau}u_0. \end{cases}$$

This is equivalent to $A(s_0, i_0, u_0)^T = 0$ where

$$A = \begin{pmatrix} \lambda + d + \overline{h}(S^*) + \beta I^* & \beta S^* & -(1-\alpha)e^{-(d+\lambda)\tau} \\ -\beta I^* & \lambda - \beta S^* + d + \mu & 0 \\ -\overline{h}(S^*) & 0 & 1 - \alpha e^{-(d+\lambda)\tau} \end{pmatrix}. \tag{4.9}$$

4.4.1 Local stability of any disease-free equilibrium

We remind that any disease-free equilibrium is denoted by $E_0^i = (S_f^i, 0, u_f^i)$ with $i = 1, 2, 3$. From 4.9, we set

$$\begin{vmatrix} \lambda + d + \overline{h}(S_f^i) & \beta S_f^i & -(1-\alpha)e^{-(d+\lambda)\tau} \\ 0 & \lambda - \beta S_f^i + d + \mu & 0 \\ -\overline{h}(S_f^i) & 0 & 1 - \alpha e^{-(d+\lambda)\tau} \end{vmatrix} = 0.$$

The characteristic equation is given by

$$(\lambda - \beta S_f^i + d + \mu)\left[(\lambda + d + \overline{h}(S_f^i))(1 - \alpha e^{-(d+\lambda)\tau}) - \overline{h}(S_f^i)(1-\alpha)e^{-(d+\lambda)\tau}\right] = 0,$$

which is equivalent to

$$\begin{aligned} (\lambda - (d+\mu)(R_0^i - 1))\Big[\lambda + d + \overline{h}(S_f^i) \\ - \left[\alpha(\lambda + d + \overline{h}(S_f^i)) + \overline{h}(S_f^i)(1-\alpha)\right] e^{-d\tau} e^{-\lambda\tau}\Big] = 0. \end{aligned} \tag{4.10}$$

We can then state the following result.

Theorem 4.2. *For $i = 1$ or 3, if we assume that $R_0^i > 1$, then $(S_f^i, 0, u_f^i)$ is unstable when it exists. Inversely if $R_0^i < 1$ and additionally if*

$$d > -\tilde{M}\overline{h}(S_f^i), \qquad \text{with} \quad \tilde{M} := \frac{1 + e^{-d\tau}}{1 + \alpha e^{-d\tau}} > M,$$

then, the steady state $(S_f^i, 0, u_f^i)$ of system (4.2) is locally asymptotically stable. If E_0^2 exists, then it is always unstable.

Proof. By considering the characteristic equation (4.10), there exists a real root of

(4.10) given by $\lambda = (d+\mu)(R_0^i - 1)$ and it is positive under the hypothesis $R_0^i > 1$. Consequently, each $(S_f^i, 0, u_f^i)$ is unstable when $R_0^i > 1$.

Under the assumption $R_0^i < 1$ for $i = 1$ or 3, we have $\lambda = (d+\mu)(R_0^i - 1) < 0$. To complete the stability study, we need to check the sign of the real part of $\lambda \in \mathbb{C}$ satisfying

$$\lambda + d + \overline{h}(S_f^i) - \left[\alpha(\lambda + d + \overline{h}(S_f^i)) + \overline{h}(S_f^i)(1-\alpha)\right] e^{-d\tau} e^{-\lambda\tau} = 0.$$

We rewrite this equation as

$$\lambda + d + \overline{h}(S_f^i) = \left[\alpha(\lambda + d) + \overline{h}(S_f^i)\right] e^{-d\tau} e^{-\lambda\tau}. \tag{4.11}$$

Suppose by contradiction that $\lambda = a + ib$ with $a, b \in \mathbb{R}$ and $a \geq 0$. The equation (4.11) leads to $\left|\lambda + d + \overline{h}(S_f^i)\right| \leq \left|\alpha(\lambda + d)e^{-d\tau} + \overline{h}(S_f^i)e^{-d\tau}\right|$. Taking square of both sides, we get

$$\begin{aligned}
&(\lambda + d + \overline{h}(S_f^i))(\overline{\lambda} + d + \overline{h}(S_f^i)) \\
&\qquad \leq [\alpha(\lambda + d)e^{-d\tau} + \overline{h}(S_f^i)e^{-d\tau}][\alpha(\overline{\lambda} + d)e^{-d\tau} + \overline{h}(S_f^i)e^{-d\tau}],
\end{aligned}$$

which implies that

$$\begin{aligned}
&(1 - (\alpha e^{-d\tau})^2)|\lambda + d|^2 \\
&\qquad + (1 - \alpha(e^{-d\tau})^2)\overline{h}(S_f^i)(\lambda + \overline{\lambda} + 2d) + [\overline{h}(S_f^i)]^2(1 - (e^{-d\tau})^2) \leq 0.
\end{aligned}$$

This is a contradiction since

$$\begin{aligned}
&(1 - (\alpha e^{-d\tau})^2)|\lambda + d|^2 \\
&\qquad + (1 - \alpha(e^{-d\tau})^2)\overline{h}(S_f^i)(\lambda + \overline{\lambda} + 2d) + [\overline{h}(S_f^i)]^2(1 - (e^{-d\tau})^2) > 0.
\end{aligned} \tag{4.12}$$

In fact, we have $\lambda + \overline{\lambda} = 2a \geq 0$, then (4.12) is equivalent to

$$(1 - (\alpha e^{-d\tau})^2)((a+d)^2 + b^2)$$
$$+2(1 - \alpha(e^{-d\tau})^2)\overline{h}(S_f^i)(a+d) + [\overline{h}(S_f^i)]^2(1 - (e^{-d\tau})^2) > 0.$$

To show this, it suffices to obtain

$$P(a+d) := (1 - (\alpha e^{-d\tau})^2)(a+d)^2$$
$$+2(1 - \alpha(e^{-d\tau})^2)\overline{h}(S_f^i)(a+d) + (1 - (e^{-d\tau})^2)[\overline{h}(S_f^i)]^2 > 0.$$

Clearly, if $\overline{h}(S_f^i) \geq 0$, then the above equality holds leading to a contradiction. Now, if $\overline{h}(S_f^i) < 0$, the discriminant of P is calculated and gives

$$\begin{aligned}\Delta_P &= [2(1 - \alpha(e^{-d\tau})^2)\overline{h}(S_f^i)]^2 - 4(1 - (\alpha e^{-d\tau})^2)(1 - (e^{-d\tau})^2)[\overline{h}(S_f^i)]^2, \\ &= 4(\alpha - 1)^2(e^{-d\tau})^2[\overline{h}(S_f^i)]^2 > 0.\end{aligned}$$

In another side, P is positive if

$$a + d > \frac{-2(1 - \alpha(e^{-d\tau})^2)\overline{h}(S_f^i) + [4(\alpha-1)^2(e^{-d\tau})^2[\overline{h}(S_f^i)]^2]^{\frac{1}{2}}}{2(1 - (\alpha e^{-d\tau})^2)} = -\tilde{M}\overline{h}(S_f^i),$$

where

$$\tilde{M} := \frac{1 + e^{-d\tau}}{1 + \alpha e^{-d\tau}}.$$

Therefore, if $d > -\tilde{M}\overline{h}(S_f^i)$ for $i = 1$ or 3, then (4.12) holds true which leads to the contradiction. Consequently, $a < 0$. We conclude that each (S_f^i, u_f^i), for $i = 1$ or 3, is locally asymptotically stable.

For E_0^2, we consider the following real function, for $x \in \mathbb{R}$,

$$\Delta_0(x) := x + d + \overline{h}(S_f^2) - \left[\alpha(x + d + \overline{h}(S_f^2)) + \overline{h}(S_f^2)(1-\alpha)\right] e^{-d\tau} e^{-x\tau}.$$

Using Remark 2, we have

$$\Delta_0(0) = d + \overline{h}(S_f^2) - \left[\alpha d + \overline{h}(S_f^2)\right] e^{-d\tau} = d(1 - \alpha e^{-d\tau}) + (1 - e^{-d\tau})\overline{h}(S_f^2) < 0.$$

Moreover, $\lim_{x\to+\infty} \Delta_0(x) + \infty$. This ensures the existence of a positive real root for equation (4.10) at E_0^2. Thus, E_0^2 is always unstable. □

We can remark that if $\overline{h}(S_f^i) \geq 0$, which means that S_f^i is located in the increasing part of the function $h(x)x$, then the condition $d > -\tilde{M}\overline{h}(S_f^i)$ becomes satisfied. This possibility occurs only for E_0^1. The next theorem improves the result stated above, mainly when $\overline{h}(S_f^i) < 0$. The proof is based also on the contradiction.

Theorem 4.3. *For $i = 1$ or 3, if*

$$d > -\frac{1}{\alpha}\overline{h}(S_f^i), \qquad \text{with} \quad \alpha \neq 0,$$

then, the steady state (S_f^i, u_f^i) of system (4.2) is locally asymptotically stable. If E_0^2 exists, then it is always unstable.

Proof. The case of instability is already proven in the proof of Theorem 4.2. Again, we need to see the sign of the real part of $\lambda \in \mathbb{C}$ satisfying

$$D_0(\lambda) := \lambda + d + \overline{h}(S_f^i) - \left[\alpha(\lambda + d + \overline{h}(S_f^i)) + \overline{h}(S_f^i)(1-\alpha)\right] e^{-d\tau} e^{-\lambda\tau} = 0. \quad (4.13)$$

Since the case $\overline{h}(S_f^i) \geq 0$ is included in the previous theorem, we consider here only the case $\overline{h}(S_f^i) < 0$. First, we can see that there exists a negative real root λ_0 of (4.13). In fact, we consider D_0 as a real function and for $\lambda_0 = -d$ we get $D_0(\lambda_0) = 0$.

Now, we suppose that $\lambda = \mu + i\omega$ is a solution of (4.13) with nonnegative real part

$\Re(\lambda) = \mu \geq 0$. For simplicity, we put $\overline{h} := \overline{h}(S_f^i)$. We obtain,

$$D_0(\lambda) = \lambda + d + \overline{h} - \left[\alpha(\lambda + d) + \overline{h}\right] e^{-d\tau} e^{-\lambda\tau} = 0.$$

By separating real part in the equation (4.13), we obtain

$$\begin{aligned} \mu - \lambda_0 &= (\alpha(\mu + d) + \overline{h}) e^{-d\tau} \cos(\omega\tau) e^{-\mu\tau} - (\alpha(\lambda_0 + d) + \overline{h}) e^{-d\tau} e^{-\lambda_0\tau} \\ &\quad + \omega\alpha \sin(\omega\tau) e^{-d\tau} e^{-\mu\tau}. \end{aligned}$$

Since $\mu \geq 0$, we have

$$\mu - \lambda_0 < (\mu - \lambda_0)\alpha + \omega\alpha \sin(\omega\tau) e^{-d\tau} e^{-\mu\tau}. \tag{4.14}$$

Also, by separating imaginary part in the equation (4.13), we obtain

$$\omega - \omega\alpha \cos(\omega\tau) e^{-d\tau} e^{-\mu\tau} + (\alpha(\mu + d) + \overline{h}) \sin(\omega\tau) e^{-d\tau} e^{-\mu\tau} = 0.$$

Then,

$$\sin(\omega\tau) e^{-d\tau} e^{-\mu\tau} = -\frac{\omega \left[1 - \alpha \cos(\omega\tau) e^{-d\tau} e^{-\mu\tau}\right]}{\alpha(\mu + d) + \overline{h}}.$$

Therefore, (4.14) implies that

$$0 < (1 - \alpha)(\mu - \lambda_0) < -\omega^2 \alpha \frac{\left[1 - \alpha \cos(\omega\tau) e^{-d\tau} e^{-\mu\tau}\right]}{\alpha(\mu + d) + \overline{h}} < 0.$$

We obtain a contradiction. The conclusion is that $\mu < 0$. Hence, all characteristic roots have negative real part and (S^0, u^0) is locally asymptotically stable. □

4.4.2 Local stability of the endemic steady state

In this part, we study the stability of the endemic steady state $E_I = (S_I, I_I, u_I)$ and a possible Hopf bifurcation to our main system. Through the rest of the paper, we

assume the existence of E_I. We still suppose that

$$\Lambda > dS_I + \frac{1-e^{-d\tau}}{1-\alpha e^{-d\tau}} h(S_I)S_I.$$

This is equivalent to

$$\tau < \tau_{\max} := \begin{cases} \dfrac{1}{d}\ln\left(\dfrac{1-\alpha L}{1-L}\right), & 0 < L < 1, \\ +\infty, & 1 \leq L, \end{cases}$$

where

$$L := \frac{\Lambda - dS_I}{h(S_I)S_I}.$$

We consider our system 4.2 as a special case of Neutral Delay Differential Equation (NDDE). We get the following system:

$$\begin{cases} S'(t) = \Lambda - (d + h(S(t)))S(t) - \beta S(t)I(t) + (1-\alpha)e^{-d\tau}u(t-\tau), \\ I'(t) = \beta S(t)I(t) - (d+\mu)I(t), \\ \dfrac{d}{dt}[u(t) - h(S(t))S(t) - \alpha e^{-d\tau}u(t-\tau)] = 0, \end{cases} \tag{4.15}$$

which is completed by the initial conditions

$$S(0) = S_0, \;\; I(0) = I_0 \;\text{ and }\; u(t) = \phi(t), \;\; \text{for} \;\; -\tau \leq t \leq 0. \tag{4.16}$$

This system has the following form

$$\begin{cases} \dfrac{d}{dt}G(S(t), I(t), u_t)) = F(S(t, I(t), u_t)), \\ S(0) = S_0, I(0) = I_0 \quad \text{and} \quad u_0 = \phi. \end{cases} \tag{4.17}$$

avec

$$\begin{cases} G(S, I, \phi) = (S, I, \phi(0) - h(S)S - e^{-d\tau}\phi(-\tau)), \\ F(S, I, \phi) = (\Lambda - (d + h(S))S - \beta SI + (1 - \alpha)e^{-d\tau}\phi(-\tau), \beta SI - (d + \mu)I, 0) \end{cases}$$

Qualitative theory of such systems can be found in the litterature [12, 13]. To obtain the equivalence of systems 4.2 and 4.17, we consider the initial data in the following set

$$\Big\{(S_0, I_0, \phi) \in (R^+)^2 \times C([-\tau, 0], \mathbb{R}^+) : \phi(0) - h(S_0)S_0 - e^{-d\tau}\phi(-\tau) = 0\Big\}$$

.

We consider linearization of system 4.15 around an equilibrium point $(\overline{S}, \overline{I}, \bar{u})$

$$\begin{cases} \dfrac{d}{dt}D(S(t), I(t), u_t) = L(S(t), I(t), u_t), \quad t > 0, \\ S(0) = S_0, I(0) = I_0 \quad u_0(s) = \phi(s), \quad s \in [-\tau, 0], \end{cases} \tag{4.18}$$

with

$$\begin{cases} D(S,I,\phi) = \Big(S, I, \phi(0) - \bar{h}(S)S - \alpha e^{-d\tau}\phi(-\tau)\Big), \\ L(S,I,\phi) = \Big(- dS - \bar{h}(S)S - \beta(\bar{S}I + \bar{I}S) + (1-\alpha)e^{-d\tau}\phi(-\tau), \\ \qquad\qquad \beta(\bar{S}I + \bar{I}S) - (d+\mu)I, 0\Big), \end{cases}$$

where

$$\overline{h}(\bar{S}) := \frac{d[h(x)x]}{dx}\,|_{x=\bar{S}} = h(\bar{S}) + h'(\bar{S})\bar{S}.$$

To apply the general Hopf bifurcation theorem for neutral delay differential equations, it is a fundamental prerequisite to ensure the strong stability of the difference operator D. The following proposition demonstrates that the neutral component of the system is intrinsically stable.

Proposition 4.2 (Strong Stability of D)**.** *Let $D : \mathbb{R}^3 \times \mathcal{C}([-\tau, 0], \mathbb{R}) \to \mathbb{R}^3$ be the continuous difference operator associated with the linearized system 4.18, defined by:*

$$D(S_t, I_t, u_t) = \begin{pmatrix} S_t(0) \\ I_t(0) \\ u_t(0) - \overline{h}(\bar{S})S_t(0) - \alpha e^{-d\tau}u_t(-\tau) \end{pmatrix} \tag{4.19}$$

For all biologically relevant parameter values ($0 \leq \alpha < 1$ and $d, \tau > 0$), the operator D is strongly (uniformly) stable.

Proof. By definition, the difference operator D is strongly stable if all the roots of its associated characteristic equation have strictly negative real parts. The characterstic

equation is given by:

$$\Delta_D(\lambda) = \begin{pmatrix} 1 & 0 & 0 \\ 0 & 1 & 0 \\ -\overline{h}(\bar{S}) & 0 & 1 - \alpha e^{-d\tau} e^{-\lambda\tau} \end{pmatrix} \tag{4.20}$$

The characteristic roots are the solutions to the algebraic equation $\det(\Delta_D(\lambda)) = 0$. Since $\Delta_D(\lambda)$ is a lower triangular matrix, its determinant is simply the product of its diagonal entries. We obtain:

$$\det(\Delta_D(\lambda)) = (1 - \alpha e^{-d\tau} e^{-\lambda\tau}) = 0 \tag{4.21}$$

This simplifies to the transcendental equation:

$$e^{\lambda\tau} = \alpha e^{-d\tau} \tag{4.22}$$

Let $\lambda = \mu + i\omega$, where $\mu, \omega \in \mathbb{R}$. Substituting this into the equation and taking the modulus of both sides, we get:

$$|e^{\mu\tau} e^{i\omega\tau}| = \alpha e^{-d\tau} \implies e^{\mu\tau} = \alpha e^{-d\tau} \tag{4.23}$$

Solving for the real part μ, we find:

$$\mu = \Re(\lambda) = \frac{1}{\tau} \ln(\alpha e^{-d\tau}) \tag{4.24}$$

From the parameter definitions of the model, $\alpha \in [0, 1)$ represents a probability, and $d > 0$, $\tau > 0$. Therefore, the product $\alpha e^{-d\tau}$ is strictly less than 1 (and strictly

positive). Consequently, its natural logarithm is strictly negative:

$$\ln(\alpha e^{-d\tau}) < 0 \implies \Re(\lambda) < 0 \tag{4.25}$$

Since there exists a strictly negative upper bound for the real parts of all characteristic roots of D, the difference operator D is strongly stable. This completes the proof. □

The characteristic equation related to the endemic steady state is :

$$\begin{aligned} &\lambda^2 + (d + \overline{h}(S_I) + \beta I_I)\lambda + \beta I_I(d+\mu) \\ &\quad - \left[\alpha e^{-d\tau}(\lambda^2 + (d+\beta I_I)\lambda + \beta I_I(d+\mu)) + \overline{h}(S_I)e^{-d\tau}\lambda\right] e^{-\lambda\tau} = 0. \end{aligned} \tag{4.26}$$

Note that if $\tau = 0$, the characteristic equation is simplified to

$$(1-\alpha)(\lambda^2 + (d+\beta I_I)\lambda + \beta I_I(d+\mu)) = 0,$$

and thanks to the Routh-Hurwitz criterion, all roots have negative real parts. This suggests that there can be no recurrent epidemic wave if the duration of the protection phase is reduced to zero.

Coming back to $\tau > 0$, we analyze if the roots of the characteristic equation stay in the left half plane for all $\tau \in [0, \tau_{\max})$. A first result, due to the Theorem 6.3 of [95] is given below.

Theorem 4.4. *If $\overline{h}(S_I) \geq 0$, then all roots of (4.26) have negative real parts, and the endemic steady state is locally asymptotically stable.*

Next, we look for the case where $\overline{h}(S_I) < 0$. Considering eigenvalues of the form

$\lambda = iw$ leads into the equation (4.26) and separating the real and the imaginary part

$$\begin{cases} a\cos(w\tau) - bw\sin(w\tau) = w^2 - (d+\mu)\beta I_I, \\ bw\cos(w\tau) + a\sin(w\tau) = w(\beta I_I + d + \overline{h}(S_I)), \end{cases}$$

with

$$a = e^{-d\tau}[\alpha w^2 - \alpha(d+\mu)\beta I_I] \quad \text{and} \quad b = e^{-d\tau}[\alpha\beta I_I + \alpha d + \overline{h}(S_I)].$$

Therefore, we get

$$\begin{cases} \cos(w\tau) = \dfrac{a(w^2 - (d+\mu)\beta I_I) + w^2 b(\beta I_I + d + \overline{h}(S_I))}{a^2 + (bw)^2}, \\ \sin(w\tau) = \dfrac{wa(\beta I_I + d + \overline{h}(S_I)) - bw(w^2 - (d+\mu)\beta I_I)}{a^2 + (bw)^2}. \end{cases} \tag{4.27}$$

This implies that

$$a^2 + w^2 b^2 = (w^2 - (d+\mu)\beta I_I)^2 + w^2(\beta I_I + d + \overline{h}(S_I))^2. \tag{4.28}$$

We note

$$\Gamma := (d+\mu)\beta I_I.$$

Equation (4.28) is then written as

$$(1-\alpha^2 e^{-2d\tau})w^4 + \left(-2(1-\alpha^2 e^{-2d\tau})\Gamma + \vartheta(\tau)\right) w^2 + (1-\alpha^2 e^{-2d\tau})\Gamma^2 = 0,$$

with

$$\vartheta(\tau) := (\beta I_I + d + \overline{h}(S_I))^2 - e^{-2d\tau}(\alpha(\beta I_I + d) + \overline{h}(S_I))^2).$$

Setting $X = w^2$ we get

$$(1-\alpha^2 e^{-2d\tau})X^2 + \left(-2(1-\alpha^2 e^{-2d\tau})\Gamma + \vartheta(\tau)\right) X + (1-\alpha^2 e^{-2d\tau})\Gamma^2 = 0. \tag{4.29}$$

The following proposition is a direct conclusion of the Routh-Hurwitz criterion.

Proposition 4.3. *Assume that* $\vartheta(\tau) \geq \vartheta^*(\tau) := 2(1-\alpha^2 e^{-2d\tau})\Gamma$ *for all* $\tau \in [0, \tilde{\tau})$ *with* $0 < \tilde{\tau} < \tau_{\max}$. *Then, the endemic steady-state* $E_I := (S_I, I_I, u_I)$ *is locally asymptotically stable for* $\tau \in [0, \tilde{\tau})$.

Suppose next that $\vartheta(\tau) < \vartheta^*(\tau) = 2(1-\alpha^2 e^{-2d\tau})\Gamma$ for some $\tau \in (0, \tau_{\max})$, see Figure 4.5.

The discriminant of (4.29) is calculated by

$$\Delta(\vartheta(\tau)) = \vartheta^2(\tau) - 4(1-\alpha^2 e^{-2d\tau})\Gamma\vartheta(\tau).$$

Since

$$\vartheta(\tau) < \vartheta^*(\tau) = 2(1-\alpha^2 e^{-2d\tau})\Gamma < 4(1-\alpha^2 e^{-2d\tau})\Gamma,$$

no destabilization occurs when $0 < \vartheta(\tau) < \vartheta^*(\tau)$.

Proposition 4.4. *Assume that* $\vartheta(\tau) > 0$ *for all* $\tau \in [0, \tilde{\tau})$ *with* $0 < \tilde{\tau} < \tau_{\max}$, *then, the endemic steady-state* $E_I := (S_I, I_I, u_I)$ *is locally asymptotically stable for* $\tau \in [0, \tilde{\tau})$.

Clearly, if $\overline{h}(S_I)) \geq 0$, which means that S_I is located in the increasing part of the function $h(x)x$, then $\vartheta(\tau) > 0$ for all $\tau \in [0, \tau_{\max})$ and no destabilization occurs.
Now, we focus on the case where $\vartheta(\tau) \leq 0$ for $\tau \in [0, \tilde{\tau})$, with $0 < \tilde{\tau} \leq \tau_{\max}$, for instance see example in Figure 4.5. Then, there are two possible roots $w_{\pm}(\tau)$ given by

$$w_-(\tau) = \left[\frac{-\left(-2(1-\alpha^2 e^{-2d\tau})\Gamma + \vartheta(\tau)\right) - \sqrt{\Delta(\vartheta(\tau))}}{2(1-\alpha^2 e^{-2d\tau})}\right]^{\frac{1}{2}},$$

and

$$w_+(\tau) = \left[\frac{-\left(-2(1-\alpha^2 e^{-2d\tau})\Gamma + \vartheta(\tau)\right) + \sqrt{\Delta(\vartheta(\tau))}}{2(1-\alpha^2 e^{-2d\tau})} \right]^{\frac{1}{2}}.$$

We define by (4.27) the angles $\theta_\pm(\tau) \in [0, 2\pi]$ which satisfies

$$\begin{cases} \cos(\theta_\pm(\tau)) = \dfrac{a(w_\pm^2(\tau) - (d+\mu)\beta I_I) + w_\pm^2(\tau) b(\beta I_I + d + \overline{h}(S_I))}{a^2 + (b w_\pm(\tau))^2}, \\ \sin(\theta_\pm(\tau)) = \dfrac{w_\pm(\tau) a(\beta I_I + d + \overline{h}(S_I)) - b w_\pm(\tau)(w_\pm^2(\tau) - (d+\mu)\beta I_I)}{a^2 + (b w_\pm(\tau))^2}, \end{cases}$$

and write that

$$w_\pm(\tau)\tau = \theta_\pm(\tau) + 2k\pi, \qquad \text{with} \quad k \in \mathbb{N}.$$

As in [87, 32], these angles are given by

$$\begin{aligned}
&\theta_\pm(\tau) = \arctan(D_1(\tau)/D_2(\tau)), && \text{if} \quad \sin(\theta_\pm(\tau)) > 0, \quad \cos(\theta_\pm(\tau)) > 0, \\
&\theta_\pm(\tau) = \pi/2, && \text{if} \quad \sin(\theta_\pm(\tau)) = 1, \quad \cos(\theta_\pm(\tau)) = 0, \\
&\theta_\pm(\tau) = \pi + \arctan(D_1(\tau)/D_2(\tau)), && \text{if} \quad \cos(\theta_\pm(\tau)) < 0, \\
&\theta_\pm(\tau) = 3\pi/2, && \text{if} \quad \sin(\theta_\pm(\tau)) = -1, \quad \cos(\theta_\pm(\tau)) = 0, \\
&\theta_\pm(\tau) = 2\pi + \arctan(D_1(\tau)/D_2(\tau)), && \text{if} \quad \sin(\theta_\pm(\tau)) < 0, \quad \cos(\theta_\pm(\tau)) > 0,
\end{aligned}$$

where

$$D_1(\tau) := w_\pm(\tau) a(\beta I_I + d + \overline{h}(S_I)) - b w_\pm(\tau)(w_\pm^2(\tau) - (d+\mu)\beta I_I),$$

$$D_2(\tau) := a(w_\pm^2(\tau) - (d+\mu)\beta I_I) + w_\pm^2(\tau) b(\beta I_I + d + \overline{h}(S_I)).$$

The critical value of $\tau \in (0, \tilde{\tau})$ for which the stability change occurs are the roots of

the following functions, for $k \in \mathbb{N}$,

$$\begin{aligned} Z_k^{\pm} : \ (0, \tilde{\tau}) &\to \mathbb{R}, \\ \tau &\mapsto Z_k^{\pm}(\tau) = \tau - \frac{\theta_{\pm}(\tau) + 2k\pi}{w_{\pm}(\tau)}. \end{aligned}$$

More precisely, a pair of simple conjugate pure imaginary roots $\lambda = \pm iw(\tau^*)$ exist at τ^* if and only if τ^* is a root of Z_k^+ or Z_k^-, $k \in \mathbb{N}$.

As in [87], we rewrite the characteristic equation (4.26) in the following suitable form

$$\Delta(\tau, \lambda) := P(\tau, \lambda) + Q(\tau, \lambda)e^{-\lambda\tau} = 0.$$

We define the polynomial function

$$F(\tau, \omega) = |P(\tau, i\omega)|^2 - |Q(\tau, i\omega)|^2.$$

Then,

$$\begin{aligned} F(\tau, \omega) = (w^2 - \Gamma)^2 + w^2 \left(d + \beta I_I + \overline{h}(S_I)\right)^2 \\ - \left(\alpha e^{-d\tau} w^2 - \Gamma\right)^2 - w^2 e^{-2d\tau} (\alpha(\beta I_I + d) + \overline{h}(S_I))^2. \end{aligned}$$

Recall that if $\lambda(\tau)$ is a branch of roots of (4.26) such that $\lambda(\tau^*) = iw(\tau^*)$, then a Hopf bifurcation exists around the endemic equilibrium when $\tau = \tau^*$ if

$$\left[\left(\frac{\mathrm{d}(\lambda(\tau))}{\mathrm{d}\tau}\right)_{\tau=\tau^*}\right] > 0.$$

From [87], we have

$$\left[\left(\frac{\mathrm{d}(\lambda(\tau))}{\mathrm{d}\tau}\right)_{\tau=\tau^*}\right] = \left(\frac{\partial F}{\partial w}(\tau^*, w(\tau^*))\right)\left(\frac{\mathrm{d}Z_0^{\pm}(\tau^*)}{\mathrm{d}\tau}\right),$$

Using the formula of F, we get

$$\frac{\partial F}{\partial w}(\tau, w(\tau)) = 2w\left(2\left(1-\left(\alpha e^{-d\tau}\right)^2\right)w^2 - 2\Gamma\left(1-\alpha e^{-d\tau}\right) + \vartheta(\tau)\right).$$

Since the functions $Z_k^{\pm}(\tau)$ are given implicitly, then we are not able to provide a characterization of their roots. Therefore, as in our illustrations bellow, the roots can be found numerically. Next, we state some straightforward properties of $Z_k^{\pm}$.

Lemma 4.1. *For all $k \in \mathbb{N}$ and $\tau \in [0, \tilde{\tau})$,*

$$Z_k^{\pm}(0) < 0 \quad \textit{and} \quad Z_{k+1}^{\pm}(\tau) < Z_k^{\pm}(\tau).$$

From this lemma, if $Z_k^{\pm}$ has no root on $[0, \tilde{\tau})$, then no function $Z_j^{\pm}$, with $j > k$, have roots on $[0, \tilde{\tau})$. The following result is a direct consequence of lemma 4.1.

Proposition 4.5. *If both Z_0^+ and Z_0^- have no root on the interval $[0, \tilde{\tau})$, then then the endemic equilibrium does not undergo any Hopf bifurcation for any $\tau \in [0, \tau_{\max})$.*

The following theorem states the stability switch located at the smallest root of $Z_k^{\pm}$.

Theorem 4.5 (Hopf Bifurcation at the Endemic Equilibrium)**.** *Assume that the endemic equilibrium $E_I = (S_I, I_I, u_I)$ exists. Suppose there exists a critical delay $\tau^* \in (0, \tau_{max})$ such that:*

1. *$\vartheta(\tau^*) \leq 0$, ensuring the existence of the critical frequency $\omega_0 = w_+(\tau^*) > 0$.*
2. *τ^* is the minimum positive root of $Z_0^+(\tau) = 0$.*
3. *The transversality condition is satisfied: $\left.\frac{dZ_0^+(\tau)}{d\tau}\right|_{\tau=\tau^*} > 0$.*

Then, the following dynamical properties hold:

- *The endemic equilibrium E_I is locally asymptotically stable for $\tau \in [0, \tau^*)$.*

- *E_I loses its stability at $\tau = \tau^*$.*
- *A Hopf bifurcation occurs at $\tau = \tau^*$, leading to the emergence of a family of periodic solutions bifurcating from the endemic steady state E_I.*

Proof. To prove the occurrence of a Hopf bifurcation for a NDDE, following the general theoretical framework [13, 12], four fundamental conditions must be verified at the critical parameter $\tau = \tau^*$, strong stability of the difference operator, existence of simple purely imaginary root, non-resonance condition and tranversaility condition. As demonstrated in Proposition 4.2, the operator D is uniformly strongly stable.

Under the condition $\vartheta(\tau^*) \leq 0$, Proposition 2 establishes that the transcendental characteristic equation $\Delta(\tau^*, \lambda) = 0$ admits a pair of purely imaginary roots $\lambda_0 = \pm i\omega_0$, where $\omega_0 = w_+(\tau^*) > 0$. Furthermore, it was proven that $\frac{\partial F}{\partial \omega}(\tau^*, \omega_0) = 2\omega_0\sqrt{\Delta_G(\tau^*)} > 0$. This strict positivity analytically guarantees that $\frac{\partial \Delta}{\partial \lambda}\Big|_{\lambda = i\omega_0} \neq 0$, meaning the purely imaginary roots are simple.

By definition, τ^* is the *minimum* positive root of $Z_0^+(\tau) = 0$. Because the sequence of threshold functions $Z_k^+(\tau)$ is strictly monotonically decreasing with respect to k, τ^* is the very first instance where any characteristic root reaches the imaginary axis as the delay τ increases from 0. Consequently, at $\tau = \tau^*$, all other characteristic roots still possess strictly negative real parts.

To ensure that the roots genuinely cross the imaginary axis, we must prove that the crossing velocity $\frac{d}{d\tau}\Re(\lambda(\tau))$ is strictly positive at $\tau = \tau^*$. Using the established implicit differentiation relation for delay systems, the sign of the real part derivative is governed by:

$$\operatorname{sign}\left[\frac{d\Re(\lambda)}{d\tau}\bigg|_{\tau=\tau^*}\right] = \operatorname{sign}\left[\frac{\partial F}{\partial \omega}(\tau^*, w_+(\tau^*)) \cdot \frac{dZ_0^+(\tau)}{d\tau}\bigg|_{\tau=\tau^*}\right] \tag{4.30}$$

We know that $\frac{\partial F}{\partial \omega}(\tau^*, w_+(\tau^*)) > 0$. Thus, the direction of the crossing is entirely determined by the derivative of the Z_0^+ function. By assumption (3) of the theorem,

$\left.\frac{dZ_0^+(\tau)}{d\tau}\right|_{\tau=\tau^*} > 0$. Consequently:

$$\left.\frac{d\Re(\lambda(\tau))}{d\tau}\right|_{\tau=\tau^*} > 0 \tag{4.31}$$

The pair of complex conjugate roots crosses the imaginary axis from the left half-plane to the right half-plane with a strictly positive velocity.

All four required conditions for the Hopf bifurcation theorem in neutral functional differential equations are rigorously satisfied. The endemic steady state E_I transitions from asymptotically stable to unstable precisely at $\tau = \tau^*$, giving birth to a limit cycle. □

In the next part, we illustrate our theoretical result by some numerical simulations. Our interest is to provide numerical examples in which the Hopf bifurcation arises, that is, the recurrent epidemic waves occur. For this, we remind that the function h is define as

$$h(S)S = \frac{\gamma S}{K^2 + S^2}$$

It is a unimodal function. The parameter γ represents the maximal effort according to ressources available. The parameter K represents the size of population targeted by PrEP.

The values of parameters are chosen to be

$$\begin{aligned} &\Lambda = 1 \quad \text{indiv} \cdot \text{time}^{-1} && \mu = 0.1 \quad \text{time}^{-1} \\ &\beta = 0.03 \quad (\text{indiv} \cdot \text{time})^{-1} && d = 0.01 \quad \text{time}^{-1} \\ &\alpha = 0.3 \end{aligned}$$

The delay τ is fixed for each situation. In Figure 4.5, the set of parameters is considered to get $\vartheta(\tau) \leq 0$ for $\tau \in [0, 17.219]$. It is demonstrated that in such case, the endemic equilibrium may become unstable through the Hopf bifurcation. In the

same figure, the function Z_0^+ intersects alone the x-axis, which means that a root of this function exists leading to the existence of a purely imaginary solution for the characteristic equation. It is denoted $\tau^* = 1.39$ and the associated characteristic root by $\lambda = iw_+(\tau^*)$, where

$$w_+(\tau^*) = \left[\frac{-\left(-2(1-\alpha^2 e^{-2d\tau^*})\Gamma + \vartheta(\tau^*)\right) + \sqrt{\Delta(\vartheta(\tau^*))}}{2(1-\alpha^2 e^{-2d\tau^*})}\right]^{\frac{1}{2}}.$$

In this case, we obtain

$$\frac{\partial F}{\partial w}(\tau^*, w_+(\tau^*)) = 2w_+(\tau^*)\left[2\Gamma\alpha e^{-d\tau^*}\left(1-\alpha e^{-d\tau^*}\right) + \sqrt{\Delta(\vartheta(\tau^*))}\right] > 0.$$

Therefore,

$$\left(\frac{\partial F}{\partial w}(\tau^*, w_+(\tau^*))\right) = +1,$$

and we get

$$\left[\left(\frac{\mathrm{d}(\lambda(\tau))}{\mathrm{d}\tau}\right)_{\tau=\tau^*}\right] = \left(\frac{\mathrm{d}Z_0^+(\tau^*)}{\mathrm{d}\tau}\right).$$

In the case of this numerical simulation, we observe from Figure 4.5 that

$$\left[\left(\frac{\mathrm{d}(\lambda(\tau))}{\mathrm{d}\tau}\right)_{\tau=\tau^*}\right] = \left(\frac{\mathrm{d}Z_0^+(\tau^*)}{\mathrm{d}\tau}\right) > 0.$$

The above statement confirms the occurrence of the Hopf bifurcation around the endemic steady state at $\tau^* = 1.39$ months. In Figure, 4.6, the solution is drawn for $\tau = 0.4 < \tau^* = 1.39$. Clearly, the local asymptotic stability of the endemic equilibrium is ensured. We can check that for this case the equilibrium E_f^3 exists alone and the basic reproduction number $R_0 > 1$ with $I_I = 8.62$. The figure 4.7 gives a clear confirmation of the existence of solution with periodic oscillations for $\tau > \tau^*$. In the Figure 4.8, we vary τ to be $30 < \tau_{\max}$. This time, the three equilibria E_f^i, for $i = 1, 2, 3$, exist with $S_f^1 = 1.17$, $S_f^2 = 4.70$, $S_f^3 = 54.11$ and we have $R_0^1 = 0.09$, $R_0^2 = 0.85$ and $R_0^3 = 26.33$. In this case, $R_0^1 < R_0^2 < 1 < R_0^3$ leading to the existence

of the endemic equilibrium, with $S_I = (d+\mu)/\beta = 3.66$ and $I_I = 1.06$. Despite the existence of endemic equilibrium, the solution converge to E_f^1. The fact that $R_0^1 < R_0^2 < 1$ suggests the convergence to the disease-free equilibrium instead of the endemic one. All these observations are summarized in the Figure 4.9 where the diagram of bifurcation and the amplitude of the oscillations as a function of τ are drawn.

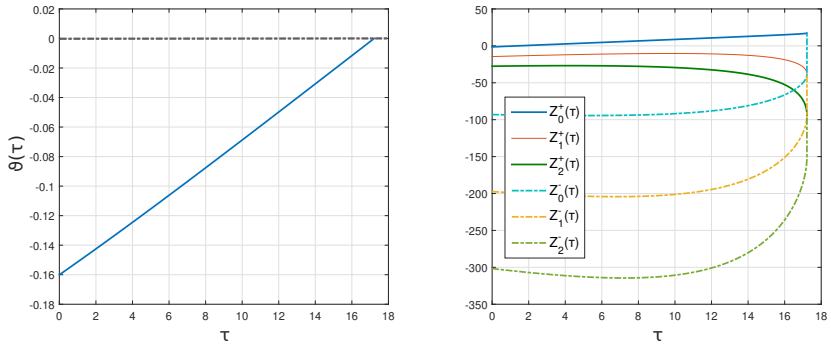


Figure 4.5:
]Left: we have $\vartheta(\tau) \leq 0$ for $\tau \in [0, 17.219]$, in this situation a possible Hopf bifurcation may occur. Right: the only function Z_0^+ intersects the x-axis at $\tau^* = 1.39$. Following our theoretical result, a Hopf bifurcation produces at this root and the system may exhibits a periodic behavior. Parameters are: $\Lambda = 1$, $\mu = 0.1$, $\beta = 0.03$, $d = 0.01$, $\Gamma = 10$, $K = 1$ and $\alpha = 0.3$.

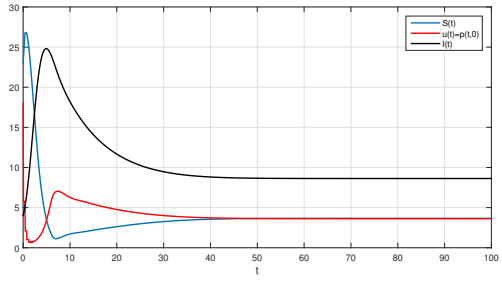


Figure 4.6: This simulation is done for $\tau = 0.4 < \tau^* = 1.39$. The equilibrium E_f^3 exists alone. The endemic equilibrium is $I_I = 8.62$. Of course, the local asymptotic stability of this equilibrium is ensured under the condition $\tau < \tau^*$. Parameters are: $\Lambda = 1$, $\mu = 0.1$, $\beta = 0.03$, $d = 0.01$, $\Gamma = 10$, $K = 1$ and $\alpha = 0.3$.

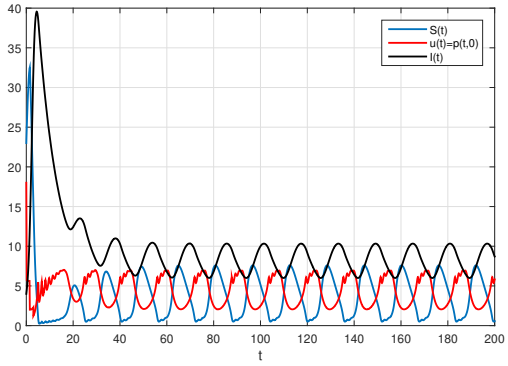


Figure 4.7: This simulation is done for $\tau = 1.5 > \tau^* = 1.39$. The equilibrium E_f^3 exists alone. In this case, we have $I_I = 8.26$. Since $\tau > \tau^*$, we expected the occurrence of oscillations due to Hopf bifurcation at $\tau = \tau^*$. Parameters are: $\Lambda = 1$, $\mu = 0.1$, $\beta = 0.03$, $d = 0.01$, $\Gamma = 10$, $K = 1$ and $\alpha = 0.3$.

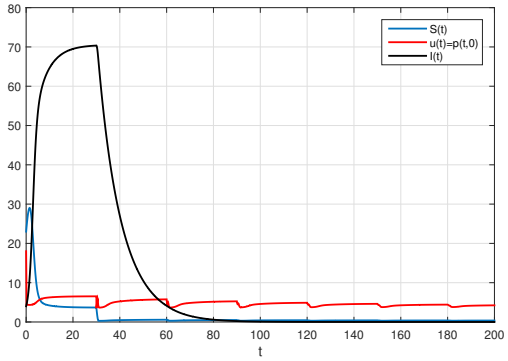


Figure 4.8: The equilibria E_f^i, for $i = 1, 2, 3$, exist with $S_f^1 = 0.33$, $S_f^2 = 3.11$, $S_f^3 = 54.1196.54$ and we have $R_0^1 = 0.09$, $R_0^2 = 0.85$ and $R_0^3 = 26.33$. In this case, $R_0^1 < R_0^2 < 1 < R_0^3$ leading to the existence of the endemic equilibrium, with $S_I = (d + \mu)/\beta = 3.66$ and $I_I = 1.06$. The fact that $R_0^1 < R_0^2 < 1$ suggests the convergence to the disease-free equilibirum. Parameters are: $\Lambda = 1$, $\mu = 0.1$, $\beta = 0.03$, $d = 0.01$, $\Gamma = 10$, $K = 1$ and $\alpha = 0.3$. This simulation is done for $\tau = 30 < \tau_{\max} = 35.63$.

4.5 Discussion

In this work, we extend previous models based on the Susceptible-Infectious-Protected (SIP) model that incorporates two critical real workd complexities: temporary pro-

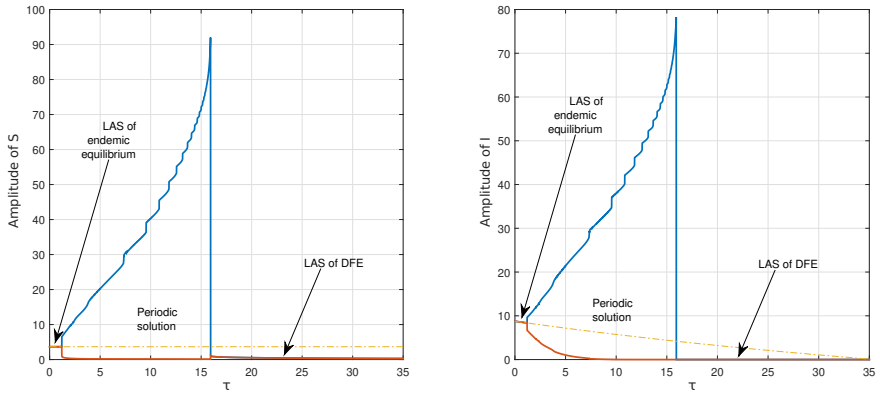


Figure 4.9: Diagram of bifurcation and the amplitude of the oscillations as a function of τ are drawn. Parameters are: $\Lambda = 1$, $\mu = 0.01$, $\beta = 0.03$, $d = 0.1$, $\Gamma = 10$, $K = 51$ and $\alpha = 0.3$. This simulation is done for $\tau \in [0, \tau_{\max}]$, with $\tau_{\max} = 35.63$. On this interval of τ, the existence of endemic equilibrium is ensured.

tection phase and non-monotonic recruitment rate for PrEP uptake. This approach allows for a more nuanced understanding of the impact of political and economics decisions on PrEP uptake. The non-monotonic recruitment term, $h(S)S$ (Holling type III modified), is designed to capture the combined impact of policy-driven ressource limitations when susceptible population size (S) increases. This type of function is often used to model psychological effects of behavioral changes like saturation or protection measures in a susceptible population when the infected numbers are high. By simplifying the initial age-structured system into a coupled differential-difference system (4.1) with a discrete delay τ (representing the $\approx$ 3-month prescription renewal cycle), we captured the period of protection and potential vulnerability that is essential to PrEP adherence modeling. Our analysis yielded three principal results that challenge conclusions drawn from simpler models.

The non-monotonic recruitment function allows for the coexistence of up to three DFEs (Table (4.2), Figure (4.3)). These equilibria, E_0^1, E_0^2, E_0^3, correspond to distinct epidemiological settings: E_0^1 (low-risk/low-recruitment populations), E_0^2 (medium density/maximal recruitment, like the core MSM group in France), and E_0^3 (high density/saturated uptake). Crucially, the intermediate equilibrium E_0^2 is always un-

stable, leading to complex convergence scenarios.

We established clear basic reproduction number thresholds (R_0^i) for the existence and local stability of both the DFE and the endemic equilibrium E_I. When multiple DFEs coexist, the system's long-term behavior depends on the initial conditions, suggesting that even if an endemic equilibrium exists ($R_0^3 > 1$), the epidemic may still be eliminated if the population converges to a stable DFE (E_0^1 or E_0^3) with $R_0^i < 1$, as shown in Figure (4.8).

For the endemic equilibrium E_I, we demonstrated that the protection duration delay (τ) can be a destabilizing factor. When the DFE recruitment term falls in the decreasing part of $h(S)S$ ($\overline{h}(S_I) < 0$), the delay can induce a Hopf bifurcation at a critical value τ^*. This leads to the existence of recurrent periodic epidemic waves (Figure (4.7)). This result highlights that inadequate public health logistics or delayed policy response, represented by a longer effective τ, may inadvertently sustain oscillating HIV prevalence, even when PrEP uptake is significant.

A key public health implication of our analysis lies in the concept of the critical delay, τ^*. Clinically, PrEP is typically prescribed for three months ($\tau \approx 3$ months in model time), a period that coincides with the recommended window for mandatory STI and HIV re-screening for prescription renewal. The World Health Organization (WHO) and UNAIDS track "PrEP continuation at 3 months" as a crucial indicator of program retention and adherence. Our mathematical result shows that if the intrinsic dynamics of the system (determined by parameters like Λ, β, γ, and K) place the endemic equilibrium such that the actual effective renewal delay exceeds the critical delay ($\tau > \tau^*$), the system destabilizes.

In our numerical simulation, the calculated $\tau^* = 1.39$ time units is less than the standard three-month renewal period used for context, suggesting that delays even shorter than the WHO recommendation could be detrimental.This suggests that for populations vulnerable to policy-driven saturation effects ($\overline{h}(S_I) < 0$), the standard three-month τ should be viewed as an absolute maximum, and public health programs must aim for an effective delay significantly shorter than τ^* to ensure local asymptotic stability and prevent a shift from stable endemic control to perpetual oscillations. The critical role of τ^* thus mathematically formalizes the clinical urgency

of maintaining high rates of adherence and follow-up, especially in communities where the recruitment is operating in the saturation phase of the $h(S)S$ curve.

While this work provides local stability results, a complete understanding of this system requires further investigation into several avenues. Establishing global stability conditions for the disease-free and endemic equilibria is the next step for future works.

Introducing control variables for PrEP resources (γ and K) into the model could inform optimal resource allocation strategies for targeted populations, maximizing PrEP's cost-effectiveness while managing the resource saturation effect that leads to the non-monotonic uptake dynamics.

4.6 Comparaison between deterministic and stochastic approaches

The mathematical modeling of infectious diseases and their respective biomedical interventions demands an epistemological alignment between the biological characteristics of the pathogen, the clinical dynamics of the intervention, and the selected mathematical architecture. Modern mathematical epidemiology requires methodological pluralism; no single modeling framework can capture the entirety of an epidemic's complexity across all spatial and temporal scales . This thesis has navigated this complexity by intentionally shifting paradigms based on the research question at hand. Chapters 2 through 4 utilized continuous, deterministic differential-difference equations to uncover macro-level systemic thresholds and resource constraints associated with PrEP for HIV. In contrast, Chapter 5 employed a discrete, stochastic Agent-Based Model (ABM) to navigate the micro-level network heterogeneity and path-dependent biological sequelae underlying Chlamydia trachomatis (CT) and a hypothetical vaccine.The evaluation of a top-down public health policy, such as the deployment of HIV PrEP, fundamentally necessitates the analytical tractability provided by deterministic frameworks. By defining populations as continuous aggregates moving through mutually exclusive states, the DDE framework deployed in the preceding chapters permitted the exact, closed-form derivation of the basic reproduction number, $\mathcal{R}_0$ [8, 21]. This expression yields the critical threshold for the monthly PrEP recruitment rate required to constrain the reproduction number below unity. This is critical information for health policies to adapt funding accordingly.Furthermore, it enabled mathematical proofs regarding asymptotic stability. In chapter 4, the deterministic framework incorporated a unimodal functional response, denoted as $h(S(t))S(t)$, to model the recruitment of susceptible individuals into the protected compartment. This non-linear recruitment function mathematically encapsulates the macroeconomic reality of healthcare saturation: as the at-risk population expands beyond finite clinical capacities and budgetary limits, the rate of new PrEP initiations is constrained. Additionally, the framework integrated a discrete delay parameter, τ ,

representing the World Health Organization's mandated three-month clinical renewal cycle for PrEP [121]. This approach allows to encapture the particular schedule of PrEP combining tractability of deterministic model and still incorporating personal decision in the model through parameter θ.Another advantage of this approach lies in the discovery of Hopf bifurcations. Through rigorous stability analysis of the characteristic equation, we mathematically proved that if the clinical renewal delay τ exceeds a critical threshold τ^*, the disease-free equilibrium destabilizes. This demonstrates that logistical delays, interacting with resource saturation, can intrinsically generate recurring epidemic waves independent of stochastic environmental noise. While an agent-based model can highlight this behavior, deterministic models offers a white box vision and provide insights about nature of such oscillations, their durations and ways to mitigate them.Despite their analytical power for macro-policy evaluation, classical compartmental models exhibit structural limitations when applied to the microdynamics of STIs at a general level.The assumption of deterministic systems, homogeneous mixing and mass-action incidence is violated by STI transmission [18]. STI propagation is strictly constrained by the intricate topology of sexual networks, assortative mixing patterns, and the existence of highly connected core groups [17, 16].Traditional ODEs and DDEs essentially model infectious contacts as instantaneous collisions, struggling significantly to represent concurrent relationships and precise partnership durations. Moreover, continuous models assume exponentially distributed, memoryless residence times within compartments. They are structurally incapable of tracking an individual's unique, cumulative clinical history over a lifetime of sexual activity, a deficiency that becomes critical when evaluating path-dependent sequelae. However, HIV situation is different from others STIs. Because HIV establishes an irreversible infection, it is not subject to the complex reinfection cycles characteristic of other STIs; consequently, its transmission dynamics can be effectively modeled as an aggregate flow from the susceptible compartment. Considering a large population and focusing on the macro-level impact, it is reasonnable to use law of mass action. [179]. To resolve the limitations of homogeneous mixing, the evaluation of the Chlamydia trachomatis vaccine in Chapter 5 necessitated a transition to a stochastic Agent-Based Model. Unlike the irreversible Susceptible-Infected

dynamics of HIV, CT is a highly prevalent bacterial infection characterized by rapid Susceptible-Infected-Susceptible reinfection cycles and waning natural immunity [110]. The ABM framework operates on the principles of discrete, autonomous microsimulation, explicitly generating a dynamic sexual network where agents form persistent relationships. It successfully models concurrency and distinct gap times between partnerships. Most importantly, the primary public health burden of CT is not the acute asymptomatic infection, but severe, long-term reproductive sequelae such as Pelvic Inflammatory Disease (PID) [109]. The risk of developing PID is a cumulative, highly path-dependent phenomenon that escalates with repeated, untreated infections. By tracking discrete individuals, the ABM retains the clinical memory required to apply escalating PID risk multipliers based on an agent's precise infection history.The stochastic realism of the ABM comes at a severe computational and analytical cost. While DDEs offer mathematical computational speed, ABMs are inherently black box systems. The complex network parameters of the CT model required painstaking calibration against empirical demographic data, such as the National Survey of Family Growth (NSFG) and the National Health and Nutrition Examination Survey (NHANES) [163], frequently relying on computationally exorbitant Approximate Bayesian Computation (ABC) methods [55]. This complexity introduces inherent challenges regarding parameter identifiability and structural uncertainty. Unlike the deterministic derivation of global stability limits, ABM outputs yield probabilistic confidence intervals and variance metrics across Monte Carlo simulations. The choice between these paradigms is therefore a fundamental trade-off between absolute mathematical certainty and stochastic biological realism.The comparative analysis of deterministic DDEs and stochastic ABMs reveals that their scientific utility is strictly contingent upon the specific epidemiological question being posed. DDEs excel at answering macro-policy questions regarding systemic thresholds and logistical delays, whereas ABMs are indispensable for micro-targeting questions involving network topology and cumulative biological risk. Looking forward, the frontier of mathematical epidemiology lies in the development of hybrid architectures, specifically Mixed Agent-Based Compartmental frameworks [172]. Future research must seek to synthesize the strengths of both paradigms. For instance, researchers can

utilize the granular network outputs of an ABM to empirically derive exact contact probabilities and partnership durations, and subsequently integrate these parameters into a coupled deterministic compartmental structure. This hybrid approach promises to retain the analytical tractability required to compute R_0 and bifurcation risks, while remaining firmly grounded in the structural realism of complex sexual networks. Ultimately, the most robust epidemiological insights will be forged at the intersection of these diverse modeling paradigms.

Chapter 5

An agent-based platform for simulating the impact of chlamydia vaccine in the US population

5.1 Introduction

Chlamydia trachomatis (CT) is the most frequently reported bacterial sexually transmitted infection (STI) worldwide [160]. In 2023, the US Centers for Disease Control and Prevention reported 1.6 million cases of chlamydia, which represents two-thirds of all STIs reported that year. Nonetheless, chlamydia is mainly asymptomatic (>80%) at any infection site [27, 131, 110, 130], and reporting cases from surveillance data are likely to underestimate the prevalence of the disease [99]. The data are also likely to be biased by opportunistic screening practices because of the focus on young women and at-risk groups in the population (like man who have sex with men (MSM) and sex workers) [164]. Untreated infections can lead to severe reproductive health outcomes, especially in women as infection can ascend the reproductive tract causing pelvic inflammatory disease (PID) that may lead to ectopic pregnancy and infertility [43]. Some countries have implemented CT control programs using the

'test and treat' approach for asymptomatic at-risk groups [111], but evidence of their effectiveness in reducing infection prevalence or preventing PID is limited. Despite screening recommendations, uptake remains suboptimal, and some scientists suggest that these programs might detect transient self-resolving infections [112]. While CT has not shown significant antimicrobial resistance (AMR)[133, 166], this has been described in association with other pathogens like gonorrhea [86]. Routine screening in low-prevalence populations may not be cost-effective [38, 48, 155], leading some health agencies to consider more targeted approaches for high-risk groups or behavioral interventions [86, 38]. The development of a vaccine against CT represents a promising avenue to enhance existing control [154, 90]. Several vaccine candidates are under development in preclinical and early clinical trials [105, 93, 7]. Thus, a flexible, user-friendly modeling platform would be particularly timely as a tool to simulate CT transmission in a population and to investigate how pharmacological interventions can mitigate the disease burden. The value of such a platform would be further amplified if it were built in such a way as to be readily extensible to other sexually transmitted diseases. Mathematical modelling studies can be a useful tool for evaluating the impact of vaccines [154, 75, 59, 96]. Recently, Makhoul et al. [154] examined the potential population-level impact of a hypothetical chlamydia vaccine in the US using a deterministic compartmental framework. They demonstrated that a moderately efficacious CT vaccine could substantially reduce chlamydia prevalence. Such compartmental models provide valuable insights into forming chlamydia epidemiology and vaccination policy, particularly for large-scale projections.

In our study, we focused on questions that require explicit representation of individual infection histories, dynamics of sexual partnerships and the accumulation of long-term sequelae. Addressing these outcomes requires tracking individuals over time and linking transmission events to downstream health consequences, which is more naturally represented within an agent-based modeling (ABM) framework[24, 33, 50]. We therefore develop an ABM to simulate CT transmission dynamics and evaluate candidate vaccination strategies under realistic scenarios. For this analysis, we will explore the impact of a chlamydia vaccination program on two main outcomes: 1)

CT infection rates in the community (males and females), and 2) PID rates in the overall female population. We implement different vaccination scenarios, varying vaccine efficacy, uptake and recommendations in people aged 15-44 years (Table 1). We explore the potential benefit of the vaccine in reducing the risk of infection and CT transmission and test the impact of population prioritization.

5.2 Methods

Our ABM tracks 20,000 sexually active agents, aged 15 to 54 years, with equal numbers of males and females over time. The age distribution of the simulated population mimics that of the US population within the corresponding age range [183]. Each agent is characterized by a set of attributes, including age, sex, sexual behavior (heterosexual, female sex workers (FSW) or MSM), preferred number of concurrent partners (pnp), vaccination status, CT infection status and age-specific immunity level against CT infection. We did not consider male sex workers as they constitute a marginalized subgroup of overall group [169] and women who have sex with women as they contribute very little to STI transmission [46]. The values and distributions of model parameters, along with their sources, are provided in Table 5.2. Note that parameters sampled from normal distributions are truncated at lower bounds to prevent non-physical negative. For example, the duration of treated chlamydia infection was sampled from a normal distribution with mean 2 weeks and variance 2 weeks, with a lower bound of 1 week [33]. The model simulation operates with a time step of one week. The algorithmic description of our model implementation is provided at the end of this part (Algorithm 1). At each simulation step, the model executes three main operations: the removal and addition of agents, the formation and dissolution of dynamic relationships, and the transmission of disease.

Algorithm 1: Pseudocode for the IBM/ABM algorithm for modeling chlamydia transmission

```
   // Model initialization
1  for t = 0 to T' do
       // Agent removal and addition
2      for agent from 1 to N do
3          if agent.age > agent.maximum_age then
4              remove this agent and create a new agent
       // Dynamic relationship formation and dissolution
5      for agent from 1 to N do
6          if agent.existing_partners < agent.pnp and agent.gap_time ≥ 0 then
7              for other_agent from 1 to N do
8                  if sexual orientation and gender are compatible then
9                      form relationship
10     for agent from 1 to N do
11         if agent.duration < 0 then
12             relationship ends and assigns gap time
       // Disease transmission
13     for agent from 1 to N do
14         for partner in agent.existing_partners_list do
15             if agent or partner is infected then
16                 CT transmitted with sex/age-dependent probability
```

Agent removal and addition

To maintain a dynamic yet constant population size, each agent ages by one week at every simulation time step. Once an agent reaches 55 years of age, they are immediately removed from the network, and any relationships involving that agent are dissolved. Simultaneously, a new 15 year-old agent is introduced into the network to replace the departing individual. The new agent is assigned a sex that balance the female: male ratio over time. The sexual behavior of new agents is randomly assigned in accordance with the predefined distribution of characteristics. Upon entering the population, new agents have no existing relationships but are immediately available to form them. These incoming agents are considered naïve, meaning they are neither infected nor vaccinated. It is assumed that all agents retain consistent sexual behavior throughout their lifetime.

Dynamic relationship formation and dissolution

The formation and dissolution of relationships are strongly related to agents' age, sexual behavior and predefined partnership preference. In the model, heterosexual individuals form partnerships exclusively with agents of the opposite sex, while MSM form partnerships exclusively with other MSM individuals. FSW can establish relationships with any heterosexual male. Let p_{ij} denote the probability that agent i forms a relationship with agent j. This probability is assumed to follow a Gaussian distribution centered around the age difference between the agents. Specifically, let age_i and age_j be the ages of the two agents, age_{male} and age_{female} be the ages of male and female agents from the network, and μ and σ denote the mean and standard deviation of the preferred age difference, respectively, then the relationship probability is defined as:

$$p_{ij} = \begin{cases} 1, & \text{if agent is FSW,} \\ e^{-\frac{1}{2}\left(\frac{\Delta}{\sigma}\right)^2}, & \text{otherwise.} \end{cases}$$

in which Δ is the age difference between agents and is defined based on the relationship type: for homosexual pairs $\Delta = |\text{age}_i - \text{age}_j|$; for heterosexual pairs $\Delta = |\text{age}_{male} - \text{age}_{female} - \mu|$. The sex workers are likely to have sexual relationship with people of a wide age range. Thus, if either agent is a sex worker, the probability of relationship formation is set to 1, regardless of age. This formulation ensures that: (1) agents of a similar age are more likely to form a relationship; (2) male agents are likely to form a relationship with females who are younger than themselves. This aligns with the observed facts in the US [153]. Once a relationship is formed, it is probabilistically designated as either long-term or short-term. The duration of relationships is geometrically distributed, with long- and short-term relationships having different average values; the duration of each partnership is then stochastically drawn from the appropriate distribution. Partnerships involving FSW are treated separately: they are always modeled as short-term encounters, with durations drawn from normal distribution (mean 2 weeks, variance 2 weeks). In reality, FSWs may maintain longer-term relationships, which are not explicitly represented in the model. However, given the relatively small size of the FSW population and the focus of our analyses on population-level vaccination effects, this simplifying assumption is unlikely to materially influence the main conclusions. At each simulation step, the model decrements the duration between the partners by one week. When the duration reaches zero, the relationship is dissolved. Following dissolution, both agents enter a gap period during which they are temporarily ineligible to form new relationships. This ensures a realistic turnover rate in partnerships and mimics social network stability. An exception is made for sex workers, who do not experience a gap period between partnerships. While most agents prefer to maintain monogamous relationships, a minority (5% of the population) engage in concurrent partnerships, with each participating agent allowed up to three simultaneous partners.

Disease transmission

We consider the rates of chlamydia infection in the general population of both males and females. Initially, a proportion of agents is assumed to be infected with chlamydia

based on the age- and sexspecific prevalence estimates in the US [108]. Then, at each simulation step, chlamydia transmission occurs through sexual contact. The model has Susceptible - Exposed - Infected - Recovered – Susceptible (SEIRS) transmission dynamics. In this model, susceptible agents are those who are not currently infected with chlamydia and lack immunity, rendering them at risk of acquiring infection upon exposure. A susceptible agent becomes infected following sexual contact with an infectious partner, with the per-contact probability of transmission determined by the direction of transmission: from an infected male to a susceptible female, the probability is $\beta_{m\to f}$, whereas from an infected female/male to a susceptible male, the probability is $\beta_{f/m\to m}$. The frequency of sexual contact is relationship-type specific: on average, long-term partnerships involve 1.75 sexual encounters per week, short-term partnerships involve 3 weekly encounters [33], and partnerships FSW include 10 encounters per week. Then the weekly probability that a susceptible female in a long-term relationship with an infected male becomes exposed $P(male \to female)$ is calculated as:

$$P(male \to female) = 1 - (1 - \beta_{m\to f})^{1.75}.$$

Analogous expressions are used to compute the weekly transmission probabilities in other cases, including short-term relationships, transmission from infected females to susceptible males, and contacts involving FSW. Following infection, susceptible agents transition to the exposed state, during which they are not yet infectious. After an incubation period of two weeks [33], exposed agents move into either the asymptomatic infected state with a probability of 85% or into the symptomatic infected state [110, 130]. Symptomatic individuals have a weekly probability of seeking treatment, while the asymptomatic agents have a chance to be screened and detected. Infected agents who are detected and treated are assumed to recover within two weeks [33]. Those who remain undiagnosed and untreated experience prolonged infection durations, which are randomly drawn from a normal distribution with a mean of 52 weeks and a variance of 52 weeks. A lower bound with 45 weeks was applied to reflect

the typically prolonged duration of untreated infection [54, 40]. Recovered agents acquire partial and temporary natural immunity, meaning their susceptibility to reinfection after exposure is reduced relative to susceptible agents. The magnitude of this reduction is modeled by stochastically drawing from a uniform distribution spanning 20% to 80%. This assumption is consistent with estimates reported by the work [89], which inferred a mean reduction in susceptibility of 67% [95% uncertainty interval: 24%–88%] based on US data. Following recovery, individuals enter a refractory period representing temporary post-infection immunity, before gradually returning to the fully susceptible state. The average refractory duration after recovery defines the mean length of this post-recovery immune period and is modeled as a stochastic process with a mean of 6 weeks following natural recovery and 2 weeks following treatment, consistent with [33]. This representation of partial, waning immunity acting through reduced susceptibility is consistent with prior mathematical modeling studies of CT, which suggest that long-lasting or complete immunity is incompatible with observed reinfection patterns and endemic persistence [89, 69].

Female agents have an age-dependent weekly probability (P_{base}) of developing all-cause PID independent of CT infection. For treated CT-infected women, studies indicate PID risk increases by 55% after initial infection, an additional 17% following second infection, and 35% after third or subsequent infections, compared to uninfected women [56], on top of P_{base}. Untreated CT-infected women face a one-time 16% probability of developing PID [110, 67], independent of P_{base} or infection history. Model calibration varied P_{base} to match U.S. female population PID prevalence estimates [109], confirming P_{base} is well below 1%, with untreated CT-infected individuals having substantially higher overall PID risk than treated ones.

Output of model simulation under different vaccination scenarios

The model runs for 50 years to stabilize sexual network and disease dynamics, then calibrates to match US chlamydia prevalence. PID is introduced and simulated for

another 50 years, with recalibration to reflect observed PID prevalence (Table 5.1.

Table 5.1: Calibration prevalence targets for Chlamydia and PID

Metric	**Values and ranges**
Chlamydia infection % (25th–75th percentile)	
Total	2.138 (2.001–2.279)
Age group	
15–39	3.673 (3.415–3.935)
25–39	1.149 (0.989–1.318)
Gender	
Female	2.410 (2.201–2.616)
Male	1.881 (1.691–2.072)
Source	[79]
1+ lifetime PID episodes % (95% CI)	
Total	4.1 (3.2–5.1)
Age Group	
15–24	2.8 (1.2–4.3)
25–34	3.6 (2.3–5.0)
35–44	5.4 (3.4–7.5)
Source	[183]

We further perform model validation using epidemiological datasets that were not used as calibration targets. Using the calibrated and validated model, we evaluate various vaccination scenarios' impact on chlamydia prevalence in males and females, and all-cause PID in US females (Table 5.2). Vaccination targets individuals under

44 years, regardless of infection history, until simulation end. Vaccine coverage is the proportion of the target population vaccinated. For example, a coverage level of 60% implies that 60% of the targeted population currently has vaccine protection. The model doesn't account for multiple doses or boosters. Each scenario was simulated using 20 independent stochastic realizations to account for random variability inherent to the ABM. To assess whether this number of simulations adequately captures stochastic uncertainty, we conducted a sensitivity analysis using 10, 20, 50 and 100 simulations. Across these analyses, mean outcome trajectories and relative differences between scenarios were highly consistent, without altering qualitative conclusions or scenario rankings (5.7). Based on this convergence behavior and the substantial computational cost of the model, we therefore report results based on 20 simulations per scenario. The base scenario systematically examined different combinations of vaccine efficacy (VE) and coverage (VC) for substantial chlamydia and PID reduction. It assumed constant vaccine protection (i.e., susceptibility reduction to infection) for uninfected individuals. Recognizing vaccine-induced immunity may wane over time due to immune memory degradation or pathogen evolution [93], we extended this to include time-varying VE with fixed VC, modeling exponentially declining immunity. In addition, to assess the impact of a gradual uptake of the vaccine while considering wanning of vaccine-induced immunity, we conducted a scenario analysis in which VC gradually increases to 60% over 5 or 10 years, while VE exponentially declines from an initial value of 80%. While vaccines often aim for sterilizing immunity, many provide partial protection by reducing susceptibility, disease severity, or infectiousness [117, 23]. For a potential chlamydia vaccine, protection could reduce susceptibility (as in previous scenarios) and lower infectiousness among vaccinated infected individuals, potentially by decreasing bacterial load via vaccine-induced immune responses [33, 117, 23]. We simulated three scenarios where vaccines: (1) reduce susceptibility only, (2) reduce infectiousness only, or (3) reduce both, administered to individuals aged 15-44 years. Finally, we explored targeted vaccination strategies by age and sex versus broader population approaches. Although simulations were conducted in a finite population, demographic turnover through agent aging and replacement ensured continuous population renewal and reduced the likelihood of stochastic ex-

tinction unrelated to intervention effects. Importantly, extinction was not observed in isolated or sporadic simulation replicates across all scenario's runs. When near elimination occurred, it did so consistently across all stochastic realizations within a given scenario.

Model calibration

Most model parameters are obtained and inferred from existing literature and epidemiological data (Table 5.2). Several key parameters, including the average gap time between partnerships (long- and short-term), the transmission probabilities per sexual contact $\beta_{(m\to f)}, \beta_{(f/m\to m)}$, and the age-specific baseline probability of developing PID in female agents, that cannot be estimated directly, are calibrated so that the model outputs match the available datasets [113, 108, 163, 109]. We use a simulation-based, rejection-style Approximate Bayesian Computation (ABC) calibration approach to ensure that the model reproduces key behavioral and epidemiological patterns observed in US. Model calibration proceeds in three sequential stages: sexual network calibration, CT transmission calibration and PID prevalence calibration. After running the model for 50 years, a stable sexual network with a population of 20,000 individuals is established. To align the simulated network with empirical behavioral data, we calibrate parameters governing the average gap between the dissolution of a partnership and the formation of a new one, separately for long-term and short-term partnerships. Motivated by the works [33, 24], we assume nominal distributions over plausible ranges for these two parameters and sample values from the priors to simulate dynamic partnership formation and dissolution. For each sampled parameter combination, we compute the average number of lifetime sexual partners per individual, and compare it with corresponding estimate, which is around six, from the National Survey of Family Growth (NSFG) [113]. Parameter combinations that reproduced the NSFG partnership patterns are retained. The retained samples form empirical posterior distributions for the average durations of short-term and long-term partnerships. After calibrating the sexual network, CT infection is introduced into the network. In this phase, the model is further calibrated to CT prevalence

rates in the US, which were taken from Kreisel et al [108]. These prevalence estimates pertain to the general population aged 15-39 years and are stratified by gender (male and female) and age group (15-24 and 25-39 years), based on data from 2015-2018 cycles of the National Health and Nutrition Examination Survey (NHANES) [163]. Due to limited prior information on the values of $\beta_{(m\to f)}$ and $\beta_{(f/m\to m)}$, we assume a uniform prior distribution for $\beta_{(m\to f)}$ and set $\beta_{(f/m\to m)} = 0.4\beta_{(m\to f)}$. Values of $\beta_{(m\to f)}$ are sampled from the prior distribution and used to run the model. For each sampled parameter value, we compute three summary statistics from model output: (i) overall chlamydia prevalence, (ii) age-specific prevalence, and (iii) sex-specific prevalence. These model-derived prevalence estimates are compared against corresponding estimates derived from NHANES data [108, 163]. Parameter values are retained if all three simulated prevalence rates jointly fall within predefined tolerance ranges around the empirical targets. The retained parameter values form an empirical approximation to the posterior distribution of the $\beta_{(m\to f)}$. The calibration results, presented in the 5.1 Fig., suggest that $\beta_{(m\to f)}$ values in the range of 0.32 to 0.38 yield prevalence estimates that closely aligned with the targets.

We then select the simulations that reach stable endemic equilibrium and store them as a pool of baseline simulations for subsequent simulation. This approach aims to conserve computational resources by skipping the initialization step. Following the calibration of CT prevalence, we calibrate the age-specific baseline probability of developing PID to reproduce observed PID prevalence in the US population [109]. During CT prevalence calibration, both background PID rate and the probability of getting PID induced by CT infection were set to zero, such that no PID occurred in the population. For PID calibration, we fix probability of getting PID induced by CT infection according to the existing literature and vary the background probability to reproduce the PID prevalence. At this stage, simulations are initialized using previously stored calibrated baseline simulations rather than reinitializing agents. We assume uniform prior distributions over plausible ranges for the baseline PID probabilities and conduct simulations analogous to the CT calibration step. For each sample parameter set, we run the model and compute age-specific lifetime prevalence

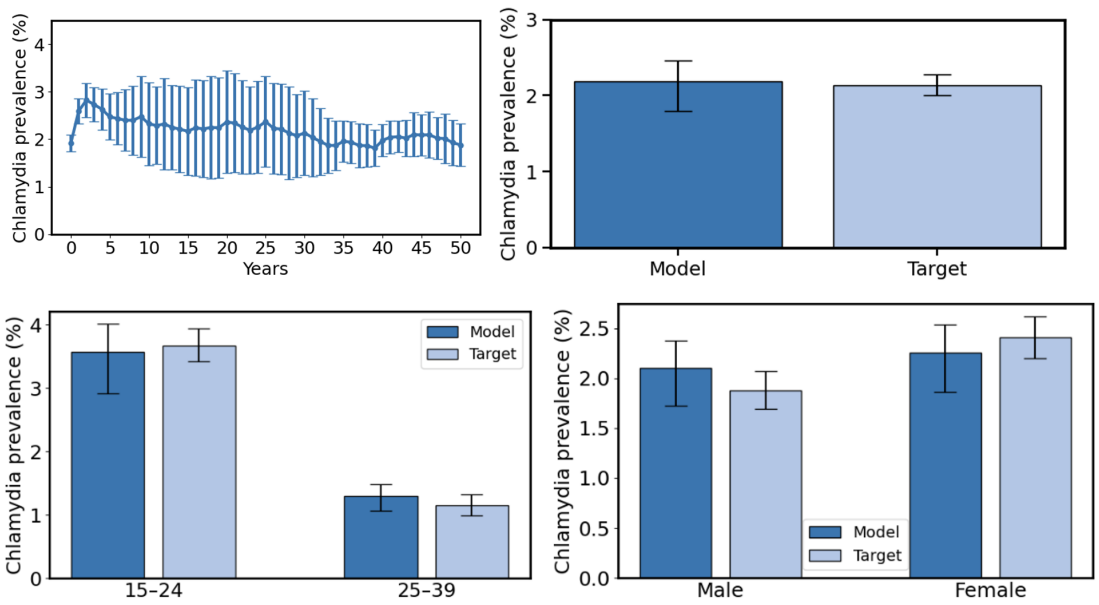


Figure 5.1: **Model calibration of CT prevalence, with comparison to prevalence estimates.** This figure shows the model-predicted CT prevalence in comparison with targets reported by Kreisel et al [108]. The model is simulated 10 times over a 50-year period to ensure equilibrium, and prevalence estimates of the last year are shown as median values with error bars indicating the interquartile range (25th to 75th percentiles) across simulations. The model outputs indicate that the overall prevalence, gender- and age- stratified prevalences align closely with empirical data. The estimated transmission probability $\beta_{m\to f}$ ranged from 0.32 to 0.38, and $\beta_{f/m\to m}$ ranged from 0.13 to 0.15.

of all-cause PID. These outputs are compared with NHANES-derived lifetime PID prevalence estimates by age group [109]. Parameter values producing close agreement with observed PID prevalence are retained, yielding an approximate posterior distribution for age-specific baseline PID risk. Importantly, calibration targeted all-cause PID prevalence rather than PID attributable to chlamydia specifically, allowing chlamydia-attributable PID to emerge endogenously from simulated infection histories. As shown in 5.2 Fig., we have two base PID probabilities that match the PID prevalence targets. Simulations incorporating these calibrated PID parameters are then added to the simulation pool used in subsequent vaccination scenarios analyses.

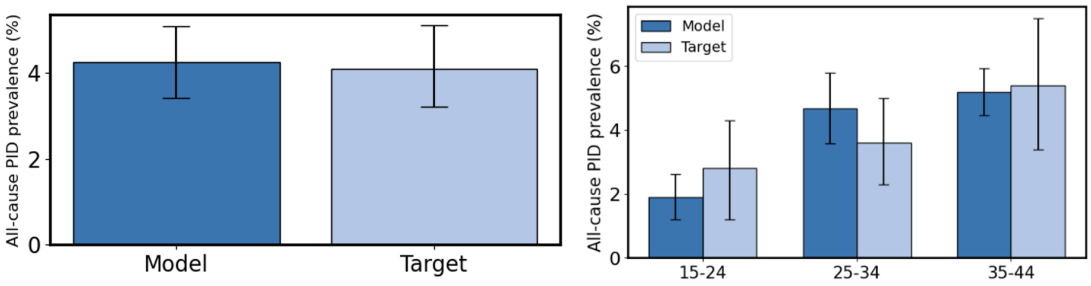


Figure 5.2: **PID prevalence calibration results.** This figure shows the model-predicted CT prevalence in comparison with targets reported by Kreisel et al [109]. The model is simulated 10 times over an 80-year period to ensure equilibrium, and prevalence estimates of the last three years are shown as median values with error bars indicating the 95% confidence interval across simulations. The model outputs indicate that the overall prevalence and age- stratified prevalences align closely with empirical data. The estimated baseline weekly probability of developing PID P_{base} is in the interval $[2 \times 10^{-5}, 10^{-4}]$ for females under 24 years of age and $[10^{-5}, 1.5 \times 10^{-5}]$ for those aged 24 years and older.

There are several limitations of the calibration approach. First, the rejection-based ABC framework does not yield a formal likelihood or a full joint posterior distribution over all model parameters. Instead, parameters are calibrated sequentially, and dependencies between different parameter sets may not be fully characterized. Second, tolerance thresholds for accepting parameter values necessarily involve subjective choices, and alternative thresholds could yield slightly different posterior approximations. Third, due to computational constraints, calibration is performed using a finite number of stochastic simulations, which may not exhaustively explore the full parameter space. Despite these limitations, this calibration strategy is well suited to complex stochastic ABMs for which likelihood-based inference is infeasible. To further address uncertainties inherent in the calibration process, we perform model validation using epidemiological datasets that were not used as calibration targets, as described in the subsequent section.

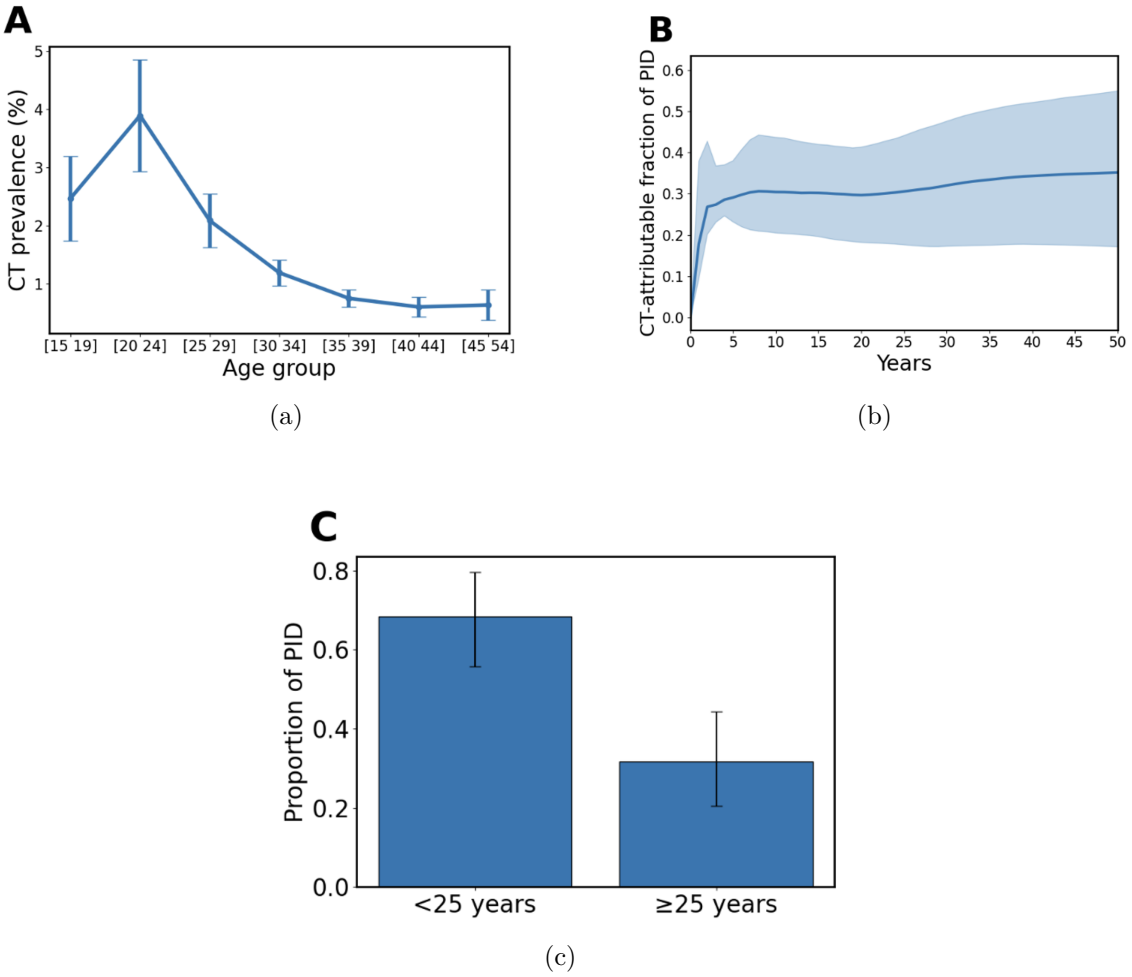
Model validation using non-calibration targets

We perform model validation using epidemiological datasets that were not used as calibration targets [149, 73, 14, 120]. Specifically, we examine whether the model could reproduce (i) the age-specific surveillance pattern of reported CT cases, (ii) the fraction of PID attributable to CT infection, and (iii) the age distribution of first PID onset. None of these outcomes were directly constrained during model calibration. Instead, they arise naturally from the model simulations and are compared directly with independent empirical datasets, providing an external assessment of model validity beyond the calibration targets. We first compare model outputs with age-specific chlamydia rates reported in the US Sexually Transmitted Infections Surveillance reports published by the Centers for Disease Control and Prevention [149], which were not used in model calibration. According to the Centers for Disease Control and Prevention, Sexually Transmitted Infections Surveillance 2020-2024 report, chlamydia reported case rates were highest among individuals aged 20–24 years, followed by those aged 15–19 years and 25-29 years, with lower rates in older age groups. Clearly, the model's age-specific prevalence outputs exhibit a highly consistent ordering across age groups (Figure 5.3).

This quantitative alignment in age gradients between model output and Centers for Disease Control and Prevention reported rates strengthens our confidence that the model captures realistic age-dependent transmission dynamics. While surveillance data are not direct measures of true prevalence, the consistent relative age pattern (20–24 > 15–19 > 25–29, etc.) between model output and surveillance data supports model validity. In the model, PID was considered as all-cause outcome. Model calibration therefore targeted lifetime prevalence of all-cause PID using estimates derived from NHANES data [163, 109]. As part of model validation, we examine the fraction of PID attributable to CT infection. Price et al. [73] synthesized evidence from multiple methodological approaches and reported that, in high-income settings, an estimated mean of 35% of PID cases are attributable to CT with a wide 95%CI of 11%–69%. Earlier national surveillance summaries from the US Centers for Disease Control and Prevention [14] similarly suggested that chlamydia accounts

for a substantial proportion of PID burden at the population level.

Our model estimates that 37.9% of PID cases are attributable to CT infection, with a simulated 95% CI of 17.6%–60.4% (Figure 5.3). This estimate lies well within the range reported in the literature [73, 14]. Finally, we evaluate the model's ability to reproduce the age distribution of first PID onset. According to the US Sexually Transmitted Infections Treatment Guidelines, the peak incidence of PID occurs among females aged 15–25 years, and that approximately 70% of the estimated one million annual PID cases in the US occur in women under 25 years of age [120]. In the simulated population, first PID episodes are similarly concentrated at younger ages, with the majority occurring before age 25 and a clear peak in early adulthood (Figure 5.3). This close agreement in age distribution provides additional support for the model's ability to capture age-dependent risk accumulation leading to PID.



(a) (b)

(c)

Figure 5.3: **Model validation results.** (A) Age-specific CT prevalence without vaccination, showing higher prevalence among younger age groups. Points represent the mean prevalence across stochastic simulations, with error bars indicating 95%CI. (B) Time series of the fraction of PID cases attributable to CT, with the solid line indicating the mean across stochastic simulations and the shaded region representing the 95%CI. (C) Distribution of age at first PID onset, grouped as < 25 and ≥ 25 years. Bars represent the proportion of first PID cases in each age group averaged across simulations, with error bars indicating 95%CI, showing that the majority of PID cases occur before age 25.

Table 5.2: Parameters for the model simulation (No vaccination case)

Parameter	Values	Distribution	Reference
Sexual behavior			
Size of the population	20,000	—	—
Age range in the model	15–54 years	—	—
Percentage of MSM	3.3 %	—	[148]
Percentage of FSW	0.023 %	—	[84]
Preferred concurrent partners	1, 2, or 3	—	[33]
Average lifetime partners	6	—	Model output
Agents with concurrent partners	5 %	—	[181]
Probability that an agent is available to form additional partnerships:			
Second relationship	0.75	—	[33]
Third relationship	0.25	—	[33]
Prob. long-term partnership	0.4	—	[33]
Average duration:			

Continued on next page...

Parameter	Values	Distribution	Reference
Long-term	8 years	Geometric	[33]
Short-term	2 weeks	Geometric	[24, 33]
Number of sexual contacts per week:			
Long-term	1.75	—	[33]
Short-term	3	—	[33]
FSW	10	—	Assumed
Gap between partnerships:			
Long-term (weeks)	$\max(25, \mathcal{N}(45, 30))$	Trunc. Normal	Fitted
Short-term (weeks)	$\max(4, \mathcal{N}(20, 15))$	Trunc. Normal	Fitted
CT infection parameters			
Transmission probability:			
Male to female	$[0.32, 0.38]$	Uniform	Fitted
Female to male	$[0.13, 0.15]$	Uniform	Fitted
Incubation period	2 weeks	—	[33]
Asymptomatic infections	0.85	—	[110, 130]

Continued on next page...

Parameter	Values	Distribution	Reference
Infection duration (weeks):			
Without treatment	$\max(45, \mathcal{N}(52, 52))$	Trunc. Normal	[56, 67]
With treatment	$\max(1, \mathcal{N}(2, 2))$	Trunc. Normal	[33]
Prob. seeking treatment:			
Female	0.14 / week	—	[79]
Male	0.25 / week	—	[79]
Reinfection susceptibility	$[0.2, 0.8]$	Uniform	[71, 98]
Refractory duration:			
Natural recovery	6 weeks	Uniform	[33]
Post-treatment	2 weeks	Uniform	[33]
Background screening:			
Female ≤ 24 / 24+	0.00525 / 0.00598	—	[79]
Male ≤ 24 / 24+	0.00277 / 0.00338	—	[79]
Detection sensitivity	0.9	—	Assumed
PID parameters			
Baseline prob. (female):			

Continued on next page...

Parameter	Values	Distribution	Reference
≤ 24 years old	$[2 \times 10^{-5}, 10^{-4}]$	Uniform	Fitted
> 24 years old	$[10^{-5}, 1.5 \times 10^{-5}]$	Uniform	Fitted
Risk multiplier (treated):			
One episode	1.55	—	[175]
Two episodes	1.8135	—	[175]
Three+ episodes	2.0925	—	[175]
Untreated PID prob. (one-time)	0.16	—	[110, 150]

Table 5.3: Vaccination scenarios

Scenario	**Assumptions**	**Implementation**
Base scenario	Protection mechanism: reducing susceptibility in uninfected individuals. Targeted population: individuals aged 15–44 years.	For each (VC, VE)pair, simulations are conducted under the assumption that both parameters remain constant over time.
Impact of VE waning rate	Protection mechanism: reducing susceptibility in uninfected individuals. Targeted population: individuals aged 15-44 years.	VC is fixed at 60%, while VE declines exponentially according to specified waning rates.
Impact of vaccination scale-up under waning immunity	Protection mechanism: reducing susceptibility in uninfected individuals Targeted population: individuals aged 15–44 years.	VC increases gradually from 0 to 60% over 5, 10, or 20 years. VE decays exponentially from 80% with a decay rate of 1/(10 years).
Impact of different vaccine mechanisms	Protection mechanism: reducing susceptibility in uninfected individuals or/and infectiousness in infected individuals Targeted population: individuals aged 15–44 years.	VC is fixed at 60%; VE decays exponentially over time an initial value of 80% with a decay rate of 1/(10 years).

Following on the next page

Table 5.3 – suite de la page précédente

Scenario	Assumptions	Implementation
Impact of target population prioritisation	Protection mechanism: reducing susceptibility in uninfected individuals. Targeted population: grouped by age and sex.	VC fixed at 60% or 90%; VE decays exponentially ove time from an initial value of 80% with a decay rate of 1/(10 years).

5.3 Results

Vaccine efficacy (VE) and vaccine coverage (VC) required to reduce prevalence of chlamydia infection in the community.

An ongoing vaccination campaign with a moderately efficacious vaccine (VE = 50%) and moderate coverage (VC = 60%) resulted in chlamydia prevalence decreased by 64.2% [95%CI: 43.0–68.1] relative to the baseline scenario without vaccination (figure 5.4 panels **a** and **c**), while PID prevalence declined by 14.3% [95%CI: 10.1–29.4] (figure 5.4 panels **b** and **c**). Our simulations suggested that an efficacy of at least 80% with 60% coverage, or alternatively 50% efficacy with 90% coverage, is necessary to achieve reductions in chlamydia prevalence exceeding 80%. The greatest reductions in both chlamydia and PID burden, however, are observed when both VE and VC exceed 80%. Under these conditions, chlamydia prevalence declines to near-zero levels, highlighting the potential for disease elimination with a high-performing vaccine and widespread implementation.

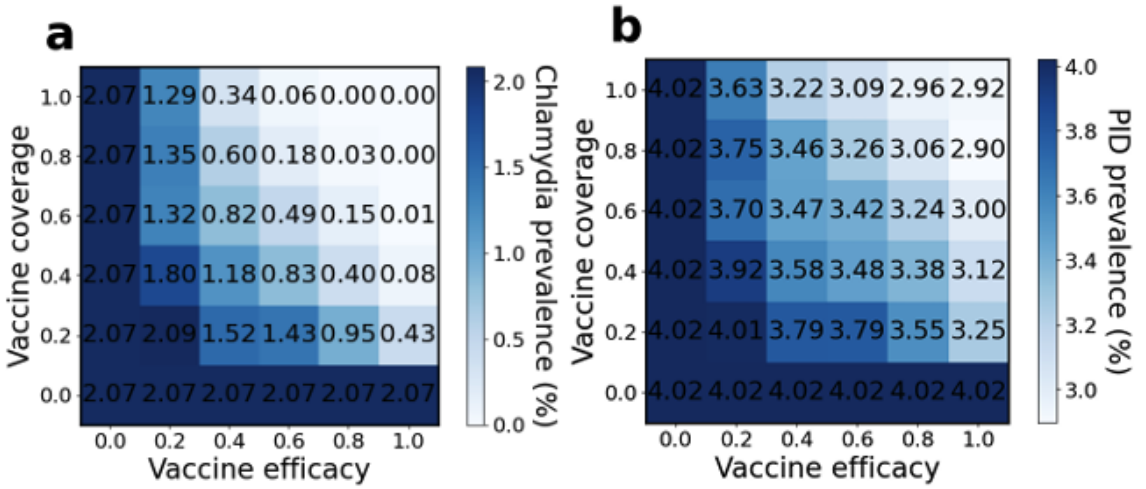


Figure 5.4: Chlamydia a and PID b prevalence rates across combinations of vaccine efficacy and coverage. Each cell represents the mean prevalence calculated from 20 independent simulations per combination. Vaccine efficacy ranges from 0 to 1, indicating the degree to which the vaccine reduces susceptibility to infection. Vaccine coverage ranges from 0 to 1, representing the proportion of the population (males and females) aged 15–44 years that is vaccinated.

Impact of VE waning rates.

A vaccine with rapid waning rates (decay rates of $(1year)^{-1}$ or $(5years)^{-1}$) may have limited longterm effectiveness (5.5), assuming a fixed VC of 60%. In contrast, vaccines with slower waning rates, such as $(10years)^{-1}$ or longer, are associated with substantially greater reductions. Specifically, a vaccine with a 10-year decay rate achieves a 60.8% [95% CI: 50.8–75.9] reduction in chlamydia prevalence, although this was 33.7% [95% CI: 14.5–48.0] less reduction compared to a vaccine with constant VE. We adopt a 10-year half-life assumption for VE decay in all subsequent vaccination scenario analyses. Under this assumption, vaccine-induced immunity decreases by half every decade and can be considered to have almost disappeared approximately 40 years after vaccination.

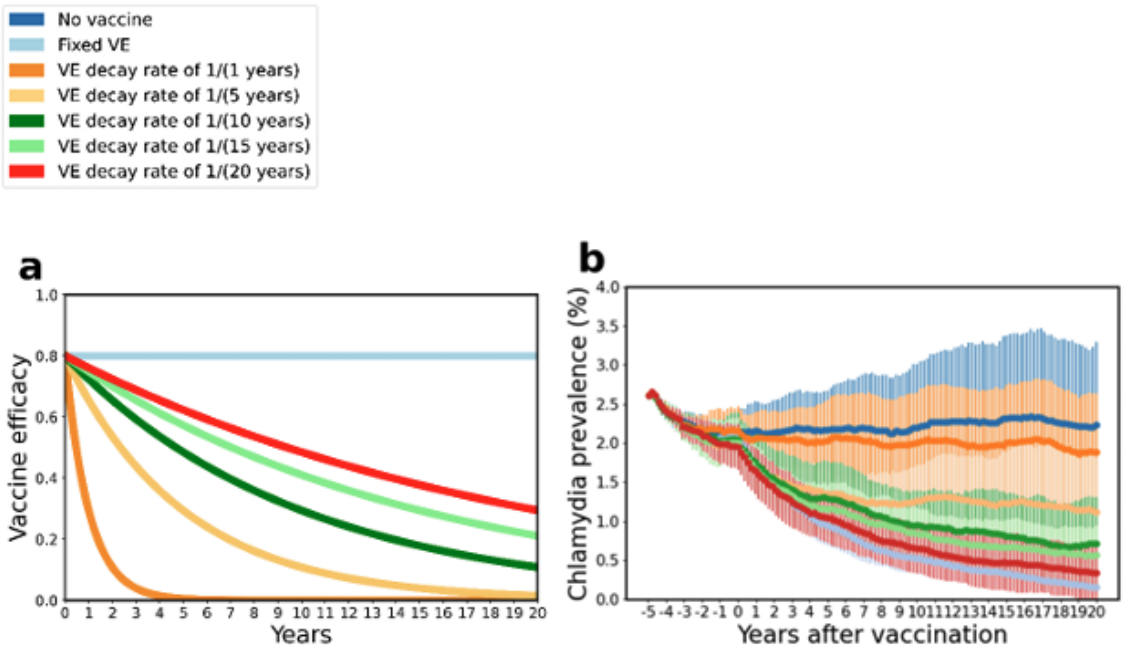


Figure 5.5: **a** Vaccine efficacy changes with time over 20 years. The solid light blue line represents a vaccine with fixed efficacy (80%) throughout the simulation while other curves represent vaccines with exponentially decaying efficacy, corresponding to decay half-lives of 1, 5, 10, 15, and 20 years. **b** Chlamydia prevalence under different vaccine efficacy dynamics. X-axis represents simulation time in years, where year 0 marks the introduction of vaccination, and y-axis shows the chlamydia prevalence. The solid lines represent the mean prevalence from 20 simulations, with error bars indicating 95% confidence intervals.

Impact of vaccination scale-up under waning immunity.

Figure 5.6 panel **a** shows the resulting population-level effective immunity over time, defined as the average individual-level vaccine protection across the population. Under immediate coverage, effective immunity rises sharply following vaccine introduction but subsequently declines as vaccine-induced protection wanes. In contrast, gradual scale-up scenarios generate slower accumulation of population immunity, with peak effective immunity occurring later and at lower levels as scale-up duration increases. These patterns illustrate the competition between immunity gains from vaccine rollout

and losses due to waning protection. Immediate coverage achieves the largest relative reduction in chlamydia prevalence (59.0% [95% CI: 45.9–72.1]), followed by 5-year (52.5% [95% CI: 31.1–73.9]) and 10-year scale-up scenarios (51.9% [95% CI: 27.7–76.1]) (5.6 panel **b**). In the subsequent scenario analyses, we adopt the immediate scale-up assumption to provide clearer comparison across vaccine characteristics and targeting strategies.

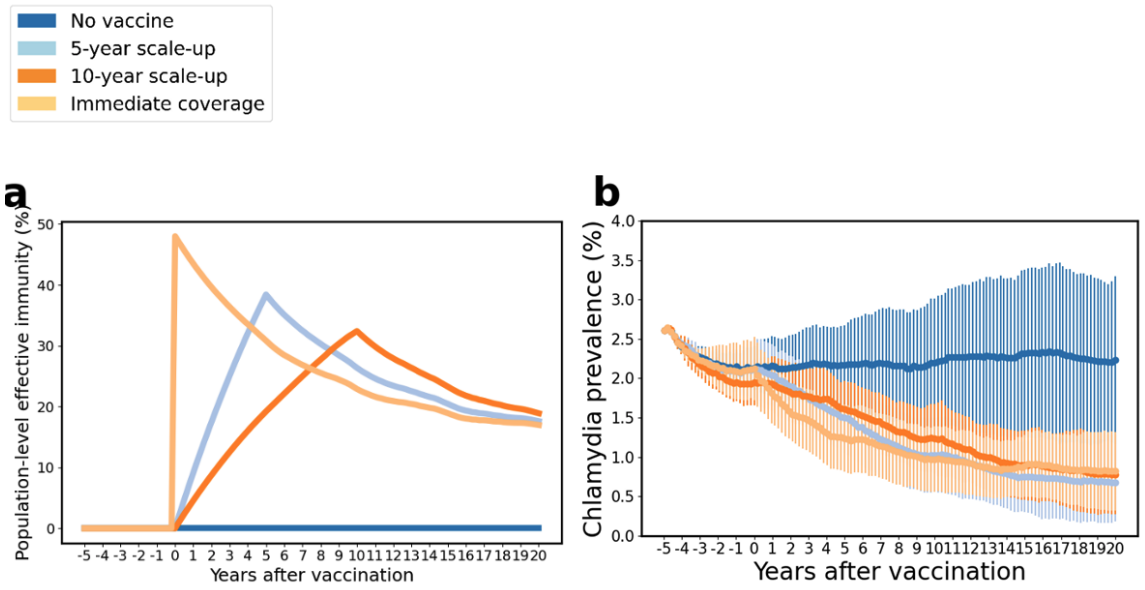


Figure 5.6: **a** Population-level effective immunity over time under different vaccination scale-up scenarios. Effective immunity is defined as the mean individual-level vaccine-induced protection across the population, jointly accounting for vaccine uptake, waning efficacy, and population turnover. **b** Chlamydia prevalence under the corresponding vaccination scale-up scenarios. The x-axis represents years relative to vaccine introduction (year 0), and the y-axis shows chlamydia prevalence in the population. The solid lines represent the mean prevalence from 20 simulations, with error bars indicating 95% confidence intervals.

Impact of different vaccine mechanisms.

In the absence of vaccination, chlamydia prevalence remains around 2 to 2.5% (figure 5.7 panel **a**). The most pronounced reduction is observed when the vaccine reduces both susceptibility to infection and infectiousness, resulting in the theoretical elimination of CT infection within 20 years. Vaccines that target either susceptibility or infectiousness alone also led to significant reductions in CT infections and PID, though the decline is slower. Figure 5.7 panel **b** presents chlamydia and PID prevalences at year 20 following vaccine implementation. Notably, there is no statistically significant difference between the prevalences obtained in the susceptibility-reduction-only versus the infectiousnessreduction-only scenarios. The simulation predicts an 83.7% [95% CI: 75.1–92.3] reduction in chlamydia prevalence and a 21.6% [95% CI: 16.3–26.9] reduction in PID prevalence in the general population under the dual-mechanism vaccine.

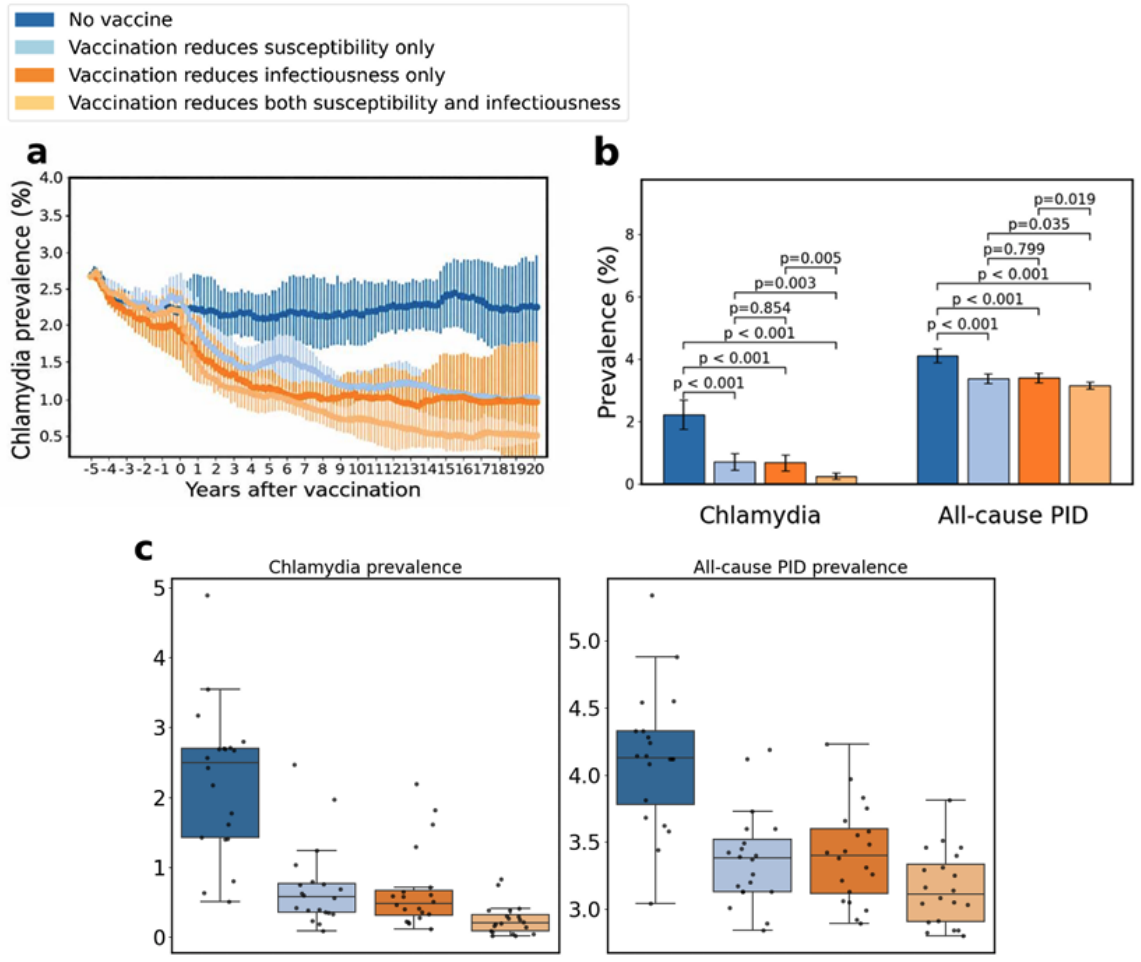


Figure 5.7: **a** Projected weekly CT prevalence over 20 years under four vaccination scenarios. Time (years) starts at vaccine introduction (year 0). VE decays exponentially from 80% with a rate of $(10 \text{ years})^{-1}$, and VC is 60% among individuals aged 15–44. Solid lines show means of 20 simulations; error bars indicate standard deviation.**b** Predicted CT and PID prevalence at year 20 across scenarios. Bars show mean values from 20 simulations; error bars represent 95% confidence intervals. Statistical significance ($p < 0.05$) is based on 20 stochastic simulations per scenario and should be interpreted as indicative. **c** Distribution of CT and all-cause PID prevalence at year 20. Boxplots summarize 20 simulations: median (line), IQR (box), and $1.5 \times IQR$ (whiskers). Points denote individual simulation outcomes.

Impact of target population prioritisation.

Our simulations indicate that prioritizing vaccination for females only or for older adults (ages 25-44 years) leads to relatively modest reductions in disease burden (**??**). Notably, even when vaccine coverage among these groups reaches 90%, the reduction in chlamydia prevalence (22.6% [95% CI: 12.6–47.5]) is comparable to that achieved by vaccinating only 60% of young individuals aged 15–24 years (23.2% [95% CI: 15.0–57.5]). Given that achieving 60% vaccine coverage is generally more feasible than achieving 90% coverage, targeting younger populations may represent a more efficient strategy. The most substantial reductions are observed when vaccination targets both males and females across the broader 15–44-year age range. Vaccinating 60% of both males and females aged 15–44 years led to a 61.2% [95% CI: 46.9–75.5] reduction in chlamydia prevalence, and increasing coverage to 90% achieved a reduction of 84.6% [95% CI: 76.5–91.7]. Similar but less pronounced patterns are observed for PID outcomes, reflecting the cumulative nature of PID development (5.8). Under the most comprehensive strategy (90% vaccination of both sexes), PID prevalence decreases by 23.4% [95% CI: 22.0–24.8] after 20 years. To complement prevalence-based comparisons, we calculate the number of vaccinations needed to avert one chlamydia infection (VNAI) under each prioritization strategy (Table 5.8, 5.8 fig.). Vaccination strategies targeting younger individuals (ages 15-24 years) are consistently the most efficient and robust, with a median VNAI of 3.7 and a mean of 6.6 at 60% coverage. In contrast, programs prioritizing older adults (ages 25-44 years) required substantially more vaccinations per infection averted and exhibited much greater uncertainty, with a median VNAI of 5.1, a mean of 18.0, and a wide uncertainty interval (2.6-113.6) at 60% coverage. Vaccinating both females and males yields a lower median VNAI (4.2) than vaccinating females only (4.7), with a narrower uncertainty interval. This advantage becomes more pronounced at higher coverage levels: at 90% coverage, the median VNAI decreases to 3.1 under gender-neutral vaccination compared with 3.5 for female-only strategies, alongside a substantially reduced upper tail of the distribution.

Table 5.4: Relative reduction in chlamydia and PID prevalence across VE and VC combinations

Vaccine coverage	**Vaccine efficacy**	**Reduction in Chlamydia prevalence (%) (95% CI)**	**Reduction in PID prevalence (%) (95% CI)**
0.2	0.2	7.8 (0, 20.6)	0.25 (0, 25.1)
0.2	0.4	26.6 (9.2, 74.0)	5.7 (0, 24.9)
0.2	0.6	30.9 (5.8, 62.0)	5.7 (0, 16.2)
0.2	0.8	54.1 (48.4, 90.7)	11.7 (10.3, 20.0)
0.2	1.0	79.2 (54.9, 98.8)	19.2 (2.3, 37.5)
0.4	0.2	13.0 (10.2, 77.4)	2.5 (0, 20.7)
0.4	0.4	43.0 (15.8, 86.8)	10.6 (4.1, 18.4)
0.4	0.6	59.9 (35.5, 69.9)	13.4 (7.0, 28.6)
0.4	0.8	80.7 (73.4, 94.9)	15.9 (13.5, 32.3)
0.4	1.0	96.1 (95.2, 99.9)	22.4 (20.5, 37.3)
0.6	0.2	36.2 (20.1, 74.6)	8.0 (0, 19.6)
0.6	0.4	60.4 (30.3, 87.8)	13.7 (0, 21.1)
0.6	0.6	76.3 (79.5, 93.7)	14.9 (12.5, 24.7)
0.6	0.8	92.8 (91.7, 99.2)	19.4 (20.7, 30.9)
0.6	1.0	99.5 (99.2, 100)	25.4 (23.8, 35.6)
0.8	0.2	34.8 (29.7, 89.7)	6.7 (0, 29.9)
0.8	0.4	71.0 (46.8, 89.5)	13.9 (2.1, 26.3)
0.8	0.6	91.3 (89.6, 97.3)	18.8 (13.6, 31.5)
0.8	0.8	98.6 (94.1, 99.9)	23.9 (17.3, 33.5)
0.8	1.0	100.0 (100.0, 100.0)	27.9 (21.7, 39.3)
1.0	0.2	37.7 (24.9, 90.0)	9.7 (3.8, 24.3)
1.0	0.4	83.6 (79.4, 98.5)	19.9 (10.7, 37.7)
1.0	0.6	97.1 (97.0, 99.9)	23.1 (17.4, 34.8)
1.0	0.8	99.9 (99.9, 100.0)	26.4 (20.8, 40.6)
1.0	1.0	100.0 (100.0, 100.0)	27.4 (16.5, 37.5)

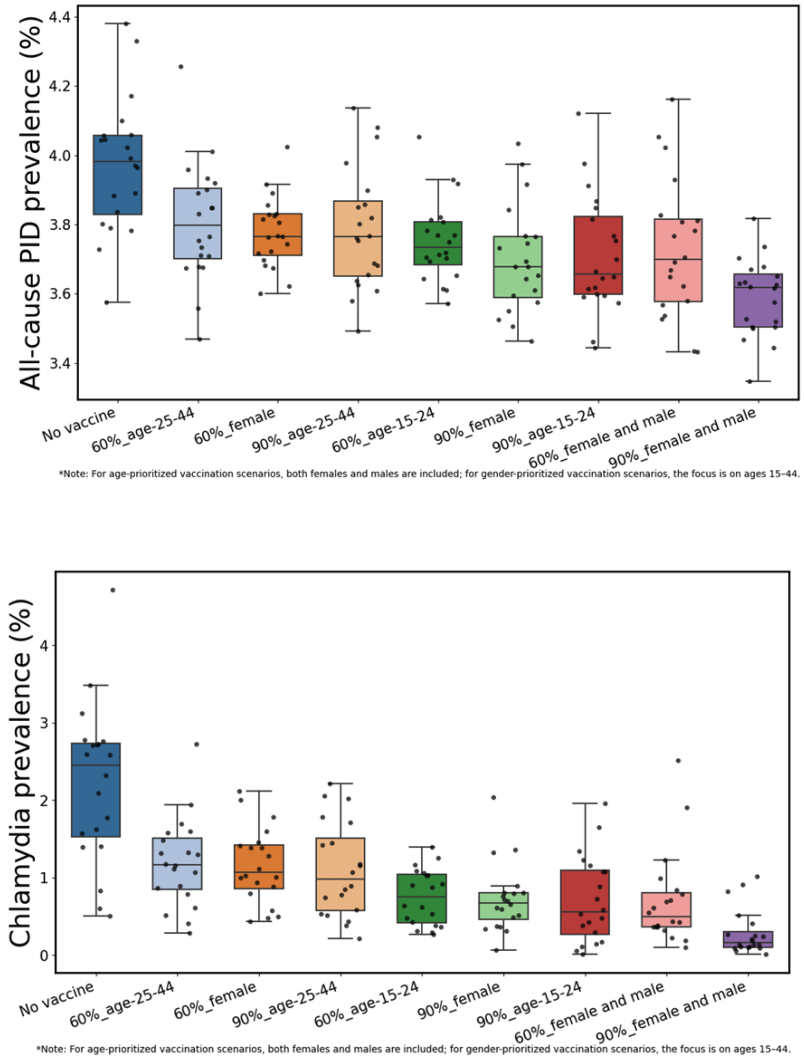


Figure 5.8: Chlamydia (**a**) and PID (**b**) prevalence at year 20 under vaccination programs by age (15–24 vs. 25–44), gender (female only vs. both), and coverage (60% vs. 90%). Age-based scenarios include both sexes; gender-based target ages 15–44. VE starts at 80% and decays exponentially at rate $(10 \text{ years})^{-1}$. Boxplots (20 simulations) show median, IQR, and $1.5 \times IQR$; points denote individual outcomes.

Table 5.5: Relative reduction in chlamydia across VE waning rates

Vaccine scenario	**Reduction in Chlamydia prevalence (%) (95% CI)**
Fixed VE	91.7 (89.5, 93.8)
VE decay 1/(1 year)	14.0 (0, 23.0)
VE decay 1/(5 years)	36.7 (16.8, 56.5)
VE decay 1/(10 years)	60.8 (50.8, 75.9)
VE decay 1/(15 years)	63.3 (41.0, 80.7)
VE decay 1/(20 years)	74.1 (55.5, 92.7)

Table 5.6: Relative reduction in chlamydia across vaccination scale-up years

Vaccination scale-up	**Reduction in Chlamydia prevalence (%) (95% CI)**
Immediate coverage	59.0 (45.9, 72.1)
5-year scale-up	52.5 (31.1, 73.9)
10-year scale-up	51.9 (27.7, 76.1)
20-year scale-up	38.6 (17.9, 59.3)

Table 5.7: Relative reduction in chlamydia and PID prevalence across vaccine mechanisms

Vaccine mechanisms	**Reduction in Chlamydia prevalence (%) (95% CI)**	**Reduction in PID prevalence (%) (95% CI)**
Susceptibility only	63.3 (50.5, 76.0)	16.6 (11.1, 22.0)
Infectiousness only	61.6 (46.8, 76.4)	15.8 (10.6, 21.0)
Susceptibility & Infectiousness	83.7 (75.1, 92.3)	21.6 (16.3, 26.9)

Table 5.8: Relative reduction in chlamydia and PID prevalence across different vaccine programs

Vaccine programs	**Reduction in Chlamydia prevalence (%) (95% CI)**	**Reduction in PID prevalence (%) (95% CI)**
60% age-25-44	25.0 (11.9, 63.9)	9.9 (9.3, 10.7)
60% female	23.2 (15.0, 57.5)	12.2 (11.4, 13.0)
60% age-15-24	53.5 (15.8, 37.1)	16.3 (15.4, 17.3)
90% age-25-44	22.6 (12.6, 47.5)	11.0 (10.3, 11.7)
60% female and male	61.2 (46.9, 75.5)	17.6 (16.3, 18.8)
90% female	50.8 (25.5, 75.6)	17.6 (16.4, 18.8)
90% age-15-24	58.6 (34.7, 82.7)	18.3 (17.1, 19.5)
90% female and male	84.6 (76.5, 91.7)	23.4 (22.0, 24.8)

5.4 Discussion

Previous agent-based modeling studies have provided important insights into chlamydia transmission and control, including sexual network models of screening and reinfection dynamics [38, 24], analyses of male screening [111], partner notification strategies [50], and vaccine impact assessments [33].

Our model builds on these works but extends them in several critical ways. First, we incorporate greater population heterogeneity, including heterosexuals, MSM, and FSW, with dynamic relationship patterns. Second, we explicitly track infection histories and lifetime allcause PID prevalence, allowing direct estimation of vaccine effects on the broader reproductive health. Third, we perform a rigorous three steps model calibration: (i) sexual network calibration to the National Survey of Family Growth (NSFG) data, (ii) chlamydia prevalence calibration across age and sex to the NHANES data and (iii) all-cause PID calibration across age to the NHANES data. Fourth, we conduct model validation using epidemiological datasets that are independent of the calibration targets. This validation demonstrates that the model can reproduce multiple age- and time-related features of CT infection and PID without direct calibration to these outcomes, thereby increasing confidence that the model captures key mechanisms governing disease progression and long-term sequelae. We believe that these extensions support the use of the model for evaluating vaccination scenarios and provide complementary insights into the potential long-term public health impact of chlamydia vaccination.

Our simulations show that vaccine against CT infection can significantly reduce both CT cases and all cause PID in the US population, even with a moderate efficacy (50%) and coverage (60%), respectively. This result underscores the value of vaccine candidates currently under development, even if they do not include sterilizing immunity [105, 93, 117], consistent with evidence that natural protective immunity to CT infection is partial and wanes over time [39]. In the context of persistent transmission despite decades of screening efforts, a vaccine offering partial protection could provide a critical new tool in chlamydia control. Further, our analyses also reveal the flexible tradeoff between VE and VC. We show that high coverage can

partially offset lower efficacy, and vice versa. For example, either 80% VE with 60% VC or 50% VE with 90% VC achieved reductions in CT prevalence exceeding 80%. This finding has important implications for public health programs, suggesting that tailored strategies may be viable in different settings depending on logistical constraints, vaccine hesitancy, and health system capacity.

A key determinant of vaccine impact is the duration of protection. For example, a vaccine with a 10-year half-life reduced prevalence by nearly 60%, whereas one with a 1-year half-life achieved only a 14% reduction. These results reinforce the importance of designing vaccines with longlasting immune responses and suggest that boosters may be needed to maintain population-level benefits if durability is limited.

Mechanistically, we find that vaccines that reduce both susceptibility to infection and infectiousness among infected individuals have the greatest impact, with the potential to reduce CT prevalence to zero. While most vaccine evaluations focus on susceptibility alone, our results demonstrate that incorporating reduced infectiousness can dramatically amplify public health benefits [154, 33, 56, 67]. This suggests that clinical trials should measure not only infection endpoints but also bacterial load and transmission potential, and that vaccine developers should consider immune responses capable of lowering pathogen shedding. The scale-up scenarios further highlight the interaction between vaccination rollout and waning immunity. Our results show that slower rollout in coverage leads to delayed and attenuated reductions in CT prevalence, although long-term prevalence levels converge once target coverage is reached. These findings underscore that population-level impact depends not only on the eventual coverage achieved but also on the pace of vaccine deployment. This is particularly relevant for adult vaccination programs, which typically lack school-based delivery infrastructure and face substantial logistical and behavioral constraints.

Consistent with real-world experience from adult hepatitis A/B vaccination in the US [79], our results suggest that vaccine durability and sustained rollout efforts will be critical determinants of the public health impact of a chlamydia vaccine. Targeting vaccination to specific subgroups also affects overall program efficiency. We show that prioritizing younger individuals aged 15–24 years, even at moderate coverage levels, is more effective than high-coverage programs focused on older adults or females only.

This is consistent with chlamydia epidemiology and suggests that adolescent or early young adult vaccination, analogous to current HPV vaccination strategies, would be an efficient and impactful policy. Including both males and females in vaccination programs further enhances impact, highlighting the importance of gender-inclusive approaches. Across prioritization programs, the median VNAI over a 20-year horizon ranged from 3 to 5 (Table 5.8, 5.8 fig.).

Vaccination strategies targeting younger individuals or adopting gender-neutral approaches were consistently more efficient and robust. Increasing coverage from 60% to 90% further reduced both the median and mean VNAI and the upper tail of the distribution, particularly for gender-neutral strategies. These estimates are closely aligned with previously reported values [154]. Despite substantial reductions in chlamydia incidence, declines in lifetime PID prevalence were more modest. It is important to recall, though, that this is reduction in all-cause PID, with non-CTassociated PID modelled as a baseline PID background. In our simulations, the CT attributable fraction of PID is 37.9% [95%CI: 17.6- 60.4], consistent with epidemiological reports [73, 14]. We nevertheless chose all-cause PID reduction as our outcome due to its greater relevance for assessing the overall public health burden and the potential impact of a CT vaccine on healthcare needs. Indeed, it is critical to remember that PID is strongly associated with other significant reproductive health issues in women, including infertility and ectopic pregnancy. PID-related tubal damage can obstruct the passage of eggs or sperm, leading to these severe outcomes. Thus, the projected reduction in PID cases indirectly implies a potential reduction in the burden of infertility and ectopic pregnancy.

Furthermore, while not modeled here, it is important to note that CT infection can also contribute to infertility in men [71, 98]. Several previous deterministic modeling studies have also examined the impact of a hypothetical chlamydia vaccines in the US. In particular, Makhoul et al. [154] observed sustained reductions in chlamydia burden across a wide range of vaccine efficacy, duration of protection and coverage assumptions. Our findings are broadly consistent with these conclusions. At the same time, our study extends prior work by using an agent-based framework that explicitly captures individuallevel heterogeneity, reinfection histories, waning immunity, and

gradual vaccine scale-up. This allows direct assessment of long-term PID burden alongside prevalence reduction.

Our study has several limitations. The agent-based model simplifies sexual networks, maintaining a constant 20,000-agent population where 55-year-olds are replaced by 15-year-olds, without considering other demographic changes. The age range (15-54) balances computational feasibility with epidemiological relevance, as US data indicates minimal sexual activity below 15 [48, 175] and minimal CT transmission above 54 [150]. Although key aspects of partnership formation and dissolution were informed by empirical data, the sexual network structure necessarily relies on structural assumptions. In particular, the agent-based interaction rules may generate heterogeneity in cumulative partnership exposure and concurrency over time. While such heterogeneity is plausible, CT transmission is characterized by substantial general-population exposure rather than strong concentration within narrowly defined core groups. Network heterogeneity is known to amplify the apparent population-level impact of interventions such as vaccination and may therefore contribute to the magnitude of vaccine effects observed in some scenarios. The results presented should thus be interpreted as scenario-based projections under plausible network assumptions, rather than precise quantitative forecasts for the US population.

We do not explicitly model vaccination's effect on CT infection duration [154, 33]; instead incorporating it within vaccine efficacy against infectiousness. Transmission probabilities remain constant across individuals and time, omitting variations due to condom use, partner notification, treatment behaviors, or biological heterogeneity. Regarding PID risk in untreated CT infections, available data only supports a one-time probability [110, 67], without evidence on risk changes with repeated untreated episodes. Our fixedrisk assumption for untreated cases may underestimate cumulative PID burden. These aspects warrant future research.

In conclusion, this modeling study strongly supports the development and deployment of a chlamydia vaccine as a valuable addition to current control strategies. Even partially effective vaccines with moderate uptake could meaningfully reduce the burden of infection and PID, and by extension, other associated sequelae in women. Optimizing vaccine characteristics, especially durability and the ability to

reduce infectiousness, and targeting both males and females will be essential to achieving maximal public health impact. Our findings provide actionable insights for researchers, policymakers, and funders, and underscore the need for continued investment and collaborative efforts to translate vaccine development into real-world disease reduction and improved public health outcomes for both women and men. We emphasize that the modeling framework developed here can be readily adapted to other sexually transmitted infections; the sexual network simulation component is by itself agnostic about the STI being transmitted, and thus, in principle, other diseases, or indeed, combinations of diseases, could be "dropped in".

Chapter 6

Conclusion

6.1 Discussion

Mathematical modeling of epidemics provides valuable insights into their mechanisms and impact. In this thesis, we studied two types of prevention measures for distinct epidemics: PrEP (Pre-Exposure Prophylaxis) for HIV and a hypothetical vaccine for the bacterium Chlamydia trachomatis.

Epidemics are complex phenomena that depend on both the time and the location of their emergence. Consequently, various perspectives can be adopted to understand their underlying mechanisms. However, it is impossible to encompass all these factors within a single model. For this research, we chose to focus on temporal dynamics and the various timescales within an epidemic. These aspects are often difficult to capture using classical compartmental models described by ordinary differential equations.

To achieve this, we considered the unique temporality of PrEP, which consists of specific renewal cycles. This led us to describe this compartment using an age-structured hyperbolic equation. By reducing our models through the method of characteristics, we transformed our systems into differential systems coupled with a difference equation featuring a discrete delay. This specific parameter is central to the recommendations of the World Health Organization.

By doing so, we directly account for the temporal organization of PrEP. We pay particular attention to accessibility and the mechanisms governing it. Therefore, we incorporated non-linearities into our models capable of capturing key factors: the economic and political decisions governing PrEP access in countries where it is available.

In the final chapter of this thesis, we maintain our focus on temporal dynamics. Because Chlamydia results primarily in asymptomatic infections, it is necessary to account for differing individual reactions and timelines. To represent this, we utilize ABM. This approach allows us to account for complex behaviors specific to STIs, such as sexual dynamics and different types of relationships. The prevention method studied here is a hypothetical vaccine. We analyze its impact on the prevalence of Chlamydia and Pelvic Inflammatory Disease.

In chapter 2, we obtained results regarding the global stability of our model. Our modeling shows that the "reservoir effect" of PrEP helps maintain HIV incidence at a low level. Conversely, abruptly stopping PrEP would trigger a resurgence of the epidemic. Furthermore, numerical simulations highlight the importance of targeted intervention. By applying our model to French data for Truvada and distinguishing the population of Men who have Sex with Men (MSM) into two groups based on acquisition risk, we observed a significant difference in PrEP's impact on incidence. This is due to logistical constraints that produce a dilution effect.

In chapter 3, we assumed that PrEP recruitment depends on incidence. Adopting a purely mathematical approach, we obtained local stability results. We investigated whether the model could be destabilized by a Hopf bifurcation. While we proved that no destabilization is possible under specific conditions, an interval remains where we cannot reach a definitive conclusion. However, our numerical simulations suggest that this phenomenon is unlikely to occur in this model, which is consistent with the theory of monotone dynamical systems.

In chapter 4, we observed the impact of non-monotone recruitment. This was motivated by the results of the previous chapter and a more realistic view of the population size with PrEP access. This model incorporates rich dynamics. We observed several scenarios leading to the coexistence of up to three disease-free equilibria. These

equilibria are directly related to the level of recruitment and access. The main results include hysteresis phenomena and destabilization via a Hopf bifurcation. The hysteresis highlights the system's sensitivity to initial conditions and illustrates how poor PrEP management could have significant long-term consequences. Regarding the Hopf bifurcation, we calculated the critical delay.
In chapter 5, the incorporation of vaccine scenarios shows that even a moderately effective vaccine with average coverage can significantly decrease the prevalence of Chlamydia and PID. Furthermore, the ABM shows that targeting 15–24-year-olds is the optimal scenario. Finally, a vaccine that reduces both susceptibility and infectiousness offers the greatest potential for epidemic reduction. We also demonstrated the trade-off between vaccine coverage and efficacy, as one can compensate for deficiencies in the other. Another crucial factor is the duration of protection: as expected, longer-lasting vaccines yield a greater positive impact. Lastly, the speed of deployment plays a significant role in the epidemic burden, suggesting that vaccination campaigns should prioritize rapid availability.

These results demonstrate that the efficacy of biomedical interventions is inherently dependent on human behavior. As established in the literature, adherence to PrEP is a critical parameter. The calculation of the critical delay τ^* highlights the impact of public health policies on logistical bottlenecks; specifically, delays in prescription renewal and treatment accessibility can exert a long-term influence on the course of the epidemic. These findings underscore the stark reality of the current budget cuts affecting health program funding in aid-dependent countries [162]. Furthermore, resource limitations necessitate the precise targeting of individuals for various prevention methods to maximize impact—a perspective adopted in Chapters 1, 3, and 4.The results of Chapter 5 provide a clear roadmap regarding the characteristics of a potential Chlamydia vaccine. Clinical trials should focus on reducing both susceptibility and infectiousness. Additionally, these results account for logistical constraints on vaccine deployment speed and allow for the prioritization of specific age groups, in alignment with existing scientific literature.

6.2 Future works

For future work, it would be valuable to incorporate treatment as prevention. Incorporating viral suppression into future models would provide a more realistic framework. Furthermore, the model would benefit from accounting for different disease stages and awareness (or lack thereof) of seropositive status. Official estimates of actual case numbers play a vital role in developing strategies to combat the epidemic. In 2024, more than 50% of HIV diagnoses were classified as "late-stage." This leads to severe consequences for those affected, including higher mortality risks and long-term sequelae. Recent studies indicate an increased risk of dementia and severe cognitive impairment during aging for late-stage cases [35, 137]. Moreover, the funding crisis of 2025–2026 is expected to result in a significant number of new infections [162]. In this context, a cost-effectiveness analysis would better reflect state-level funding decisions.Methodological AdvancementsSeveral approaches are possible. A comparative study across different countries would better illustrate the impact of specific policies, as would modeling the differential costs between lifelong care for affected individuals versus the unit cost of maintaining an individual within the "protected" compartment.To measure the impact of this crisis under real-world constraints, our models should be coupled with optimal control for delay equations. This is a dynamic field of research given the current abundance of data. It is natural to analyze prevention strategies—which are intrinsically limited—through this lens. Recent developments in machine learning, specifically Physics-Informed Neural Networks (PINNs), offer promising new possibilities.Finally, our model's current assumption—that no individual on PrEP discontinues treatment before their next medical appointment—is unrealistic. One potential improvement is to introduce an age-dependent dropout term $\gamma(a)$ into the age-structured hyperbolic equation:

$$\frac{\partial p}{\partial t}(t,a) + \frac{\partial p}{\partial a}(t,a) = -(\mu + \gamma(a))p(t,a)$$

This would transform the equation for the susceptible population into one with a distributed delay:

$$\frac{dS(t)}{dt} = \Lambda - \mu S(t) - \beta I(t)S(t) - \psi(I(t))f(S(t)) + \int_0^\tau \gamma(a)p(t,a)da + (1-\theta)p(t,\tau)$$

.This would represent an interesting coupling with the aforementioned optimal control for delay systems. Regarding PrEP, considering a non-constant renewal rate is another avenue for improvement. This could be achieved classically with a time-dependent term. Alternatively, one could consider variability within the three-month period by introducing a distribution kernel $K(a)$, representing the probability density that protection ends at age a, resulting in:

$$u(t) = \psi(I(t))f(S(t)) + \int_0^\infty \theta(a)K(a)e^{-\mu a}u(t-a)da$$

Our Agent-Based Model (ABM) provides a solid foundation for capturing the heterogeneity of individual behaviors. However, its structure imposes significant computational constraints. This makes it difficult to rapidly explore vast parameter spaces or simulate very long-term equilibria. An interesting research avenue consists of developing a hybrid approach by using the detailed outputs of the ABM to derive the mixing parameters of a deterministic compartmental model.One could propose stratifying this deterministic model by age $\mathcal{I}$ (in 5-year age groups from 15 to 44 years) and by sexual behaviors $\mathcal{G}$ (including subgroups such as MSM, sex workers, and heterosexual men/women). The ABM would allow for the empirical calculation of a sexual mixing matrix $\mathcal{M}_{g\to h}$. This matrix could be more finely defined by combining a matrix $\mathcal{S}$ representing the proportion of sexual acts occurring between different groups and a perturbation matrix $\mathcal{J}$ to model specific epidemiological bridges between these populations.The force of infection $\lambda_{i,g}(t)$ of the system of differential equations for a given group (i,g) would be:

$$\lambda_{i,g}(t) = \sum_j \sum_h \beta_{i,g\to j,h} \cdot c_{i,g} \cdot \mathcal{M}_{g\to h} \cdot \frac{I_{S,j,h}(t) + I_{A,j,h}(t)}{N_{j,h}(t)}$$

In this formulation, β represents the transmission rate per contact, $c_{i,g}$ captures the dynamics and frequency of partnerships (weighted by the short-term or long-term nature of the relationships), and the final quotient represents the prevalence of symptomatic (I_S) and asymptomatic (I_A) infections within the targeted partner group.Integrating this force of infection into a complete compartmental system would open new analytical perspectives. It would facilitate the use of Bayesian calibration methods and allow for the extraction of fundamental public health metrics. Notably, the next-generation matrix calculation would allow for the isolation of the basic reproduction number $\mathcal{R}_0$ by subgroup to determine which populations contribute most to the epidemic. The ordinaries differential equations model would also facilitate the estimation of herd immunity thresholds and target reproduction numbers to guide intervention policies.Finally, independently of this mathematical coupling, future iterations must focus on addressing certain current limitations regarding clinical disease progression. For example, relaxing the assumption of a fixed probability of developing PID in the event of an untreated infection would allow for more accurate modeling of the cumulative burden associated with successive reinfections.

Bibliography

[1] A. G. McKendrick W. O. Kermack and G. T. Walker. "A Contribution to the Mathematical Theory of Epidemics". In: *Proc. R. Soc. Lond. A* 115 (1927). Reprinted in 1997, pp. 700–721. DOI: 10.1098/rspa.1927.0118.

[2] M. A. Cruz and J. K. Hale. "Stability of Functional Differential Equations of Neutral Type". In: *Journal of Differential Equations* 7.2 (1970), pp. 334–355. DOI: 10.1016/0022-0396(70)90114-2.

[3] V. Capasso and G. Serio. "A Generalization of the Kermack-McKendrick Deterministic Epidemic Model". In: *Mathematical Biosciences* 42.1–2 (1978), pp. 43–61. DOI: 10.1016/0025-5564(78)90006-8.

[4] G. F. Webb. *Theory of Nonlinear Age-Dependent Population Dynamics*. New York: Marcel Dekker, 1985. 294 pp.

[5] R. M. Anderson et al. "A Preliminary Study of the Transmission Dynamics of the Human Immunodeficiency Virus (HIV), the Causative Agent of AIDS". In: *IMA J. Math. Appl. Med. Biol.* 3.4 (1986), pp. 229–263. DOI: 10.1093/imammb/3.4.229.

[6] V. Isham. "Mathematical Modelling of the Transmission Dynamics of HIV Infection and AIDS: A Review". In: *J. Roy. Statist. Soc. Ser. A* 151.1 (1988), pp. 5–49. DOI: 10.2307/2982179.

[7] H. Buhaug et al. "Cost effectiveness of testing for chlamydial infections in asymptomatic women". In: *Medical Care* 27.8 (1989), pp. 833–841. ISSN: 0025-7079. DOI: 10.1097/00005650-198908000-00007.

[8] O. Diekmann and J. A. P. Heesterbeek. "On the definition and the computation of the basic reproduction ratio R0 in models for infectious diseases in heterogeneous populations". In: *J. Math. Biol.* 28 (1990), pp. 365–382. DOI: 10.1007/BF00178324.

[9] H. I. Freedman and P. Moson. "Persistence definitions and their connections". In: *Proc. Amer. Math. Soc.* 109.4 (1990), pp. 1025–1033.

[10] R. M. Anderson and R. M. May. *Infectious Diseases of Humans: Dynamics and Control*. Oxford University Press, May 1991. ISBN: 978-0-19-854599-6. DOI: 10.1093/oso/9780198545996.001.0001.

[11] D. E. Kirschner A. S. Perelson and R. De Boer. "Dynamics of HIV infection of CD4+ T cells". In: *Mathematical Biosciences* 114.1 (1993), pp. 81–125. ISSN: 0025-5564. DOI: 10.1016/0025-5564(93)90043-A.

[12] J. K. Hale and S. M. Verduyn Lunel. *Introduction to Functional Differential Equations*. 1st ed. Vol. 99. Applied Mathematical Sciences. Springer-Verlag New York, 1993. ISBN: 978-1-4612-8741-4.

[13] Y. Kuang. *Delay Differential Equations: With Applications in Population Dynamics*. Mathematics in Science and Engineering v. 191. Boston: Academic Press, 1993. ISBN: 978-0-12-427610-9.

[14] Centers for Disease Control and Prevention (CDC). "Ten leading nationally notifiable infectious diseases–United States, 1995". In: *MMWR Morbidity and Mortality Weekly Report* 45.41 (1996), pp. 883–884. ISSN: 0149-2195.

[15] K. L. Cooke and P. van den Driessche. "Analysis of an SEIRS epidemic model with two delays". In: *Journal of Mathematical Biology* 35.2 (1996), pp. 240–260. ISSN: 1432-1416. DOI: 10.1007/s002850050051.

[16] Geoffrey P. Garnett et al. "Sexual Mixing Patterns of Patients Attending Sexually Transmitted Diseases Clinics". In: *Sexually Transmitted Diseases* 23.3 (May–June 1996), p. 248. ISSN: 0148-5717.

[17] S. O. Aral. "Sexual Network Patterns as Determinants of STD Rates: Paradigm Shift in the Behavioral Epidemiology of STDs Made Visible". In: *Sexually Transmitted Diseases* 26.5 (May 1999), p. 262. ISSN: 0148-5717.

[18] R. M. Anderson and G. P. Garnett. "Mathematical Models of the Transmission and Control of Sexually Transmitted Diseases". In: *Sexually Transmitted Diseases* 27.10 (Nov. 2000), pp. 636–643. ISSN: 0148-5717. DOI: 10.1097/00007435-200011000-00012. PMID: 11099079.

[19] R. V. Culshaw and S. Ruan. "A Delay-Differential Equation Model of HIV Infection of CD4+ T-cells". In: *Mathematical Biosciences* 165.1 (2000), pp. 27–39. DOI: 10.1016/S0025-5564(00)00006-7.

[20] H. W. Hethcote. "The mathematics of infectious diseases". In: *SIAM Rev.* 42.4 (2000), pp. 599–653. DOI: 10.1137/S0036144500371907.

[21] P. van den Driessche and J. Watmough. "Reproduction numbers and sub-threshold endemic equilibria for compartmental models of disease transmission". In: *Math. Biosci.* 180.1 (2002), pp. 29–48. DOI: 10.1016/S0025-5564(02)00108-6.

[22] P. W. Nelson and A. S. Perelson. "Mathematical analysis of delay differential equation models of HIV-1 infection". In: *Math. Biosci.* 179.1 (2002), pp. 73–94. DOI: 10.1016/S0025-5564(02)00099-8.

[23] J. U. Igietseme et al. "Delivery of Chlamydia vaccines". In: *Expert Opin. Drug Deliv.* 2.3 (2005), pp. 549–562. DOI: 10.1517/17425247.2.3.549.

[24] K. M. E. Turner et al. "Developing a realistic sexual network model of Chlamydia transmission in Britain". In: *Theor. Biol. Med. Model.* 3 (2006), p. 3. DOI: 10.1186/1742-4682-3-3.

[25] "Models of HIV-1 disease: A review of current status". In: *Drug Discov. Today Dis. Models* 3.1 (2006). Visited on 09/22/2025, pp. 113–119. DOI: 10.1016/j.ddmod.2006.03.016.

[26] D. Greenhalgh N. Dalal and X. Mao. "A stochastic model of AIDS and condom use". In: *J. Math. Anal. Appl.* 325.1 (2007), pp. 36–53. DOI: 10.1016/j.jmaa.2006.01.055.

[27] R. C. Brunham and M. L. Rekart. "The arrested immunity hypothesis and the epidemiology of Chlamydia control". In: *Sex. Transm. Dis.* 35.1 (2008), p. 53. DOI: 10.1097/OLQ.0b013e31815e41a3.

[28] F. Brauer. "Compartmental models in epidemiology". In: *Mathematical Epidemiology*. Ed. by P. van den Driessche F. Brauer and J. Wu. Berlin, Heidelberg: Springer, 2008, pp. 19–79.

[29] L. Bettencourt and R. Ribeiro. "Real time Bayesian estimation of the epidemic potential of emerging infectious diseases". In: *PloS One* 3.5 (2008), e2185. DOI: 10.1371/journal.pone.0002185.

[30] S. J. Clark S. Cassels and M. Morris. "Mathematical models for HIV transmission dynamics". In: *J. Acquir. Immune Defic. Syndr.* 47 (2008), S34–S39. DOI: 10.1097/QAI.0b013e3181605da3.

[31] The Lancet Collaborative Analysis. "Life expectancy of individuals on combination antiretroviral therapy in high-income countries: a collaborative analysis of 14 cohort studies". In: *The Lancet* 372.9635 (2008), pp. 293–299. DOI: 10.1016/S0140-6736(08)61113-7.

[32] G. Fan, M. Min-Oo, and G. S. K. Wolkowicz. "Hopf bifurcation of delay differential equations with delay dependent parameters". In: *Canadian Applied Mathematics Quaterly* 17 (2009), pp. 37–69.

[33] R.T. Gray et al. "Modeling the impact of potential vaccines on epidemics of sexually transmitted Chlamydia trachomatis infection". In: *J. Infect. Dis.* 199.11 (2009), pp. 1680–1688. DOI: 10.1086/598983.

[34] Haute Autorité de Santé. *Argumentaire dépistage VIH*. Tech. rep. HAS, 2009. URL: https://solidarites-sante.gouv.fr/IMG/pdf/argumentaire_depistage_vih_HAS_2009-2.pdf (visited on 02/24/2026).

[35] M. Kaul. "HIV-1 associated dementia: update on pathological mechanisms and therapeutic approaches". In: *Curr Opin Neurol* 22.3 (June 2009), pp. 315–320. DOI: 10.1097/WCO.0b013e328329cf3c.

[36] O. M. Akpa and B. A. Oyejola. "Modeling the transmission dynamics of HIV/AIDS epidemics: an introduction and a review". In: *J. Infect. Dev. Ctries.* 4.10 (2010), pp. 597–608. DOI: 10.3855/jidc.542.

[37] R. J. Smith et al. "Evolutionary Dynamics of Complex Networks of HIV Drug-Resistant Strains: The Case of San Francisco". In: *Science* 327.5966 (2010), pp. 697–701. DOI: 10.1126/science.1180556.

[38] C. L. Althaus et al. "Transmission dynamics of Chlamydia trachomatis affect the impact of screening programmes". In: *Epidemics* 2.3 (2010), pp. 123–131. DOI: 10.1016/j.epidem.2010.04.002.

[39] B.E.Batteiger et al. "Protective immunity to Chlamydia trachomatis genital infection: evidence from human studies". In: *J. Infect. Dis.* 201.S2 (2010), S178–S189. DOI: 10.1086/652400.

[40] W. M. Geisler. "Duration of untreated, uncomplicated Chlamydia trachomatis genital infection and factors associated with Chlamydia resolution: A review of human studies". In: *J. Infect. Dis.* 201.S2 (2010), S104–S113. DOI: 10.1086/652402.

[41] H. Liu and L. Li. "A class age-structured HIV/AIDS model with impulsive drug-treatment strategy". In: *Discrete Dyn. Nat. Soc.* 2010 (2010). DOI: 10.1155/2010/758745.

[42] H. Smith and H. Thieme. *Dynamical Systems and Population Persistence*. American Mathematical Society, 2010. DOI: 10.1090/gsm/118. URL: https://www.ams.org/gsm/118.

[43] C.L. Haggerty et al. "Risk of sequelae after Chlamydia trachomatis genital infection in women". In: *J. Infect. Dis.* 201.S2 (2010), S134–S155. DOI: 10.1086/652395.

[44] M. S. Cohen et al. "Prevention of HIV-1 Infection with Early Antiretroviral Therapy". In: *N. Engl. J. Med.* 365.6 (2011), pp. 493–505. DOI: 10.1056/NEJMoa1105243.

[45] et al. D. Van Manen. "Genome-Wide Association Scan in HIV-1-Infected Individuals Identifying Variants Influencing Disease Course". In: *PLoS One* 6.7 (2011), e22208. DOI: 10.1371/journal.pone.0022208.

[46] L. M. Gorgos and J. M. Marrazzo. "Sexually Transmitted Infections among Women Who Have Sex with Women". In: *Clin. Infect. Dis.* 53.S3 (2011), S84–S91. DOI: 10.1093/cid/cir697.

[47] H. Smith. *An Introduction to Delay Differential Equations with Applications to the Life Sciences*. 1st. Vol. 57. Texts in Applied Mathematics. New York: Springer-Verlag, 2011. ISBN: 978-1-4419-7645-1.

[48] I. V. Van Den Broek et al. "Effectiveness of Yearly, Register-Based Screening for Chlamydia in the Netherlands: Controlled Trial with Randomised Stepped Wedge Implementation". In: *BMJ* 345 (2012), e4316–e4316. ISSN: 1756-1833. DOI: 10.1136/bmj.e4316.

[49] J.M. Baeten et al. "Antiretroviral Prophylaxis for HIV Prevention in Heterosexual Men and Women". In: *N. Engl. J. Med.* 367.5 (2012), pp. 399–410. DOI: 10.1056/NEJMoa1108524.

[50] M. Kretzschmar et al. "Effects of Screening and Partner Notification on Chlamydia Positivity in the United States: A Modeling Study". In: *Sex. Transm. Dis.* 39.5 (2012), pp. 325–331. ISSN: 1537-4521. DOI: 10.1097/OLQ.0b013e31824e52c2.

[51] G. Yamey S. F. Morin and G. W. Rutherford. "HIV Pre-Exposure Prophylaxis". In: *BMJ* 345 (2012), e5412. ISSN: 1756-1833. DOI: 10.1136/bmj.e5412.

[52] World Health Organization. *Programmatic Update: Antiretroviral Treatment as Prevention (TasP) of HIV and TB: Executive Summary*. Tech. rep. WHO/HIV/2012.12, 2012.

[53] D. Liu and B. Wang. "A novel time-delayed HIV/AIDS model with vaccination & antiretroviral therapy and its stability analysis". In: *Appl. Math. Model.* 37.7 (2013), pp. 4608–4625. ISSN: 0307-904X. DOI: 10.1016/j.apm.2012.09.065.

[54] W. M. Geisler et al. "Spontaneous Resolution of Genital Chlamydia trachomatis Infection in Women and Protection from Reinfection". In: *J. Infect. Dis.* 207.12 (2013), pp. 1850–1856. ISSN: 1537-6613.

[55] M. Sunnåker et al. "Approximate Bayesian Computation". In: *PLoS Computational Biology* 9.1 (Jan. 10, 2013), e1002803. ISSN: 1553-734X. DOI: 10.1371/journal.pcbi.1002803. PMID: 23341757. URL: https://pmc.ncbi.nlm.nih.gov/articles/PMC3547661/ (visited on 05/28/2026).

[56] B. Davies et al. "Heterogeneity in Risk of Pelvic Inflammatory Diseases after Chlamydia Infection: A Population-Based Study in Manitoba, Canada". In:

J. Infect. Dis. 210.S2 (2014), S549–S555. ISSN: 1537-6613. DOI: 10.1093/infdis/jiu483.

[57] R.M. Grant et al. "Uptake of Pre-Exposure Prophylaxis, Sexual Practices, and HIV Incidence in Men and Transgender Women Who Have Sex with Men: A Cohort Study". In: *The Lancet Infect. Dis.* 14.9 (2014), pp. 820–829. ISSN: 1474-4457. DOI: 10.1016/S1473-3099(14)70847-3.

[58] P.S. Rivadeneira et al. "Mathematical Modeling of HIV Dynamics After Antiretroviral Therapy Initiation: A Review". In: *BioResearch Open Access* 3.5 (2014), pp. 233–241. DOI: 10.1089/biores.2014.0024.

[59] D. M. Vickers and N. D. Osgood. "The Arrested Immunity Hypothesis in an Immunoepidemiological Model of Chlamydia Transmission". In: *Theoretical Population Biology* 93 (2014), pp. 52–62. ISSN: 0040-5809. DOI: 10.1016/j.tpb.2014.01.005.

[60] M. Adimy, A. Chekroun, and T. Touaoula. "Age-Structured and Delay Differential-Difference Model of Hematopoietic Stem Cell Dynamics". In: *Discrete and Continuous Dynamical Systems - B* 20.9 (2015), pp. 2765–2791. ISSN: 1531-3492. DOI: 10.3934/dcdsb.2015.20.2765.

[61] C.F. Cáceres et al. "PrEP Implementation: Moving from Trials to Policy and Practice". In: *Journal of the International AIDS Society* 18.4S3 (2015), p. 20222. ISSN: 1758-2652. DOI: 10.7448/IAS.18.4.20222.

[62] F. Cazein et al. "Découvertes de séropositivité VIH et sida - France, 2003-2013". In: *Bull Epidémiol Hebd.* 9-10 (2015), pp. 152–161.

[63] M. Martcheva. *An Introduction to Mathematical Epidemiology*. Vol. 61. Texts in Applied Mathematics. Boston, MA: Springer US, 2015. ISBN: 978-1-4899-7611-6 978-1-4899-7612-3. DOI: 10.1007/978-1-4899-7612-3.

[64] J. Molina et al. "On-Demand Preexposure Prophylaxis in Men at High Risk for HIV-1 Infection". In: *New England Journal of Medicine* 373.23 (2015), pp. 2237–2246. ISSN: 0028-4793. DOI: 10.1056/NEJMoa1506273.

[65] D. J. Pilowsky and L.-T. Wu. "Sexual Risk Behaviors and HIV Risk among Americans Aged 50 Years or Older: A Review". In: *Substance Abuse and Rehabilitation* 6 (2015), pp. 51–60. DOI: 10.2147/SAR.S78808.

[66] I. Zablotska et al. "PrEP Implementation in the Asia-Pacific Region: Opportunities, Implementation and Barriers". In: *Journal of the International AIDS Society* 19 (2016), p. 21119.

[67] M. J. Price et al. "The Natural History of Chlamydia Trachomatis Infection in Women: A Multi-Parameter Evidence Synthesis". In: *Health Technology Assessment* 20.22 (2016), pp. 1–250. DOI: 10.3310/hta20220.

[68] V. A. Fonner et al. "Effectiveness and safety of oral HIV preexposure prophylaxis for all populations". In: *AIDS* 30.12 (2016), p. 1973. ISSN: 0269-9370. DOI: 10.1097/QAD.0000000000001145.

[69] L. F. Johnson and N. Geffen. "A comparison of two mathematical modeling frameworks for evaluating sexually transmitted infection epidemiology". In: *Sex. Transm. Dis.* 43.3 (2016), pp. 139–146. ISSN: 1537-4521. DOI: 10.1097/OLQ.0000000000000412.

[70] S. McCormack et al. "Pre-exposure prophylaxis to prevent the acquisition of HIV-1 infection (PROUD): effectiveness results from the pilot phase of a pragmatic open-label randomised trial". In: *The Lancet* 387.10013 (2016), pp. 53–60. ISSN: 0140-6736, 1474-547X. DOI: 10.1016/S0140-6736(15)00056-2.

[71] N. Mesbah and H. K. Salem. "Genital tract infection as a cause of male infertility". In: *Genital Infections and Infertility*. IntechOpen, June 2016. ISBN: 978-953-51-2487-0. DOI: 10.5772/62740.

[72] B. Dubey P. Dubey and U. S. Dubey. "An SIR model with nonlinear incidence rate and Holling type III treatment rate". In: *Applied Analysis in Biological and Physical Sciences*. Ed. by J. M. Cushing et al. New Delhi: Springer India, 2016, pp. 63–81. ISBN: 978-81-322-3640-5. DOI: 10.1007/978-81-322-3640-5_4.

[73] M.J. Price et al. "Proportion of pelvic inflammatory disease cases caused by Chlamydia trachomatis: consistent picture from different methods". In: *J. Infect. Dis.* 214.4 (2016), pp. 617–624. ISSN: 0022-1899. DOI: 10.1093/infdis/jiw178.

[74] K. Afassinou, F. Chirove, and K. S. Govinder. "Pre-Exposure Prophylaxis and Antiretroviral Treatment Interventions with Drug Resistance". In: *Mathematical Biosciences* 285 (2017), pp. 92–101. DOI: 10.1016/j.mbs.2017.01.005.

[75] M. M. Rönn et al. "The Use of Mathematical Models of Chlamydia Transmission to Address Public Health Policy Questions: A Systematic Review". In: *Sexually Transmitted Diseases* 44.5 (2017), pp. 278–283. DOI: 10.1097/OLQ.0000000000000598.

[76] C. J. Silva and D. F. M. Torres. "A SICA compartmental model in epidemiology with application to HIV/AIDS in Cape Verde". In: *Ecological Complexity* 30 (2017), pp. 70–75. DOI: 10.1016/j.ecocom.2016.12.001.

[77] L. Simpson and A. B. Gumel. "Mathematical assessment of the role of pre exposure prophylaxis on HIV transmission dynamics". In: *Applied Mathematics and Computation* 293 (2017). DOI: 10.1016/j.amc.2016.07.043.

[78] G. Röst et al. "Global Dynamics of an Epidemiological Model with Age-of-Infection Dependent Treatment Rate". In: *Ricerche di Matematica* 67.1 (2018), pp. 125–140. DOI: 10.1007/s11587-018-0360-5.

[79] P. K. Ghaswalla et al. "Hepatitis A, B, and A/B Vaccination Series Completion among US Adults: A Claims-Based Analysis". In: *Human Vaccines & Immunotherapeutics* 14.11 (2018), pp. 2780–2785. DOI: 10.1080/21645515.2018.1489189.

[80] I. Durand-Zaleski et al. "Costs and Benefits of On-Demand HIV Preexposure Prophylaxis in MSM". In: *AIDS* 32.1 (Jan. 2, 2018), pp. 95–102. ISSN: 1473-5571. DOI: 10.1097/QAD.0000000000001658. PMID: 29210777.

[81] M. U. Nsuami and P. J. Witbooi. "A model of HIV/AIDS population dynamics including ARV treatment and pre-exposure prophylaxis". In: *Advances in Difference Equations* (2018). DOI: 10.1186/s13662-017-1458-x.

[82] C. M. A. Pinto and A. R. M. Carvalho. "The impact of pre-exposure prophylaxis (PrEP) and screening on the dynamics of HIV". In: *Journal of*

Computational and Applied Mathematics 339 (2018), pp. 231–244. DOI: 10.1016/j.cam.2017.10.019.

[83] C. J. Silva and D. F. M. Torres. "Modeling and optimal control of HIV/AIDS prevention through PrEP". In: *Discrete and Continuous Dynamical Systems* 11.1 (2018), pp. 119–141. DOI: 10.3934/dcdss.2018008.

[84] D. A. Sawicki et al. "Culturally Competent Health Care for Sex Workers: A Examination of Myths That Stigmatize Sex-Work and Hinder Access to Care". In: *Sexual and relationship therapy* 34.3 (2019), pp. 355–371. DOI: 10.1080/14681994.2019.1574970.

[85] F. Cazein et al. "Bulletin de Santé Publique. Découvertes de séropositivité VIH et diagnostique de SIDA - France, 2018". In: *Bulletin de santé publique VIH / sida* (2019).

[86] F. Y. S. Kong et al. "Pharmacokinetic Considerations Regarding the Treatment of Bacterial Sexually Transmitted Infections with Azithromycin: A Review". In: *Journal of Antimicrobial Chemotherapy* 74.5 (2019), pp. 1157–1166. DOI: 10.1093/jac/dky548.

[87] Q. An et al. "Geometric Stability Switch Criteria in Delay Differential Equations with Two Delays and Delay Dependent Parameters". In: *Journal of Differential Equations* 266.11 (2019), pp. 7073–7100. DOI: 10.1016/j.jde.2018.11.025.

[88] Q. Hu et al. "Efficacy and Cost-Effectiveness of Early Antiretroviral Therapy and Partners' Pre-Exposure Prophylaxis among Men Who Have Sex with Men in Shenyang, China: A Prospective Cohort and Costing Study". In: *BMC Infectious Diseases* 19.1 (2019), p. 663. DOI: 10.1186/s12879-019-4275-x.

[89] R. Omori et al. "Does Infection with Chlamydia Trachomatis Induce Long-Lasting Partial Immunity? Insights from Mathematical Modelling". In: *Sexually Transmitted Infections* 95.2 (2019), pp. 115–121. DOI: 10.1136/sextrans-2018-053543.

[90] S. Abraham et al. "Safety and Immunogenicity of the Chlamydia Vaccine Candidate CTH522 Adjuvanted with CAF01 Liposomes or Aluminium

Hydroxide: A First-in-Human, Randomised, Double-Blind, Placebo-Controlled, Phase 1 Trial". In: *The Lancet Infectious Diseases* 19.10 (2019), pp. 1091–1100. DOI: 10.1016/S1473-3099(19)30279-8.

[91] S. Wood et al. "Barriers and Facilitators of PrEP Adherence for Young Men and Transgender Women of Color". In: *AIDS and Behavior* 23.10 (2019), pp. 2719–2729. DOI: 10.1007/s10461-019-02502-y.

[92] S. Billioti de Gage, T. Le Tri, and R. Dray-Spira. "Suivi de l'utilisation de Truvadaou génériques pour une prophylaxie pré-exposition (PrEP) au VIH à partir des données du Système National des Données de Santé (SNDS)". In: (Nov. 2019).

[93] S. Phillips, B. L. Quigley, and P. Timms. "Seventy Years of Chlamydia Vaccine Research – Limitations of the Past and Directions for the Future". In: *Frontiers in Microbiology* 10 (2019). DOI: 10.3389/fmicb.2019.00070.

[94] VIH.org. *Stabilité des chiffres du VIH en France*. 2019. URL: https://vih.org/20190328/stabilite-des-chiffres-du-vih-en-france/ (visited on 02/24/2026).

[95] M. Adimy, A. Chekroun, and C. Ferreira. "Global dynamics of a differential difference system: A case of Kermack-McKendrick SIR model with age-structured protection phase". In: *Mathematical Biosciences and Engineering* 17 (2020), pp. 1329–1354. DOI: 10.3934/mbe.2020067.

[96] M. D. Akinlotan, D. G. Mallet, and R. P. Araujo. "Mathematical Modelling of the Role of Mucosal Vaccine on the Within-Host Dynamics of Chlamydia Trachomatis". In: *Journal of Theoretical Biology* 497 (2020), p. 110291. DOI: 10.1016/j.jtbi.2020.110291.

[97] D. P. Serota et al. "Pre-Exposure Prophylaxis Uptake and Discontinuation Among Young Black Men Who Have Sex With Men in Atlanta, Georgia: A Prospective Cohort Study". In: *Clinical Infectious Diseases* 71.3 (2020), pp. 574–582. DOI: 10.1093/cid/ciz894.

[98] E. Babakhanzadeh et al. "Some of the Factors Involved in Male Infertility: A Prospective Review". In: *International Journal of General Medicine* 13 (2020), pp. 29–41. DOI: 10.2147/IJGM.S241099.

[99] E. R. Learner et al. "The Influence of Screening, Misclassification, and Reporting Biases on Reported Chlamydia Case Rates Among Young Women in the United States, 2000 Through 2017". In: *Sexually Transmitted Diseases* 47.6 (2020), pp. 369–375. DOI: 10.1097/OLQ.0000000000001157.

[100] K. A. McManus et al. "Regional Disparities in Qualified Health Plans' Prior Authorization Requirements for HIV Pre-exposure Prophylaxis in the United States". In: *JAMA Network Open* 3.6 (2020), e207445. DOI: 10.1001/jamanetworkopen.2020.7445.

[101] M. M. Paschen-Wolff et al. "HIV Treatment Knowledge in the Context of "Treatment as Prevention" (TasP)". In: *AIDS and Behavior* 24.10 (2020), pp. 2984–2994. DOI: 10.1007/s10461-020-02849-7.

[102] A. Buratto, R. Cesaretto, and R. Zamarchi. "Mathematical Models for HIV Treatment: A Schematic Review". In: *Journal of Interdisciplinary Mathematics* 23.3 (2020), pp. 707–725. DOI: 10.1080/09720502.2020.1732049.

[103] S. K. Calabrese. "Understanding, Contextualizing, and Addressing PrEP Stigma to Enhance PrEP Implementation". In: *Current HIV/AIDS Reports* 17.6 (2020), pp. 579–588. DOI: 10.1007/s11904-020-00533-y.

[104] P. M. T. Djomegni, A. Tekle, and M. Y. Dawed. "Pre-Exposure Prophylaxis HIV/AIDS Mathematical Model with Non Classical Isolation". In: *Japan Journal of Industrial and Applied Mathematics* 37.3 (2020), pp. 781–801. DOI: 10.1007/s13160-020-00422-2.

[105] E. D. G. McIntosh. "Development of Vaccines against the Sexually Transmitted Infections Gonorrhoea, Syphilis, Chlamydia, Herpes Simplex Virus, Human Immunodeficiency Virus and Zika Virus". In: *Therapeutic Advances in Vaccines and Immunotherapy* 8 (2020), p. 2515135520923887. DOI: 10.1177/2515135520923887.

[106] UNAIDS. *Global HIV & AIDS statistics 2020 fact sheet*. 2020. URL: https://www.unaids.org/en/resources/fact-sheet (visited on 02/24/2026).

[107] E. O. Murchu et al. *Oral Pre-exposure Prophylaxis (PrEP) to Prevent HIV: A Systematic Review and Meta-Analysis of Clinical Effectiveness, Safety,*

Adherence and Risk Compensation in All Populations. Pre-published. 2021. DOI: 10.1101/2021.09.24.21264095.

[108] K. M. Kreisel et al. "Estimates of the Prevalence and Incidence of Chlamydia and Gonorrhea Among US Men and Women, 2018". In: *Sexually Transmitted Diseases* 48.4 (2021), pp. 222–231. DOI: 10.1097/OLQ.0000000000001382.

[109] K. M. Kreisel et al. "The Burden of and Trends in Pelvic Inflammatory Disease in the United States, 2006-2016". In: *The Journal of Infectious Diseases* 224.12 Suppl 2 (2021), S103–S112. DOI: 10.1093/infdis/jiaa771.

[110] L. A. Barbee et al. "The Natural History of Rectal Gonococcal and Chlamydial Infections: The ExGen Study". In: *Clinical Infectious Diseases* 74.9 (2021), pp. 1549–1556. DOI: 10.1093/cid/ciab680.

[111] Z. Qu et al. "Effect of Screening Young Men for Chlamydia Trachomatis on the Rates among Women: A Network Modelling Study for High-Prevalence Communities". In: *BMJ Open* 11.1 (2021), e040789. DOI: 10.1136/bmjopen-2020-040789.

[112] J. E. A. M. van Bergen et al. "Where to Go to in Chlamydia Control? From Infection Control towards Infectious Disease Control". In: *Sexually Transmitted Infections* 97.7 (2021), pp. 501–506. DOI: 10.1136/sextrans-2021-054992.

[113] CDC. *NSFG - Listing N - Key Statistics from the National Survey of Family Growth*. https://www.cdc.gov/nchs/nsfg/key$_s$*tatistics*/n_k*eystat.htm*. Accessed: 2023-23-02. 2021.

[114] Centers for Disease Control and Prevention and U.S. Public Health Service. *Preexposure prophylaxis for the prevention of HIV infection in the United States: 2021 update*. Atlanta, GA: CDC, 2021. URL: https://www.cdc.gov/hiv/pdf/risk/prep/cdc-hiv-prep-guidelines-2021.pdf.

[115] Centers for Disease Control and Prevention and U.S. Public Health Service. *Preexposure Prophylaxis for the Prevention of HIV Infection in the United States – 2021 Update: A Clinical Practice Guideline*. Tech. rep. Accessed: 2026-01-20. Atlanta, GA: CDC, 2021. URL: https://www.cdc.gov/hiv/pdf/risk/prep/cdc-hiv-prep-guidelines-2021.pdf.

[116] European Centre for Disease Prevention and Control. *HIV Pre-Exposure Prophylaxis in the EU/EEA and the UK: Implementation, Standards and Monitoring*. Accessed: 2026-01-19. Stockholm: ECDC, 2021. URL: https://www.ecdc.europa.eu/en/publications-data/HIV-PrEP-eueea-and-uk-implementation-standards-monitoring-guidance.

[117] L. M. de la Maza, T. L. Darville, and S. Pal. "Chlamydia Trachomatis Vaccines for Genital Infections: Where Are We and How Far Is There to Go?" In: *Expert Review of Vaccines* 20.4 (2021), pp. 421–435. DOI: 10.1080/14760584.2021.1899817.

[118] J. B. Reed et al. "HIV PrEP Is More than ART-lite: Longitudinal Study of Real-World PrEP Services Data Identifies Missing Measures Meaningful to HIV Prevention Programming". In: *Journal of the International AIDS Society* 24.10 (Oct. 2021), e25827. ISSN: 1758-2652. DOI: 10.1002/jia2.25827. PMID: 34648678.

[119] L. Wang et al. "Mathematical Modelling of the Influence of Serosorting on the Population-Level HIV Transmission Impact of Pre-Exposure Prophylaxis". In: *AIDS* 35.7 (June 1, 2021), p. 1113. ISSN: 0269-9370. DOI: 10.1097/QAD.0000000000002826. URL: https://journals.lww.com/aidsonline/fulltext/2021/06010/mathematical_modelling_of_the_influence_of.12.aspx.

[120] K.A. Workowski et al. "Sexually Transmitted Infections Treatment Guidelines, 2021". In: *MMWR. Recommendations and reports: Morbidity and mortality weekly report. Recommendations and reports* 70.4 (July 23, 2021), pp. 1–187. ISSN: 1545-8601. DOI: 10.15585/mmwr.rr7004a1. PMID: 34292926.

[121] World Health Organization. *Consolidated Guidelines on HIV Prevention, Testing, Treatment, Service Delivery and Monitoring: Recommendations for a Public Health Approach*. Tech. rep. Accessed: 2026-01-20. Geneva: World Health Organization, 2021. URL: https://www.who.int/publications/i/item/9789240031593.

[122] M. Adimy et al. "Forecasting the Effect of Pre-Exposure Prophylaxis (PrEP) on HIV Propagation with a System of Differential–Difference Equations with Delay". In: *Mathematics* 10.21 (Jan. 2022), p. 4093. ISSN: 2227-7390. DOI: 10.3390/math10214093.

[123] AIDS Action Europe. *Rapid Assessment on Access to PrEP in EU/EEA Countries*. Tech. rep. Co-funded by the Health Programme of the European Union. Berlin, Germany: AIDS Action Europe, Dec. 2022. URL: https://www.prepwatch.org/resources/rapid-assessment-on-access-to-prep-in-eu-eea-countries-2022/.

[124] A. Alrubayyi et al. "Functional Restoration of Exhausted CD8 T Cells in Chronic HIV-1 Infection by Targeting Mitochondrial Dysfunction". In: *Frontiers in Immunology* 13 (July 5, 2022). ISSN: 1664-3224. DOI: 10.3389/fimmu.2022.908697.

[125] J. Ballreich, T. Levengood, and R. M. Conti. "Opportunities and Challenges of Generic Pre-Exposure Prophylaxis Drugs for HIV". In: *Journal of Law, Medicine & Ethics* 50.S1 (June 2022), pp. 32–39. ISSN: 1073-1105, 1748-720X. DOI: 10.1017/jme.2022.33.

[126] C. Comer and R. Fernández. "Health Departments and PrEP: A Missed Opportunity for Public Health". In: *Journal of Law, Medicine & Ethics* 50.S1 (June 2022), pp. 64–68. ISSN: 1073-1105, 1748-720X. DOI: 10.1017/jme.2022.39. URL: https://www.cambridge.org/core/journals/journal-of-law-medicine-and-ethics/article/health-departments-and-prep-a-missed-opportunity-for-public-health/83F9A9C6D2851E0CC5FB963F7BEFE08B (visited on 09/22/2025).

[127] P. Godfrey-Faussett et al. "HIV Prevention for the next Decade: Appropriate, Person-Centred, Prioritised, Effective, Combination Prevention". In: *PLOS Medicine* 19.9 (Sept. 26, 2022), e1004102. ISSN: 1549-1676. DOI: 10.1371/journal.pmed.1004102.

[128] Joint United Nations Programme on HIV/AIDS. *Dangerous inequalities: World AIDS Day report 2022*. UNAIDS, 2022.

[129] H. Jourdain et al. "Real-World Effectiveness of Pre-Exposure Prophylaxis in Men at High Risk of HIV Infection in France: A Nested Case-Control Study". In: *The Lancet Public Health* 7.6 (June 1, 2022), e529–e536. ISSN: 2468-2667. DOI: 10.1016/S2468-2667(22)00106-2. PMID: 35660214.

[130] A. Lau, J.S.Hocking, and F.Y.S. Kong andY.S. Fabian. "Rectal Chlamydia Infections: Implications for Reinfection Risk, Screening, and Treatment Guidelines". In: *Current Opinion in Infectious Diseases* 35.1 (Feb. 1, 2022), pp. 42–48. ISSN: 1473-6527. DOI: 10.1097/QCO.0000000000000804. PMID: 34840272.

[131] C. M.Khosropour et al. "Incidence and Duration of Pharyngeal Chlamydia Among a Cohort of Men Who Have Sex With Men". In: *Clinical Infectious Diseases: An Official Publication of the Infectious Diseases Society of America* 75.5 (Sept. 14, 2022), pp. 875–881. ISSN: 1537-6591. DOI: 10.1093/cid/ciab1022. PMID: 34893806.

[132] S. Mashaphu et al. "Condom Use Consistency among South African HIV Serodiscordant Couples Following an HIV Risk-Reduction Intervention". In: *International Journal of STD & AIDS* 33.5 (Apr. 1, 2022), pp. 479–484. ISSN: 0956-4624. DOI: 10.1177/09564624221076617.

[133] R. Rodrigues et al. "Therapeutic Options for Chlamydia Trachomatis Infection: Present and Future". In: *Antibiotics* 11.11 (Nov. 16, 2022), p. 1634. ISSN: 2079-6382. DOI: 10.3390/antibiotics11111634. PMID: 36421278.

[134] M. Adimy, A. Chekroun, and T. Kuniya. "Global Asymptotic Stability for a Distributed Delay Differential–Difference System of a Kermack–McKendrick SIR Model". In: *Applicable Analysis* 102.12 (Aug. 13, 2023), pp. 3463–3475. ISSN: 0003-6811. DOI: 10.1080/00036811.2022.2075352.

[135] M. Adimy et al. "Global Asymptotic Stability of a Hybrid Differential–Difference System Describing SIR and SIS Epidemic Models with a Protection Phase and a Nonlinear Force of Infection". In: *Qualitative Theory of Dynamical Systems* 23.1 (Oct. 31, 2023), p. 34. ISSN: 1662-3592.

[136] L. Bekker et al. "HIV Infection". In: *Nature Reviews Disease Primers* 9.1 (Aug. 17, 2023), p. 42. ISSN: 2056-676X. DOI: 10.1038/s41572-023-00452-3.

[137] A. Cornea et al. "Assessment and diagnosis of HIV-associated dementia". In: *Viruses* 15.2 (Jan. 2023), p. 378. DOI: 10.3390/v15020378.

[138] R. Giddings et al. "Infectious Disease Modelling of HIV Prevention Interventions: A Systematic Review and Narrative Synthesis of Compartmental Models". In: *PharmacoEconomics* 41.6 (June 1, 2023), pp. 693–707. ISSN: 1179-2027. DOI: 10.1007/s40273-023-01260-z.

[139] J. Harper et al. "Progress Note 2024: Curing HIV; Not in My Lifetime or Just Around the Corner?" In: *Pathogens and Immunity* 8.2 (2023), pp. 115–179. ISSN: 2469-2964.

[140] Joint United Nations Programme on HIV/AIDS (UNAIDS). *The Path That Ends AIDS: UNAIDS Global AIDS Update 2023*. Geneva: UNAIDS, 2023. URL: https://thepath.unaids.org/wp-content/themes/unaids2023/assets/files/2023_report.pdf.

[141] Joint United Nations Programme on HIV/AIDS (UNAIDS). *UNAIDS Data 2023*. Licence: CC BY-NC-SA 3.0 IGO. Geneva: UNAIDS, 2023. URL: https://www.unaids.org/sites/default/files/media_asset/data-book-2023_en.pdf.

[142] R. J. Landovitz, H. Scott, and S. G. Deeks. "Prevention, Treatment and Cure of HIV Infection". In: *Nature Reviews Microbiology* 21.10 (Oct. 2023), pp. 657–670. ISSN: 1740-1534. DOI: 10.1038/s41579-023-00914-1.

[143] M. Magnus et al. "Overcoming Structural Barriers to Diffusion of HIV Pre-Exposure Prophylaxis". In: *The Journal of Medicine Access* 7 (Jan. 1, 2023), p. 27550834231214958. ISSN: 2755-0834. DOI: 10.1177/27550834231214958.

[144] M. Saade, S. Aniţa, and V. Volpert. "Dynamics of Persistent Epidemic and Optimal Control of Vaccination". In: *Mathematics* 11.17 (Jan. 2023), p. 3770. ISSN: 2227-7390. DOI: 10.3390/math11173770.

[145] P. Wu et al. "PrEP Intervention in the Mitigation of HIV/AIDS Epidemics in China via a Data-Validated Age-Structured Model". In: *Bulletin of Mathematical Biology* 85.5 (Apr. 11, 2023), p. 41. ISSN: 1522-9602. DOI: 10.1007/s11538-023-01145-4.

[146] *Actualisation des chiffres d'utilisation de la PrEP*. EPI-PHARE. Nov. 29, 2024. URL: https://www.epi-phare.fr/rapports-detudes-et-publications/prep-vih-2024/ (visited on 12/26/2025).

[147] M. Adimy et al. "Stability Analysis of a New Differential-Difference Model Applied to the Pre-exposure Prophylaxis (PrEP) Effect on the Spread of HIV". In: *Qualitative Theory of Dynamical Systems* 23.5 (July 11, 2024), p. 238. ISSN: 1662-3592. DOI: 10.1007/s12346-024-01093-x.

[148] B.W. Bennett et al. "Population Percentage and Population Size of Men Who Have Sex With Men in the United States, 2017-2021: Meta-Analysis of 5 Population-Based Surveys". In: *JMIR Public Health and Surveillance* 10.1 (June 11, 2024), e56643. DOI: 10.2196/56643. URL: https://publichealth.jmir.org/2024/1/e56643 (visited on 02/18/2026).

[149] Centers for Disease Control and Prevention. *Sexually Transmitted Infections Surveillance, 2023*. Annual Report. Atlanta, GA: U.S. Department of Health and Human Services, Nov. 12, 2024. URL: https://www.cdc.gov/sti-statistics/annual/index.html.

[150] Centers for Disease Control and Prevention. *Table 32. Chlamydia — Reported Cases and Rates of Reported Cases by Age Group and Sex, United States*. STI Statistics. 2024. URL: https://www.cdc.gov/sti-statistics/data-vis/table-ct-agesex.html.

[151] Z. Chazuka, E. Mudimu, and D. Mathebula. "Stability and Bifurcation Analysis of an HIV Model with Pre-Exposure Prophylaxis and Treatment Interventions". In: *Scientific African* 23 (Mar. 1, 2024), e01979. ISSN: 2468-2276. DOI: 10.1016/j.sciaf.2023.e01979.

[152] T. Chou, N.S. Maggirwar, and M.D. Marsden. "HIV Persistence, Latency, and Cure Approaches: Where Are We Now?" In: *Viruses* 16.7 (July 2024), p. 1163. ISSN: 1999-4915. DOI: 10.3390/v16071163.

[153] R. Fry. *A Growing Share of U.S. Husbands and Wives Are Roughly the Same Age*. Pew Research Center. Aug. 15, 2024. URL: https://www.pewresearch.org/short-reads/2024/08/15/a-growing-share-of-us-husbands-and-wives-are-roughly-the-same-age/.

[154] M. Makhoul et al. "Impact of a Potential Chlamydia Vaccine in the USA: Mathematical Modelling Analyses". In: *BMJ Public Health* 2.1 (Jan. 2024), e000345. ISSN: 2753-4294. DOI: 10.1136/bmjph-2023-000345.

[155] E. Mataand et al. "Unveiling the Cost-Effectiveness of Chlamydia Screening Strategies: A Systematic Review". In: *Portuguese Journal of Public Health* 43.1 (Nov. 19, 2024), pp. 47–58. ISSN: 2504-3137. DOI: 10.1159/000542685.

[156] A. N. Schemelev et al. "Involvement of Human Cellular Proteins and Structures in Realization of the HIV Life Cycle: A Comprehensive Review, 2024". In: *Viruses* 16.11 (Nov. 2024), p. 1682. ISSN: 1999-4915. DOI: 10.3390/v16111682.

[157] *UNAIDS Data 2024*. Tech. rep. Licence: CC BY-NC-SA 3.0 IGO. Geneva: Joint United Nations Programme on HIV/AIDS, 2024. URL: https://www.unaids.org/sites/default/files/media_asset/data-book-2024_en.pdf.

[158] I. F. Unigwe et al. "Trajectories of Adherence to Oral Pre-exposure Prophylaxis and Risks of HIV and Sexually Transmitted Infections". In: *Open Forum Infectious Diseases* 11.10 (Oct. 1, 2024), ofae569. ISSN: 2328-8957. DOI: 10.1093/ofid/ofae569.

[159] World Health Organization. *Guidelines on lenacapavir for HIV prevention and testing strategies for long-acting injectable pre-exposure prophylaxis*. Accessed 2026. Geneva, Switzerland: World Health Organization, 2024. URL: https://www.who.int/publications.

[160] World Health Organization. "Implementing the Global Health Sector Strategies on HIV, Viral Hepatitis and Sexually Transmitted Infections, 2022–2030". In: (2024).

[161] S. Bamouni et al. "Effect of Extending PrEP Initiation to Primary Care Settings: A Nationwide Cohort Study in France". In: *The Lancet Public*

Health 10.5 (May 1, 2025), e362–e370. ISSN: 2468-2667. DOI: 10.1016/S2468-2667(25)00062-3.

[162] C. Bendana. "Trump's cuts to international aid are stifling Africa's HIV research". In: *Nature* (May 2025). DOI: 10.1038/d41586-025-01424-1.

[163] Centers for Disease Control and Prevention. *National Health and Nutrition Examination Survey*. National Health and Nutrition Examination Survey. Dec. 18, 2025. URL: https://www.cdc.gov/nchs/nhanes/index.html.

[164] Centers for Disease Control and Prevention. *STI screening recommendations*. 2025. URL: https://www.cdc.gov/std/treatment-guidelines/screening-recommendations.htm.

[165] European Centre for Disease Prevention and Control. *HIV/AIDS surveillance in Europe 2025 – 2024 data*. 2025. URL: https://www.ecdc.europa.eu/en/publications-data/hivaids-surveillance-europe-2025-2024-data (visited on 01/16/2026).

[166] L. Giacani et al. "Antimicrobial Resistance in Curable Sexually Transmitted Infections". In: *Current HIV/AIDS reports* 22.1 (Jan. 25, 2025), p. 14. ISSN: 1548-3576. DOI: 10.1007/s11904-025-00722-7. PMID: 39856345.

[167] Joint United Nations Programme on HIV/AIDS. *UNAIDS Global AIDS Update 2025: AIDS, Crisis and the Power to Transform*. Geneva: United Nations, 2025.

[168] K. Łupina et al. "Pharmacological Advances in HIV Treatment: From ART to Long-Acting Injectable Therapies". In: *Archives of Virology* 170.9 (2025), p. 195. ISSN: 0304-8608. DOI: 10.1007/s00705-025-06381-8. PMID: 40826301.

[169] N. McKeever. "Is Sex Work Inherently Gendered?" In: *Hypatia* 40.3 (Aug. 2025), pp. 633–652. ISSN: 0887-5367, 1527-2001. DOI: 10.1017/hyp.2024.56.

[170] Y. Merad et al. "Determinants of Mpox Vaccination Uptake among MSM during the 2022 Outbreak: A Single-Centre Retrospective Study at Lyon University Hospital, France". In: *BMC Public Health* 25 (Oct. 15, 2025),

p. 3496. ISSN: 1471-2458. DOI: 10.1186/s12889-025-24728-3. PMID: 41094414.

[171] R. Wittenauer et al. "Health and Economic Impact of Oral PrEP Provision across Subgroups in Western Kenya: A Modelling Analysis". In: *BMJ Global Health* 10.1 (Jan. 11, 2025). ISSN: 2059-7908. DOI: 10.1136/bmjgh-2024-015835. PMID: 10.1136/bmjgh-2024-015835.

[172] R. Gudeli, K. Mangu, and H. Agarwal. "Optimizing Vaccine Allocation: A Review of Epidemiological Models with Behavioral Adaptation". In: *Clinical and Experimental Vaccine Research* 15.1 (Jan. 2026), pp. 9–14. ISSN: 2287-3651. DOI: 10.7774/cevr.2026.15.e3. PMID: 41660220.

[173] S. M. Topp et al. "Advancing Functional and Systemic Integration of HIV Prevention into Public Health Systems". In: *The Lancet Global Health* 14.1 (Jan. 1, 2026), e121–e130. ISSN: 2214-109X. DOI: 10.1016/S2214-109X(25)00397-3. PMID: 41349553.

[174] H. Wang et al. "Extended PrEP Cascades and Determinants of Long-Acting PrEP Intention and Unmet PrEP Needs among Transgender Women, Transgender Men, and Non-Binary Individuals in 20 European Countries". In: *International Journal of Transgender Health* 0.0 (June 26, 2026), pp. 1–17. ISSN: 2689-5269. DOI: 10.1080/26895269.2026.2693596.

[175] Wikipedia contributors. *Adolescent sexuality in the United States*. Wikipedia. 2026. URL: https://en.wikipedia.org/w/index.php?title=Adolescent_sexuality_in_the_United_States&oldid=1336313907.

[176] AVAC. *MSM in Europe*. URL: https://www.avac.org/sites/default/files/u3/MSM_in_Europe_Euro_Rave.pdf (visited on 04/04/2023).

[177] HIV.gov. *HIV basics: Overview: About HIV & AIDS: Symptoms of HIV*. URL: https://www.hiv.gov/hiv-basics/overview/about-hiv-and-aids/symptoms-of-hiv (visited on 07/08/2026).

[178] INSEE. *Statistiques*. URL: https://www.insee.fr/fr/statistiques/2383440 (visited on 02/24/2026).

[179] S. Olaniyi et al. "Mathematical Analysis of Non-Autonomous HIV/AIDS Transmission Dynamics with Efficient and Cost-Effective Intervention Strategies | Contemporary Mathematics". In: ().

[180] V. Ssempijja et al. "Dynamics of Pre-Exposure (PrEP) Eligibility Because of Waxing and Waning of HIV Risk in Rakai, Uganda". In: *Journal of Acquired Immune Deficiency Syndromes (1999)* 93.2 (), pp. 143–153. ISSN: 1944-7884. DOI: 10.1097/QAI.0000000000003182. PMID: 36889304.

[181] *U.S.: Reported to Infidelity 2021*. Statista. URL: https://www.statista.com/statistics/1367073/us-reported-to-infidelity/.

[182] UNAIDS. *France*. URL: https://www.unaids.org/en/regionscountries/countries/france (visited on 02/24/2026).

[183] US Census Bureau. *Age and Sex Composition in the United States: 2018*. Census.gov. URL: https://www.census.gov/data/tables/2018/demo/age-and-sex/2018-age-sex-composition.html.

[184] World Health Organization. *HIV/AIDS fact sheet*. URL: https://www.who.int/news-room/fact-sheets/detail/hiv-aids (visited on 02/24/2026).

Modélisation mathématique de la propagation d'épidemies avec traitement à éfficacité temporaire

Résumé : Cette thèse s'articule autour de la modélisation mathématique et de l'analyse de l'impact épidémiologique de deux interventions biomédicales: la Prophylaxie Pré-Exposition (PrEP) contre le Virus de l'Immunodéficience Humaine (VIH) et la vaccination contre Chlamydia trachomatis (CT). Dans la première partie, nous développons des modèles compartimentaux pour le VIH intégrant un compartiment spécifique pour les individus sous PrEP. L'originalité du modèle réside dans la prise en compte de la durée limitée de protection via une équation hyperbolique structurée en âge (temps depuis la dernière prise). Ce formalisme permet de transformer le modèle en un système hybride d'équations différentielles à retard discret, représentant le délai entre les rendez-vous médicaux selon les directives de l'OMS. Nous menons une analyse mathématique (stabilité locale et globale) et explorons l'influence de taux de recrutement non-linéaires. Nos résultats mettent en évidence l'existence de phénomènes d'hystérésis et l'émergence de bifurcations de Hopf, identifiant des délais critiques au-delà desquels la dynamique épidémique devient oscillatoire. Les simulations numériques, calibrées sur des données françaises (Truvada), quantifient l'impact de l'adhérence au traitement et de la durée de protection sur le contrôle de l'épidémie. Dans la seconde partie, la thèse change d'échelle pour évaluer l'impact populationnel d'un futur vaccin contre la chlamydia aux États-Unis. Nous avons développé un modèle à agents (ABM), calibré sur les données de l'enquête NHANES, pour simuler les réseaux de transmission. Ce modèle permet de tester différentes stratégies vaccinales, démontrant que des approches ciblant des tranches d'âge spécifiques ou adoptant une stratégie inclusive de genre sont essentielles pour réduire significativement la prévalence de l'infection. Ce travail interdisciplinaire combine analyse qualitative des systèmes dynamiques et simulations stochastiques pour offrir des outils d'aide à la décision en santé publique, soulignant l'importance des facteurs comportementaux et économiques dans la réussite des politiques de prévention.

Mots-clés : Modélisation mathématique, Épidémies, Traitement temporaire, Équations differentielles à retard, Modèle à agents, Infections sexuellement transmissibles

---

Mathematical modeling of epidemics spreading dealing with temporary treatment efficiency

Abstract : This dissertation focuses on the mathematical modeling and epidemiological impact analysis of two major biomedical interventions: Pre-Exposure Prophylaxis (PrEP) for the Human Immunodeficiency Virus (HIV) and vaccination against Chlamydia trachomatis (CT). In the first part, we develop HIV compartmental models that incorporate a specific PrEP compartment. The originality of the model lies in accounting for the limited duration of protection through an age-structured hyperbolic equation (where age represents the time elapsed since the last dose). This formalism allows the model to be reduced to a hybrid system of differential-difference equations with a discrete delay, representing the interval between medical appointments according to WHO guidelines. We perform a rigorous mathematical analysis (including local and global stability) and explore the influence of non-linear recruitment rates. Our results highlight the existence of hysteresis phenomena and the emergence of Hopf bifurcations, identifying critical delays beyond which epidemic dynamics become oscillatory. Numerical simulations, calibrated using French data (Truvada), quantify the impact of treatment adherence and protection duration on epidemic control. In the second part, the thesis shifts scale to evaluate the population-level impact of a potential vaccine for Chlamydia in the United States. We developed an Agent-Based Model (ABM), calibrated using National Health and Nutrition Examination Survey (NHANES) data, to simulate transmission networks. This model tests various vaccination strategies, demonstrating that age-targeted approaches or gender-inclusive strategies are essential for significantly reducing infection

prevalence. This interdisciplinary work combines the qualitative analysis of dynamical systems with stochastic simulations to provide decision-support tools for public health, emphasizing the importance of behavioral and economic factors in the success of prevention policies.

Keywords : Mathematical Modeling, Epidemics, Temporary treatment, Delay differential equations, Agent-based model, Sexually transmitted infections

Université Claude Bernard Lyon 1
École Doctorale InfoMaths (ED 512)
Discipline : Mathématiques
Laboratoire : Institut Camille Jordan (ICJ)